Epigraph

Nothing in life is to be feared, it is only to be understood. Now is the time to understand more, so that we may fear less.

— Marie Curie

University of Alberta

A role for the nuclear pore complex protein Nup170p in defining chromatin structure and regulating gene expression

by

David Wallace Van de Vosse

A thesis submitted to the Faculty of Graduate Studies and Research
in partial fulfillment of the requirements for the degree of

Doctor of Philosophy

Department of Cell Biology

Fall 2012
Edmonton, Alberta

Dedication

To my courageous wife Tania, may we be at eighty, as we were at twenty…ridiculously compatible.

Abstract

The spatial organization of chromosomal loci within the nucleus can have a significant influence on transcriptional activity. Transcriptionally active genes are generally positioned within the nuclear interior. By contrast, the positioning of genes at the nuclear periphery is often correlated with transcriptional silencing as evident by the preferential localization of condensed, transcriptionally silent heterochromatin at the nuclear envelope (NE). This generality of the NE fostering silencing is lost at regions of the NE occupied by nuclear pore complexes (NPCs). Here heterochromatin bound to the inner nuclear membrane is abruptly interrupted at the nucleoplasmic face of NPCs by associated, transcriptionally active euchromatin channels. Thus, NPCs are positioned at the interface between heterochromatin and euchromatin. These morphological observations have long led to the idea that NPCs play an important role in defining chromatin structure and in gene expression. In recent years, this premise has been reinforced by studies in the yeast model system. For example, both active and silenced genes have been detected in association with NPCs. These and other observations have led ourselves and others to hypothesize that NPCs function in the transition of chromatin between transcriptional states. We have investigated this role of NPCs in chromatin organization through analyses of its components. We have focused on Nup170p, as the role of this protein in transcriptional repression was indicated by phenotypic manifestations suggestive of derepression of cell-type-dependent genes. We showed that Nup170p genetically interacts with multiple chromatin complexes involved in transcriptional silencing. Consistent with these

observations, we detected Nup170p in physical association with the RSC chromatin-remodeling complex, and both the RSC complex and Nup170p are required for repression of subtelomeric genes and the regulation of ribosomal protein (RP) gene expression. Moreover, Nup170p associates with and is required for proper chromatin structure at these loci. The subtelomeric chromatin association of Nup170p is mediated by its interaction with the silencing factor Sir4p. Conversely, the binding of Sir4p to telomeres and their normal association with the inner nuclear membrane are dependent on Nup170p. Importantly, these interactions are prominent during periods of telomere association with the NE at the end of mitosis.

Acknowledgments

I am beholden to a great many individuals whose assistance and support have guided me through my graduate studies. Foremost, I am thankful to have had the opportunity to study under Rick Wozniak. Rick, your understanding and appreciation of science is to be admired, though it is your application of the scientific method and the rigor in which you apply it that is truly inspiring. I am grateful for all that I have learned. Thank you.

This work would not have been possible without the close collaboration of John Aitchison, whose expertise in systems biology proved to be both invaluable and unparalleled. I thank you and your group members, particularly Yakun Wan, for your insights and contributions over the years.

I am appreciative of the support, both personal and professional, that I received from all members of the Wozniak Lab, past and present. In chronological order they are: Patrick Lusk, Robert Scott, Jana Mitchell, Tadashi Makio, Chris Ptak, Lucas Cairo, Chris Neufeldt, Neil Adames, Diego Lapetina, Juliana Capitanio, and Nogi Park. I no doubt owe any successes during my studies to your thorough, diligent, and seemingly endless critiquing of my work. For this I am truly grateful, as to meet your scientific standards means that one's work is of exceptional quality. Above all I am thankful for your friendships. Pat and Rob, your early lessons continue to guide me. Jana, our graduate careers progressed in parallel and as a friend you were always there to share these experiences with. A great amount of gratitude is owed to Neil Adames. Your spectacular insight and comprehensive knowledge of yeast biology is uncanny and, perhaps, only

matched by your voracious laughter. Luc and Chris, your ability to view seemingly subtle scientific details in a much broader perspective will serve you well in your future careers. Most of all thank you for the experience, I have gained much and your presence will be missed.

I am privileged to have a tremendously supportive family, especially my wife, Tania, your love and encouragement through the years is everything. To my mother, Carrie Van de Vosse, whose lessons and love provided me with all the tools to succeed in life and my father, Henry Van de Vosse, for teaching me the virtues of hard work, determination, and sacrifice.

Table of Content

List of Tables

List of Figures

List of Symbols, Abbreviations and Nomenclature

μ	micro
μm	microns/micrometres
μg	micrograms
μL	microlitres
˚C	degrees celsius
5-FOA	5-fluoroorotic acid
bp	base pairs
CCD	charge-coupled device
ChIP	chromatin immunoprecipitation
d	days
DNA	deoxyribonucleic acid
ECL	enhanced chemiluminescence
EM	electron microscopy
FG	phenylalanine glycine
Fig	figure
g	grams
G1	gap 1 phase
G2	gap 2 phase
GAP	GTPase activating protein
GDP	guanosine-5'-diphosphate
GEF	guanine nucleotide exchange factor
GFP	green fluorescent protein
GST	glutathione-S-transferase
GTP	guanosine-5'-triphosphate
GTPase	guanosine-5'-triphosphate hydrolase
h	hours
HA	hemagluttinin
pA	protein A
HDAC	histone deacetylase complex
HML	hidden *MAT* left

HMR ..... hidden *MAT* right

HU ..... hydroxyurea

IgG ..... immunoglobulin G

IGR ..... intergenic region

INM ..... inner nuclear membrane

IPTG ..... isopropyl beta-D-1-thiogalactopyranoside

KAT ..... lysine acetyltransferase

kDa ..... kilodalton

KMT ..... lysine methyltransferase

LacI ..... lactose repressor

lacO ..... lactose operator

$lexA^{op}$ ..... lexA operator

m ..... milli

M ..... molarity/mega

MAT ..... mating-type locus

mCherry ..... monomeric cherry

MDa ..... megadalton

mg ..... milligrams

min ..... minutes

mL ..... millilitres

mRNA ..... messenger ribonucleic acid

mRNP ..... messenger ribonucleoprotein

n ..... nano

NAD ..... nicotinamide adenine dinucleotide

NE ..... nuclear envelope

NES ..... nuclear export sequence

NFR ..... nucleosome free region

NLS ..... nuclear localization sequence

NOC ..... nocodazole

NPC ..... nuclear pore complex

Nup ..... nucleoporin

OD ..... optical density
ONM ..... outer nuclear membrane
ORF ..... open reading frame
PCR ..... polymerase chain reaction
POM ..... pore membrane
Pom ..... pore membrane protein
qPCR ..... quantitative real-time PCR
rDNA ..... ribosomal DNA
RFP ..... red fluorescent protein
RNA ..... ribonucleic acid
RNAi ..... RNA interference
RNP ..... ribonucleoprotein
RSC ..... remodel the structure of chromatin
RT-PCR ..... semi-quantitative reverse transcription PCR
SC ..... synthetic complete media
SDS-PAGE ..... sodium dodecyl sulfate polyacrylamide gel electrophoresis
sec ..... seconds
SGA ..... synthetic genetic array
SGD ..... *Saccharomyces cerevisiae* genome database
SIR ..... silent information regulator
SUMO ..... small ubiquitin like modifier
TCA ..... trichloroacetic acid
Tel ..... telomere
TEM ..... transmission electron microscopy
TSS ..... transcriptional start site
TTS ..... transcriptional termination site
WT ..... wild type
YPD ..... yeast extract peptone dextrose media

Chapter I: *Introduction**

***** Portions of this chapter were reproduced from: Van de Vosse, D.W., Wan, Y., Aitchison, J.D., and R.W. Wozniak. (2011). **Role of the nuclear envelope in genome organization and gene expression.** *Wiley Interdisciplinary Reviews Systems Biology and Medicine*. 3(2), 147-166.

1.1 Preface

A defining feature of eukaryotic cells is the presence of internal membrane structures that separate and compartmentalize cellular processes into organelles. The nucleus is one such organelle. Common among all eukaryotes, the nucleus contains the nuclear genome and all DNA metabolic processes associated with it and it is delineated by a membrane system: the nuclear envelope (NE). The presence of the NE establishes a communication barrier between the nucleoplasm and the cytoplasm that requires a transport mechanism to facilitate macromolecular movement across the NE (reviewed in: Walde and Kehlenbach, 2010; Wente and Rout, 2010). All nucleocytoplasmic transport across the NE is restricted to large, proteinaceous structures permeating the NE, termed nuclear pore complexes (NPCs)(reviewed in: Aitchison and Rout, 2012). In addition to regulating access of soluble factors to the genome, NPCs function in several non-transport related nuclear processes including transcriptional regulation and genome organization (reviewed in: Kohler and Hurt, 2010; Liang and Hetzer, 2010; Chatel and Fahrenkrog, 2012).

Transcriptionally silenced regions of the genome preferentially associate with the NE, while transcriptionally active regions predominate the nuclear interior. However, upon activation, certain genes relocate to the NE, indicating that both transcriptionally active and silenced chromatin co-exist at the NE. Through interactions with both forms of chromatin states, NPCs modulate the transcriptional status of attached chromatin and are ideally situated at the interface between transcriptionally active and silent chromatin domains, raising the notion

that NPCs may facilitate the transition between transcriptional states. Identification of the molecular mechanisms that establish and maintain these distinct chromatin structures at the NE is critical to understanding how genome organization influences transcriptional regulation.

1.2 Nuclear envelope

The nuclear envelope (NE) is comprised of two phospholipid bilayers, the outer nuclear membrane (ONM) and the inner nuclear membrane (INM), which together form a physical barrier between the cytoplasm and the nucleoplasm. The bi-directional transport of soluble cargo across the NE occurs through trans-cisternal pores formed by the fusion of the ONM and the INM. Consequently, at the fusion site an additional and sharply bent membrane domain is formed, the pore membrane (POM). The protein composition of each of these membrane domains is distinct from one another. The ONM is continuous with that of the endoplasmic reticulum (ER)(Watson, 1955) and contains numerous protein complexes also present at the ER, including membrane attached ribosomes. In addition, there are proteins specific to the ONM (Kvam and Goldfarb, 2006; Mellad et al., 2011).

The INM harbors a diverse set of membrane proteins involved in a wide range of nuclear processes including intranuclear signalling, chromosome segregation, and, importantly, genome organization (Dreger et al., 2001; Schirmer et al., 2003; Zuleger et al., 2011). Underlying the INM of higher eukaryotes is the nuclear lamina, a complex meshwork of intermediate filaments (formed by lamin

polymers) connected to the INM through integral inner membrane proteins and NPCs. Importantly, the nuclear lamina provides a critical function in nuclear stability and provides attachment sites for chromatin (reviewed in: Dechat et al., 2008 and Shimi et al., 2010). Lower eukaryotes such as *Sacccharomyces cerevisiae* lack a discernable nuclear lamina, however, lamin-like functions have been proposed for several yeast protein-interaction networks (Diffley and Stillman, 1989; Strambio-de-Castillia et al., 1999; Andrulis et al., 2002; Taddei et al., 2004). Interestingly, the targeting of a subset of integral INM proteins, and thus the composition of the INM, is influenced by the POM (King et al., 2006).

The POM lines the pore created by fusion of the INM and ONM and is distinguished by the presence of a specific subset of integral membrane proteins. Here, these proteins interact with and anchor nuclear pore complexes (NPCs), the large macromolecular assemblies that regulate nucleocytoplasmic transport. Consequently, the protein constituents of the POM are, together, imperative for NPC formation.

1.3 Nuclear pore complexes

Pores within the NE were first identified in early electronmicrographs of amphibian nuclei by Callan and Tomlin (1950) and would later be referred to as NPCs (Watson, 1959). Since then a plethora of electron microscopy studies across a wide range of organisms have defined the dimensions and overall structure of the NPC. Vertebrate NPCs are ~130 nm in diameter and ~80 nm in height (Akey and Radermacher, 1993; Yang et al., 1998), where as the yeast counterpart is

slightly smaller in size at ~100 nm in diameter by ~40 nm in height (Yang et al., 1998). Despite their significant differences in size, proteomic analyses have estimated the molecular mass of yeast and vertebrate NPCs to be relatively similar, ~50 MDa in yeast and ~60 MDa in vertebrates (Yang et al., 1998; Rout et al., 2000; Cronshaw et al., 2002). However, discrepancies in the estimates of NPC size, in terms of mass, have been reported and may reflect differences in the purification of the numerous NPC-associated protein complexes (Reichelt et al., 1990; Rout and Blobel, 1993). More concise is the observation that NPCs display a characteristic 8-fold radial symmetry around its nucleocytoplasmic axis, an observation made almost 5 decades ago (Gall, 1967) and 2-fold symmetry in relation to the mid-plane of the NE. Again, however, discrepancies exist, as NPCs displaying 9-fold and even 10-fold symmetry have been reported (Hinshaw and Milligan, 2003), though these are a rare exception and the significance of these rare observations has not been established.

The sheer size of the NPC prohibits the molecular structure of the NPC to be solved by standard crystallography techniques. To overcome this limitation, a recent comprehensive study of the yeast NPC used computational analysis of physical interaction data obtained from a multitude of biochemical approaches and data from extensive location analyses to approximate the position of each protein within the NPC (Alber et al., 2007a and 2007b). This work resulted in a high-resolution spatial map of the NPC (see Figure 1-1). Structurally, NPCs are comprised of several ring and spoke-like structures that are symmetrically positioned to form a cylinder-like structure surrounding a central channel ~40 nm

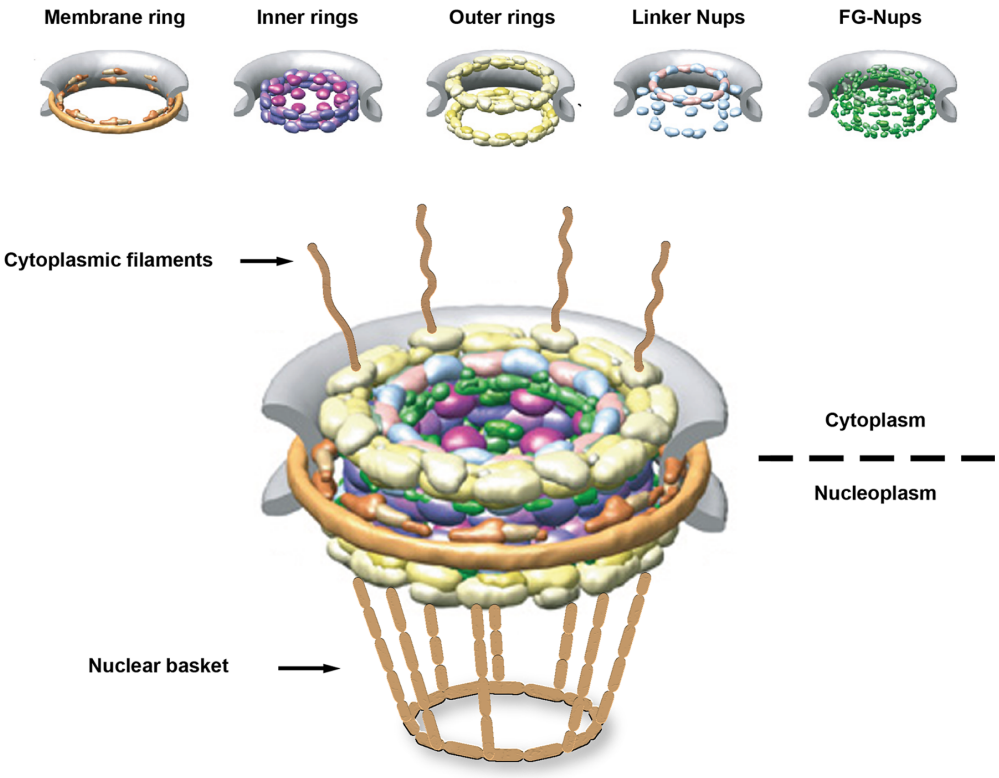

Figure 1-1. Structure and composition of the nuclear pore complex.

A graphical representation displaying the major substructures of an NPC embedded within the NE. Nucleoporins are coloured according to their predicted localization volumes within the five substructures of the NPC. The NPC is anchored to the pore membrane (POM; grey) by the lumen ring (orange). The core of the NPC is composed of the inner rings (purple), outer rings (yellow), and the linker Nups (light blue/pink). Attached to the linker Nups and lining the central channel are the FG-Nups (green). Protruding from the cytoplasmic and nucleoplasmic face of the NPC are the cytoplasmic filaments (for clarity only four of eight are shown) and the nuclear basket, respectively (brown). Adapted from Alber et al., 2007b. Reprinted by permission from Macmillan Publishers Ldt: Nature. Alber, F., Dokudovskaya, S., Veenhoff, L.M., Zhang, W., Kipper, J., Devos, D., Suprapto, A., Karni-Schmidt, O., Williams, R., Chait, B.T., Sali, A., and M.P. Rout. The molecular architecture of the nuclear pore complex. *Nature*. 2007;450(7170):695-701. Copyright 2007.

in diameter. Most nucleocytoplasmic transport is thought to occur through the central channel. The cylinder (structural core) consists of a symmetrical cytoplasmic and nucleoplasmic face, each containing an equivalent inner and outer ring. In addition, the core contains a single proteinaceous ring lying adjacent to the pore membrane within the lumenal space of the NE. The lumen ring spans the circumference of the pore and anchors the core to the POM.

Within the pore, each inner and outer ring of the core cylinder consists of repeating structural subcomplexes that, when stacked within the context of the cylinder, give rise to eight spoke-like structures responsible for the characteristic 8-fold radial symmetry of the NPC. Emanating from these spokes on the cytoplasmic face of the NPC are cytoplasmic filaments involved in the initial stages of nuclear import and the final stages of nuclear export (Jarnik and Aebi, 1991; reviewed in: Walde and Kehlenbach, 2010). A distinct set of filaments protrude into the nucleoplasm from the nucleoplasmic face, coalescing to form the nuclear basket structure that provides docking sites for the final stages of nuclear import and the initial stages of nuclear export (Goldberg and Allen, 1996; reviewed in: Walde and Kehlenbach, 2010). The nuclear basket and features of the NPC core facing the nucleoplasm mediate interactions with chromatin and, in higher eukaryotes, the nuclear lamina. In addition, these structures provide an attachment site for multiple NPC-associated proteins involved in a wide-range of nuclear processes, including, among others, post-translational modifications, genome stability, chromosome segregation, and transcriptional regulation (Galy et

al., 2000, Iouk et al., 2002; Scott et al., 2005 and 2009; Dilworth et al., 2005; Lewis et al., 2007; Luthra et al., 2007; Palancade et al., 2007).

1.4 Nucleoporins

Numerous genetic and proteomic approaches have identified the vast majority of yeast and mammalian NPC proteins, termed nucleoporins, or Nups, demonstrating that despite its immense size the NPC is composed of surprisingly few proteins, ~30 different Nups in yeast (Rout et al., 2000). A similar number of Nups have been identified in vertebrates (Cronshaw et al., 2002). A list of both yeast and vertebrate Nups are listed in Table 1-1. In comparison, the ribosome, at ~4 MDa in mass, is less than 10% of the mass of an NPC, yet contains nearly three times the number of proteins (Wool et al., 1995). This disparity is overcome by the presence of each Nup in multiple copies, usually 16 per NPC, resulting in an individual NPC consisting of approximately 456 individual proteins (Rout et al., 2000; Alber et al., 2007b).

Until recently experimentally derived atomic structures were limited to a small number of Nups, however several groups, the Blobel and Schwartz laboratories in particular, have made significant progress in this area, and high-resolution structures of numerous individual Nups and subcomplexes of interacting Nups have now been determined (Berke et al., 2004; Weirich et al., 2004; Hsia et al., 2007; Jeudy and Schwartz, 2007; Melcak et al., 2007; Debler et al., 2008; Kampmann and Blobel, 2009; reviewed in: Brohawn et al., 2009 and Hoelz et al., 2011). These structural studies, in addition to structures predicted by

Table 1-1. Mammalian and *Saccharomyces cerevisiae* nucleoporin homologs.

Mammalian	*S. cerevisiae*	Nup category
Nup358 (RanBP2)	—	FG
Nup214	Nup159p	FG
Nup153	Nup1p/Nup2/Nup60p	FG
Nup98	Nup145-N/Nup100p/Nup116p	FG
Nup62 (p62)	Nsp1p	FG
Nup58/Nup45	Nup49p	FG
Nup54	Nup57p	FG
Nup53 (Nup35)	Nup53p/Nup59p	FG
Nup50	Nup2p	FG
NLP1 (hCG1)	Nup42p	FG
Nup205	Nup192p	Non-FG
Nup188	Nup188p	Non-FG
Nup160	Nup120p	Non-FG
Nup155	Nup157p/Nup170p	Non-FG
Nup133	Nup133p	Non-FG
Nup107	Nup84p	Non-FG
Nup96	Nup145-C	Non-FG
Nup93	Nic96p	Non-FG
Nup88	Nup82p	Non-FG
Nup85 (Nup75)	Nup85p	Non-FG
Nup43	—	Non-FG
Nup37	—	Non-FG
ALADIN	—	Non-FG
Gle1	Gle1p	Non-FG
RAE1 (Gle2)	Gle2p	Non-FG
Sec13	Sec13p	Non-FG
Seh1	Seh1p	Non-FG
Tpr	Mlp1p/Mlp2p	Non-FG
Pom121	—	Pom
gp210	—	Pom
NDC1	Ndc1p	Pom
—	Pom34p	Pom
—	Pom152p	Pom

* Adapted from: D'Angelo and Hetzer, et al., 2008.

primary sequence analysis of Nups (Devos et al., 2006; Alber et al., 2007b), revealed that the simplicity in composition of the NPC is similarly reflected by the presence of relatively few protein folding domains. Based on these fold domains, Nups partition into three groups distributed spatially within the NPC: a transmembrane domain-containing group (the Poms) positioned within the pore membrane domain, a β-propeller and α-solenoid group that populates the core cylinder of the NPC (the core scaffold Nups), and a third group of Nups containing phenylalanine-glycine (FG) repeats (the FG-Nups) that play a direct role in nucleocytoplasmic transport.

1.4.1 Pore membrane proteins (Poms)

The yeast NPC contains three intregal pore membrane proteins (Poms), Pom34p, Pom152, and Ndc1p, a component shared with spindle pole bodies (Wozniak et al., 1994; Chial et al., 1998; Miao et al., 2006). A fourth trans-membrane containing protein, Pom33p, is required for NPC distribution along the NE and *POM33* displays genetic interactions with several nucleoporin genes including *NDC1*; however, its inclusion in the Pom-family of proteins is questioned based on its transient association with NPCs and a lack of physical interactions with other Poms (Chadrin et al., 2010). Poms form extensive physical interactions with one another and, as such, have been proposed to assemble a distinct subcomplex that forms the membrane-associated lumenal ring that circumscribes the pore (Alber et al., 2007b; Onischenko et al., 2009). Each Pom is predicted to contain one or more transmembrane α-helices that extend through the

pore membrane and, through their interactions with core scaffold Nups, the Poms are proposed to anchor the NPC to the NE.

Poms appear to be functionally redundant as only loss of Ndc1p is lethal, a likely consequence of its essential function in spindle pole body formation (Winey et al., 1993). Functional redundancy is further evident by the shared set of genetic interactions with scaffold Nups described for *POM34* and *POM152* (Marelli et al., 1998; Tcheperegine et al., 1999; Miao et al., 2006; Onischenko et al., 2009). Single null mutations of either *POM34* or *POM152* do not impede nuclear import, while import is inhibited following depletion of Ndc1p (Madrid et al., 2006). Loss of Ndc1p was also accompanied by mislocalization of both cytoplasmic and nucleopolasmic Nups, and upon further loss of Pom152p, led to NPCs with an increased diameter and a lack of proteinceous material, suggesting that both are required for NPC assembly (Madrid et al., 2006). Consistent with this view, a role for Pom34p and Pom152p in targeting newly synthesized Nups to the NE has been determined, however, their role in this process was only apparent in the absence of one or both of their core scaffold-binding partners, Nup53p and Nup59p (Onischenko et al., 2009).

The role vertebrate Poms play in NPC assembly is more clearly defined. Similar to NPC assembly in yeast, verebrate NPCs assemble across an intact NE during interphase. However unlike yeast, vertebrate NPCs also undergo mitotic disassembly and reassembly as cell progress through mitosis (reviewed in: Fernandex-Martinex and Rout, 2009 and Doucet et al., 2010). NPC assembly in the latter stages of mitosis has been reconstituted *in vitro* using *Xenopus laevis*

oocytes and this assay has revealed key roles for the vertebrate Poms Pom121 and NDC1 in forming a pore intermediate structure required for subsequent recruitment of core scaffold Nups (Antonin et al., 2005; Mansfeld et al., 2006). These studies identified a similar role for the core scaffold components Nup155 and Nup160, which were later determined to be direct binding partners of Pom121 (Mitchell et al., 2010). Thus, whether in yeast or vertebrate cells, the Pom interaction network performs a critical role in NPC assembly and anchoring the core scaffold to the pore membrane.

1.4.2 Core scaffold Nups

The nucleoporins that form the inner and outer rings of the core scaffold are often referred to as non-FG-Nups, as they lack the characteristic phenylalanine-glycine repeats found in the peripheral FG-Nups (see section 1.4.3). Non-FG-Nups are formed almost exclusively from two protein-folding domains, a β-propeller folding domain and an α-solenoid-like folding domain, which may be present together in a β-propeller followed by an α-solenoid-like fold orientation or each may occur individually on separate Nups (Devos et al., 2004 and 2006). Strikingly, these protein-folding domains are common among membrane-bending proteins that form the clathrin, COPI, and COPII vesicle-coating complexes (Devos et al., 2004). From this developed the "protocoatamer" hypothesis that suggests that the protein-folding domains of Non-FG-Nups and vesicle-coating complexes originated within a common ancestor as a functional module to bend membranes and generate internal membrane structures that were

precursors to present day eukaryotic organelles (Devos et al., 2004; Brohawn et al., 2008; Field and Dacks, 2009; Field et al., 2011). Physical and genetic interaction networks between the scaffold Nups containing both protein-folding domains and Poms suggest that these Nups are positioned along the pore membrane domain (Aitchison et al., 1995; Miao et al., 2006; Alber et al., 2007b; Onischenko et al., 2009; Mitchell et al., 2010). Here, they may coat the membrane to mediate bending and/or stabilization of membrane curvature, similar to vesicle coating complexes (Devos et al., 2004 and 2006; Kampmann and Blobel, 2009).

In yeast, the NPC core is formed by three abundant subcomplexes, the Nup84 complex containing seven Nups that form a repeating structural unit to generate the outer rings, the Nup170 complex containing Nup157p and Nup170p and two additional Nups that form a repeating subcomplex to generate the inner rings, and the Nic96p complex that links many FG-Nups to the core scaffold (Alber et al., 2007b). Together these complexes make up the bulk of the NPC protein composition and form a lattice to which the FG-Nups attach. The structure of the Nup84 complex has been extensively studied and these studies revealed that it adopts a Y-shaped conformation with Nup145C/Sec13p forming the long arm and Nup120 and Nup85p/Seh1p forming the two shorter arms, respectively (Siniossoglou et al., 2000; Lutzmann et al. 2002; Hsia et al., 2007; Debler et al., 2008; Kampmann and Blobel, 2009). As a result, the Nup84 complex bears a striking resemblance to proteins of the COPII vesicle-coating complex. In fact, Sec13p and Seh1p are shared components among these complexes (Devos et al., 2004), providing further support for the “protocoatamer” hypothesis discussed

above. Mutations within the Nup84 complex are associated with defects in NPC distribution and mRNA export (Doye et al., 1994; Aitchison et al., 1995b). The vertebrate counterpart of the Nup84 complex is the Nup107-Nup160 complex and, similar to its yeast counterpart, is required for mRNA export and NPC assembly (Vasu et al., 2001; Walther et al., 2003).

The Nup170 complex in yeast (Nup155 complex in vertebrates) forms the inner rings, which are proposed to be positioned in the same plane as the Pom-containing membrane ring. Extensive physical and genetic interaction networks functionally link Poms to the Nup170 complex, generating a protein bridge through which NPCs are anchored to the pore (Alber et al., 2007b; Onischenko et al., 2009). Nup157p and Nup170p share a high degree of sequence similarity and, along with numerous other gene duplications in *Saccharomyces cerevisiae*, are believed to have arisen from a whole genome duplication event (Aitchison et al., 1995a; Wolfe and Shields, 1997; Scannell et al., 2007). Consequently, Nup170p and Nup157p are functionally redundant, loss of either one individually does not greatly affect NPC structure or cell viability; however concomitant loss of both proteins results in lethality (Aitchison et al., 1995a). Consistent with a role for these Nups in NPC assembly, loss of both proteins results in decreased NPC number, Nup mislocalization, and the appearance of NPC intermediate structures attached to the INM (Makio et al., 2009). Furthermore, the stoichiometry of the FG-Nups Nup1p and Nup2p is dependent on Nup170p (Kenna et al., 1996). In agreement with its role in maintaining NPC structure, the size exclusion barrier of the NPC is increased in a *NUP170* null mutant, a phenotype also observed in a

NUP188 null mutant (Shulga et al., 2000). Despite its affects on NPC structure, no defects in active transport have been reported in a *nup170* mutant (Aitchison et al., 1995a; Makio et al., 2009). Alhough it should be noted that targeting of a subset of integral INM proteins appears to be compromised in a *nup170Δ* mutant (King et al., 2006; reviewed in Lusk et al., 2007). Interestingly, deletion of *NUP170,* but not *NUP157*, leads to defects in chromosome segregation and alterations in centromeric chromatin structure (Kerscher et al., 2001), suggesting that, despite sequence similarity, Nup170p functions in chromatin dynamics independent of Nup157p.

1.4.3 FG-repeat containing Nups

As their name suggests, the group of phenylalanine-glycine (FG) repeat-containing Nups (FG-Nups) are characterized by the presence of multiple FG dipeptide repeats that form natively unfolded protein domains that interact with the soluble transport machinery (Radu et al., 1995a and 1995b; Denning et al., 2003). FG-Nups represent roughly one third of all nucleoporins, and are functionally redundant in nature as over half of the total mass of FG domains can be deleted without significant affects on yeast viability (Strawn et al., 2004). FG-Nups can be divided into two main groups based on the amino-acid residues flanking the FG repeats, either as GLFG or FxFG. These intrinsically unstructured domains are proposed to form flexible filaments attached to the NPC through linker Nups such as Nic96p and Nup82p via α-helical and coiled-coil domains present within the FG-Nups (Grandi et al., 1993; Belgareh et al., 1998; Devos et

al., 2006; Alber et al., 2007b). In doing so, the innermost layer of the NPC central channel is lined with FG-Nups that contribute to the permeability barrier of the NPC (Patel et al., 2007) and whose FG domains facilitate translocation through the pore. Consistent with their peripheral localization, FG-Nups are last to be recruited to a newly forming NPC (Dultz et al., 2008) and assembly of at least one FG-Nup, Nup53p, is dependent on nuclear transport (Lusk et al., 2002).

In addition to the FG-Nups lining the central channel, there are others that are asymmetrically located on either the cytoplasmic or nucleoplasmic face of the NPC. On the cytoplasmic face, these Nups form the eight cytoplasmic filaments emanating into the cytoplasm and, in yeast, are formed by Nup42p, Nup82p and Nup159p (Belgareh et al., 1998; Hurwitz et al., 1998; Strahm et al., 1999; Rout et al., 2000). In vertebrates, Nup358 forms ~36 nm long filaments and is thought to constitute the majority of the cytoplasmic filament structure along with Nup214 (Wu et al., 1995; Bastos et al., 1997; Delphin et al., 1997). These Nups are anchored to the NPC through the cytoplasmic facing Nup88 (Bernad et al., 2004; Roth et al., 2003). Located on the nucleoplasmic face are the FG-Nups, Nup1p, Nup2p, and Nup60p in yeast or Nup50, and Nup153 in vertebrates (Sukegawa and Blobel, 1993; Guan et al., 2000; Rout et al., 2000; Dilworth et al., 2001). Extending from this face is the nuclear basket stucture proposed to be formed by Mlp1p and Mlp2p in yeast and Tpr in vertebrates (Cordes et al., 1997; Strambio-de-Castilla et al., 1999; Frosst et al., 2002). Proper assembly and maintenance of the nuclear basket in vertebrates requires nuclear lamina formation (Smythe et al., 2000). In a similar fashion, assembly of the yeast nuclear basket requires the

INM-associated protein Esc1p (Lewis et al., 2007), which has been proposed to be a functional counterpart of the nuclear lamina or lamin-associated proteins (Andrulis et al., 2002; Taddei et al., 2004). Extension of the nuclear basket 50 to 100 nm into the nucleus situates it in a prime location to facilitate interactions with the underlying chromatin (Fahrenkrog et al., 1998; Strambio-de-Castillia et al., 1999; Krull et al., 2004).

1.4.4 NPC-associated proteins

Both the nuclear basket and cytoplasmic filaments provide a platform for additional non-Nup proteins to associate with the NPC. Binding of Dyn2p, the light chain of the dynein microtubule motor protein, to Nup159p in yeast causes the cytoplasmic filaments to become rigid and thus provides structure to an otherwise heavily unstructured filament (Stelter et al., 2007). Nup159p also mediates the association of an additional NPC-associated protein, Dbp5p, a DEAD-box helicase that functions in the terminal step of mRNA export by remodeling mRNP particles exiting the NPC (Snay-Hodge et al., 1998; Schmitt et al., 1999; Weirich et al., 2004; Montpetit et al., 2011). Moreover, Gle1p, a protein with DEAD-box helicase activating properties is similarly localized to the cytoplasmic face of the NPC (Weirich et al., 2006; Alcazar-Roman et al., 2006).

In vertebrates, the cytoplasmic filaments provide binding sites for enzymes functioning in the post-translational modification of proteins by the small ubiquitin like modifier, SUMO. The SUMO-E2-conjugating enzyme Ubc9 stably associates with Nup358, also known as RanBP2 (Saitoh et al., 1997; Lee et al.,

1998), while Nup358 itself is a bona fide SUMO E3 ligase (Pichler et al., 2002). Notably, SUMO modification targets cytoplasmic RanGAP1 to the NPC (Mahajan et al., 1997; Matunis and Blobel, 1998) where it forms a stable complex with Nup358 and Ubc9 (Werner et al., 2012). Thus this complex is ideally situated at the cytoplasmic face of the NPC to facilitate dissociation of export cargoes and their cognate karyopherins through its RanGAP activity and the SUMO-dependent release of ribonucleoproteins from exported mRNP particles (Bernad et al., 2004; Vassileva et al., 2004).

Located on the nucleoplasmic face of the NPC are the SUMO deconjugating enzymes SENP1 and SENP2 in vertebrates and their yeast counterpart Ulp1p (Li and Hochstrasser, 2000; Panse et al., 2003; Hang et al., 2002; Zhang et al., 2002a; Bailey et al., 2004); thus, further emphasizing the role of NPCs in regulating sumoylation. Surprisingly, Ulp1p does not appear to be tethered at the NPC through direct interactions with Nups but rather through its association with the karyopherins Kap121p and the Kap60/Kap90 complex (Panse et al., 2003; Makhnevych et al., 2007). A temperature sensitive Ulp1p mutant with reduced enzymatic activity caused leakage of unspliced pre-mRNA (Lewis et al., 2007), further linking NPC-associated SUMO regulatory processes with mRNA export.

As stated above, the coiled-coil domain containing myosin-like proteins Mlp1p and Mlp2p and their homolog Tpr in vertebrates extend from the nucleoplasmic face of the NPC and form the nuclear basket (Cordes et al., 1997; Strambio-de-Castilla et al., 1999; Frosst et al., 2002). A copious-array of

functions have been attributed to the Mlps including roles in pre-mRNA surveillance (Galy et al., 2004), spindle pole body formation (Niepel et al., 2005), transcriptional activation (Luthra et al., 2007), formation of gene loops (Tan-Wong et al., 2009), mRNA export (Green et al., 2003; Fasken et al., 2008), and a disputed role in silencing (Galy et al., 2000; Feuerbach et al., 2002; Hediger et al., 2002a and 2002b). The role of these proteins in various aspects of genome organization and transcriptional regulation will be discussed throughout the remaining sections (gene activation 1.8.2, transcriptional memory 1.8.3, gene silencing 1.8.5 and telomere function 1.10.5). Cumulatively, these results implicate the NPC and its associated transport machinery not only as a scaffold for attachment of nuclear proteins, but also as an active participant in multiple nuclear processes.

1.5 Nuclear transport

NPCs form a diffusion barrier that excludes certain macromolecules while remaining permeable to others. Notably, small molecules such as ions and metabolites are free to diffuse through NPCs, while diffusion of larger macromolecules (i.e. proteins greater than ~30 kDa in mass or molecules greater than ~5 nm in diameter) are inhibited (Paine et al., 1975). The FG-Nups contribute to this barrier in a redundant manner as over half of the total mass of FG-domains can be deleted without significant affects on the permeability barrier (Strawn et al., 2004; Patel et al., 2007). The structural core also contributes to the barrier as loss of Nup170p or Nup188p drastically increases the size exclusion

limit (Shulga et al., 2000). Transport of macromolecules larger than the diffusion limit, including some approaching ~39 nm in diameter such as the hepatitis B viral capsid (Pante and Kann, 2002), is highly regulated and requires interactions with soluble transport factors. Transport factors facilitate translocation of cargo molecules through the NPC by mediating a series of low-affinity interactions with FG-Nups lining the central channel. Despite significant progress in this area, the precise molecular events involving translocation through the NPC remain unclear, however several hypotheses have been proposed and are discussed below (see section 1.5.3).

1.5.1 Karyopherins and nuclear transport sequences

Nuclear transport factors mediate the transport of a wide variety of cargoes including but not limited to proteins, RNAs such as mRNPs and tRNAs, ribosomal subunits, and viral capsids. Most transport factors are members of a family of structurally related proteins termed karyopherins or Kaps. Kaps can be divided into two groups, α-karyopherins (α-Kaps) and β-karyopherins (β-Kaps). In yeast there is a single α-Kap and 14 β-Kaps (reviewed in: Wozniak et al., 1998; Pemberton and Paschal, 2005). Both α- and β-Kaps can recognize protein cargoes through their binding to topogenic sequences, but only β-Kaps interact with FG-Nups. As such, α-Kaps (Kap60p in yeast and karyopherin α in vertebrates) form a heterodimer with a β-Kap (Kap95p in yeast and karyopherin β1 in vertebrates) to mediate cargo translocation (Goldfarb et al., 2004). Protein cargoes destined for import contain a nuclear localization sequence (NLS) within

their peptide sequence that is recognized by an import Kap. Several distinct NLSs have been described and are typified by a stretch of basic amino acid residues. For example, the classical NLS (cNLS) is a lysine-rich pentapeptide (KKKRK) recognized by Kap60p (Kalderon et al., 1984; Siomi and Dreyfuss, 1995). Other NLSs are more complex. For instance the bipartite cNLS consists of two stretches of basic amino acid residues separated by a spacer ~10 residues in length (Dingwall, et al., 1988). Similarly, protein cargoes destined for export contain a nuclear export sequence (NES) that is recognized by an export Kap. The amino acids that constitute NESs are much less conserved and appear to be more specific for their cognate export Kap than their NLS counterparts. Perhaps the best-characterized NES is that recognized by Xpo1p (CRM1 in vertebrates) and consists of a short, hydrophobic leucine-rich region (Fornerod et al., 1997; Stade et al., 1997). Nuclear transport is a promiscuous process and transport of a particular cargo protein is often not limited to a single Kap. Furthermore, a Kap can recognize multiple cargo proteins. Thus, a significant level of functional redundancy exists, providing alternative means of transport for essential proteins.

1.5.2 Directionality of transport

Nuclear import is initiated when the NLS of a cargo is recognized by its import Kap. The Kap then mediates translocation of the Kap/cargo complex through the NPC via interactions with FG-Nups. Upon entry into the nucleus the import Kap/cargo complex encounters the small GTPase Ran, present in its active GTP bound form (RanGTP). Binding of RanGTP to the import Kap results in a

conformational change and dissociation of the Kap/cargo complex (Rexach and Blobel 1995; Gorlich et al., 1996; Chook and Blobel, 2001). Conversely, formation of nuclear export Kap/cargo complexes within the nucleus occurs cooperatively with RanGTP binding and forms a trimeric export complex that stabilizes the export Kap/cargo interaction (Rexach and Blobel, 1995; Fornerod et al., 1997; Wente and Rout, 2010). Following export to the cytoplasm, RanGTP is stimulated to undergo GTP hydrolysis causing dissociation of the export complex (Fornerod et al., 1997). Directionality of nuclear transport is determined by the differential localization of two Ran effector molecules that influence the nucleotide bound state of Ran (see Figure 1-2; Klebe et al., 1995). Ran-GTPase activating protein, Ran-GAP, is strictly localized to the cytoplasm where it stimulates the intrinsic GTP hydrolytic activity of Ran (Hopper et al., 1990; Bischoff et al., 1994), causing accumulation of Ran-GDP in the cytoplasm. In vertebrates, this activity is performed by RanGAP1, which forms a stable complex with the cytoplasmic filament component Nup358p (Matunis et al., 1996). By contrast, the Ran guanine nucleotide exchange factor, Ran-GEF, is retained in the yeast nucleus through interactions with chromatin where it exchanges RanGDP for RanGTP (Ohtsubo et al., 1989; Bischoff and Ponstingl, 1991). Thus, directionality is provided by the differential localization of Ran and its nucleotide bound state, with RanGDP predominant in the cytoplasm and RanGTP predominantly inside the nucleus.

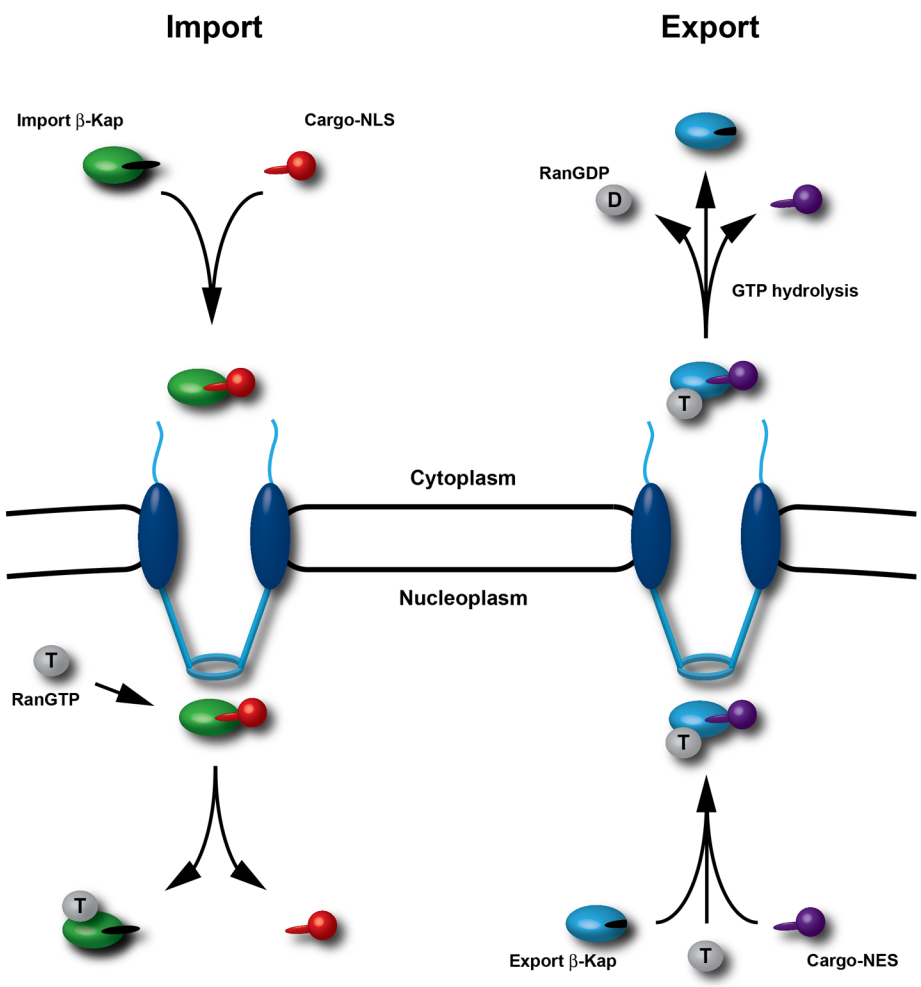

Figure 1-2. Karyopherin-mediated nucleocytoplasmic transport.

Cargoes (red) destined for karyopherin (Kap)-mediated import contain a nuclear localization sequence (NLS) recognized in the cytoplasm by an import Kap (green). The Kap then facilitates translocation of the import Kap/cargo complex through the NPC. Upon entry to the nucleoplasm GTP-bound Ran (RanGTP; grey) binds the import Kap causing a conformational change and release of the import cargo. Conversely, an export cargo (purple) contains a nuclear export sequence (NES) recognized by an export Kap (blue), with formation of the export Kap/cargo complex occuring cooperatively with RanGTP in the nucleoplasm. Once formed the trimeric export Kap/cargo/RanGTP complex then transits through the NPC and in the cytoplasm encounters RanGAP, which stimulates Ran-mediated GTP hydrolysis and dissociation of the export complex.

1.5.3 Transport models

Despite extensive characterization of Kaps and FG-Nups, precisely how these proteins facilitate translocation through the NPC remains unclear and has been the source of much debate. Recent work has begun to illuminate this process with several transport models and variations of these models having been proposed including: the selective phase/hydrogel models, the virtual gate/polymer brush models, the forest model, and the reduction of dimensionality model. A brief synopsis of each model is provided below.

The selective phase or hydrogel model is based on the observed inter- and intra-molecular interactions among the FG-Nups lining the central channel (Ribbeck and Gorlich, 2002; Frey et al., 2006). Extensive interactions would generate a three-dimensional sieve or hydrogel that physically excludes non-interacting factors larger than the sieve, while permitting small molecules to pass relatively freely (e.g. ions). Kaps and their cargoes, however, would be transported across the NPC through their ability to interact with FG-domains. Kap binding is proposed to disrupt the inter- and intra-molecular interactions amongst FG-domains and essentially "unzip" the sieve. Support for this model comes from studies showing that addition of aliphatic alcohols, which disrupt hydrophobic interactions also disrupt the NPC permeability barrier (Ribbeck and Gorlich, 2002; Shulga and Goldfarb, 2003; Patel et al., 2007). This model is further supported by *in vitro* studies demonstrating that recombinant FG-Nups can form a hydrogel impermeable to inert proteins (Frey et al., 2006; Frey and Gorlich, 2007; Frey and Gorlich, 2009). Moreover, entry of a cargo protein into the hydrogel was

greatly enhanced by the additional of its cognate β-Kap, thus, reconstituting some properties of the selectivity barrier *in vitro* (Frey and Gorlich, 2009).

Whereas the selective phase model is based on inter- and intra-molecular forces, the virtual gate model proposed by Rout and colleagues is based on repulsive forces and the thermodynamic properties of transport (Rout et al., 2000; Rout et al., 2003). In relation to the volumes of the nucleus and cytoplasm, the volume of the central channel is extremely small. Consequently, movement of a cargo into the channel is entropically unfavorable. The presence of highly unstructured FG-filaments lining the central channel further decreases the volume of the channel generating an entropic barrier. However, the ability of Kaps to interact FG-domains can compensate for the loss of entropy such that the NPC would function analogous to an enzyme in lowering the energy of activation required for transport. Transport through the pore is predicted to occur through Brownian motion and upon completion of transport overall entropy would be increased. A variation to this model is the brush-polymer model where FG-filaments extend into the nucleoplasm and cytoplasm and act as a brush to repel molecules (Lim et al., 2006; Lim et al., 2007). Upon Kap binding, however, the FG-filaments collapse, drawing potential cargoes into the central channel. This is supported by evidence that FG-Nups are intrinsically unfolded (Denning et al., 2002; Denning et al., 2003) but collapse into a compact structure when bound by a β-Kap (Lim et al., 2007; Yamada et al., 2010).

The forest model proposed by Rexach and colleagues retains aspects of both the selective phase and virtual gate models and is essentially a hybrid of the

two (Patel et al., 2007; Yamada et al., 2010). This model is based on comprehensive structural analyses of all yeast FG-Nups that revealed they adopt either a collapsed globular conformation or an extended coil conformation (Patel et al., 2007; Krishnan et al., 2008; Yamada et al., 2010). The forest model proposes that attachment of FG-Nups to the lining of the central channel creates two transport zones a peripheral zone filled with globular domains, suggested to resemble shrubs, and a central zone filled with extended coil domains resembling trees. Inter- and intra-molecular interactions among the latter are predicted to form a hydrogel, similar to the selective phase model, while the globular, shrub FG-Nups are thought to generate an entropic exclusion barrier, similar to the virtual gate model.

Lastly, the reduction of dimensionality model posits that *in vivo* FG-domains are saturated by Kaps unbound by cargo. Thus FG-Nups adopt a collapsed confirmation against the wall of the central channel and are coated with Kaps (Peters, 2005; Peters, 2009). A Kap/cargo complex would then out compete the bound, cargo-free Kap for binding to FG-Nups and a random walk along the FG-Nups lining the channel would facilitate translocation. A prediction of this model is that nuclear transport occurs along the wall of the channel. Support for this model comes from single molecule microscopy studies showing that Kap/cargo translocation occurs at the periphery as opposed to the center of the pore (Fiserova et al., 2010; Ma and Yang, 2010).

1.6 Non-transport related NPC functions

In addition to facilitating nucleocytoplasmic transport, it is becoming clear that NPC components function in multiple processes independently of their role in transport across the NE. For example, two proteins required for the execution of the spindle assembly checkpoint, Mad1p and Mad2p, dynamically associate with the nuclear basket in both yeast and vertebrates (Campbell et al., 2001; Iouk et al., 2002; Scott et al., 2005). Upon activation of the spindle assembly checkpoint (SAC) budding yeast Mad1p is targeted to kinetochores in a manner dependent on a nuclear export sequence (NES)(Scott et al., 2009). It was further shown that the Mad1p NES is recognized by the export karyopherin Xpo1p, which, in a process analogous to nuclear export, targets Mad1p to kinetochores in a RanGTP dependent manner following SAC activation (Scott et al., 2009). Together these findings implicate the nuclear transport machinery in intranuclear trafficking independent of translocation through NPCs. Similar Kap-dependent trafficking mechanisms have been proposed to occur in the cytoplasm. Notably, Ulp1p-mediated desumoylation of the septin ring during cytokineses is Kap121p-dependent (Mahknevych et al., 2007), and targeting of Nup358/RanGAP1 to vertebrate kinetochores following nuclear envelope breakdown is sensitive to inhibition of the Xpo1p homolog Crm1 (Arnaoutov et al., 2005).

A structural role for NPCs in tethering chromatin to the NE has long been suggested, with electron micrographs from as far back as 1965 exhibiting chromatin fibres extending to the NE and attaching to what were presumably NPCs as they displayed 8-fold radial symmetry, but were referred to as annuli

(DuPraw, 1965; Comings and Okada, 1970). Only in the last decade, however, have the mechanisms involved in this process become apparent, some of which are discussed at length in sections 1.8 and 1.9.5.

1.7 Chromatin

As early as 1928, Emil Heitz noted at least two types of chromatin: highly condensed chromatin that failed to decondense during interphase and other regions on the same chromosome that did (Heitz, 1928; reviewed in Passarge, 1979). He referred to these distinct chromosomal domains as heterochromatin and euchromatin, respectively. Eighty years later we know that DNA must be highly organized and packed in order for it to fit in the nucleus of a cell and that tightly packed regions of chromatin are generally transcriptionally silent, whereas loosely packed chromatin has greater potential to be transcriptionally active. DNA organization of this sort is accomplished through multiple layers of compaction to form chromatin (reviewed in: Rando and Winston, 2012). The first order of compaction consists of ~147 base pairs of DNA wound around an octamer of histone proteins to form a nucleosome. The histone octamer consists of two H2A-H2B dimers and a core H3-H4 tetramer (Luger et al., 1997). In addition to the canonical histones, yeast encode three histone variants that are incorporated into nucleosomes that provide structural diversity. These variants are the centromere-specific histone H3 variant Cse4p (Meluh et al., 1998), histone H1 (Patterton et al., 1998), and the H2A variant H2A.Z (Htz1p in yeast; Santisteban et al., 2000). Nucleosomes oligomerize to form a 30 nm fiber and ultimately organize into a

poorly defined higher order chromatin structure. Each layer of compaction is highly regulated. Subtle changes induced by chromatin binding proteins and histone modifying enzymes can greatly influence the accessibility of DNA to transcription factors, leading to regions that are transcriptionally active or repressed, as is the case for Emil Heitz's euchromatin and heterochromatin, respectively (reviewed in: Li et al., 2007a; Clapier and Cairns, 2009). To prevent the spread of one chromatin state into an adjacent region of the opposite chromatin state, boundary regions are present that lie at the interfaces of opposing chromatin. Such boundary regions are often dynamic and contain epigenetic marks, in the form of post-translational histone modifications, typical of both active and inactive chromatin (Tackett et al. 2005; Babiarz et al., 2006; Shia et al, 2006; Wan et al., 2010).

1.7.1 Post-translational histone modifications

The N-termini of histones are extensively post-translationally and covalently modified by acetylation, methylation, phosphorylation, ubiquitination, ADP-ribosylation, glycosylation, and sumoylation (reviewed in: Bannister and Kouzarides, 2011). Together these modifications form binding surfaces recognized by additional chromatin modifiers and transcription factors. This led to the proposal of the "histone code hypothesis" whereby the function of a single histone mark cannot be understood without undestanding the function of additional combinatorial co-occurring histone modifications (Turner, 1993; Turner, 2000; Strahl and Allis, 2000). In otherwords, specific combinations of histone modifications specify unique biological outcomes. However, this

hypothesis has been the focal point of substantial debate (reviewed in: Rando and Winston, 2012). Considering over 100 different histone modifications have been described so far, with a recent proteomic analysis identifying 67 previously unknown histone modifications (Tan et al., 2011), the combinatorial complexity of a histone code is astounding.

Histone acetylation was first suggested to play a role in transcriptional regulation almost 50 years ago (Allfrey et al., 1964) and, as such, it is perhaps the most widely characterized histone modification. Acetylation of lysine residues is catalyzed by lysine acetyltransferases (KATs), often found as part of a multi-subunit protein complex. For example KAT2, (Gcn5p) can be found as part of the SAGA (Spt5-Ada2-Gcn5-Acetyltransferase) complex and is targeted to promoters containing TATA-boxes present at most stress-response genes (Robert et al., 2004; Hahn and Young, 2011). Histone acetylation is thought to counteract the positive charge of histones and, therefore, decrease the interaction between positively charged histones and the negatively charged phosphate groups of DNA, making DNA more accessible to transcription factors. This is an overly simplistic view, however, as several chromatin modifiers are targeted to chromatin through recognition of certain acetylated lysine residues by a protein-folding domain referred to as a bromodomain (Dhalluin et al., 1999; Owen et al., 2000; Zeng and Zhou, 2002). For instance, the RSC chromatin remodeling complex (remodels structure of chromatin) contains 4 bromodomain containing proteins one of which Rsc4p, along with histone acetylation, is required for RSC targeting to promoters (Kasten et al., 2004; Carey et al., 2006).

Removal of histone acetylation is catalyzed by histone deacetylases (HDACs). These enzymes are often genome-wide regulators of gene expression, which, through recruitment to promoter regions via co-repressors, such as Tup1/Cyc8, generally inhibit transcription (Ekwall, 2005). However, some HDACs are targeted to specific regions of the genome. In yeast, hypoacetylation of histones within the rDNA (encoding ribosomal RNA), the silent mating type loci (*HM*), and telomeres by Sir2p facilitates transcriptional silencing (Rusche et al., 2003). This is discussed further in section 1.7.3. In addition to their inhibitory roles, HDACs also appear to function in promoting transcriptional elongation by preventing spurious transcription from cryptic promoters within coding regions (Carrozza et al., 2005; Li et al., 2007b). Furthermore, the Set3C HDAC is targeted to the 5'-end of coding regions where deacetylation is required for full transcriptional activity (Kim and Buratowski, 2009; Govind et al., 2010).

Cross talk among histone modifications is further exemplified by ubiquitination of histone H2B and methylation of histone H3. At actively transcribed genes, ubiquitination of histone H2B on lysine 123 (H2BK123ub) by the Rad6/Bre1 complex is a prerequisite for methylation of histone H3 on lysine 4 (H3K4me) by the methyltransferase complex COMPASS (Dover et al., 2002; Sun and Allis, 2002; Wood et al., 2003; Shilatifard, 2006). Subsequently, H3K4me is recognized by a protein-folding domain (i.e. chromodomain) of a large number of chromatin-modifiers including the HDAC Set3C and the histone-acetyltransferase complex NuA3 among others, further emphasizing the role of cross talk among histone modifications in transcriptional regulation.

1.7.2 Nucleosome positioning by ATP-dependent chromatin-remodeling complexes

Nucleosomes significantly influence many aspects of gene expression, perhaps no more so than through their relative positioning within promoter regions. Here nucleosomes restrict access of transcription factors to the underlying DNA elements. Extensive mapping of nucleosome positions in yeast identified ~50,000 nucleosomes unevenly distributed throughout the genome, indicating that ~78% of the genome is occluded by nucleosomes (Shivaswamy et al., 2008). In particular, nucleosomes were shown to be canonically positioned within the majority of yeast promoters. As a general rule, the promoter region of yeast "house-keeping" or TATA-less genes are characterized by a ~150 bp nucleosome free region (NFR) flanked by two well-positioned nucleosomes (-1 and +1 nucleosomes), such that the transcriptional start site (TSS) is located within the +1 nucleosome immediately downstream of the NFR (Yuan et al., 2005; Lee et al., 2007; Shivaswamy et al., 2008; Hartley and Madhani, 2009; Weiner et al., 2010). It is generally viewed that transcriptional activation correlates with promoter nucleosome eviction. For instance, activation of the *PHO5* gene leads to eviction of promoter nucleosomes and allows the transcriptional machinery access to the TATA box (Almer et al., 1986; Boeger et al., 2003; Korber et al., 2004). In a similar fashion, promoter nucleosomes are evicted following activation of *GAL1/10* and *HSP82* (Axelrod et al., 1993; Gross et al., 1993). However, attempts to correlate nucleosome rearrangements with perturbations in transcriptional activity on a genome-wide scale have garnered

contradictory results. Several studies have reported a general, albeit weak, correlation between nucleosome depletion and transcriptional activation (Lee et al., 2004; Lee et al., 2007; Weiner et al., 2010), while others failed to observe a global correlation (Shivaswamy et al., 2008; Kaplan et al., 2009; Zawadzki et al., 2009).

While restricting access to transcription factor binding sites, nucleosomes are also a barrier to essentially all DNA metabolic processes including DNA repair, DNA replication, and transcription elongation. To overcome this, a variety of protein complexes utilize energy derived from ATP hydrolysis to evict, remodel/replace histones, or reposition nucleosomes during these processes. There are four families of chromatin remodelers in yeast: Ino80, Swi/Snf, Chd, and Iswi. Members of the Ino80 family function in histone replacement, Swi/Snf family members tend to destabilize/evict nucleosomes, while the Chd and Iswi family members function to slide nucleosomes along DNA (reviewed in: Clapier and Cairns, 2009; Rondo and Winston, 2012).

The SWR1 complex is a member of the Ino80 family of chromatin-remodelers and catalyzes the replication-independent exchange of histone H2A-H2B dimers with H2A.Z-H2B dimers (Krogan et al., 2003; Kobor et al., 2004; Mizuguchi et al., 2004). The histone variant H2A.Z (Htz1p in yeast) is enriched in NFR-flanking nucleosomes (Guillemette et al., 2005; Raisner et al., 2005) though is not required for NFR formation (Hartley and Madhani et al., 2009; Tirosh et al., 2010). Htz1p has been proposed to poise promoters for future transcriptional activity by promoting nucleosome eviction (Raisner et al., 2005; Zhang et al.,

2005) and through recruitment of the TATA-binding protein (Wan et al., 2009). Further functions for Htz1p have been reported in transcriptional memory (Brickner et al., 2007; Light et al., 2010), and demarcation of heterochromatin boundaries (Meneghini et al., 2003).

The RSC complex (remodel the structure of chromatin) is a member of the Swi/Snf family of chromatin remodelers and consists of 15 subunits, most of which are essential for yeast viability (Cairns et al., 1996). Sth1p is the catalytic subunit which possesses ATPase activity (Cairns et al., 1996), and loss of Sth1p results in an increase in nucleosome density and a reduction in NFR width, suggesting RSC complex activity is required for NFR formation (Parnell et al., 2008; Hartley and Madhani, 2009). Genome-wide localization studies have placed the RSC complex at ~700 target genes, consisting of both RNA polII and RNA polIII transcribed genes (Damelin et al., 2002; Ng et al., 2002). The RSC complex is targeted to promoters by the DNA-binding activity of the Rsc3p/Rsc30p dimer (Parnell et al., 2008; Badis et al., 2008) and through the ability of the bromodomain containing subunits Rsc1p, Rsc2p, Rsc4p, and Sth1p to bind acetylated lysine residues (Carey et al., 2006). Due to the vast number of genes regulated by the RSC complex, a multitude of pleiotropic effects arise upon loss of RSC function. Thus, teasing apart bona fide RSC functions from indirect effects presents a challenge. For example, the RSC complex has been implicated in NPC assembly, however, whether this is a direct or indirect effect has not been determined. On the other hand, the RSC complex associates with DNA double-strand breaks to assist loading of the yKu heterodimer (Chai et al., 2005; Shim et

al., 2005; Shim et al., 2007) and constitutively associates with centromeric DNA to maintain proper chromatin structure and cohesin loading (Hsu et al., 2003; Huang and Laurent, 2004), clearly demonstrating a function for the RSC complex in both DNA repair and chromosome segregation.

Unlike the previously discussed families of chromatin remodelers, the Iswi family members slide nucleosomes laterally along the DNA sequence (reviewed in: Clapier and Cairns, 2009; Rando and Winston, 2012). The ISW2 complex, for example, is a major co-repressor that repositions nucleosomes in promoter regions to occlude transcription factor binding sites. The ISW2 complex is targeted to ~20% of RNA polII genes and the vast majority of tRNA genes (White-house et al., 2007). Additionally, the ISW2 complex functions as a co-repressor for a subset of mating-type-specific genes that are actively transcribed in yeast cells of the **a**-mating type but repressed in yeast cells of the α-mating type (Sugiyama and Nikawa, 2001; Ruiz et al., 2003; Trachtulcova et al., 2004). Here the repressive function of the ISW2 complex is mediated through the positioning of nucleosomes such that the TATA box is occluded from the transcriptional initiation machinery (Morohashi et al., 2006).

1.7.3 Transcriptional silencing in budding yeast

Silent chromatin regions are characterized by large spans of tightly compacted, hypoacetylated chromatin inaccessible to DNA binding factors. Although budding yeast lack the hallmarks of heterochromatin found in higher eukaryotes, such as H3K9me3 and the compaction required to visualize heterochromatin by microscopy, silencing nonetheless occurs in heterochromatin-

like regions: rDNA, silent mating type loci, and telomeres. At telomeres, silencing is initiated by recruitment of the silent information regulator protein Sir4p by the telomere repeat binding protein Rap1p (Moretti et al., 1994; Cockell et al., 1995; Moretti and shore, 2001; Luo et al., 2002). Rap1p is a context specific transcriptional regulator that functions in transcriptional activation of ribosomal protein genes and glycolytic genes in addition to its silencing functions at telomeres and the silent mating type loci. Chromatin-bound Sir4p forms a complex with the silent information regulators Sir2p and Sir3p (Moretti et al., 1994; Hecht et al., 1996; Cubizolles et al., 2006). Once targeted to chromatin, Sir2p catalyzes the deacetylation of the N-termini of histones H3 and H4, in particular histone H4K16 (Tanny et al., 1999; Imai et al., 2000). Deacetylated histone H4K16 is a high-affinity binding site for Sir3p (Liou et al., 2005; Buchberger et al., 2008) while Sir4p has affinity for deacetylated N-terminal histone tails. Thus, the enzymatic activity of Sir2p generates additional binding sites for Sir2p/Sir3p/Sir4p (SIR) complex. Multiple rounds of recruitment and deacetylation spreads the SIR complex towards the centromere forming compact, highly structured chromatin that is transcriptionally silent.

Silencing at the two silent mating type loci, *HML* and *HMR*, occurs in a similar manner to silencing at telomeres, however initial recruitment of Sir4p differs slightly. The silent mating type loci are flanked by two cis-acting silencer elements, E and I, which nucleate SIR complex formation. The E-silencer alone is sufficient to nucleate silencing, while the I-silencer is not (Abraham et al., 1984; Brand et al., 1985). Both contain binding sites for Abf1p and ORC, but only E-

silencers contain a binding site for Rap1p. These DNA-binding sites are functionally redundant as they all, directly or indirectly, recruit Sir4p. For instance, Rap1p binds Sir4p directly (Luo et al., 2002), Abf1p associates with Sir3p, and ORC has affinity for Sir1p (Chien et al., 1993; Zhang et al., 2002b), a silent information regulator specific to *HM* silencing that associates directly with Sir4p (Triolo and Sternglanz, 1996). Once associated, Sir4p forms a complex with Sir2p and Sir3p leading to deacetylation of nearby histones and the spread of silenced chromatin along the chromosome until a chromatin boundary is reached.

1.7.4 Chromatin boundaries

Boundary regions exist to prevent silencing from spreading beyond silent regions and into sites of active transcription. Boundary regions are not precisely defined static barriers, instead they are dynamic regions that switch back and forth in a form of transcriptional tug-of-war (reviewed in: Rusche, 2003; Sun et al., 2011). As a consequence boundary chromatin contains epigenetic marks of both transcripitonally active and silent chromatin. This is perhaps best demonstrated at telomeres where boundary regions are loosely defined by competition between deacetylation and acetylation of histone H4K16. In the absence of the lysine acetyltransferase KAT8 (Sas2p), silencing spreads beyond the typical ~3 kb from chromosome ends up to ~15 kb (Kimura et al., 2002). This anti-silencing activity is attributed to Sas2p-mediated acetylation of histone H4K16, which competes with Sir2p-mediated deacetylation of histone H4K16 to restrict the spread of Sir3p/Sir4p (Kimura et al., 2002; Suka et al., 2002). Surprisingly, the HDAC Rpd3p also displays anti-silencing activity that is proposed to occur through

removal of Sir2p substrate (Sun et al., 1999; Zhou et al., 2009). Decreased Sir2p enzymatic activity would reduce the levels of the metabolite *O*-acetyl-ADP-ribose produced during the deacetylation process and contributes to SIR complex stabilization (Tanner et al., 2000; Liou et al., 2005; Onishi et al., 2007; Ehrentraut et al., 2010). Given the plethora of histone modifications it is not surprising that the formation of chromatin boundaries is not limited to a dynamic equilibrium between acetylation and deacetylation, but rather involves a complex combination of post-translational histone modifications (H3K36me, H3K79me, H2BK123ub) (Huang et al., 1997; Van Leeuwen et al., 2002; Tompa and Madhani, 2007), histone variants (Htz1p)(Meneghini et al., 2003; Babiarz et al., 2006), histone chaperones (CAF-1, Rtt106p, Chz1p)(Huang et al., 2007; Wan et al., 2010), chromatin-remodeling complexes (RSC, the Dbp4-related complexes containing Isw2p and Itc1p)(Tackett et al., 2005; Dhillon et al., 2009), and importantly the transcriptional machinery itself.

Positioned to the right of *HMR*-E is a boundary element that exhibits anti-silencing activity through its ability to recruit the transcriptional machinery. Here, a highly transcribed tRNA gene disrupts nucleosome positioning by creating a NFR within its promoter that prevents the spread of SIR complexes (Donze and Kamakaka, 2001). Essential to this process is recruitment of the RNA polIII pre-initiation complex to the NFR (Simms et al., 2008). In particular, TFIIIC plays an important role, as TFIIIC binding alone was sufficient to block Sir-mediated silencing (Simms et al., 2008). Further influencing this process are the chromatin modifiers RSC, SAGA, and Sas2p, among others (Donze and Kamakaka, 2001;

Oki and Kamakaka, 2005; Dhillon et al., 2009) and several NPC-associated proteins that are discussed further in section 1.8.4 (Ishii et al., 2002; Dilworth et al., 2005; Ruben et al., 2011).

1.8 NE-mediated chromatin organization

Early electron micrographs revealed that although highly condensed chromatin domains are found at both the nuclear periphery and nuclear interior, for many cell types these heterochromatin domains are preferentially localized to the nuclear periphery, suggesting that regions interior to the nucleus tend to promote gene expression, while regions at the periphery tend to promote gene silencing.

Consistent with these early morphological observations, advances in microscopy techniques have revealed the dynamic nature of chromosomal domains. *In-vivo* visualization and real-time tracking of discrete chromosomal loci in mammalian cells have led to the discovery that chromosomes encoding relatively few genes, said to be gene-poor, are more frequently associated with the nuclear periphery whereas gene-rich chromosomes are positioned more internally (Croft et al., 1999; Bolzer et al., 2005). Similarly, highly transcribed, co-regulated genes often cluster within chromosomal territories. This is the case for the murine immunoglobulin gene clusters *Igh* and *Igκ,* encoding genes of the immunoglobulin heavy and light chains respectively, which, in hematopoietic progenitor B-cells, associate with the nuclear lamina when inactive and relocate away from the nuclear periphery following commitment to the B-cell lineage (Jhunjhunwala et al., 2009; Kosak et al., 2002). In this context, peripheral

localization is proposed to prevent spurious immunoglobulin rearrangements by limiting accessibility of *Ig* loci to recombination factors (Reddy et al., 2008). Similar gene repositioning occurs with the *MASH1* locus during neural induction of embryonic stem cells and the *beta-globin* genes during erythrocyte maturation (Williams et al., 2006; Ragoczy et al., 2006). *NANOG* also undergoes gene repositioning during cell differentiation; however, in this case, because *NANOG* expression is required to maintain pluripotency of human embryonic stem cells, upon differentiation *NANOG* becomes transcriptionally silent and relocates from the nuclear interior to a more peripheral position (Wiblin et al., 2005). These observations correlate changes in gene positioning with changes in transcriptional activity during cell differentiation, and raise the question of whether gene relocalization is the cause or consequence of gene activation.

Preferential association of transcriptionally silent chromatin at the NE is a feature of yeast as well as higher eukaryotes. Silent regions in yeast including telomeres, the silent mating type loci (*HMR* and *HML*), and centromeres (in fission yeast), all localize in the vicinity of the nuclear periphery (Gotta et al., 1996; Jin et al., 1998; Funabiki et al., 1993; Laroche et al., 2000). Yeast telomeres are assembled into silent chromatin and coalesce to form clusters of 8-10 foci per cell (Palladino et al., 1993; Gotta et al., 1996; Maillet et al., 1996). These telomeric foci are tethered at the periphery through two redundant mechanisms (discussed in detail in section 1.9.3). Ablation of both pathways revealed a loss of subtelomeric silencing concomitant with decreased expression of non-telomeric genes, a result attributed to dispersal to ectopic chromatin sites of the SIR

silencing complex (Sir2p/Sir3p/Sir4p) (Taddei et al., 2009). Based on these results, it was proposed that telomere clustering at the periphery sequesters a limited pool of Sir proteins at concentrations high enough to permit heterochromatin formation (Gasser et al., 2004). In support of this, silencing of an *HMR* locus flanked by weakened silencing elements is enhanced when artificially tethered to the nuclear periphery, and enhanced silencing is dependent on intact peripheral telomere foci (Andrulis et al., 1998). However, peripheral tethering of an *HMR* locus lacking silencing elements failed to repress, suggesting that a peripheral localization promotes, but is not sufficient for, repression. Likewise, a peripheral localization is not necessary for silencing (Mondoux et al., 2007). Thus, subnuclear positioning influences but does not determine the transcriptional status of silent domains.

An exception to the generality presented above, where the NE associates with transcripitonally inactive chromatin, lies in the vicinity of NPCs where euchromatic channels have been observed extending through the peripheral heterochromatin subjacent to NPCs. The correlation of NPCs and euchromatin led to the "gene-gating hypothesis" (Blobel, 1985), which proposed that association of actively transcribed genes with NPCs would increase accessibility to transcription factors and facilitate export of transcription products. While these morphological characteristics have been a source of speculation regarding gene expression, the molecular mechanism(s) that determine whether a peripherally localized gene is active or repressed are not clear, but likely depend on the context of the surrounding nuclear architecture including interactions with specific

subdomains of the NE, contacts with the nuclear lamina in metazoans, the state of the surrounding chromatin and the presence of NPCs.

1.8.1 Chromatin association with NPCs in metazoa

There is accumulating evidence in higher eukaryotes that association of chromatin with NPC components plays an important regulatory role in gene expression. In mamallian cells, some genes derepressed by HDAC inhibition become associated with Nup93 through promoter-NPC interactions (Brown et al., 2008). In Drosophila, hyperactivation of the X-chromosome in males is associated with its peripheral localization and NPC association (Mendjan et al., 2006; Vaquerizas et al., 2010) and the *HSP70* locus associates with NPCs (Kurshakova et al., 2007). More recently, two papers have reported Nup association with both silent loci and developmentally regulated genes undergoing transcriptional induction in *Drosophila melanogaster* (Capelson et al., 2010; Kalverda et al., 2010). However, like yeast Nup2p, some Drosophila Nups are highly dynamic and exchange between NPCs and the nucleoplasm, and these studies demonstrated that soluble intranuclear pools of some Nups interact with chromatin. Thus Nup-chromatin interactions are not necessarily restricted to the nuclear periphery. These observations provide an important advance in our understanding of the basic roles of Nups in gene regulation in higher eukaryotes and they imply that nucleoplasmic Nups play an active role in gene regulation, perhaps as direct regulators or as scaffolds to bring modifiers, transcription factors, and the genome in proximity to one another. Given the complexities of

gene regulatory mechanisms governing development, it is reasonable to assume that remodeling of NPC-chromatin contacts could represent yet another layer of complexity on the modulation of gene expression.

1.8.2 Transcriptionally active chromatin at yeast NPCs

Over the last decade it has become increasingly evident that highly transcribed genes associate with NPC-associated proteins in yeast. Genome-wide chromatin immunopreciptation studies (ChIP-chip) have been performed on several components of the NPC as well as multiple Kaps (Casolari et al., 2004). These studies suggested that the NPC components Nup2p, Nup60p, Nup166p, Nic96p, Mlp1p and Mlp2p and the Kaps Cse1p, Kap95p and Xpo1p preferentially associate with actively transcribed genes, enriching with genes that are highly transcribed such as those involved in glycolysis and ribosome biogenesis. In contrast, the RanGEF Prp20p preferentially associates with inactive genes (Casolari et al., 2004). Prp20p is an essential transport factor that maintains Ran in a GTP-bound state in the nucleus and associates with chromatin (Aebi et al., 1990; Lee et al., 1993; Dilworth et al., 2005). Prp20p association with inactive genes has been proposed to target newly imported transcription factors directly to target gene promoters (Casolari et al., 2004). Under repressive conditions the galactose-inducible *GAL* genes associate with Prp20p, but not with nucleoporins. Following the addition of galactose, the *GAL* genes associate with nucleoporins, but no longer associate with Prp20p, suggesting that a subset of genes can be recruited to the NPC under conditions of transcriptional activation (Casolari et al., 2004; Berger et al., 2008).

In yeast, visualization of inducible genes (*INO1*, *HXK1*, *GAL1*, *GAL2*, *SUC2*, *FIG2* and *HSP104*) through chromatin tagging confirmed that these loci relocate to the nuclear periphery or NPCs upon transcriptional activation (Brickner et al., 2004; Casolari et al., 2005; Cabal et al., 2006; Dieppois et al., 2006; Taddei et al., 2006). However, the molecular mechanisms and factors that mediate recruitment and the functional significance of recruitment are poorly understood. Several laboratories have sought to address this question and have uncovered a diverse set of factors that contribute to chromatin-NPC interactions including transcription factors (Menon et al., 2005; Schmid et al., 2006), chromatin-modifying complexes (Cabal et al., 2006; Mendjan et al., 2006; Kohler et al., 2008; Kehat et al., 2011), a histone variant (Brickner et al., 2007), and mRNA processing and export factors (Fischer et al., 2002; Rodriquez-Navarro et al., 2004; Dieppois et al., 2006; Drubin et al., 2006; Taddei et al., 2006).

The nuclear basket proteins are particularly important for gene recruitment. Nup2p binds the nuclear basket through Nup60p (Denning et al., 2001), interacts with chromatin through association with chromatin-bound Prp20p (Dilworth et al., 2005) and is required for peripheral gene recruitment of *GAL1* and *INO1* (Brickner et al., 2007; Light et al., 2010). Also anchored to the nuclear basket via Nup60p are the myosin-like proteins Mlp1p and Mlp2p that form coiled-coils that extend beyond the NPC and into the nuclear interior (Strambio-de-Castillia et al., 1999; Feuerbach et al., 2002). Mlp1p is involved in gene targeting as deletion of *MLP1* prevents recruitment of *GAL1/10* and *HSP104* to the periphery (Dieppois et al., 2006). However, targeting of *INO1* to the periphery

does not require Mlp1p but does require Mlp2p (Ahmed et al., 2010), suggesting that overlapping, but distinct, targeting mechanisms exist. In an attempt to identify such a mechanism, a proteomic approach was undertaken to identify Mlp1p interacting partners, revealing a physical interaction with the SAGA complex (Luthra et al., 2007). Moreover, ChIP experiments revealed that Mlp1p and SAGA components associate at the same promoter region of the *GAL* genes and that Mlp1p association is dependent on the integrity of the SAGA complex (Luthra et al., 2007). Interestingly, the SAGA component Sus1p is also present in a Sac3p containing mRNA export complex located at NPCs and both Sac3p and Sus1p are required for efficient *GAL1/10* recruitment, providing further evidence that an NPC association is an important feature in peripheral gene targeting (Rodriquez-Navarro et al., 2004; Cabal et al., 2006). It should be stressed, however, that although many active genes have been identified in association with NPCs, interaction with the nuclear periphery is not a mandatory feature of gene activity in yeast (Taddei, 2007) and some genes appear targeted to the periphery independent of transcription (Brickner et al., 2007).

It appears that multiple aspects of transcriptional activation are required for NPC-chromatin interactions, however not all highly expressed genes associate with the periphery. Therefore, a mechanism, independent of transcription, must exist that specifies which genes will adopt an NPC association. Such a mechanism is likely to be encoded by *cis*-acting DNA elements as peripheral targeting of some yeast genes are independent of transcription (Schmid et al., 2006; Brickner et al., 2007). A recent study identified two gene recruitment sequences (GRS I and

GRS II) within the promoter region of the *INO1* gene responsible for *INO1* targeting to the NPC and were sufficient to target an ectopic locus to the nuclear periphery (Ahmed et al., 2010). Considering, GRS I elements have been identified in 94 gene promoters (Ahmed et al., 2010), it is reasonable to assume that only a small fraction of the total number of NPC interacting genes have been identified. The factors that bind GRS elements and promote recruitment remain unknown but it remains only a matter of time before they too are identified to further inform the spatial organization and regulation of the genome

1.8.3 NPCs and transcriptional memory

In yeast several of the inducible genes that are recruited to NPCs following induction appear to be retained at the periphery over multiple generations even after transcriptional repression (Brickner et al., 2007; Ahmed et al., 2010). Retention at the nuclear periphery during periods of repression is thought to serve as a memory of previous transcriptional activity to promote an accelerated transcriptional response following reactivation (Brickner et al., 2009). The fact that memory is maintained through multiple cell cycles indicates that the molecular mechanisms responsible are stable through DNA replication, mitosis, and, ultimately, inherited by daughter cells. How cells remember a previous transcriptional state is unclear, however epigenetic changes in chromatin structure are likely responsible. In this regard, alterations in nucleosome positioning mediated by the chromatin remodeling complex SWI/SNF and incorporation of the histone variant H2A.Z into assembled nucleosomes both contribute to

transcriptional memory (Brickner et al., 2007; Kundu et al., 2007; Light et al., 2010).

An additional mechanism of transcriptional memory was identified by studies that revealed a link between gene looping and transcriptional memory (Laine et al., 2009; Tan-Wong et al., 2009). Gene loops are dynamic structures formed upon transcriptional initiation through interactions between the promoter and 3'-end of a gene. Gene looping has been observed for both yeast and mammalian genes, however, not all genes form loops (O'Sullivan et al., 2004; Tan-Wong et al., 2008; Tan-Wong et al., 2009). Transcription-dependent gene loop structures were identified in two genes (*HXK1* and *GAL1*) that associate with NPCs upon transcriptional activation, and gene loops were maintained during intervening periods of transcriptional repression (Tan-Wong et al., 2009). These DNA loop structures are termed memory gene loops (MGLs) and are required for transcriptional memory but not initial gene activation. The molecular mechanisms that facilitate MGLs and establish transcriptional memory are likely to involve changes in chromatin structure through post-translational histone modifications and/or incorporation of histone variants and interactions with NPCs.

A role for NPCs in transcriptional memory is implicated by the association of MGLs with the nuclear basket protein Mlp1p (Tan-Wong et al., 2009). Mlp1p associates with MGLs through interactions with both the 5' UAS and 3'-end regions, but not with internal regions of the *HXK1* gene. Mlp1p association with MGLs is transcription dependent and it is maintained for the duration of the transcriptional memory. Furthermore, deletion of *MLP1* disrupted MGL

formation and resulted in loss of transcriptional memory (Tan-Wong et al., 2009). Gene recruitment to the NPC could enhance MGL formation by acting as a scaffold to promote interactions with both promoter elements and the 3'-end regions of activated genes. Alternatively, the NPC may provide an environment that is conducive for the chromatin reorganization necessary for transcriptional memory as suggested by the physical interaction of Nup2p and Htz1p (Dilworth et al., 2005), both of which have been implicated in transcriptional memory of *INO1* (Brickner et al., 2007; Light et al., 2010).

1.8.4 NPC-mediated boundary activity

Although much progress has been made concerning the role of NPCs in tethering active genes at the NE, little is known about their function in facilitating boundary activity. Surprisingly, components of the nuclear basket and nuclear transport machinery were identified in a yeast genetic screen as factors exhibiting robust boundary activity by preventing the spread of heterochromatin into a neighboring active region (Ishii et al., 2002). Moreover, boundary activity was dependent on physical interaction with the nuclear basket (Ishii et al., 2002; Dilworth et al., 2005), suggesting that the NPC generates a boundary between repressive and active domains. Further support for this idea comes from the observation that heterochromatin forms extensively along the NE but is excluded from regions surrounding the NPC in Hela cells infected with polio virus (Krull et al., 2010). However, knock down of Tpr and subsequent loss of the nuclear basket structure in these cells permits heterochromatin to form along the entire NE,

including areas immediately underlying NPCs, suggesting a potentially important role for the nuclear basket in demarcating transcriptional boundaries.

Nup2p transcends the classical division between the mobile and stationary phases of the transport machinery by cycling on and off the basket of the NPC in a Ran-dependent manner (Denning et al., 2001; Dilworth et al., 2001). Deletion of *NUP2* abolishes boundary activity of all NPC-associated components tested (Ishii et al., 2002; Dilworth et al., 2005). Interestingly, Nup60p, which is responsible for anchoring Nup2p to the NPC, is also required for Nup2p-dependent boundary activity, suggesting that boundary activity of Nup2p requires attachment to NPCs (Dilworth et al., 2005). Proteomic, transcriptomic, and genetic studies revealed Nup2p and together with Prp20p, physically interact with the boundary proteins Htz1p and the chromatin remodeling complex ISW2 (Dilworth et al., 2005). Furthermore, chromatin co-isolating with Nup2p and Prp20p contains epigenetic marks characteristic of boundaries (Dilworth et al., 2005). While a separate proteomic study to identify chromatin complexes at boundary regions failed to detect Prp20p or Nup2p, it did identify multiple Prp20p and Nup2p associated proteins (Tackett et al., 2005). Recently, however, it was shown that both Nup2p and Nup60p bind the tRNA gene that forms the boundary element at *HMR* and mediate its perinuclear positioning (Ruben et al., 2011). A dynamic model of NPC-mediated boundary activity has been proposed (Dilworth et al., 2005). In this model intranuclear Nup2p initially associates with chromatin-bound Prp20p at boundary regions. Re-association of Nup2p to the nuclear basket promotes localization of chromatin to the nuclear periphery where the NPC facilitates

relocation of chromatin to distinct nuclear subcompartments to stabilize either an active or inactive transcriptional state.

1.8.5 NPCs and silent chromatin

Whether NPCs are active participants in the formation of silent chromatin remains unclear and initial studies supporting such a function were met with skepticism (Galy et al., 2000; Hediger et al., 2002a). Since these early studies, there has been mounting evidence from several model systems in support of this hypothesis. In *Homo sapiens,* evidence that NPCs interact with silent chromatin comes from the determination of Nup93 binding sites in Hela cells, which revealed that Nup93 binding sites are depleted of histone modifications associated with active genes and enriched for histone modifications associated with silent genes (Brown et al., 2008). But what is perhaps the strongest evidence of a role for NPCs in transcriptional silencing comes from studies of the core scaffold Nup Nup155, a homolog of yeast Nup170p. Nup155 was shown to interact with HDAC4 in rat cardiomyocytes and localize HDAC4 to NPCs (Kehat et al., 2011). Importantly, HDAC4 repressed genes associate with NPC components, and a Nup155 truncation mutant that fails to target HDAC4 to NPCs prevents HDAC4-mediated represion. Moreover, overexpression of HDAC4 did not restore repression in the Nup155 truncation mutant suggesting that NPC association is essential for HDAC4 function. This study indicates that NPCs, particularly Nup155, have an important role in mediating transcriptional repression through the recruitment of both a chromatin modifier as well as its target loci. In yeast,

studies have also shown that silent loci associate with two components of the nuclear basket, Mlp1p and Mlp2p, further demonstrating the interactions of silent chromatin with NPCs across a variety of species (Casolari et al., 2004 and 2005).

1.9 Telomeres

Transcriptional silencing at telomeres represents a significant proportion of NE-associated silent chromatin in budding yeast. As a result, these unique chromosomal structures have been of considerable importance in understanding the mechanisms involved in silent chromatin formation and its association at the NE. Some of these processes are heavily intertwined with the unique characteristics of telomeres; consequently, to gain a better understanding of these processes several aspects of telomere biology, including telomere structure and function, must first be addressed.

Functionally, telomeres are DNA-protein complexes that protect the ends of linear chromosomes from degradation, recombination, and DNA repair pathways (Gilson and Geli, 2007; Wellinger, 2010). Moreover they function to ensure complete replication of chromosome ends (Smogorzewska and de Lange, 2004; Gilson and Geli, 2007). During DNA replication, leading strand synthesis proceeds to the chromosome end, however, lagging strand synthesis is unable to replicate the extreme end, resulting in loss of genetic information following each round of replication (Watson, 1972). Telomeres address the "end replication problem" by providing a repetitive, non-coding sequence at the chromosome ends that, when lost, does not deprive the cell of genetic information. As telomeric

repeats are lost, the telomerase complex can extend the telomere repeats in a manner similar to reverse-transcriptase (Greider and Blackburn, 1985; reviewed in: Blackburn and Collins, 2011). If, however, telomeres become critically short they are recognized by the DNA damage checkpoint and cellular senescence is induced. Cells that escape this arrest undergo DNA repair by non-homologous end-joining, generating end-to-end chromosome fusions that, during the proceeding anaphase, lead to aneuploidy, chromsome instability and transformation to a cancer cell type. It is believed that diminished telomere function late in life contributes to genome instability and the higher incidences of cancer late in life.

1.9.1 Telomere structure

In *Saccharomyces cerevisiae,* telomeres are formed by a ~300 to ~350 bp sequence of double stranded $TG_{1\text{-}3}$ repeats free of nucleosomes followed by a distal 3'-oriented G-rich single-stranded overhang of 10-15 nucleotides (Shampay and Blackburn, 1988). Bound to the single-stranded overhang is the Cdc13p/Stn1p/Ten1p (CST) telomere-capping complex. Loss of any of these proteins causes telomere degradation and activation of the DNA damage checkpoint (Wellinger, 2010). Additional telomere capping functions are performed by the yKu70p/Ku80p heterodimer that directly binds chromosome ends through its dsDNA-end-binding activity, and the telomere-associated Rif1p and Rif2p proteins that inhibit DNA-damage checkpoint kinases (Gravel et al., 1998; Hirano et al., 2009). Telomere association of Rif1p/2p occurs through

interactions with the C-terminus of the double-stranded telomeric repeat binding protein Rap1p (Mishra and Shore, 1999). Rap1p binding occurs once per 18 bp of telomeric DNA, potentially accommodating up to ~20 Rap1p molecules per telomere (Gilson et al., 1993). In addition to binding Rif1p, the C-terminus of Rap1p also contains an interaction domain for Sir4p, such that Sir4p and Rif1p compete for an overlapping binding site (Mishra and Shore, 1999). Consequently, Sir4p binding is enhanced by deletion of *RIF1*. Additional Sir4p can be recruited by the yKu70p/Ku80p heterodimer (Mishra and Shore, 1999; Roy et al., 2004) and once bound, Sir4p nucleates telomeric silencing that typically extends 3 kb to 5 kb from the chromosome ends as previously discussed (see section 1.7.3 and Figure 1-3). The abundance of Sir4p in the densely packed subtelomeric chromatin provides interaction sites for telomere bound Rap1p, causing the telomere to fold over on itself and reinforce the silent state (de Bruin et al., 2000). RNA polII-transcribed genes placed within this region are, for the most part, transcriptionally silent, a phenomenon known as telomere position effect (Gottschling et al., 1990; Tham and Zakian, 2002). For instance, insertion of a reporter gene, *ADE2,* into subtelomeric chromatin results in *ADE2* present in a semi-stable, yet heritable, transcriptionally silenced state, evident by the formation of red colonies. However, the transcriptional status of *ADE2* can switch to a stable and heritable active state, leading to the formation of white colonies (Gottschling et al., 1990; Singer et al., 1994). The extent of transcriptional silencing (TPE) and the frequency of switching between epigenetic states is telomere dependent with some telomeres displaying higher levels than others

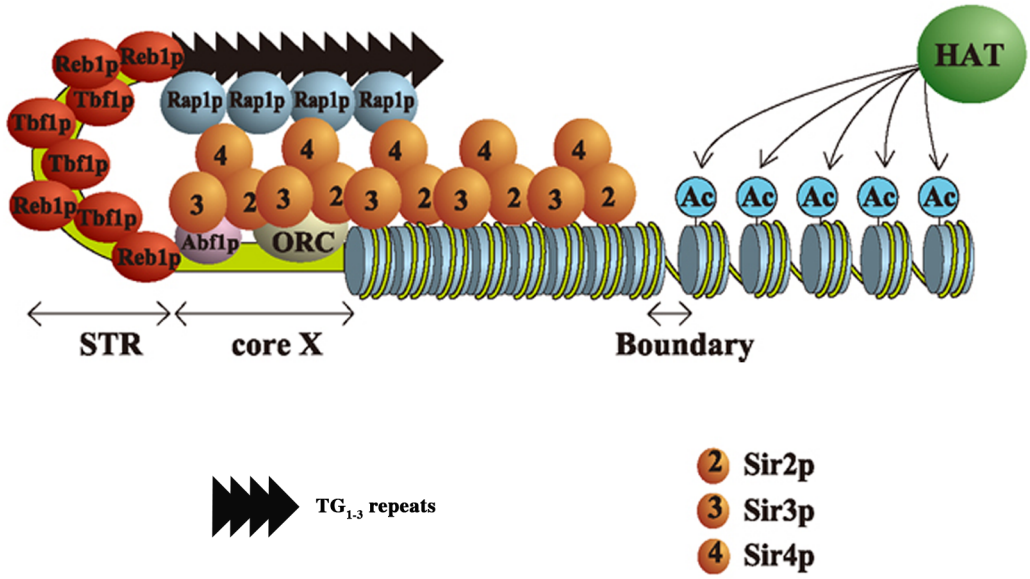

Figure 1-3. Schematic of subtelomeric gene silencing.

Transcriptional silencing at *S. cerevisiae* telomeres is initiated by binding of Rap1p to double-stranded telomeric (TG_{1-3}) repeats. Rap1 binding is followed by recruitment of the silencing factor Sir4p to the C-terminus of Rap1p. In turn, Sir4p recruits the remainder of the silent information regulators (Sir) Sir2p and Sir3p through formation of a trimeric Sir2p/Sir3p/Sir4p (SIR) complex. Once targeted to chromatin Sir2p-mediated histone deacetylation of histone N-termini tails generates hypoacetylated nucleosomes and additional binding sites for the SIR complex. Subsequent cycles of binding and deacetylation cause SIR complex spreading towards the centromere generating compact, transcriptionally silenced chromatin that continues to spread until a boundary region is reached. The spread of Sir4p generates additional Rap1p binding sites causing the telomere to fold over. In addition, the spread of silencing is further influenced by the subtelomeric repeat elements present at individual telomeres. Within these regions silencing is enhanced by binding of Abf1p and ORC to the X element (core X) and inhibited by binding of Tbf1p and Reb1p within the subtelomeric repeats (STR). Adapted from Sun et al., 2011. Reprented by permission from Genes and Genetic Systems: Sun, J.Q., Hatanaka, A., and M. Oki. Boundaries of transcriptionally silent chromatin in Saccharomyces cerevisiae. *Genes Genet Syst*. 2011;86(2):73-81. Copyright 2011.

(Pryde and Louis, 1999). Variation in TPE is due to the influence of subtelomeric elements (STE) immediately proximal to the TG_{1-3} repeats known as X and Y' elements. The size of X varies from ~300 bp to 3 kb between telomeres, but all telomeres contain a core X element with binding sites for Abf1p and ORC that promote silencing through further recruitment of SIR complexes (Louis, 1995; Tham and Zakian, 2002). In addition, X-elements can contain binding sites for the anti-silencers Tbf1p and Reb1p that prevent the spread of silencing (Fourel et al., 1999). Unlike, X-elements, the Y' element is not present at every telomere and contains additional Tbf1p and Reb1p binding sites (Fourel et al., 1999). Thus, the extent of silencing is a result of a combination of cis- and trans-acting factors that promote and inhibit the spread of silent chromatin.

1.9.2 Telomere length homeostasis

The constant length in which telomeres are maintained indicates regulatory mechanisms exist to allow only a certain amount of telomerase activity to counteract telomere loss. Numerous factors promote telomerase activity including: DNA replication, the DNA damage response, cell-cycle dependent transcription, telomere structure, and, impotantly, recruitment of telomerase itself (reviewed in: Smogorzewska and de Lange, 2004). A simplified working model for the recruitment of telomerase in yeast has emerged (reviewed in: Bianchi and Shore, 2008; Sabourin and Zakian, 2008; Wellinger et al., 2010). This model postulates that during S-phase DNA replication destabilizes the structure of the 3'overhang, exposing Cdc13p binding sites and allowing exonucleolytic cleavage

by the Mre11/Rad50/Xrs2 (MRX) complex which promotes additional Cdc13p binding through extension of the 3'overhang. Phosphorylation of Cdc13p by Cdk1p and the telomere-associated kinase Tel1p is required for Cdc13p-mediated recruitment of the telomerase subunit Est1p (Pennock et al., 2001; Tseng et al., 2006; Li et al., 2009), though the role of Tel1p in this process has been contested (Gao et al., 2010). Despite this, the phosphorylation dependent interaction of Cdc13p with Est1p is essential for recruitment of the telomerase holoenzyme. Telomerase recruitment is further aided by the yKu heterodimer through interaction with the RNA component of telomerase (Stellwagen et al., 2003). It should be noted that, in yeast, not all telomeres are extended by telomerase in every cell cycle (Teixeira et al., 2004). Thus, several rounds of DNA replication and telomere resection are required to reach a threshold at which point telomerase is recruited. In support of this view, Tel1p, the MRX complex and Cdc13p all preferentially associate with short telomeres (Bianchi and Shore, 2007).

On the other hand, the main telomerase inhibitors in yeast are Rif1p and Rif2p, which, in conjunction with Rap1, are thought to provide a counting mechanism to determine telomere length (Marcand et al., 1997; Levy and Blackburn, 2004). A postulation of the telomere-counting model is that telomere elongation, by generating additional Rap1p binding sites, increases recruitment of Rif1p and Rif2p thereby inhibiting subsequent telomerase activity. Conversely, telomere shortening leads to fewer Rap1p binding sites and a reduction in telomerase inhibition by Rif1p/2p. Additional telomerase inhibition may also occur through the formation of G-quartets by the single-stranded 3'-overhang.

Such a conformation inhibits telomerase activity *in vitro* (Zaug et al., 2005; Burge et al., 2006), and many telomeric proteins have the ability to either promote or unfold G-quartets (Fang and Cech, 1993; Giraldo and Rhodes, 1994; Pedroso et al., 2009). However, the functional significance of such structures *in vivo* remains unclear.

1.9.3 Telomere tethering at the NE

Telomere tethering at the NE in *Saccharomyces cerevisiae* is accomplished through two partially, redundant pathways involving Sir4p and the yKu heterodimer, and ablating both pathways delocalizes telomeres (Hediger et al., 2002b). Additionally, the NE associated proteins Esc1p and Mps3p are prominent factors in mediating tethering of both pathways (displayed in Figure 1-4). For instance, Sir4-mediated tethering occurs through interaction of its partitioning and anchoring domain (PAD; aa 950-1262) with the INM associated protein Esc1p (Taddei et al., 2004), and through interaction with the integral INM protein Mps3p, which tethers telomeres specifically during S-phase (Bupp et al., 2007; Schober et al., 2009). In addition, Sir4p was shown to interact with yKu80p indicating the two pathways are interconnected (Taddei et al., 2004). yKu80p, however, is capable of tethering independently of Sir4p through a series of interactions with telomerase and Mps3p (Schober et al., 2009). yKu80p binds a stem loop of the telomerase RNA component TLC1, which, in turn, interacts with the Est1p subunit of telomerase. It has been further demonstrated that Est1p interacts with Mps3p to mediate peripheral localization of telomeres specifically

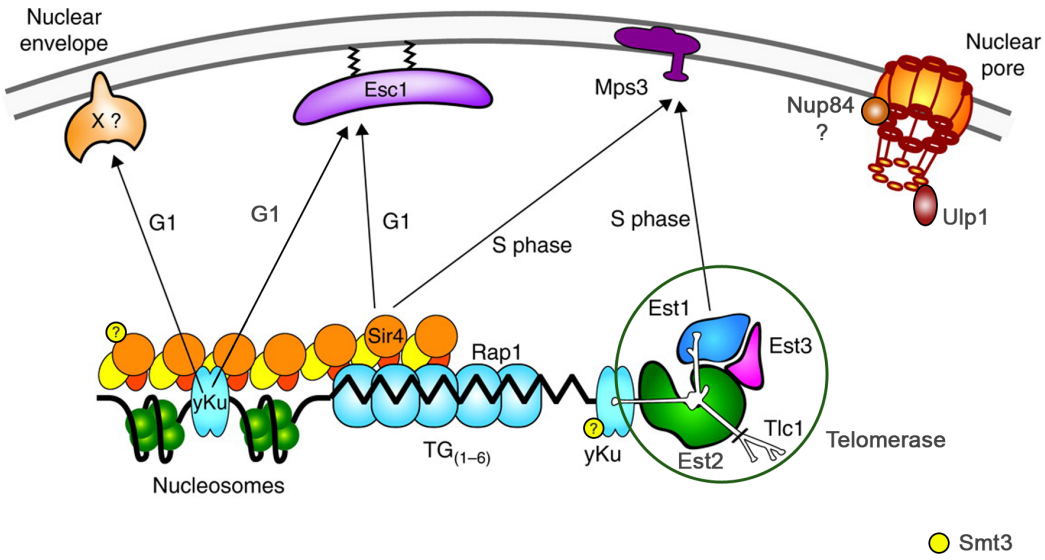

Figure 1-4. Telomere tethering mechanisms at the nuclear envelope.

Telomeres are tethered at the NE through partially redundant mechanisms involving Sir4p and the yKu70p/yKu80p heterodimer (yKu) that, during different stages of the cell cycle, attach to different inner nuclear membrane (INM) anchors. During G1-phase, yKu tethers through an as-yet-unidentified NE anchor, as well as through the INM-associated protein Esc1p. During S-phase yKu interacts with telomerase, which, in turn, interacts with the integral INM protein Mps3p. On the other hand, Sir4p-mediated telomere tethering during G1-phase occurs through interaction with Esc1p. During S-phase Sir4p tethers telomeres predominantly through interaction with the integral INM protein Mps3p. Components of the NPC (the Nup84 complex and the nuclear basket components Mlp1p/Mlp2p) have also been implicated in telomere tethering at the NE. Of note, conjugation of SUMO (Smt3p in yeast) to yKu and Sir4p promotes telomere tethering, however it remains unclear whether desumoylation by NPC-associated Ulp1p has a role in telomere tethering. Adapted from Taddei et al., 2010. Reprinted by permission from Cold Spring Harbor Laboratory Press: Cold Spring Harbor Perspectives in Biology. Taddei, A., Schober, H., and S.M. Gasser. The budding yeast nucleus. *Cold Spring Harb Perspect Biol*. 2010;2:a000612. Copyright 2010.

in S-phase (Schober et al., 2009). Interestingly, S-phase specific tethering by yKu80p is independent of yKu70p (Taddei et al., 2004; Schober et al., 2009). By contrast, yKu80p tethering during G1-phase is yKu70p dependent (Taddei et al., 2004). An additional, unknown NE anchor is likely to exist that is capable of tethering telomeres in a yKu dependent fashion during G1-phase. The existence of a third NE anchor is predicted by the finding that yKu-mediated tethering during G1-phase is maintained in the absence of Esc1p (Taddei et al., 2004), while Mps3p is believed to function specifically in S-phase.

Additional factors involved in telomere tethering have been described including: subunits of the replication factor C-like complex (RFC-like complex; Dcc1p, Ctf8p and Ctf18p), the lysine acetyltransferase Rtt109p, and the histone chaperone Asf1p (Hiraga et al., 2006 and 2008). However, the mechanisms responsible for their tethering functions were not determined and it remains unclear whether these proteins affect tethering directly or indirectly. Components of the NPC have also been proposed to function in telomere organization and tethering at the NE and are discussed in section 1.9.5.

1.9.4 Telomere dynamics through the cell cycle

Throughout the cell cycle telomere association with the NE is dynamic. During G1- and S-phase of the cell cycle yeast telomeres localize at the NE. However as cells move through G2/M-phase, telomeres are generally dislodged from the NE (Laroche et al., 2000; Hediger et al., 2002b). Similarly, foci formed by Rap1p, Sir3p, and Sir4p are maintained at the NE during interphase but are

dispersed throughout the nucleoplasm during G2/M (Laroche et al., 2000). Following nuclear division telomeres and telomeric foci reform at the NE during the late stages of cytokinesis as cells re-enter G1-phase (Laroche et al., 2000). Recent work has begun to reveal the mechanisms involving telomere dislodgement from the NE, and DNA replication appears to play an important role. A delay in DNA replication is accompanied by a delay in telomere relocalization as telomeres remain at the NE throughout the prolonged S-phase (Ebrahimi and Donaldson, 2008). Further support for this hypothesis comes from the finding that following DNA replication the yKu mediated tethering pathway is inhibited (Ebrahimi and Donaldson, 2008), though the yKu complex remains bound to telomeres (Fisher et al., 2004). A potential mechanism for yKu inhibition comes from a recent finding that both yKu70p and yKu80p are post-translationally modified by SUMO (Ferreira et al., 2011). Importantly, it was demonstrated that the SUMO E3 ligase Siz2p promotes yKu mediated telomere tethering (Ferreira et al., 2011). This raises an appealing hypothesis in which desumoylation leads to the inhibition of yKu-mediated tethering upon DNA replication. Whether the sumoylation status of yKu is cell-cycle-dependent is not known and future studies will be needed to address this possibility.

The mechanisms in which telomeres reassociate with the nuclear periphery following mitosis are largely unknown, though it is interesting to note that reassociation occurs concomitant with the re-establishment of telomeric silencing during the latter stages of mitosis. It has been proposed that telomeres are initially targeted to the NE through a silencing-independent-mechanism

mediated by yKu. At the nuclear periphery, telomere clustering would promote gene silencing and further reinforce telomere association at the NE by Sir4p-mediated tethering (Gasser et al., 2004).

1.9.5 NPC-mediated telomere organization

NPCs have been proposed to organize silent chromatin domains at the nuclear periphery in budding yeast, albeit not without controversy. Two NPC-associated components, Mlp1p and Mlp2p, were initially implicated in subtelomeric gene silencing and telomere localization at the nuclear periphery (Galy et al., 2000). In particular, Mlp2p was shown to physically interact with the telomere binding protein yKu70p, suggesting that the nuclear basket directly tethers telomeres at the NE. A subsequent study demonstrated that the Mlps and Nup60p, likely through its ability to anchor the Mlps to the NPC, are required for formation of silent domains at the NE (Feuerbach et al., 2002). However, the contribution of the Mlps in telomeric silencing and telomere tethering at the NE has been contested (Hediger et al., 2002a and 2002b). Moreover, limited colocalization has been observed between NPCs and telomeric foci in Nup mutants that cause NPCs to cluster into a single, large focus at the NE (Hediger et al., 2002b; Taddei et al., 2004; Schober et al., 2009) and has been interpreted as evidence that NPCs and telomeres do not interact (Gasser et al., 2004; Taddei et al., 2010). The reasoning behind such an argument lies in the fact that if NPCs tether telomeres at the NE, then presumably clustering of NPCs would also cause telomeres to co-cluster. It is important to note that NPC clustering mutants have

multiple pleiotropic effects on NPC structure, NE morphology, DNA repair, and nuclear transport that may potentially disrupt telomere-NPC interactions (Doye et al, 1995, Aitchison et al., 1995b; Palancade et al., 2007). Furthermore, these studies are based on static images of asynchronous populations of cells and are unlikely to reveal transient telomere-NPC interactions. Additionally, the degree of co-localization observed between the telomeric protein Sir4p and its NE anchor Esc1p is similarly limited (Taddei et al., 2004).

There is accumulating evidence that suggests a functional role for NPC components in telomere localization at the NE. Chromatin immunoprecipitation of the NPC components Mlp1p and Mlp2p revealed enrichment of silent loci, including certain subtelomeric genes, suggestive of at least a transient interaction with subtelomeric chromatin (Casolari et al., 2004 and 2005). More recently, mutations in the Nup84 complex disrupted subtelomeric silencing and the NE association of a telomere (Tel11L) and Sir3p (Therizols et al., 2006). However, in the absence of a defined molecular mechanism in which the Nup84 complex contributes to telomere tethering the significance of these observations is convoluted by the pleiotropic effects mutations in the Nup84 complex have on nuclear transport, NPC distribution and DNA repair (Doye et al., 1994; Palancade et al., 2007). Perhaps the most striking evidence of a role for NPCs in telomere localization comes from the finding that critically short telomeres localize to NPCs (Khadaroo et al., 2009), presumably to access NPC-associated proteins involved in DNA repair (Nagai et al., 2008). This suggests that NPCs are not simply a static NE anchor but likely contribute to dynamic processes in telomere

biology through the functions of NPC-associated proteins, as demonstrated for DNA repair (Nagai et al., 2008). A greater understanding of the composition of NPC-associated proteins would assist in clarifying NPC functions in telomere organization. For instance, are components involved in transcriptional repression associated with NPCs in yeast, as demonstrated for HDAC4 in vertebrates? Interestingly, the HDAC4 homolog in yeast Hda1p, although not known to interact with NPC components, is required for transcriptional repression of subtelomeric regions. Exactly how NPCs contribute to telomere organization and the repressive environment of the NE is not well-understood and future studies will be required to discriminate direct from indirect functions.

1.10 Thesis focus

In yeast, tethering chromatin at the NE promotes both gene silencing, in the case of telomeres and the mating type loci, as well as transcriptional activation. Thus, transcriptionally active and silent domains co-exist at the nuclear periphery. Although NPCs have been suggested to play a role in the organization of these domains, the molecular mechanisms responsible remain unknown. This thesis investigates the role of the NPC component Nup170p in the organization of these distinct chromatin domains. Through genetic and proteomic analyses a role for Nup170p in chromatin structure and transcriptional repression was identified. We show that Nup170p is preferentially targeted to transcriptionally silenced subtelomeric DNA where it functions in gene silencing and telomere tethering at the NE. We further demonstrate that telomeres are recruited to NPCs during

mitosis to promote the re-establishment of heterochromatin and its association at the NE.

Chapter II: *Experimental Procedures*

2.1 Yeast strains and media

All yeast strains were grown at 30˚C in YPD (1% yeast extract, 2% bactopeptone and 2% glucose) unless otherwise indicated. Strains requiring selection of prototrophic yeast markers were grown in synthetic complete medium (SC) and 2% glucose lacking the appropriate nutrients as indicated. Plates used for SGA analyses were made as described previously (Tong et al., 2001). 5-FOA containing plates were made according to (Boeke et al., 1987).

Yeast integrative and plasmid transformations were performed using a lithium acetate/polyethylene glycol based method (Gietz et al., 2002). Overnight cell cultures (5 mL) were grown to early-logarithmic growth phase ($OD_{600} \leq 0.5$), harvested by centrifugation (Eppendorf 5810R, A-4-62 rotor at 6000 x g for 2 min) and then washed with 5 mL ddH_2O followed by a wash with 1 mL transformation buffer (10 mM Tris-HCl pH 7.5, 1 mM EDTA, 100 mM LiOAc). For a list of commonly used buffers, see Table 2-3. Cells were resuspended with 50 μL transformation buffer, 5 μL of 3 mg/mL heat-denatured salmon sperm DNA, and 1-2 μg of the PCR-amplified transformation cassette of interest. To this solution 300 μL of PEG solution (0.8 g/mL polyethylene glycol 3350 in transformation buffer) was added, mixed vigorously and then incubated at 30˚C for 1 h. Following incubation, cells were heat shocked at 42˚C for 15 min in a water bath and then cooled to room temperature for 5 min. Cells were then harvested by centrifugation (Beckman Coulter microfuge 18 centrifuge, 6000 x g for 30 s) and the resulting cell pellet was resuspended in YPD medium and incubated at 30˚ C for 3 h prior to plating on appropriate marker selection plates.

Genomic integrations were performed using a PCR-based, one-step method for gene modification (Longtine et al., 1998). DNA cassettes used in integrative transformations were PCR-amplified with either the Expand High Fidelity PCR or the Expand Long Template PCR systems (Roche Applied Science, Indianapolis, IN, USA) using DNA isolated from chromosomal DNA when possible or, less preferably, from plasmid isolated DNA, see plasmids 2.2. For genomic integrations of carboxy-terminal *protein A*, 9*xMYC*, *13xMYC*, *GFP, mRFP,* and *mCherry,* ~80 bp oligonucleotide primers were designed with 60 bp 5'-overhangs that anneal to regions immediately upstream and downstream of the stop codon of the gene of interest. All integrated transformants were confirmed by PCR or, when possible, in conjunction with western blotting or microscopy. For a list of yeast strains used in this thesis, see Table 2-1. Yeast strains TMY1098 (P_{MET3}-*HA3-NUP170*) and TMY1126 (*nup157Δ* P_{MET3}-*HA3-NUP170*) have been previously described (Makio et al., 2009). Yeast strain TMY1452 was kindly provided by Tadashi Makio and generated by amino-terminal integration of a PCR-amplified *kanMX6*-P_{MET3}-*HA3* cassette from pTM1046 using primers designed with 40 bp 5'-overhangs that anneal immediately upstream and downstream of the start codon of *STH1*. Repression of P_{MET3}-*HA3-STH1* and P_{MET3}-*HA3-NUP170* were performed by growth in SC medium lacking methionine to mid-logarithmic growth phase (OD_{600} ~0.5) followed by addition of methionine to a final concentration of 200 μg/mL for the indicated times.

To limit genome instability associated with *nup170* null mutants (Kerscher et al., 2001), when possible "fresh" haploid *nup170Δ* strains were isolated by

tetrad dissection of a heterozygous *NUP170/nup170Δ* diploid strain prior to experimentation. Thus limiting the number of generations undergone prior to analysis. When unable to isolate "fresh" haploid mutants from tetrad dissections, *nup170Δ* strains were constructed by integrative transformation. Transformant colonies of sufficient size were then selected for inoculation of overnight cultures. The following day *nup170Δ* strains were confirmed by PCR analysis and used to generate frozen stocks for future experimentation.

Table 2-1. Yeast strains.

Strain	Genotype	Reference
BY4741	*MAT***a** *his3Δ1 leu2Δ0 ura3Δ0 met15Δ0*	Brachmann et al., 1998
BY4742	*MAT*α *his3Δ1 leu2Δ0 ura3Δ0 lys2Δ0*	Brachmann et al., 1998
BY4743	*MAT***a**/α *his3Δ1/his3Δ leu2Δ0/leu2Δ0 ura3Δ0/ura3Δ0 MET15/met15Δ0 LYS2/lys2Δ0*	Brachmann et al., 1998
Y3656	*MAT*α *his3Δ1 leu2Δ0 ura3Δ0 met15Δ0 lys2Δ0 can1Δ::*P_{MFA1}*-HIS3-*$P_{MFalpha1}$*-LEU2*	Tong et al., 2004
AFS173	*MAT***a** *ura3-1 trp1-1 ade2-1 can1-100 his3-11,15::GFP-LacI-HIS3 leu2-3,112::lacO-LEU2*	Hanna et al., 2001
YJH17.2	*MAT***a** *ura3-1 trp1-1 ade2-1 can1-100 his3-11,15::GFP-LacI-HIS3 leu2-3,112::lacO-LEU2 ctf18Δ::TRP1*	Hanna et al., 2001
DVY0040	*MAT***a** *ura3-1 trp1-1 ade2-1 can1-100 his3-11,15::GFP-LacI-HIS3 leu2-3,112::lacO-LEU2 nup60Δ::kanR*	Derived from AFS173
YPH278	*MAT*α *his3Δ200 leu2Δ1 ura3-52 lys2-801 ade2-101 + CFIII (CEN3.L.YPH278) URA3 SUP11*	Spencer et al., 1990
DVY0050	*MAT*α *his3Δ200 leu2Δ1 ura3-52 lys2-801 ade2-101 nup53Δ::kanR + CFIII (CEN3.L.YPH278) URA3 SUP11*	Derived from YPH278
DVY0051	*MAT*α *his3Δ200 leu2Δ1 ura3-52 lys2-801 ade2-101 nup60Δ::kanR + CFIII (CEN3.L.YPH278) URA3 SUP11*	Derived from YPH278
DVY0052	*MAT*α *his3Δ200 leu2Δ1 ura3-52 lys2-801 ade2-101 nup170Δ::kanR + CFIII (CEN3.L.YPH278) URA3 SUP11*	Derived from YPH278
YPH277	*MAT***a** *leu2Δ1 ura3-52 lys2-801 trp1Δ1 ade2-101 + CFVII (RAD2.d.YPH277) URA3 SUP11*	Spencer et al., 1990
DVY0055	*MAT***a**/α *HIS3/his3Δ200 leu2Δ1/leu2Δ1 ura3-52/ura3-52 lys2-801/lys2-801 TRP1/trp1Δ1 ade2-101/ade2-101*	Derived from

	+ CFVII (RAD2.d.YPH277) URA3 SUP11	YPH277
DVY0056	*MAT***a**/α *HIS3/his3Δ200 leu2Δ1/leu2Δ1 ura3-52/ura3-52 lys2-801/lys2-801 TRP1/trp1Δ1 ade2-101/ade2-101 nup60Δ::kanR/nup60Δ::kanR + CFVII (RAD2.d.YPH277) URA3 SUP11*	Derived from YPH277
DVY0057	*MAT***a**/α *HIS3/his3Δ200 leu2Δ1/leu2Δ1 ura3-52/ura3-52 lys2-801/lys2-801 TRP1/trp1Δ1 ade2-101/ade2-101 nup170Δ::kanR/nup170Δ::kanR + CFVII (RAD2.d.YPH277) URA3 SUP11*	Derived from YPH277
DVY0100	*MAT***a** *his3Δ1 leu2Δ0 ura3Δ0 met15Δ0 lys2Δ0 can1Δ::*P_{MFA1}*-HIS3-*$P_{MFalpha1}$*-LEU2 nup53Δ::natR*	Derived from Y3656
DVY0101	*MAT***a** *his3Δ1 leu2Δ0 ura3Δ0 met15Δ0 lys2Δ0 can1Δ::*P_{MFA1}*-HIS3-*$P_{MFalpha1}$*-LEU2 nup60Δ::natR*	Derived from Y3656
DVY0102	*MAT***a** *his3Δ1 leu2Δ0 ura3Δ0 lys2Δ0 can1Δ::*P_{MFA1}*-HIS3-*$P_{MFalpha1}$*-LEU2 nup170Δ::natR*	Derived from Y3656
DVY1134	*MAT***a** *his3Δ1 leu2Δ0 ura3Δ0 nup157Δ::URA3*	This study
DVY1136	*MAT*α *his3Δ1 leu2Δ0 ura3Δ0 lys2Δ0 nup188Δ::kanR*	This study
DVY1171	*MAT*α *his3Δ1 leu2Δ0 ura3Δ0 lys2Δ0 nup170Δ::kanR*	This study
DVY1171.1	*MAT*α *his3Δ1 leu2Δ0 ura3Δ0 lys2Δ0 nup170Δ::hphR*	This study
DVY1234	*MAT*α *his3Δ1 leu2Δ0 ura3Δ0 lys2Δ0 nup170Δ::hphR bar1Δ::kanR*	This study
DVY1172	*MAT*α *his3Δ1 leu2Δ0 ura3Δ0 met15Δ0*	This study
DVY1173	*MAT***a** *his3Δ1 leu2Δ0 ura3Δ0 met15Δ0 nup170Δ::kanR*	This study
DVY1174	*MAT***a** *his3Δ1 leu2Δ0 ura3Δ0 lys2Δ0*	This study
DVY1190	*MAT*α *his3Δ1 leu2Δ0 ura3Δ0 ade1 sst2Δ ste3*^{L194Q}	Gift from N. Adames
DVY1191	*MAT***a** *his3Δ1 leu2Δ0 ura3Δ0 ade1 bar1Δ*	Gift from N. Adames
DVY1199	*MAT*α *his3Δ1 leu2Δ0 ura3Δ0 lys2Δ0 NUP170-pA::HIS3-URA3*	This study
DVY1202	*MAT***a**/α *his3Δ1/his3Δ1 leu2Δ0/leu2Δ0 ura3Δ0/ura3Δ0 MET15/met15Δ0 LYS2/lys2Δ0 NUP170/NUP170-pA::HIS3-URA3 HTZ1/HTZ1-GFP::HIS3*	This study
DVY1204	*MAT***a**/α *his3Δ1/his3Δ1 leu2Δ0/leu2Δ0 ura3Δ0/ura3Δ0 MET15/met15Δ0 LYS2/lys2Δ0 NUP170/NUP170-pA::HIS3-URA3 STH1/STH1-GFP::HIS3*	This study
DVY1207	*MAT***a**/α *his3Δ1/his3Δ1 leu2Δ0/leu2Δ0 ura3Δ0/ura3Δ0 MET15/met15Δ0 LYS2/lys2Δ0 NUP170/NUP170-pA::HIS3-URA3 ARP5/ARP5-GFP::HIS3*	This study
DVY1208	*MAT***a**/α *his3Δ1/his3Δ1 leu2Δ0/leu2Δ0 ura3Δ0/ura3Δ0 MET15/met15Δ0 LYS2/lys2Δ0 NUP170/NUP170-pA::HIS3-URA3 RVB1/RVB1-GFP::HIS3*	This study
DVY1209	*MAT***a**/α *his3Δ1/his3Δ1 leu2Δ0/leu2Δ0 ura3Δ0/ura3Δ0 MET15/met15Δ0 LYS2/lys2Δ0 NUP170/NUP170-pA::HIS3-URA3 TAF14/TAF14-GFP::HIS3*	This study
DVY1218	*MAT***a**/α *his3Δ1/his3Δ1 leu2Δ0/leu2Δ0 ura3Δ0/ura3Δ0 MET15/met15Δ0 LYS2/lys2Δ0 NUP170/NUP170-pA::HIS3-URA3 RAD6/RAD6-GFP::HIS3*	This study
DVY1219	*MAT***a**/α *his3Δ1/his3Δ1 leu2Δ0/leu2Δ0 ura3Δ0/ura3Δ0*	This study

	MET15/met15Δ0 LYS2/lys2Δ0 NUP170/NUP170-pA::HIS3-URA3 ADA2/ADA2-GFP::HIS3	
DVY1224	*MAT***a**/α *his3Δ1/his3Δ1 leu2Δ0/leu2Δ0 ura3Δ0/ura3Δ0 MET15/met15Δ0 LYS2/lys2Δ0 NUP170/NUP170-pA::HIS3-URA3 RPD3/RPD3-GFP::HIS5*	This study
DVY1226	*MAT***a**/α *his3Δ1/his3Δ1 leu2Δ0/leu2Δ0 ura3Δ0/ura3Δ0 MET15/met15Δ0 LYS2/lys2Δ0 NUP170/NUP170-pA::HIS3-URA3 SET3/SET3-GFP::HIS5*	This study
DVY1227	*MAT***a**/α *his3Δ1/his3Δ1 leu2Δ0/leu2Δ0 ura3Δ0/ura3Δ0 MET15/met15Δ0 LYS2/lys2Δ0 NUP170/NUP170-pA::HIS3-URA3 SWC5/SWC5-GFP::HIS5*	This study
DVY1394	*MAT*α *his3Δ1 leu2Δ0 ura3Δ0 lys2Δ0 STH1-13xMYC::kanR*	This study
DVY1395	*MAT*a *his3Δ1 leu2Δ0 ura3Δ0 lys2Δ0 NUP170-pA::HIS3-URA3 STH1-13xMYC::kanR*	This study
DVY1398	*MAT*α *his3Δ1 leu2Δ0 ura3Δ0 lys2Δ0 STH1-pA::HIS5 NUP170-13xMYC::kanR*	This study
DVY1399	*MAT*α *his3Δ1 leu2Δ0 ura3Δ0 lys2Δ0 NUP170-13xMYC::kanR*	This study
DVY1414	*MAT*α *his3Δ1 leu2Δ0 ura3Δ0 lys2Δ0 NUP188-pA::HIS5 STH1-13xMYC::kanR*	This study
DVY1455	*MAT*α *his3Δ1 leu2Δ0 ura3Δ0 lys2Δ0 STH1-pA::HIS5 NUP170-13xMYC::kanR nup53Δ::natR*	This study
DVY1457	*MAT*α *his3Δ1 leu2Δ0 ura3Δ0 lys2Δ0 STH1-pA::HIS5 nup170Δ::kanR*	This study
DVY1459	*MAT*α *his3Δ1 leu2Δ0 ura3Δ0 met15Δ0 NUP84-pA::HIS5 STH1-13xMYC::kanR*	This study
DVY1730	*MAT***a** *his3Δ1 leu2Δ0 ura3Δ0 met15Δ0 NUP170-pA::HIS3-URA3 YKU70-13xMYC::kanR bar1Δ::natR*	This study
DVY1732	*MAT***a** *his3Δ1 leu2Δ0 ura3Δ0 met15Δ0 NUP170-pA::HIS3-URA3 RAP1-13xMYC::kanR bar1Δ::natR*	This study
DVY2166	*MAT***a** *his3Δ1 leu2Δ0 ura3Δ0 SIR4-13xMYC::kanR bar1Δ::natR*	This study
DVY2171	*MAT***a** *his3Δ1 leu2Δ0 ura3Δ0 met15Δ0 NUP170-pA::HIS3-URA3 SIR4-13xMYC::kanR bar1Δ::natR*	This study
DVY2180	*MAT***a** *his3Δ1 leu2Δ0 ura3Δ0 NUP157-pA::HIS5 SIR4-13xMYC::kanR bar1Δ::natR*	This study
DVY2186	*MAT***a** *his3Δ1 leu2Δ0 ura3Δ0 lys2Δ0 NUP84-pA::HIS5 SIR4-13xMYC::kanR*	This study
DVY2206	*MAT***a** *his3Δ1 leu2Δ0 ura3Δ0 lys2Δ0 SIR4-pA::HIS5 NUP170-13xMYC::kanR*	This study
ROY648	*MAT*α *his3-11,15 leu2-3,112 ura3-1 trp1-1 ade2-1 ppr1Δ::HIS3 HMR::URA3*	Donze et al., 1999
DVY1303	*MAT*α *his3-11,15 leu2-3,112 ura3-1 trp1-1 ade2-1 ppr1Δ::HIS3 HMR::URA3 sir3Δ::kanR*	Derived from ROY648
DVY1305	*MAT*α *his3-11,15 leu2-3,112 ura3-1 trp1-1 ade2-1 ppr1Δ::HIS3 HMR::URA3 nup170Δ::kanR*	Derived from ROY648

KIY54	*MAT***a** *his3-11,15 leu2-3,112 ura3-1 trp1-1 ade2-1 can1-100 hml::E-4xUAS$_{GAL}$-ADE2-4xUAS$_{GAL}$-URA3-I$^{\Delta 242}$*	Ishii et al., 2002
DVY1332	*MAT***a** *his3-11,15 leu2-3,112 ura3-1 trp1-1 ade2-1 can1-100 hml::E-4xUAS$_{GAL}$-ADE2-4xUAS$_{GAL}$-URA3-I$^{\Delta 242}$ sir3Δ::kanR*	Derived from KIY54
DVY1334	*MAT***a** *his3-11,15 leu2-3,112 ura3-1 trp1-1 ade2-1 can1-100 hml::E-4xUAS$_{GAL}$-ADE2-4xUAS$_{GAL}$-URA3-I$^{\Delta 242}$ nup2Δ::kanR*	Derived from KIY54
DVY1335	*MAT***a** *his3-11,15 leu2-3,112 ura3-1 trp1-1 ade2-1 can1-100 hml::E-4xUAS$_{GAL}$-ADE2-4xUAS$_{GAL}$-URA3-I$^{\Delta 242}$ nup60Δ::kanR*	Derived from KIY54
DVY1336	*MAT***a** *his3-11,15 leu2-3,112 ura3-1 trp1-1 ade2-1 can1-100 hml::E-4xUAS$_{GAL}$-ADE2-4xUAS$_{GAL}$-URA3-I$^{\Delta 242}$ nup170Δ::kanR*	Derived from KIY54
UCC3505	*MAT***a** *his3Δ200 leu2Δ1 ura3-52 lys2-801 trp1Δ63 ade2-101 ppr1::HIS3 adh4::URA3-TEL-VIIL ADE2-TEL-VR*	Singer et al., 1994
DVY1361	*MAT***a** *his3Δ200 leu2Δ1 ura3-52 lys2-801 trp1Δ63 ade2-101 ppr1::HIS3 nup2Δ::kanR adh4::URA3-TEL-VIIL ADE2-TEL-VR*	Derived from UCC3505
DVY1364	*MAT***a** *his3Δ200 leu2Δ1 ura3-52 lys2-801 trp1Δ63 ade2-101 ppr1::HIS3 nup60Δ::kanR adh4::URA3-TEL-VIIL ADE2-TEL-VR*	Derived from UCC3505
DVY1367	*MAT***a** *his3Δ200 leu2Δ1 ura3-52 lys2-801 trp1Δ63 ade2-101 ppr1::HIS3 nup170Δ::kanR adh4::URA3-TEL-VIIL ADE2-TEL-VR*	Derived from UCC3505
DVY1370	*MAT***a** *his3Δ200 leu2Δ1 ura3-52 lys2-801 trp1Δ63 ade2-101 ppr1::HIS3 nup188Δ::kanR adh4::URA3-TEL-VIIL ADE2-TEL-VR*	Derived from UCC3505
DVY1373	*MAT***a** *his3Δ200 leu2Δ1 ura3-52 lys2-801 trp1Δ63 ade2-101 ppr1::HIS3 sir3Δ::kanR adh4::URA3-TEL-VIIL ADE2-TEL-VR*	Derived from UCC3505
DVY1760	*MAT***a** *his3Δ200 leu2Δ1 ura3-52 lys2-801 trp1Δ63 ade2-101 ppr1::HIS3 nup53Δ::natR adh4::URA3-TEL-VIIL ADE2-TEL-VR*	Derived from UCC3505
DVY1766	*MAT***a** *his3Δ200 leu2Δ1 ura3-52 lys2-801 trp1Δ63 ade2-101 ppr1::HIS3 rsc1Δ::kanR adh4::URA3-TEL-VIIL ADE2-TEL-VR*	Derived from UCC3505
DVY1770	*MAT***a** *his3Δ200 leu2Δ1 ura3-52 lys2-801 trp1Δ63 ade2-101 ppr1::HIS3 rsc3Δ::kanR adh4::URA3-TEL-VIIL ADE2-TEL-VR*	Derived from UCC3505
DVY1771	*MAT***a** *his3Δ200 leu2Δ1 ura3-52 lys2-801 trp1Δ63 ade2-101 ppr1::HIS3 rsc7Δ::kanR adh4::URA3-TEL-VIIL ADE2-TEL-VR*	Derived from UCC3505
DVY1774	*MAT***a** *his3Δ200 leu2Δ1 ura3-52 lys2-801 trp1Δ63 ade2-101 ppr1::HIS3 rsc30Δ::kanR adh4::URA3-TEL-VIIL ADE2-TEL-VR*	Derived from UCC3505
DVY1776	*MAT***a** *his3Δ200 leu2Δ1 ura3-52 lys2-801 trp1Δ63*	Derived

	ade2-101 ppr1::HIS3 htl1Δ::kanR adh4::URA3-TEL-VIIL ADE2-TEL-VR	from UCC3505
DLY171	*MAT***a** *his3Δ200 leu2Δ1 ura3-52 lys2-801 trp1Δ63 ade2-101 ppr1::HIS3 rif1Δ::kanR adh4::URA3-TEL-VIIL ADE2-TEL-VR*	Derived from UCC3505
DLY172	*MAT***a** *his3Δ200 leu2Δ1 ura3-52 lys2-801 trp1Δ63 ade2-101 ppr1::HIS3 rif1Δ::kanR nup170Δ::natR adh4::URA3-TEL-VIIL ADE2-TEL-VR*	Derived from UCC3505
DLY176	*MAT***a** *his3Δ200 leu2Δ1 ura3-52 lys2-801 trp1Δ63 ade2-101 ppr1::HIS3 nup170Δ::natR adh4::URA3-TEL-VIIL ADE2-TEL-VR*	Derived from UCC3505
TMY1098	*MAT*α *his3Δ1 leu2Δ0 ura3Δ0 lys2Δ0 NUP170::kanR-*P_{MET3}*-HA3-NUP170*	Makio et al., 2009
TMY1126	*MAT*α *his3Δ1 leu2Δ0 ura3Δ0 lys2Δ0 nup157Δ::URA3 NUP170::kanR-*P_{MET3}*-HA3-NUP170*	Makio et al., 2009
TMY1452	*MAT*α *his3Δ1 leu2Δ0 ura3Δ0 lys2Δ0 sth1::kanR-*P_{MET3}*-HA3-STH1*	Gift from T. Makio
YWY003	*MAT*α *his3Δ1 leu2Δ0 ura3Δ0 lys2Δ0*	This study
YWY284	*MAT*α *his3Δ1 leu2Δ0 ura3Δ0 lys2Δ0 SIR2-9xMYC::natR*	Wan et al., 2010
YWY286	*MAT*α *his3Δ1 leu2Δ0 ura3Δ0 lys2Δ0 SIR3-9xMYC::natR*	Wan et al., 2010
YWY296	*MAT*α *his3Δ1 leu2Δ0 ura3Δ0 lys2Δ0 SIR4-9xMYC::natR*	Wan et al., 2010
YWY655	*MAT*α *his3Δ1 leu2Δ0 ura3Δ0 lys2Δ0 NUP170-9xMYC::hphR*	This study
YWY798	*MAT*α *his3Δ1 leu2Δ0 ura3Δ0 lys2Δ0 RAP1-9xMYC::hphR*	Wan et al., 2010
YWY895	*MAT*α *his3Δ1 leu2Δ0 ura3Δ0 lys2Δ0 SIR2-9xMYC::natR nup170Δ::hphR*	This study
YWY896	*MAT*α *his3Δ1 leu2Δ0 ura3Δ0 lys2Δ0 SIR3-9xMYC::natR nup170Δ::hphR*	This study
YWY897	*MAT*α *his3Δ1 leu2Δ0 ura3Δ0 lys2Δ0 SIR4-9xMYC::natR nup170Δ::hphR*	This study
YWY908	*MAT*α *his3Δ1 leu2Δ0 ura3Δ0 lys2Δ0 RAP1-9xMYC::hphR nup170Δ::natR*	This study
YWY953	*MAT*α *his3Δ1 leu2Δ0 ura3Δ0 lys2Δ0 NUP157-9xMYC::hphR*	This study
YWY954	*MAT*α *his3Δ1 leu2Δ0 ura3Δ0 lys2Δ0 NUP188-9xMYC::hphR*	This study
YWY971	*MAT*α *his3Δ1 leu2Δ0 ura3Δ0 lys2Δ0 NUP170-9xMYC::hphR sir2Δ::natR*	This study
YWY973	*MAT*α *his3Δ1 leu2Δ0 ura3Δ0 lys2Δ0 nup170Δ::natR*	This study
YWY1501	*MAT*α *his3Δ1 leu2Δ0 ura3Δ0 lys2Δ0 NUP170-9xMYC::hphR sir4Δ::natR*	This study
YWY1502	*MAT*α *his3Δ1 leu2Δ0 ura3Δ0 lys2Δ0 NUP170-9xMYC::hphR yku70Δ::natR*	This study
YWY1066	*MAT***a** *his3Δ1 leu2Δ0 ura3Δ0 met15Δ0 NUP170-9xMYC::hphR bar1Δ::kanR*	This study

YWY906	*MAT***a** *his3Δ1 leu2Δ0 ura3Δ0 lys2Δ0 NUP170-9xMYC::hphR STH1::kanR-* P_{MET3}*-HA3-STH1*	This study
DVY2142	*MAT***a** *his3Δ1 leu2Δ0 ura3Δ0 met15Δ0 SIR4-GFP::HIS3 SEC63-mCherry::natR*	This study
DVY2143	*MAT***a** *his3Δ1 leu2Δ0 ura3Δ0 SIR4-GFP::HIS3 SEC63-mCherry::natR nup170Δ::hphR*	This study
DVY2144	*MAT***a** *his3Δ1 leu2Δ0 ura3Δ0 met15Δ0 SIR4-GFP::HIS3 SEC63-mCherry::natR nup157Δ::URA3*	This study
DVY2146	*MAT***a** *his3Δ1 leu2Δ0 ura3Δ0 met15Δ0 SIR4-GFP::HIS3 SEC63-mCherry::natR yku70Δ::kanR*	This study
DVY1483	*MAT*α *his3Δ1 leu2Δ0 ura3Δ0 met15Δ0 SIR4-GFP::HIS3 SEC63-mCherry::natR*	This study
DVY1497.1	*MAT*α *his3Δ1 leu2Δ0 ura3Δ0 SIR4-GFP::HIS3 SEC63-mCherry::natR nup170Δ::hphR*	This study
DLY161	*MAT*α *his3Δ1 leu2Δ0 ura3Δ0 SIR4-GFP::HIS3 SEC63-mCherry::natR nup170Δ::hphR rif1Δ::kanR*	This study
DLY162	*MAT*α *his3Δ1 leu2Δ0 ura3Δ0 SIR4-GFP::HIS3 SEC63-mCherry::natR rif1Δ::kanR*	This study
GA1459	*MAT***a** *leu2-3,112 ura3-1 trp1-1 ade2-1 can1-100 TELVI-R::256xlacO-lexAop-TRP1 his3-11,15::GFP-lacI-HIS3 nup49::NUP49-GFP-URA3*	Hediger et al., 2002b
DVY2050	*MAT***a** *leu2-3,112 ura3-1 trp1-1 ade2-1 can1-100 TELVI-R::256xlacO-lexAop-TRP1 his3-11,15::GFP-lacI-HIS3 SEC63-GFP-natR*	Derived from GA1459
DVY2056	*MAT*α *leu2-3,112 ura3-1 trp1-1 ade2-1 can1-100 TELVI-R::256xlacO-lexAop-TRP1 yku70Δ::kanR his3-11,15::GFP-lacI-HIS3 SEC63-GFP-natR*	Derived from GA1459
DVY2057	*MAT***a** *leu2-3,112 ura3-1 trp1-1 ade2-1 can1-100 TELVI-R::256xlacO-lexAop-TRP1 nup2Δ::kanR his3-11,15::GFP-lacI-HIS3 SEC63-GFP-natR*	Derived from GA1459
DVY2059	*MAT***a** *leu2-3,112 ura3-1 trp1-1 ade2-1 can1-100 TELVI-R::256xlacO-lexAop-TRP1 sir4Δ::kanR his3-11,15::GFP-lacI-HIS3 SEC63-GFP-natR*	Derived from GA1459
DVY2061	*MAT***a** *leu2-3,112 ura3-1 trp1-1 ade2-1 can1-100 TELVI-R::256xlacO-lexAop-TRP1 nup157Δ::URA3 his3-11,15::GFP-lacI-HIS3 SEC63-GFP-natR*	Derived from GA1459
DVY2062.1	*MAT***a** *leu2-3,112 ura3-1 trp1-1 ade2-1 can1-100 TELVI-R::256xlacO-lexAop-TRP1 nup170Δ::kanR his3-11,15::GFP-lacI-HIS3 SEC63-GFP-natR*	Derived from GA1459
GA1986	*MAT***a** *leu2-3,112 ura3-1 trp1-1 ade2-1 can1-100 TELVIII-L::256xlacO-lexAop-TRP1 his3-11,15::GFP-lacI-HIS3 nup49::NUP49-GFP-URA3*	Hediger et al., 2002b
DVY2044	*MAT*α *leu2-3,112 ura3-1 trp1-1 ade2-1 can1-100 TELVIII-L::256xlacO-lexAop-TRP1 his3-11,15::GFP-lacI-HIS3 SEC63-GFP-natR*	Derived from GA1986
DVY2063	*MAT*α *leu2-3,112 ura3-1 trp1-1 ade2-1 can1-100 TELVIII-L::256xlacO-lexAop-TRP1 sir4Δ::kanR his3-11,15::GFP-lacI-HIS3 SEC63-GFP-natR*	Derived from GA1986
DVY2065	*MAT*α *leu2-3,112 ura3-1 trp1-1 ade2-1 can1-100*	Derived

	TELVIII-L::256xlacO-lexAop-TRP1 yku70Δ::kanR his3-11,15::GFP-lacI-HIS3 SEC63-GFP-natR	from GA1986
DVY2067	*MAT*α *leu2-3,112 ura3-1 trp1-1 ade2-1 can1-100 TELVIII-L::256xlacO-lexAop-TRP1 nup2Δ::kanR his3-11,15::GFP-lacI-HIS3 SEC63-GFP-natR*	Derived from GA1986
DVY2069	*MAT*α *leu2-3,112 ura3-1 trp1-1 ade2-1 can1-100 TELVIII-L::256xlacO-lexAop-TRP1 nup170Δ::kanR his3-11,15::GFP-lacI-HIS3 SEC63-GFP-natR*	Derived from GA1986
DVY2071	*MAT*α *leu2-3,112 ura3-1 trp1-1 ade2-1 can1-100 TELVIII-L::256xlacO-lexAop-TRP1 nup157Δ::kanR his3-11,15::GFP-lacI-HIS3 SEC63-GFP-natR*	Derived from GA1986
SLJ2499	*MAT***a** *ura3-1 trp1-1 ade2-1 can1-100 TELXIV-L::256xlacO-TRP1 his3::GFP-lacI-HIS3 nup49::NUP49-GFP mps3Δ::natR leu2::MPS3-LEU2*	Bupp et al., 2007
DVY1534	*MAT***a** *leu2-3,112 ura3-1 trp1-1 ade2-1 can1-100 TELXIV-L::256xlacO-TRP1 his3::GFP-lacI-HIS3 SEC63-GFP-natR*	Derived from SLJ2499
DVY1535	*MAT***a** *leu2-3,112 ura3-1 trp1-1 ade2-1 can1-100 TELXIV-L::256xlacO-TRP1 nup157Δ::URA3 his3::GFP-lacI-HIS3 SEC63-GFP-natR*	Derived from SLJ2499
DVY1536	*MAT***a** *leu2-3,112 ura3-1 trp1-1 ade2-1 can1-100 TELXIV-L::256xlacO-TRP1 nup170Δ::kanR his3::GFP-lacI-HIS3 SEC63-GFP-natR*	Derived from SLJ2499
DVY1537	*MAT***a** *leu2-3,112 ura3-1 trp1-1 ade2-1 can1-100 TELXIV-L::256xlacO-TRP1 nup2Δ::kanR his3::GFP-lacI-HIS3 SEC63-GFP-natR*	Derived from SLJ2499
DVY1539	*MAT***a** *leu2-3,112 ura3-1 trp1-1 ade2-1 can1-100 TELXIV-L::256xlacO-TRP1 sir4Δ::kanR his3::GFP-lacI-HIS3 SEC63-GFP-natR*	Derived from SLJ2499
DVY1539.1	*MAT***a** *leu2-3,112 ura3-1 trp1-1 ade2-1 can1-100 TELXIV-L::256xlacO-TRP1 yku70Δ::kanR his3::GFP-lacI-HIS3 SEC63-GFP-natR*	Derived from SLJ2499
DVY1150	*MAT***a**/α *his3Δ1/his3Δ leu2Δ0/leu2Δ0 ura3Δ0/ura3Δ0 MET15/met15Δ0 LYS2/lys2Δ0 NUP170/nup170Δ::kanR*	This study
DVY1160.1	*MAT***a**/α *his3Δ1/his3Δ leu2Δ0/leu2Δ0 ura3Δ0/ura3Δ0 MET15/met15Δ0 LYS2/lys2Δ0 NUP170/nup170Δ::natR*	This study
DVY1160.2	*MAT***a**/α *his3Δ1/his3Δ leu2Δ0/leu2Δ0 ura3Δ0/ura3Δ0 MET15/met15Δ0 LYS2/lys2Δ0 NUP170/nup170Δ::hphR*	This study
DVY1551	*MAT***a**/α *his3Δ1/his3Δ leu2Δ0/leu2Δ0 ura3Δ0/ura3Δ0 MET15/met15Δ0 LYS2/lys2Δ0 NUP170/nup170Δ::hphR rpd3Δ::kanR*	This study
DVY1553	*MAT***a**/α *his3Δ1/his3Δ leu2Δ0/leu2Δ0 ura3Δ0/ura3Δ0 MET15/met15Δ0 LYS2/lys2Δ0 NUP170/nup170Δ::hphR swc1Δ::kanR*	This study
DVY1554	*MAT***a**/α *his3Δ1/his3Δ leu2Δ0/leu2Δ0 ura3Δ0/ura3Δ0 MET15/met15Δ0 LYS2/lys2Δ0 NUP170/nup170Δ::hphR set3Δ::kanR*	This study
DVY1572	*MAT***a**/α *his3Δ1/his3Δ leu2Δ0/leu2Δ0 ura3Δ0/ura3Δ0 MET15/MET15 lys2Δ0/lys2Δ0 CAN1/can1Δ::*P_{MFA1}-	This study

	HIS3-$P_{MFalpha1}$*-LEU2 NUP170/nup170Δ::natR arp6Δ::kanR*	
DVY1573	*MAT***a**/α *his3Δ1/his3Δ leu2Δ0/leu2Δ0 ura3Δ0/ura3Δ0 MET15/met15Δ0 LYS2/lys2Δ0 CAN1/can1Δ::*P_{MFA1}*-HIS3*-$P_{MFalpha1}$*-LEU2 NUP170/nup170Δ::natR lge1Δ::kanR*	This study
DVY1574	*MAT***a**/α *his3Δ1/his3Δ leu2Δ0/leu2Δ0 ura3Δ0/ura3Δ0 MET15/met15Δ0 LYS2/lys2Δ0 CAN1/can1Δ::*P_{MFA1}*-HIS3*-$P_{MFalpha1}$*-LEU2 NUP170/nup170Δ::natR rad6Δ::kanR*	This study
DVY1575	*MAT***a**/α *his3Δ1/his3Δ leu2Δ0/leu2Δ0 ura3Δ0/ura3Δ0 MET15/met15Δ0 LYS2/lys2Δ0 CAN1/can1Δ::*P_{MFA1}*-HIS3*-$P_{MFalpha1}$*-LEU2 NUP170/nup170Δ::natR swc5Δ::kanR*	This study
DVY1454	*MAT*α *his3Δ1 leu2Δ0 ura3Δ0 lys2Δ0 apq12Δ::kanR*	This study
DVY1620	*MAT***a** *his3Δ0 leu2Δ0 ura3Δ0 Nup82-GFP-HIS3*	This study
DVY1621	*MAT*α *his3Δ0 leu2Δ0 ura3Δ0 met15Δ0 lys2Δ0 nup170Δ::hphR Nup82-GFP-HIS3*	This study
DVY1622	*MAT*α *his3Δ0 leu2Δ0 ura3Δ0 met15Δ0 lys2Δ0 bre1Δ::kanR Nup82-GFP-HIS3*	
DVY1623	*MAT***a** *his3Δ0 leu2Δ0 ura3Δ0 met15Δ0 lys2Δ0 rpd3Δ::kanR Nup82-GFP-HIS3*	This study
DVY1624	*MAT***a** *his3Δ0 leu2Δ0 ura3Δ0 met15Δ0 set3Δ::kanR Nup82-GFP-HIS3*	This study
DVY1625	*MAT***a** *his3Δ0 leu2Δ0 ura3Δ0 met15Δ0 swc1Δ::kanR Nup82-GFP-HIS3*	This study
DVY1626	*MAT*α *his3Δ0 leu2Δ0 ura3Δ0 swr1Δ::kanR Nup82-GFP-HIS3*	This study
DVY1627	*MAT***a** *his3Δ0 leu2Δ0 ura3Δ0 nup170Δ::hphR bre1Δ::kanR Nup82-GFP-HIS3*	This study
DVY1628	*MAT*α *his3Δ0 leu2Δ0 ura3Δ0 lys2Δ0 nup170Δ::hphR rpd3Δ::kanR Nup82-GFP-HIS3*	This study
DVY1629	*MAT*α *his3Δ0 leu2Δ0 ura3Δ0 lys2Δ0 nup170Δ::hphR set3Δ::kanR Nup82-GFP-HIS3*	This study
DVY1630	*MAT***a** *his3Δ0 leu2Δ0 ura3Δ0 lys2Δ0 nup170Δ::hphR swc1Δ::kanR Nup82-GFP-HIS3*	This study
DVY1631	*MAT***a** *his3Δ0 leu2Δ0 ura3Δ0 met15Δ0 lys2Δ0 nup170Δ::hphR swr1Δ::kanR Nup82-GFP-HIS3*	This study
DVY1632	*MAT*α *his3Δ0 leu2Δ0 ura3Δ0 Nup159-GFP-HIS5*	This study
DVY1633	*MAT***a** *his3Δ0 leu2Δ0 ura3Δ0 met15Δ0 lys2Δ0 nup170Δ::hphR Nup159-GFP-HIS5*	This study
DVY1634	*MAT*α *his3Δ0 leu2Δ0 ura3Δ0 bre1Δ::kanR Nup159-GFP-HIS5*	This study
DVY1635	*MAT*α *his3Δ0 leu2Δ0 ura3Δ0 rpd3Δ::kanR Nup159-GFP-HIS5*	This study
DVY1636	*MAT***a** *his3Δ0 leu2Δ0 ura3Δ0 met15Δ0 lys2Δ0 set3Δ::kanR Nup159-GFP-HIS5*	This study
DVY1637	*MAT*α *his3Δ0 leu2Δ0 ura3Δ0 met15Δ0 swc1Δ::kanR Nup159-GFP-HIS5*	This study

DVY1638	*MAT***a** *his3Δ0 leu2Δ0 ura3Δ0 met15Δ0 lys2Δ0 swr1Δ::kanR Nup159-GFP-HIS5*	This study
DVY1639	*MAT***a** *his3Δ0 leu2Δ0 ura3Δ0 met15Δ0 nup170Δ::hphR bre1Δ::kanR Nup159-GFP-HIS5*	This study
DVY1640	*MAT*α *his3Δ0 leu2Δ0 ura3Δ0 nup170Δ::hphR rpd3Δ::kanR Nup159-GFP-HIS5*	This study
DVY1641	*MAT*α *his3Δ0 leu2Δ0 ura3Δ0 met15Δ0 nup170Δ::hphR set3Δ::kanR Nup159-GFP-HIS5*	This study
DVY1642	*MAT***a** *his3Δ0 leu2Δ0 ura3Δ0 lys2Δ0 nup170Δ::hphR swc1Δ::kanR Nup159-GFP-HIS5*	This study
DVY1643	*MAT***a** *his3Δ0 leu2Δ0 ura3Δ0 lys2Δ0 nup170Δ::hphR swr1Δ::kanR Nup159-GFP-HIS5*	This study
DVY1734	*MAT*α *his3Δ0 leu2Δ0 ura3Δ0 Gle1-GFP-HIS3*	This study
DVY1438	*MAT*α *his3Δ0 leu2Δ0 ura3Δ0 nup170Δ::hphR Gle1-GFP-HIS3*	This study
DVY1736	*MAT***a** *his3Δ0 leu2Δ0 ura3Δ0 lys2Δ0 bre1Δ::kanR Gle1-GFP-HIS3*	This study
DVY1737	*MAT***a** *his3Δ0 leu2Δ0 ura3Δ0 met15Δ0 lys2Δ0 rpd3Δ::kanR Gle1-GFP-HIS3*	This study
DVY1738	*MAT*α *his3Δ0 leu2Δ0 ura3Δ0 met15Δ0 lys2Δ0 set3Δ::kanR Gle1-GFP-HIS3*	This study
DVY1739	*MAT*α *his3Δ0 leu2Δ0 ura3Δ0 swc1Δ::kanR Gle1-GFP-HIS3*	This study
DVY1740	*MAT*α *his3Δ0 leu2Δ0 ura3Δ0 lys2Δ0 swr1Δ::kanR Gle1-GFP-HIS3*	This study
DVY1741	*MAT*α *his3Δ0 leu2Δ0 met15Δ0 ura3Δ0 nup170Δ::hphR bre1Δ::kanR Gle1-GFP-HIS3*	This study
DVY1742	*MAT***a** *his3Δ0 leu2Δ0 ura3Δ0 met15Δ0 nup170Δ::hphR rpd3Δ::kanR Gle1-GFP-HIS3*	This study
DVY1743	*MAT*α *his3Δ0 leu2Δ0 ura3Δ0 nup170Δ::hphR set3Δ::kanR Gle1-GFP-HIS3*	This study
DVY1744	*MAT*α *his3Δ0 leu2Δ0 ura3Δ0 nup170Δ::hphR swc1Δ::kanR Gle1-GFP-HIS3*	This study
DVY1745	*MAT*α *his3Δ0 leu2Δ0 ura3Δ0 nup170Δ::hphR swr1Δ::kanR Gle1-GFP-HIS3*	This study
DVY1512	*MAT***a** *his3Δ1 leu2Δ0 ura3Δ0 met15Δ0 lys2Δ0 ESC1-GFP-HIS3**	This study
DVY1514	*MAT***a** *his3Δ1 leu2Δ0 ura3Δ0 met15Δ0 lys2Δ0 ESC1-GFP-HIS3 nup170Δ::hphR**	This study
DVY1588	*MAT his3Δ1 leu2Δ0 ura3Δ0 met15Δ0 lys2Δ0 MPS3-mRFP-HIS3**	This study
DVY2119	*MAT his3Δ1 leu2Δ0 ura3Δ0 met15Δ0 lys2Δ0 MPS3-mRFP-HIS3 nup170Δ::hphR**	This study
DVY1595	*MAT***a** *his3Δ1 leu2Δ0 ura3Δ0 met15Δ0 NUP82-GFP-HIS5 NUP159-mRFP-natR*	This study
DVY2108	*MAT***a** *his3Δ1 leu2Δ0 ura3Δ0 met15Δ0 NUP170-GFP-HIS5 NUP53-mCHERRY-natR*	This study
DVY2109	*MAT***a** *his3Δ1 leu2Δ0 ura3Δ0 met15Δ0 NUP170-GFP-HIS5 NUP159-mRFP-natR*	This study

DVY2032	*MAT***a** *his3Δ1 leu2Δ0 ura3Δ0 met15Δ0 SIR4-GFP-HIS3 NUP60-mCHERRY*	This study
GA1461	*MAT***a** *leu2-3,112 ura3-1 trp1-1 ade2-1 can1-100 ARS607::lacO-4xlexA^{op}-TRP1 his3-11,15::GFP-LacI-HIS3 nup49::NUP49-GFP-URA3*	Taddei et al., 2004
DVY2043	*MAT leu2-3,112 ura3-1 trp1-1 ade2-1 can1-100 ARS607::lacO-4xlexA^{op}-TRP1 his3-11,15::GFP-LacI-HIS3 SEC63-GFP-NAT**	Derived from GA1461
DVY2048	*MAT leu2-3,112 ura3-1 trp1-1 ade2-1 can1-100 ARS607::lacO-4xlexA^{op}-TRP1 nup170Δ::kanR his3-11,15::GFP-LacI-HIS3 SEC63-GFP-natR**	Derived from GA1461
DVY2051	*MAT leu2-3,112 ura3-1 trp1-1 ade2-1 can1-100 ARS607::lacO-4xlexA^{op}-TRP1 esc1::kanR his3-11,15::GFP-LacI-HIS3 SEC63-GFP-natR**	Derived from GA1461
DVY1052	*MAT***a**/α *his3Δ1/his3Δ leu2Δ0/leu2Δ0 ura3Δ0/ura3Δ0 MET15/met15Δ0 LYS2/lys2Δ0 NUP170/nup170Δ::natR ELM1/elm1Δ::kanR*	This study
DVY1499	*MAT***a**/α *his3Δ1/his3Δ leu2Δ0/leu2Δ0 ura3Δ0/ura3Δ0 MET15/met15Δ0 LYS2/lys2Δ0 NUP170/nup170Δ::natR ITC1/itc1Δ::kanR*	This study
DVY1000	*MAT***a**/α *his3Δ1/his3Δ leu2Δ0/leu2Δ0 ura3Δ0/ura3Δ0 MET15/met15Δ0 LYS2/lys2Δ0 NUP53/nup53Δ::kanR*	This study
DVY1000.1	*MAT***a**/α *his3Δ1/his3Δ leu2Δ0/leu2Δ0 ura3Δ0/ura3Δ0 MET15/met15Δ0 LYS2/lys2Δ0 NUP60/nup60Δ::kanR*	This study
DVY1126	*MAT***a**/α *his3Δ1/his3Δ leu2Δ0/leu2Δ0 ura3Δ0/ura3Δ0 MET15/met15Δ0 LYS2/lys2Δ0 NUP157/nup157Δ::URA3*	This study
DVY1128	*MAT***a**/α *his3Δ1/his3Δ leu2Δ0/leu2Δ0 ura3Δ0/ura3Δ0 MET15/met15Δ0 LYS2/lys2Δ0 NUP2/nup2Δ::kanR*	This study
DVY1134	*MAT***a**/α *his3Δ1/his3Δ leu2Δ0/leu2Δ0 ura3Δ0/ura3Δ0 MET15/met15Δ0 LYS2/lys2Δ0 NUP188/nup188Δ::kanR*	This study
DVY1540.1	*MAT***a**/α *his3Δ1/his3Δ leu2Δ0/leu2Δ0 ura3Δ0/ura3Δ0 MET15/met15Δ0 LYS2/lys2Δ0 SIR2/sir2Δ::kanR*	This study

* These strains were isolated from matings; alleles for *MAT*, *ura3*, *his3*, *leu2*, *met15* and *lys2* were, therefore, not determined.

2.2 Plasmids

The following plasmids were provided by others and used in this thesis: pRS313, *CEN/HIS3* (Sikorski and Hieter, 1989); pRS315, *CEN/LEU2* (Sikorski and Hieter, 1989); pHNP170, pRS315 containing the *NUP170* ORF (Aitchison et al., 1995a); pRS316, *CEN/URA3* (Sikorski and Hieter, 1989); pRS316A-NUP170,

pRS316 containing the *NUP170* and *ADE3* ORFs (Marelli et al., 1998). For expression of LexA fusion proteins the following plasmids were a gift of Dr. Susan Gasser, Friedrich Miescher Institute, Basel, Switzerland: pAT4, 2*μ*/*LEU2* containing P_{ADH1}-*lexA* (Taddei et al., 2004); pAT4-SIR4^{PAD}, pAT4 containing Sir4p residues 960-1262 (Taddei et al., 2004); pAT4-ESC1^{C}, pAT4 containing Esc1p residues 1124-1658 (Taddei et al., 2004); pAT4-yku80-4, pAT4 containing *yku80-4*^{P437L} (Taddei et al., 2004). Galactose inducible expression of full length *NUP170* and truncations of *NUP170* the following plasmids were gifts of Dr. David S. Goldfarb, University of Rochester, Rochester, NY, USA: pNS276 ($P_{GAL1/10}$), pNS288 ($P_{GAL1/10}$-*NUP170*$^{1-1502}$; full length *NUP170* aa 1-1502), pNS312 ($P_{GAL1/10}$-*NUP170*$^{1-750}$), pNS313 ($P_{GAL1/10}$-*NUP170*$^{750-1502}$), pNS333 ($P_{GAL1/10}$-*NUP170*$^{500-1502}$), pNS337 ($P_{GAL1/10}$-*NUP170*$^{1000-1502}$). The plasmid pTM1046 (pFA6a-kanMX6-P_{MET3}-*HA3*) was used to integrate the P_{MET3}-*HA3-STH1* DNA cassette and has been described previously (Makio et al., 2009). Genomic integrations of carboxy-terminal gene fusions were carried out by generating PCR products derived from plasmids pGFP/HIS5 (*EGFP*^{F64L,S65T}-*HIS5*; Dilworth et al., 2001), pmCherry/NAT (*mCherry-NatR*) and pRFP/NAT (*mRFP-NatR*) were kind gifts from Dr. Richard Rachubinski, University of Alberta, AB, Canada; pProtA/HU (*protein A-HIS3-URA3*; Aitchison et al., 1995a); pBXA (*protein A-HIS5*; Aitchision et al., 1995), pFA6a-13Myc-kanMX6 (*13xMYC-KanR*; Longtine et al., 1998), pYM20 (*9xMYC-HphR*; Janke et al., 2004), and pYM21 (*9xMYC-NatR*; Janke et al., 2004).

The following plasmids were generated for this work in which the inserts were PCR-amplified from genomic DNA using the Expand High Fidelity PCR system (Roche Applied Science, Indianapolis, IN, USA). The plasmid pRS316-NUP60 was generated by introducing a 2.5 kb PCR product that includes the *NUP60* ORF plus its flanking endogenous promoter and terminator sequences, nucleotides -455 to +2070, into SpeI digested pRS316 (Sikorski and Hieter, 1989). To generate pGEX-6P1-NUP60, the entire *NUP60* ORF, nucleotides +1 to +1620, was amplified from yeast genomic DNA and inserted into BamHI digested pGEX-6P1 (GE Healthcare, Chalfont St. Giles, United Kingdom).

2.3 Antibodies

Table 2-2. Antibodies.

Antibody Reactivity	Antibody name	Raised in	Dilution for Western blot	Reference
GFP	3B4 Final Bleed	rabbit	1:5000 in PBS-T	R.J. Scott
Gsp1p	4G9 Final Bleed	rabbit	1:10000 in PBS-T	R.J. Scott
HA	F-7 (sc-7392)	Mouse	1:3333 in PBS-I	Santa Cruz Biotechnology Inc.
Myc	9E10	Mouse	1:5000 in PBS-I	Roche Applied Science
Nup53p	H174 Final Bleed	Rabbit	1:5000 in PBS-T	Marelli et al., 1998
Nup60p	4-5 Final Bleed	Rabbit	1:5000 in PBS-T	This study
protein A	Gsp1p (4G9 FB)	rabbit	1:10000 in PBS-T	R.J. Scott
Rsc3p	Rsc3p (aa237-456)	rabbit	1:1000 in PBS-T	Angus-Hill et al., 2001
Rsc30p	Rsc30p (aa652-875)	rabbit	1:1000 in PBS-T	Angus-Hill et al., 2001
Mouse IgG	Anti-mouse IgG, HRP-conjugated (NXA931)	sheep	1:10000 in PBS-T	GE Healthcare
Rabbit IgG	Anti-rabbit IgG, HRP-conjugated (NA934)	donkey	1:10000 in PBS-T	GE Healthcare

2.3.1 Generation of antibodies against Nup60p

Plasmid pGEX 6P1-NUP60 was transformed into *Escherichia coli* strain BL21 codon and 50-250 mL cultures were grown at 37˚C to an OD_{550} ~1.0, at which point expression of GST-Nup60p was induced with 0.5 M IPTG for 3.5 h at 23˚C. Following induction, cells were harvested by centrifugation (Eppendorf 5810R, A-4-62 rotor at 6000 x g for 10 min) and then resuspended in 15 mL GST Lysis Buffer containing 300 mM NaCl (see Table 2-3) per 50 mL of cell culture volume. Cell lysis was facilitated by the addition of lysozyme (0.67 mg/mL) and incubation on ice for 20-30 min. Lysates were vigorously sonicated to shear DNA (Branson 250 Sonifier output level 6 for 30 sec followed by incubation on ice for 2 min and repeated until lysate becomes transparent). Sonicated lysates were then cleared by centrifugation (Beckman Coulter, JA17 rotor at 14,000 rpm for 20 min at 4˚C). Cleared lysates were then incubated with ~125 μL of pre-equilibrated glutathione sepharose 4B beads (GE Healthcare, Chalfont St. Giles, United Kingdom) for 1.5 h at 4˚C with rotation. Following binding, beads were washed four times with 1 mL of GST Lysis Buffer containing 300 mM NaCl. Washed beads were then resuspended in 1 mL of GST Lysis Buffer supplemented with 4.5 mg/mL ATP and 10 mM $MgSO_4$ and incubated in a 37˚C water bath for 10 min to dislodge non-specifically bound heat shock proteins. Beads were then washed twice with 1 mL GST Lysis Buffer and then resuspended in 100-300 μL of GST Lysis Buffer. Bound GST-Nup60p was then cleaved with 3 U of PreScission protease (GE Healthcare, Chalfont St. Giles, United Kingdom) for 3 h at 4˚C. Cleaved Nup60p was incubated with ~30 μL of pre-equilibrated Glutathione

sepharose beads to remove excess PreScission Protease. The quantity of purified Nup60p was determined by Bradford Assay (Bio-Rad Laboratories Inc., Hercules, CA, USA) while quality was assessed by SDS-PAGE and coommassie blue staining.

New Zealand White Rabbits were immunized against purified Nup60p. For the initial immunization, 100 μg of Nup60p was emulsified in 800 μL of PBS buffered Freud's Complete Adjuvant (Sigma-Aldrich, St. Louis, MO, USA). Subsequent booster injections used 100 μg purified Nup60p emulsified in PBS buffered Freud's Incomplete Adjuvant (Sigma-Aldrich, St. Louis, MO, USA). Rabbits were immunized monthly and antibody titres were monitored two weeks post-injection by western blotting using WT, *nup60Δ* and *NUP60-GFP* cell lysates as controls. The resulting antibodies (anti-Nup60p 4-5 and anti-Nup60p 4-6) were subsequently used at a 1:5000 dilution for western blot analyses. For a complete list of antibodies used in this work, see Table 2-2.

Table 2-3. Buffers.

Buffer	Composition
FACS buffer	50 mM Tris-HCl, pH8.0
GST lysis buffer	10 mM Tris-HCl, pH 7.5, 150 mM KOAc, 2 mM MgOAc, 10% glycerol, 0.1% Igepal CA-630
IP buffer	20 mM HEPES-KOH, pH 7.4, 110 mM KOAc, 2 mM $MgCl_2$, 0.1% Tween-20, 1:5000 dilution antifoam B
K-Pi buffer	100 mM potassium phosphate, pH 6.5
PBS	137 mM NaCl, 2.7 mM KCl, 4.3 mM Na_2HPO_4, 1.4 mM KH_2PO_4, pH 7.4
Pi-citrate buffer	170 mM KH_2PO_4, 30 mM sodium citrate, pH 5.8
pre-lysis IP wash buffer	20 mM HEPES-KOH, pH 7.4, 110 mM KOAc, 2 mM $MgCl_2$
SDS-PAGE sample buffer	0.5 M Tris-base, 100 mM DTT, 15% glycerol, 6.5% SDS, 0.25% bromophenol blue

sodium phosphate buffer	81 mM Na_2HPO_4, 19 mM NaH_2PO_4, pH 7.4
TE	10 mM Tris-HCl, 1 mM EDTA, pH 7.5
TES buffer	10 mM Tris-HCl, 10 mM EDTA, pH 7.5, 0.5% SDS
transformation buffer	10 mM Tris-HCl, pH 7.5, 1 mM EDTA, 100 mM LiOAc

2.4 Affinity purification

2.4.1 Affinity purification of protein A fusion proteins

Nup84p, Nup157p, Nup170p, Nup188p, Sir4p, and Sth1p were C-terminally tagged with the *Staphylococcus aureus* protein A (pA) and affinity purified from yeast whole cell lysates as previously described (Alber et al., 2007a) with slight modification. Yeast cells synthesizing the respective proteins Nup84-pA, Nup157-pA, Nup170-pA, Nup188-pA, Sir4-pA or Sth1-pA were grown in 1 L cultures of YPD medium to an OD_{600} of 0.8-1.0 and then harvested by centrifugation (Beckman Coulter; JLA 10.5, 5000 x g for 3 min at 23˚C). Protein A purification from cell cycle arrested cells were performed from cultures grown to an OD_{600} 1.3 in 500 mL of YPD. Cells were washed twice with 100 mL ddH_2O and once with 100 ml Pre-lysis IP Wash buffer (see Table 2-3). Washed cells were pelleted and the resulting cell pellet was transferred to a syringe. Cells were then flash frozen by passage into liquid nitrogen to generate frozen yeast "noodles". Frozen cells were subsequently lysed using a planetary ball mill (PM100; Retsch, Haan, Germany; ~12 cycles at 450 rpm for 2 min with intermittent cooling in liquid N_2) generating 0.8-1.0 g of lysed cell powder. The lysed cell powder was briefly warmed on ice to ~4˚C prior to resuspension in cold IP buffer containing protease inhibitor pellets (Roche Applied Science,

Indianapolis, IN, USA) at a 1:2 ratio, 1 g of lysed cell powder to 2 mL IP buffer for 30 min on ice. Thawed lysates were then cleared by centrifugation (Eppendorf 5810R, A-4-62 rotor at 1500 x g for 10 mins at 4˚C). IgG-conjugated magnetic beads were added to cleared lysates at a ratio of 3 mg of beads to 2 mL of cleared lysates and incubated with rotation for 1 h at 4˚C. Epoxy-activated Dynabeads (Invtirogen, Carlsbad, CA, USA) were conjugated with rabbit IgG (Sigma-Aldrich, St. Louis, MO, USA); see section 2.4.2 for procedures. Following incubation, magnetic beads were separated with a magnet and washed 10 times with 1 mL of cold IP Buffer. Bead-bound protein complexes were eluted using a step gradient of 50, 500, and 2000 mM $MgCl_2$ followed by a final elution of 0.5 M acetic acid. For each elution step, proteins were eluted in 500 μL volumes for 3 min at 4˚C with rotation. Eluates were TCA precipitated overnight at 4˚C and lyophilized in a CentriVap Centrifugal Vacuum (15 mins; Labconco, Kansas City, MO, USA) and analyzed by SDS-PAGE and western blotting.

2.4.2 IgG-conjugated magnetic beads

Conjugation of IgG to magnetic beads was performed as previously described (Alber et al., 2007a). In brief, 8 mg rabbit IgG (Sigma-Aldrich, St. Louis, MO, USA) was dissolved in 800 μL sodium-phosphate buffer (0.1 M $NaPO_4$ pH 7.4) and then cleared by centrifugation (Eppendorf 5810R, F45-30-11 rotor at 20800 x g for 10 min at 4˚C). To the cleared IgG, 2 mL sodium-phosphate buffer was added followed by 1.33 mL of 3 M ammonium sulfate pH 7.5 and the solution was then passed through a 0.22 μm low-protein binding PVDF filter

syringe (Millipore, Billerica, MA, USA). The filtered IgG solution was used to resuspend 60 mg of pre-washed Epoxy M-270 Dynabeads (Invitrogen, Carlsbad, CA, USA). Prior to IgG addition, magnetic beads were equilibrated with 3.6 mL sodium-phosphate buffer with rotation for 10 min at room temperature and then washed once with 1 mL sodium-phosphate buffer. Conjugation of IgG to the magnetic beads was facilitated by incubation at 30˚C for 18-24 h with rotation. Following incubation, IgG-conjugated beads were washed extensively with rotation in the following order: once with 1 mL 100 mM glycine pH 2.5, once with 1 mL 10 mM Tris pH 8.8, once with 1 mL 100 mM triethylamine pH 6.0, four times with 1 mL PBS for 5 min, once with 1 mL PBS + 0.5% triton X-100 for 5 min, once with 1 mL PBS + 0.5% triton X-100 for 15 min, followed by three consecutive washes with 1 mL PBS for 5 min. Washed beads were then resuspended in 2 mL PBS + 0.02% sodium azide and stored at 4˚C.

2.5 Western blotting

Protein samples were resolved by SDS-PAGE gels containing 6-10% acrylamide in BioRad Mini Protean III units (BioRad, Hercules, CA, USA) and then transferred to nitrocellulose membranes using a GE Healthcare TE 22 Mini Tank Transfer Unit (GE Healthcare, Chalfont St. Giles, United Kingdom; 100 V for 1.5 h at 4˚C). The transfer efficiency of proteins was assessed by amido-black staining and excess stain was removed with extensive H_2O washes. Post-transfer nitrocellulose membranes were blocked with 5% skim milk powder resuspended in PBS-T (PBS containing 0.1% Tween-20) for 1 h at 23˚C. Primary antibodies

listed in Table 2-2 were used to detect proteins of interest by probing membranes overnight at 4˚C in 5% skim milk powder resuspended in PBS-T. Membranes were then washed three times with liberal volumes of PBS-T or PBS-I (PBS containing 0.05% Igepal; for anti-HA and anti-Myc primary antibodies) for 10 min. Bound primary antibodies were detected using sheep anti-mouse or donkey anti-rabbit HRP-conjugated secondary antibodies (see Table 2-2) and ECL detection (GE Healthcare, Chalfont St. Giles, United Kingdom). Exposure times varied between 15 sec and 45 min.

2.6 Cell-cycle arrests

All cell-cycle arrests were performed in YPD medium and were monitored microscopically for cell morphology and/or for DNA content by FACS analysis. To arrest cells in G1-phase, cells were grown to early-mid logarithmic growth phase (OD_{600} 0.3-0.5) and then arrested with either 7 μg/mL α-factor (Sigma-Aldrich, St. Louis, MO, USA) for *BAR1* strains or 50 ng/mL α-factor for *bar1Δ* strains for 2.5 h at 25˚C. G1 arrest was monitored microscopically for accumulation of cells with a shmoo phenotype. For arrest and release experiments, cells were harvested and then washed extensively with YPD medium prior to release into fresh YPD medium at 25˚C.

For S-phase arrests, cells were grown to early-mid logarithmic growth phase (OD_{600} 0.3-0.5) and arrested with 200 mM hydroxyurea (Sigma-Aldrich, St. Louis, MO, USA) for 2.5 h at 25˚C. Arrest efficiency was monitored microscopically for accumulation of large-budded cells.

To arrest cells in G2/M-phase, early-mid logarithmic growth phase cells were treated with 15 mg/mL nocodazole (Calbiochem, Division of Merck KGaA, Darmstadt, Germany) for 2.5 h at 25˚C. G2/M arrest was confirmed microscopically by accumulation of large-budded cells.

2.7 FACS analysis

Cells were fixed in 70% EtOH overnight at 4˚C. Following fixation cells were washed once with FACS buffer (see Table 2-3) and resuspended in 500 μL of FACS buffer. RNA was degraded by the addition of 1 mg/mL RNase A (Sigma-Aldrich, St. Louis, MO, USA) and incubation for 2 h at 37˚C with rotation. RNase A digested cells were then pelleted and resuspended in pepsin solution (5 mg/mL pepsin dissolved in acidic ddH_2O pH ~2.0) with rotation for 1 h at 37˚C. Cells were then washed once with FACS buffer followed by staining of DNA by resuspension in 200 μl of propidium iodide solution (180 mM Tris-HCl pH 7.5, 190 mM NaCl, 70 mM $MgCl_2$, and 50 ng/mL propidium iodide) for 1 h at 23˚C with rotation. Cells were then diluted 1 to 25 with FACS buffer and sonicated for 3 min in a water bath (FS30 Sonic Cleaner, Thermo Fisher Scientific Inc., Waltham, MA, USA) immediately prior to data collection by a FACScan (BD Biosciences, San Jose, CA, USA). Data analysis was performed using CellQuest software (BD Biosciences, San Jose, CA, USA).

2.8 Chromosome loss assays

2.8.1 Haploid chromosome loss assay

For quantification of chromosome missegregation events, both chromosome loss (1:0 segregation) and non-disjunction (2:0 segregation), haploid yeast strains were derived from the YPH278 background containing the ochre allele *ade2-101* and bearing a non-essential chromosome fragment, CFIII (*CEN3.L.YPH278*), which carries the ochre suppressor tRNA gene, *SUP11* (Spencer et al., 1990). In haploids, *ade2* mutations, such as the ochre allele *ade2-101,* confer a red colony phenotype. However, the presence of a single copy of *SUP11* suppresses the *ade2-101* allele and gives rise to a wild type, white colony phenotype. Haploid cells were grown to an OD_{600} ~1.0 and then plated at a density of ~500 colonies per plate on YPD medium for 2-4 d at 30˚C, followed by an additional 10 d at 4˚C to facilitate pigment development. Loss of the ochre suppressor gene *SUP11,* due to chromosome missegration during the first mitotic division, was indicated by the formation of half-red, half-white colonies. The frequency of these events expressed as a percentage was calculated by dividing the number of half-red, half-white colonies by the total number of colonies.

2.8.2 Diploid chromosome loss assay

For analysis of chromosome segregation defects, diploid yeast strains were derived from the YPH277 background containing the ochre allele *ade2-101* and bearing one copy of a non-essential chromosome fragment, CFVII (*RAD2.d.YPH277*), carrying the ochre suppressor tRNA gene *SUP11* (Spencer et

al., 1990). A single copy of *SUP11* in *ade2-101/ade2-101* homozygous diploid cells results in partial suppression of the ochre mutation, resulting in pink colonies. Cells were grown to an OD_{600} ~1.0 and plated at a density of ~500 colonies per plate on YPD medium for 2-4 d at 30˚C followed by an additional 10 d at 4˚C to facilitate pigment development. Chromosome loss events were indicated by the formation of red colonies and non-disjunction events were indicated by the formation of white colonies.

2.9 Mating pheromone secretion assay

A single colony derived from a haploid yeast strain hypersensitive to either the mating pheromone **a**-factor or α-factor (yeast strains DVY1190 [*MAT*α *sst2Δ* $ste3^{L194Q}$] and DVY1191 [*MAT***a** *bar1Δ*], respectively; gifts from Dr. Neil Adames) were selected and resuspended in 1 mL of ddH_2O. Cells were then further diluted by a factor of 10 with ddH_2O. 200 μL of diluted cells were then spread evenly over the surface of a YPD plate to generate a cell lawn and allowed to dry (~15 min). Once dry, single colonies of the yeast strains of interest were streaked over top of the cell lawn and incubated at 30˚C for 2-3 d. Secretion of α-factor by the strain of interest was indicated by growth inhibition of the lawn formed by *MAT***a** DVY1191 cells, resulting in the formation of a halo surrounding the strain of interest. Conversely, secretion of **a**-factor by the strain of interest resulted in a halo of growth inhibition of the lawn formed by *MAT*α DVY1190 cells.

2.10 Synthetic genetic array analysis

For each query strain, synthetic genetic array (SGA) analyses were performed in duplicate as previously described (Tong et al., 2001) with minor modification. Query strains DVY0101 (*nup60Δ*) harboring pRS316-NUP60, DVY0102 (*nup170Δ*) harboring pRS316A-NUP170, and DVY0100 (*nup53Δ*) encoding *HIS3* under control of the *MAT***a** specific *MFA1* promoter and *LEU2* under control of the *MAT*α specific promoter *MFalpha1* (*can1Δ::*P_{MFA1}-*HIS3*-$P_{MFalpha1}$-*LEU2*) were mated to a collection of ~4985 individual yeast deletions arrayed in quadruplicate such that each deletion mutant was represented by four individual colonies (Winzeler et al., 1999; Open Biosystems, Huntsville, AL, USA). The resulting diploid cells were then pinned to sporulation medium. Following sporulation, haploid meiotic progeny of the *MAT***a** mating type were selected for growth on SC medium lacking histidine. Lastly, selected *MAT***a** progeny were then pinned to medium to select for growth of either single or double deletion mutants using an automated Qpix colony picker (Genetix, San Jose, CA, USA). Plates for final selection of single and double deletion mutants derived from query strains DVY0101 (*nup60Δ*) and DVY0102 (*nup170Δ*) and contained 1 mg/mL 5-FOA (Toronto Research Chemicals, North York, ON, Canada) to select against plasmids pRS316-NUP60 and pRS316A-NUP170, respectively. Reduced fitness was determined by visual inspection of colony size. Genetic interactions were scored if ≥ 3 of 4 double mutant colonies displayed reduced fitness in two independent SGA analyses. Gene deletions that previously displayed a synthetic fitness defect with a wild type strain (Tong et al., 2001) were

removed from further analysis, as were genes genetically linked to the query gene (defined as genes separated by ≤ 10 centimorgan, ~25 kb). Genetic interactions were confirmed by tetrad analysis of heterozygous double mutants generated by mating DVY0101, DVY0102 and DVY0100 to the gene deletion strain of interest contained in the yeast deletion collection (Open Biosystems, Huntsville, AL, USA). Genetic interaction networks were generated using *Cytoscape v2.8.2* software (Shannon et al., 2003).

2.11 Gene silencing assays

2.11.1 Subtelomeric gene silencing assay

Yeast strains used in the assessment of subtelomeric gene silencing are derivatives of UCC3505, in which the reporter genes *URA3* and *ADE2* are integrated adjacent to Tel7L and Tel5R, respectively (Singer et al., 1994). Specifically, introduction of *URA3* and an adjacent 81 bp sequence of telomeric repeats (TG_{1-3}) into chromosome VII at *ADH4* resulted in a ~15 kb truncation of the left arm of chromosome VII and the removal of native subtelomeric elements. Consequently, in these cells, the 81 bp telomeric sequence is extended to ~300 bp by telomerase, generating a new telomere (*adh4:URA3-TEL*) such that the *URA3* promoter is located ~1.3 kb from Tel7L with transcription directed towards the telomere (Gottschling et al., 1990; Singer et al., 1994). The *ADE2* gene and an adjacent 81 bp sequence of telomeric repeats (TG_{1-3}) was integrated directly into the Y' element of Tel5R creating a new telomere, *ADE2-TEL,* with minimal truncation of chromosome V-R (Singer et al., 1994).

10-fold serial dilutions of cell cultures were spotted onto one of three sets of plates: 1) YPD medium, 2) synthetic complete medium (SC), SC-ura-ade and SC + 1 mg/mL 5-FOA, or 3) SC-leu, SC-leu-ura-ade and SC-leu + 1 mg/mL 5-FOA when required to maintain selection of pRS315 or pRS315-NUP170. Plates were incubated for 2-5 d at 30˚C and then placed at 4˚C for an additional 10 d to permit color development.

2.11.2 Assaying gene silencing at the silent mating type loci

Yeast strains used in the assessment of gene silencing at the mating type loci are derivatives of either ROY648 (*URA3* reporter gene inserted between the *E* and *I* silencers of the *HMR* locus at ChrIII coordinate 292140, ~640 bp to the right of *HMR-E;* Donze et al., 1999), or KIY54 (*ADE2* and *URA3* reporter genes inserted between the *E* and *I* silencers of the *HML* locus, *HML-E-4xUAS*$_{GAL}$-*ADE2-4xUAS*$_{GAL}$-*URA3-I*$^{\Delta 242}$; Ishii et al., 2002; Dilworth et al., 2005). 10-fold serial dilutions of cell cultures were spotted onto SC-leu, SC-leu-ura-ade, and SC-leu + 1 mg/mL 5-FOA. Plates were incubated for 2-5 d at 30˚C and then placed at 4˚C for an additional 10 d to permit color development.

2.12 Gene Expression analyses

2.12.1 Isolation of yeast RNA

Cells were grown to an OD_{600} 0.8-1.0 in 10 mL YPD cultures and harvested by centrifugation (Eppendorf 5810R, A-4-62 rotor at 6000 x g for 2 min). Cell pellets were then flash frozen in liquid nitrogen and total RNA was

subsequently isolated using the hot acidic phenol extraction method. In brief, cell pellets were resuspended in 1.2 mL RNase free TES buffer (for a list of buffers see Table 2-3) and 1.2 mL unbuffered acidic phenol and vortexed vigorously for 4 min prior to incubation in a 60˚C water bath for 1 h. Following incubation, the resulting cell lysates were centrifuged (Eppendorf 5810R, A-4-62 rotor at 6000 x g for 5 min). The aqueous layer was then re-extracted with an equal volume of acidic phenol and brief vortexing prior to centrifugation (Eppendorf 5810R, A-4-62 rotor at 6000 x g for 2 min). To facilitate removal of residual phenol from the newly isolated aqueous solution, a 24:1 chloroform to iso-amyl alcohol solution was added followed by a brief vortex and centrifugation (Eppendorf 5810R, A-4-62 rotor at 6000 x g for 5 min). From the resulting aqueous phase total RNA was precipitated with 95% EtOH and 3 M NaOAc (made with DEPC treated ddH_2O) at -20˚C overnight. Precipitated RNA was pelleted (Eppendorf 5810R, A-4-62 rotor at 6000 x g for 30 min at 4˚C) and washed once with 70% EtOH. Washed RNA was re-pelleted (Eppendorf 5810R, A-4-62 rotor at 6000 x g for 30 min at 4˚C) and allowed to dry for 3 h prior to resuspension in DEPC treated ddH_2O. RNA quality was evaluated by agarose gel electrophoresis under denaturing conditions and RNA quantity was determined by spectrophotometry.

2.12.2 Semi-quantitative RT-PCR

RNA was isolated from yeast cells using hot acidic phenol (see section 2.12.1) and 2 μg of total RNA was treated with DNaseI (Invitrogen, Carlsbad, CA, USA) and incubated for 15 min at 23˚C. The DNaseI digestion was quenched

by the addition of 1 μL of 25 mM EDTA and incubation for 10 min at 65˚C. cDNA was generated from the DNaseI treated RNA using random primers and SuperScript II Reverse Transcriptase (Invitrogen, Carlsbad, CA, USA) according to the manufacturers directions.

For PCR-amplification of each target cDNA, 10% of the first-strand synthesis product was used. Primers for PCR-amplification of target cDNAs were designed to anneal within the 5'-end of the coding regions of their target cDNAs and generate PCR products 110-120 bp in length. All oligonucleotide sequences used in RT-PCR are listed in Table 2-4. For each primer set the number of PCR cycles required to provide efficient, exponential amplification of the target cDNA, while preceding the linear plateau phase of amplification was determined and are listed within the appropriate figures. PCR products were resolved by agarose gel electrophoresis containing 2% agarose and imaged with a UV transilluminator (LM26E; Alpha Innotech, a division of Protein Simple, Santa Clara, CA, USA) and a CCD camera controlled by *FluorChem* software (Alpha Innotech, a division of Protein Simple, Santa Clara, CA, USA). To avoid pixel saturation, multiple dilutions of each PCR product were resolved and multiple exposure times were taken. Expression levels of the *ACT1* and/or *TUB2* genes were determined as load controls.

Table 2-4. Oligonucleotides used in semi-quantitative RT-PCR

Target cDNA	Oligonucleotide sequence	
ACT1	Forward:	CATCCCATTTAACTGTAAGAAGAAT
	Reverse:	GATCAGTCAATATAGGAGGTTATGG
ASG7	Forward:	GCATCAAGTATTGAGCATAAAACAA
	Reverse:	CACACTCATTTTACATGATTTGCAT
BAR1	Forward:	TAGATATAGGTACACCGTCCCAAAG
	Reverse:	GTATTTGAATTTGGTAAGCAGAAGG
COS12	Forward:	GAGGACGAATACTTACATGTTTGAG
	Reverse:	AGATACAGGGGTACTGAAATACCAT
HMLα2	Forward:	ACAGATGAGTTTAAATCCAGCATAC
	Reverse:	ATCCCTTAATTCAACTTCTTCTTCT
NUP170	Forward:	CTAACGGTAATGGCGGATTTTCTCA
	Reverse:	TTGACATGGGTCCTTCCAGTGATTT
PHO5	Forward:	CAACTGACGCTAGTACTTTATTCTC
	Reverse:	GTAATGGACTAATTCATCCTTGGTG
STE2	Forward:	CACTTTAGGGATTGCTACAGTTACC
	Reverse:	TGGATGCATTGAAGTATTTATCTTG
STE3	Forward:	TATGGCTTTATGTTTTGATGTCTTA
	Reverse:	AAGTACAAATCCTAGTTTGATGGAA
STE6	Forward:	ACAGCGTTGTACCCTATTTAATGAT
	Reverse:	TAAATGTCTATTTTCATTGGTGCTG
TDA8	Forward:	TCTTACACGTTCAGGTTTGCTAAGG
	Reverse:	TTGTGGATGTAATTGGAGGTTGCTC
TUB2	Forward:	TACTAGTGAAGGTATGGACGAATTG
	Reverse:	TTCTTCATCATCTTCTACAGTAGCC
VBA5	Forward:	ATGGAGGAAACTAAGTACTCTTCGC
	Reverse:	GGAAAGTCCCATTGGAGAATCATTG
YEL073C	Forward:	GCATGGTCTAATACAGTTCCGTTAG
	Reverse:	AAGGGTTTCATTCATCCAGATTACG
YFR057W	Forward:	TCTTTGCGTGGCAATATACCTCATA
	Reverse:	TCTGAGACGAAGTCGTTGCTAAAAT

2.12.3 Genome-wide gene expression profiling

Wild type, *nup157Δ*, *nup170Δ*, and *nup188Δ* cells were grown in YPD medium to mid-logarithmic phase, harvested and the cell pellets were immediately frozen in liquid nitrogen. Total RNA was isolated from cell pellets using hot acidic phenol (see section 2.12.1). For Sth1p depletion experiments, P_{MET3}-*HA3-STH1* cells were grown in SC medium lacking methionine to mid-logarithmic phase (0 h) and *STH1* was shut-off by the addition of methionine to a final concentration of 200 μg/mL for 8 h. Following 8 h of shut-off, methionine was removed by extensive washes with SC medium lacking methionine and *STH1* was reinduced by growth in SC medium lacking methionine for an additional 4 h (R4 h). Samples were taken at 0 h, 2 h, and R4 h, at which time cells were immediately pelleted and then flash frozen in liquid nitrogen. Total RNA was isolated from frozen cells using the hot acidic phenol extraction method. Labelling of cDNA and hybridization reactions were performed as described previously (Smith et al., 2007). Two-color microarrays comparing RNA between: 1) WT and *nup157Δ*, 2) WT and *nup170Δ*, 3) WT and *nup188Δ*, 4) P_{MET3}-*HA3-STH1* (0 h and 2 h), and 5) P_{MET3}-*HA3-STH1* (0 h and R4 h) were performed using Agilent whole-genome *S. cerevisiae* arrays (Agilent Technologies Inc., Santa Clara, CA, USA). For each condition, duplicate experimental and duplicate technical replicates were performed. Identification of differentially expressed genes was achieved by maximum-likelihood analysis, lambda ≥ 100 (Ideker et al., 2000; Smith et al., 2002), and genes with a ≥ 2-fold change in expression were considered significantly affected. In determining the gene expression profile of

Sth1p depleted cells methionine responsive genes, identified by microarray analysis comparing RNA between WT cells grown in the presence and absence of methionine, were omitted from analysis.

2.13 Chromatin immunoprecipitation

For each chromatin immunoprecipitation (ChIP) experiment, yeast strains producing C-terminally tagged 9xMyc fusion proteins were grown in YPD medium to an OD_{600} of 1.0 and then harvested. Chromatin immunoprecipitations were performed as described previously (Smith et al., 2007 and Wan et al., 2009). In brief, proteins were cross-linked to their respective DNA binding sites with 1% formaldehyde for 1 h at room temperature. The cross-linking reaction was quenched by a 5 min incubation with 125 mM glycine. Cells were then disrupted by glass bead lysis and the chromatin sheared to an average size of 400 bp. Sheared chromatin lysates were incubated with anti-Myc conjugated magnetic beads overnight at 4˚C with rotation. To prepare magnetic beads, 50 μL of Dynabead Pan Mouse IgG magnetic beads (Invitrogen, Carlsbad, CA, USA) were conjugated with 2 μg of anti-Myc antibody (9E10; Roche Applied Science, Indianapolis, IN, USA). 50 μl of prebound beads were added to each sheared chromatin lysate containing 1 mg of total protein. Following incubation, with beads crosslinks were reversed in both the ChIP and whole cell lysate fractions, and samples were analyzed by qPCR or DNA microarrays.

2.13.1 ChIP and qPCR

For quantitative qPCR analysis the ChIP and input DNA were used to amplify target sequences of interest using a DyNAmo Flash SYBR Green qPCR Kit (Finnzymes, Vantaa, Finland) and an iCycler instrument (ABI 7900; Applied Biosystems, Carlsbad, CA, USA). Oligonucleotide sequences used in qPCR are listed in Table 2-5. PCR amplification of each target of interest was compared to amplification of a non-transcribed intergenic region, IGR *iYMR325W,* as an internal control for normalization.

Table 2-5. Oligonucleotides used in qPCR

Target cDNA	Oligonucleotide sequence	
Tel6R 0.5 kb	Forward:	GATAACTCTGAACTGTGCATCCAC
	Reverse:	ACTGTCGGAGAGTTAACAAGCGGC
Tel6R 2.5 kb	Forward:	GAGCAATGAATCTTCGGTGCTTGG
	Reverse:	CGCAGTACCTTGGAAAAATCTAGGC
Tel6R 4.1 kb	Forward:	CGTTCTTCTTGGCCCTTATC
	Reverse:	CATCATCGGTGGTTTTGTCGTG
Tel6R 7.7 kb	Forward:	AAGTCACTATGGGTTGCCGGTATC
	Reverse:	AACTACCTCTATAGGACCTGTCTC
Tel6R 10.0 kb	Forward:	GTCTCGTAGGTAGCTTTCAC
	Reverse:	CGGTGTTCCTTTACAAACCC
Tel6R 12.6 kb	Forward:	GCCACAGAATACTTAGCCGCTGATTC
	Reverse:	GATCCAATTAGAACGGATTAGGCGGG
Tel6R 15.1 kb	Forward:	GCAATCGGTTTCACTTCCTTGG
	Reverse:	CTAGCCTGTGGTTTCTTTGG
Tel6R 17.1 kb	Forward:	GAAAGTTTGGATGCTAGCAAGGGC
	Reverse:	GCATAGCCTTTGAAAACGGCG
Tel6R 20.0 kb	Forward:	AAGAGCTCCCTTACGACGTCATCA
	Reverse:	GGCAAATTCTAAACCAAGAAGCTGG

IGR *iYMR325W*	Forward:	CAGTGTTTGTGGAGCATTTTCTG
	Reverse:	AAGTGACGCATATTCTATACGACCC
HMR A	Forward:	GGATTGTAGTGTTATCTTCA
	Reverse:	CATCCTCAGAGATTGTTCTA
HMR B	Forward:	GCCTACCTTCTTGAACAAGA
	Reverse:	CCGTCCAAGTTATGAGCTTA
HMR C	Forward:	TGACTAAAGTAGAGCAACATACATT
	Reverse:	TCTCATACGTTTATTTATGAACTAC
HMR D	Forward:	TCAATGATTAAAATAGCATAGTCGG
	Reverse:	CAATAGCAATTGTATAAACACATAG
HMR E	Forward:	GGCGATATAATTTATCATGTTTTGG
	Reverse:	TCTCTAACTTCGTTGACAAATTTTC
HMR F	Forward:	CCAATTCCGCATCTGCAGATTACTT
	Reverse:	TTCATTATTTTTCAGATGACGATGG
HMR G	Forward:	GTTCTTCTATATCCGGGTGTACCTAA
	Reverse:	ATCATCCATTGATCAGTATTCATGT
CEN3	Forward:	GCGATCAGCGCCAAACAATATGGA
	Reverse:	AACTTCCACCAGTAAACGTTTCAT
CEN4	Forward:	ACGAGCCAGAAATAGTAACTTTTGC
	Reverse:	TAAGCTATGAAAGCCTCGGCATTTT
ChrV arm region 1	Forward:	ACAAGCATCATTCATAGCCT
	Reverse:	ATCGTGGCTAGGACATTTTG
ChrV arm region 2	Forward:	GGGAAAAGTACGTGAAAGTC
	Reverse:	CTTCTTAATCTTAGCACCCT
ChrV arm region 3	Forward:	ATGAAGATGACATTGCTCCT
	Reverse:	GTATCTGGATAATGGATCTG

2.13.2 ChIP-chip analyses

For genome-wide binding analysis of Nup170p-9xMyc and Nup157-9xMyc, chromatin immunoprecipitations were performed as described (see section 2.13.1). Linkers were annealed to the ends of the ChIP and input (WCE)

DNA samples, and DNA was then amplified by PCR. Amplified DNA from the IP and input samples were labelled using a ULS aRNA Fluorescent Labeling DNA Kit (Kreatech, Amsterdam, Netherlands). Labelled DNA from the ChIP and input samples were hybridized to yeast 4x44k whole-genome tiling arrays (Agilent Technologies Inc., Santa Clara, CA, USA). Data was extracted using Agilent Feature Extraction software and analyzed with Agilent ChIP Analytics software (Agilent Technologies Inc., Santa Clara, CA, USA). To identify probes whose binding best represented binding events, probes were analyzed according to the neighborhood model; a probe was considered as significantly bound if: 1) the corresponding p-value was ≤ 0.05 and, 2) the central probe had a p-value ≤ 0.05 or a neighboring probe had a p-value ≤ 0.25. Binding intensity represents the transformation of the bound probe's p-value by $-\log_{10}$.

2.14 Nucleosome Positioning Analysis

Wild type (YWY003) and *nup170Δ* (YWY973) cells were grown in YPD medium to an OD_{600} of 1.0 and treated with 1% formaldehyde for 20 min, followed by a 5 min incubation with 125 mM glycine. Cell permeablization, micrococcal nuclease digestion, protein degradation, and DNA purification steps were performed as previously described (Yuan et al., 2005; Shivaswamy et al., 2008; Weiner et al., 2010). The resulting DNA samples were treated with RNase A and then separated in a 2% agarose gel to assess nucleosomal content. Bands corresponding to mononucleosomal DNA were extracted using a Qiagen gel extraction kit (Qiagen, Hilden, Germany). Mononucleosomal DNA libraries were

prepared and subsequently sequenced using an Illumina Genome Analyzer II (Illumina Inc., San Diego, CA, USA) according to the manufacturer's instructions. Sequencing data sets were analyzed as follows:

1) *Data processing*. Single-end sequencing reads of 35 bp were initially processed and mapped to the genomic sequence of *Saccharomyces cerevisiae* by CASAVA software (Illumina Inc., San Diego, CA, USA) allowing up to two mismatches. The raw profiles were further analyzed by in house software to obtain nucleosome profiles.

2) *Nucleosome profiling*. We developed a program, which is well-suited for problems in which the length of the DNA or RNA fragment is already known (i.e. nucleosome width ~147 bp), to quickly process high-throughput sequencing data. The workflow is broken down into four major steps as follows: 1) all reads were first mapped to the genomic sequences of *S. cerevisiae*, 2) each read was extended toward the 3'-end to 150 bp, 3) the center bp (positioned at the 75th bp) of all extended reads was taken as each read's signal, and 4) in order to detect all fine-grained or coarse-grained peak calls, we designed a flexible and customizable Gaussian filter that can define a series of Gaussian templates with different windows and standard deviations (s.d.) to infer possible nucleosome calls, written as:

$$fit(T,G) = \frac{\sum_{i}^{i+win} (t_i - T_\mu) * (g_i - G_\mu)}{win * \sigma_T * \sigma_G}$$

where *G* is Gaussian template with mean 0, s.d. *x* bp and window *y* bp, and *T* is a series of read counts in an interval based on window size in Gaussian template. In this work, we defined a sharp Gaussian template with a window of 100 bp and s.d. of 5 bp to fit the fine-grained peaks and a smooth Gaussian template with a window of 100 bp and s.d. of 20 bp to match coarse-grained peaks. All possible nucleosome calls were detected under two criteria: 1) *fit* score is as least 0.5, and 2) *occ* score (occupancy of nucleosome) is more than 3 given by:

$$occ = fit(T,G) * read\ count$$

All possible nucleosome calls detected by the Gaussian filter, will be further picked for optimal nucleosome calls by using a greedy approach under an overlap constraint that allows for an overlap of 0.3% between adjacent nucleosome calls. Finally, the 147 bp fragments surrounding the center of optimal nucleosome calls will be exported as the nucleosome profile.

3) *Normalization*. The nucleosome profile is given in GFF format, where each line denotes a nucleosome and includes information on the chromosome, the start and end coordinates of nucleosome, and the occupancy of the nucleosome (*occ* score). We normalized the nucleosome occupancy as follows: 1) for all nucleosome profiles comprising wide-type and other references, we normalized them to be equal in the sum of nucleosome occupancies and 2) for each nucleosome profile, the nucleosome occupancy was then divided by the average of *occ* score per bp.

4) *Nucleosome Free Regions*. We defined two types of nucleosome free regions (NFRs), wide and narrow. The wide NFR is from the position of the average -1 nucleosome dyad to the position of the average +1 nucleosome dyad, whereas the narrow NFR encompasses the region from -200 bp to the transcriptional start site (TSS) and excludes more nucleosomal DNA than the wide NFR.

2.15 Fluorescence Microscopy

2.15.1 Epifluorescence microcscopy

All yeast strains synthesizing C-terminally tagged GFP or mCherry fusion proteins were grown to mid-logarithmic phase in YPD medium supplemented with 40 μg/mL adenine. Cells were pelleted, washed twice with SC medium supplemented with 40 μg/mL adenine and subsequently immobilized on 2% agarose pads containing SC medium supplemented with 40 μg/mL adenine. Epifluorescence images were acquired in live cells using an Axio Observer.Z1 microscope (Carl Zeiss Inc., Oberkochen, Germany) using a UPlanS-Apochromat 100x/1.40 NA oil objective lens (Carl Zeiss Inc., Oberkochen, Germany) and an AxioCam Mrm digital camera (Carl Zeiss Inc., Oberkochen, Germany) equipped with a charge-coupled device (CCD). Images were acquired as a series of 14 section z-stacks and processed using both *Axiovision* software (Carl Zeiss Inc., Oberkochen, Germany) and *ImageJ* software (National Institutes of Health, Bethesda, MD, USA).

The subnuclear position of Sir4-GFP foci was determined relative to the nuclear envelope marker Sec63-mCherry within a single focal plane in which the

GFP signal was most intense. Foci residing in the top two or bottom two focal planes, representing the top and bottom of the nucleus, were omitted. To aid visualization of the NE, the Sec63-mCherry signal was deconvolved using an iterative algorithm to remove background signal and reassign blur using *Axiovision* software (Carl Zeiss Inc., Oberkochen, Germany). Foci were designated as peripheral if the GFP and mCherry signals partially overlapped or intranuclear if visibly distinct.

2.15.2 Live cell imaging of *lacO*-tagged loci

Yeast strains encoding ~256 tandem repeats of the *Escherichia coli* lactose operator (*lacO*) integrated ~19 kb from Tel14L are derived from SLJ2499 (a kind gift from Dr. Sue Jaspersen; University of Kansas, Kansas City, MO, USA; Bupp et al., 2007). Strains encoding ~150 *lacO* repeat sequences integrated ~14 kb from Tel6R and ~8 kb from Tel8L are derived from GA1459 and GA1986, respectively (kind gifts from Dr. Susan Gasser; Friedrich Miescher Institute, Basel, Switzerland; Hediger et al., 2002b). Yeast strains encoding 4 tandem repeats of the *lexA* operator (*lexA*^{op}) linked to ~256 *lacO* repeat sequences integrated at the autonomous replicating sequence ARS607 located within the right arm of chrVI (referred to as Chr6^{int}) were derived from GA1461 and the following plasmids were introduced: pAT4 (P_{ADH1}-*lexA*), pAT4-SIR4^{PAD}, pAT4-ESC1^{C}, and pAT4-yku80-4 (kind gifts from Dr. Susan Gasser; Friedrich Miescher Institute, Basel, Switzerland; Taddei et al., 2004). Visualization of *lacO*-tagged foci in live cells was facilitated by expression of *GFP-lacI*.

Strains containing *lacO*-tagged telomeres were grown in YPD medium supplemented with 40 μg/mL adenine to mid-logarithmic phase. Strains containing the *lacO*-tagged ARS607 locus (Chr6^{int}) were grown in SC medium lacking tryptophan supplemented with 40 μg/mL adenine to maintain plasmid selection. Cells were washed twice with SC medium supplemented with 40 μg/mL adenine and then immobilized on 2% agarose pads containing SC medium supplemented with 40 μg/mL adenine. Cells were imaged as described (see section 2.15.1). The subnuclear position of GFP foci was determined relative to the nuclear envelope marker Sec63-GFP within a single focal plane in which the GFP focus was most intense. Foci residing in the top two or bottom two focal planes, representing the top and bottom of the nucleus, were omitted. Dividing the GFP-focus-to-NE distance by the nuclear radius (r) produced a ratio that placed each focus into one of three concentric zones of equal area, with zone 1 directly underlying the NE. Zone 1 represents foci with ratios $\leq 0.184 \times r$, zone 2 represents foci with ratios between $> 0.184 \times r$ and $< 0.422 \times r$ and zone 3 represents foci with ratios $\geq 0.422 \times r$.

2.15.3 Sister chromatid cohesion assay

Yeast strain DVY0040 (*nup60Δ*) was derived from AFS173 encoding ~256 repeats of the *lac* operator *(lacO)* sequence integrated at the *LEU2* locus and P_{HIS3}-*GFP-lacI* (Hanna et al., 2001). WT, *nup60Δ,* and *ctf18Δ* cells were grown to mid-logarithmic growth phase in YPD medium. Cells were then pelleted and washed three times with SC medium lacking histidine. Washed cells were

resuspended in SC medium lacking histidine supplemented with 0.25 mg/mL adenine and 40 mM 3-amino triazole for 40 min at 23˚C to induce expression of P_{HIS3}-*GFP-lacI*. Post-induction, cells were washed twice with YPD medium and then arrested in G2/M-phase with 15 μg/mL nocodazole (Calbiochem, Merck KGaA, Darmstadt, Germany) in YPD medium containing 0.25 mg/mL adenine for 3 h at 23˚C. Cells arrested in G2/M-phase were washed twice with SC medium and then imaged on an Olympus BX50 microscope (Olympus Corporation, Tokyo, Japan) using a 100x/1.4 NA oil immersion lens. Images were acquired with a digital camera (Spot Diagnostics, Sterling Heights, MI, USA). Defects in sister chromatid cohesion were assessed by calculating the percentage of large budded cells with two distinct GFP foci.

2.15.4 Confocal microscopy

Confocal images were acquired in live cells with a microscope (Axiovert 200M; Carl Zeiss Inc., Oberkochen, Germany) equipped with a confocal laser scanning system (LSM510 META; Carl Zeiss Inc., Oberkochen, Germany) using a Plan-Apochromat 63x/1.4 NA oil objective lens (Carl Zeiss Inc., Oberkochen, Germany). A piezoelectric actuator was used to drive continuous objective movement, allowing for rapid acquisition of z-stacks. Stacks of 37 optical sections spaced 0.16 μm apart were captured and stored using *Zen* software (Carl Zeiss Inc., Oberkochen, Germany). To excite GFP, an Argon laser emitting 488 nm light and a bandpass filter (BP 514/30) was used, while a Helium/Neon laser

emitting 543 nm light was used to excite mCherry and mRFP and then collected with a bandpass filter (BP 629/20).

Acquired z-stack images were deconvolved using *Huygens Professional Software* (Scientific Volume Imaging, Hilversum, The Netherlands). Data sets were processed to remove background noise and reassign blur using an iterative algorithm and a theoretically derived point spread function. 3D deconvolved images were displayed in *Imaris 7.0* software (Bitplane, South Windsor, CT, USA) and the Spot detection feature was used to mask the channel's signals with an isosurface to generate spheres of 200 nm in diameter, representing the experimental resolution limit, using an automatic region-growing algorithm. Resulting spheres were manually cut-off to insure correct volume filling of the respective channels. Spheres were counted using the internal counting algorithm of *Imaris 7.0* software's spot function and colocalization amongst spheres was determined using *Matlab* software (MathWorks, Natick, MA, USA).

2.16 Electron microscopy

2.16.1 Osmium tetroxide staining

Transmission electron microscopy (TEM) for visualizing proteinaceous structures with osmium tetroxide staining was performed as previously described (Marelli et al., 2001; Makio et al., 2009). In order to limit genome instability associated with a *nup170* null mutant, a *NUP170/nup170Δ* heterozygous diploid strain was sporulated, tetrads were then dissected and individual spores were incubated on YPD medium for 2-3 d. *nup170Δ* haploids were identifiable by their

reduced colony size and following sufficient growth were used to inoculate overnight cultures.

Wild type and null mutant strains were grown in 50 mL YPD cultures to an OD_{600} 0.8-1.0 and harvested (Eppendorf 5810R, A-4-62 rotor at 6000 x g for 2 min). Cell pellets were washed twice with 100 mM KPO_4 buffer pH 6.5, (K-Pi buffer; see Table 2-3) and fixed with 2% glutaraldehyde and 2% formaldehyde in K-Pi buffer for 1 h on ice. Cells were then washed twice with K-Pi buffer and pretreated with 100 mM Tris-SO_4 pH 9.4 and 10 mM DTT at 30˚C for 10 min prior to cell wall digestion. Following pretreatment, cells were washed twice with 100 mM Pi-citrate buffer pH 5.8 (see Table 2-3) and resuspended in Pi-citrate buffer supplemented with 285 ng/mL 100T zymolase (MP Biomedicals, Santa Ana, CA, USA) at 30˚C to digest the cell wall (~1-2 h). Cell wall digestion was determined microscopically by observing an expansion of cell volume upon addition of 0.1% SDS. Cells were then gently washed twice with Pi-citrate buffer and postfixed with 1% osmium tetroxide in Pi-citrate buffer for 1 h on ice. Cell dehydration occurred by successive washes with increasing percentages of EtOH (30, 50, 70, 80, 90, 95 and 100% EtOH) for 5 min each with the exception of the 100% EtOH wash (2 x 15 min), followed by three washes with 100% propylene oxide for 4 min each. Cells were then infiltrated with increasing ratios of resin (TAAB 812 Embedding Resin Kit; Canemco and Marivac, Canton de Gore, QC, Canada) to propylene oxide (PO; Fisher Scientific) and which lacked a polymerization accelerant. Initially, cells were infiltrated with a 1:1 ratio of resin to PO for 1 h at 23˚C with rotation, followed by a 2:1 ratio of resin to PO for 4 h

at 23˚C, and finally with 100% resin overnight at 4˚C. Cells were then pelleted and resuspended in resin plus 185 μL of the polymerization accelerant DMP-30 (Canemco and Marivac, Canton de Gore, QC, Canada), placed in polymerizing molds and incubated at 65˚C for 48 h. Blocks were sectioned to ~60 nm, stained with 8% uranyl acetate in 50% EtOH for 10-20 min followed by 1x Reynolds lead citrate for 2-10 min and imaged on a Phillips 410 transmission electron microscope (Phillips, division of FEI Company, Hillsboro, OR, USA) at magnifications between 17,000x and 40,000x. Images were acquired with a CCD camera (Megaview III; Soft Imaging System, Munster, Germany) and *AnalySIS* software (Olympus Soft Imaging System, Munster, Germany). Post-acquisition processing (image cropping, rotation and linear measurements of the NE) was performed with *ImageJ* software (National Institutes of Health, Bethesda, MD, USA).

2.16.2 Potassium permanganate staining

TEM for visualizing membranous structures with potassium permanganate staining was performed as previously described (Marelli et al., 2001; Makio et al., 2009). WT and null mutant strains were grown to an OD_{600} 0.8-1.0 in 50 mL YPD, cells were harvested (Eppendorf 5810R, A-4-62 rotor at 6000 x g for 2 min), washed twice with ddH_2O and then stained with 3% $KMnO_4$ solution for 15 min at 23˚C. Stained cells were washed twice with ddH_2O, the cell wall was permeabilized with 1% sodium periodate for 15 min at 23˚C and washed once with ddH_2O. Addition of 1% NH_4Cl neutralized the permeabilization process and

cells were washed once with ddH_2O prior to dehydration. Cell dehydration, embedding, sectioning and staining, and imaging were performed as described in section 2.17.1.

Chapter III: *A role for the nucleoporin Nup170p in chromatin structure and gene silencing**

***** A version of this chapter has been submitted for publication and has been under review. This work was co-authored in-conjunction with Y. Wan: Van de Vosse, D.W., Wan, Y., Lapetina, D., Chen, W.M., Chiang, J.H., Aitchison, J.D., and R.W. Wozniak. (2012). **A role for the nucleoporin Nup170p in chromatin structure and gene silencing.** *Cell*, in review.

3.1 Overview

Embedded in the nuclear envelope, nuclear pore complexes (NPCs) not only regulate nuclear transport, but also interface with both transcriptionally active euchromatin and largely silenced heterochromatin, as well as the boundaries between these regions. It is unclear what functional role NPCs play in establishing or maintaining these distinct chromatin domains. Here we report that the yeast NPC protein Nup170p interacts with specific regions of the genome containing ribosomal protein and subtelomeric genes. At these locations, Nup170p functions to establish normal nucleosome occupancy and as a repressor of transcription. We show that the function of Nup170p in subtelomeric gene silencing is linked to its association with the RSC chromatin-remodeling complex and the silencing factor Sir4p, and that the binding of Nup170p and Sir4p to subtelomeric chromatin is cooperative and necessary for the association of telomeres with the nuclear envelope. Our results establish the NPC as an active participant in the formation of peripheral heterochromatin.

3.2 Results

3.2.1 Nup170p functionally interacts with chromatin-modifying complexes

We have taken an unbiased genetic approach to identify proteins and pathways whose functions are linked to yeast Nup170p. While the combined functions of Nup170p and its paralogue, Nup157p, are essential for NPC assembly and cell viability (Aitchison et al., 1995a; Makio et al., 2009), strains lacking only one of the two proteins are viable. Taking advantage of the nonlethal phenotype of the *nup170Δ* mutant, we used synthetic genetic array (SGA) analysis (Tong et al., 2001) to screen a library of non-essential gene deletion mutants for those exhibiting a synthetic sick or lethal phenotype in combination with a *nup170Δ* mutation. These double mutations are presumed to further compromise an essential structure or network, or two parallel, functionally redundant pathways contributing to an essential cellular function. We identified 73 gene deletions that displayed reduced fitness in combination with *nup170Δ* (Table 3-1). *NUP170* predictably displayed interactions with components of the NPC (Figure 3-1 and Table 3-1). However, surprisingly, a significant proportion of the interacting genes (27 of 73; p-value = 1.99×10^{-15}) encode subunits of complexes that function in chromatin organization including the chromatin-remodeling complex SWR1, the histone deacetylase complexes Rpd3L and Set3C, and genes required for ubiquitination of histone H2BK123 (Figure 3-1 and Table 3-1). These interactions appeared specific for *NUP170*. SGA analysis of *nup53Δ*, *nup60Δ*, or *kap123Δ* did not reveal similar interaction networks (Figure 3-2 and Table 3-1; Ptak et al., 2009). Moreover, the cohort of *NUP170* genetically

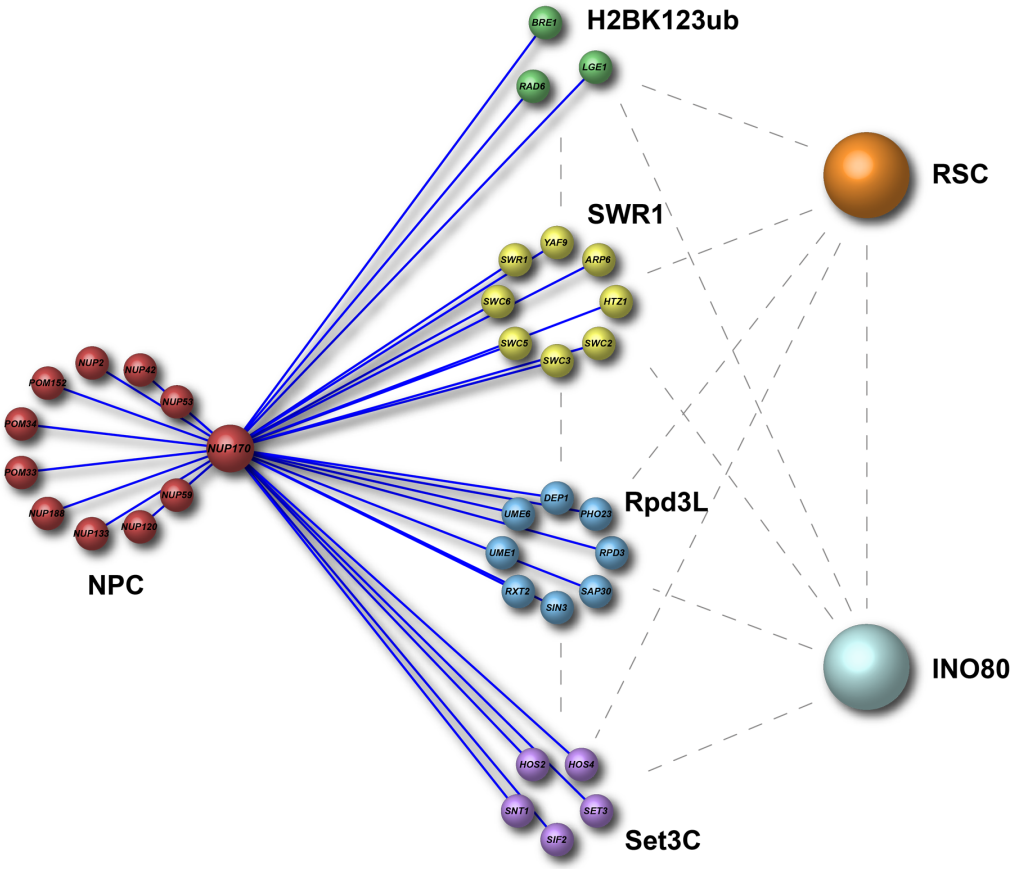

Figure 3-1. *NUP170* functionally interacts with chromatin complexes.

Graphical representation of a genetic interaction network generated for *NUP170* using *Cytoscape v2.8.2* software (Shannon et al., 2003). Nodes represent genes grouped according to functional complexes. Nodes are connected by edges that represent synthetic genetic interactions. For clarity, only those interactions of *NUP170* with multiple components of a subcomplex are shown. Grey dashed edges represent previously characterized genetic interactions among chromatin complexes as denoted by the *Saccharomyces* Genome Database (SGD; Cherry et al., 2012), blue edges represent genetic interactions identified by synthetic genetic array (SGA) analysis of *NUP170* (this study). SGA analysis involved a series of pinning procedures that mated a *nup170* null haploid mutant containing the *HIS3* ORF under control of the *MAT***a** specific *MFA1* promoter (P_{MFA1}-*HIS3*) to a collection of ~4985 individual gene deletion mutants. The resulting diploids were sporulated and meiotic haploid progeny of the *MAT***a** mating type were selected for growth on medium lacking histidine. Haploid colonies were then repinned to select for growth of either single or double deletion mutants. Genetic interactions were determined by visual inspection of colony size and were scored as synthetic interactors if reduced fitness was observed in two independent experiments. For a complete list of genetic interactions identified by SGA analyses see Table 3-1 and for a comparison of epistatic interaction profiles of *NUP2*, *NUP53*, *NUP157*, *NUP170*, and *NUP188* see Table 3-2.

Figure 3-2. *NUP53* and *NUP60* genetic interactions identified by SGA analysis.

Loss of functions associated with *nup53Δ* (A) and *nup60Δ* (B) mutations were evaluated by SGA analysis as described in Figure 3-1. Genetic interactors were grouped according to gene ontology annotations and displayed graphically using *Cytoscape v2.8.2* software (Shannon et al., 2003). Nodes represent genes and edges connecting nodes represent synthetic genetic interactions identified by SGA analysis. Functional categories are indicated. Note, 21 and 38 gene deletions were identified that displayed reduced fitness in combination with *nup53Δ* and *nup60Δ*, respectively. For a complete list of genetic interactions identified by SGA analyses see Table 3-1 and for a comparison of epistatic interaction profiles of *NUP2*, *NUP53*, *NUP157*, *NUP170*, and *NUP188* see Table 3-2.

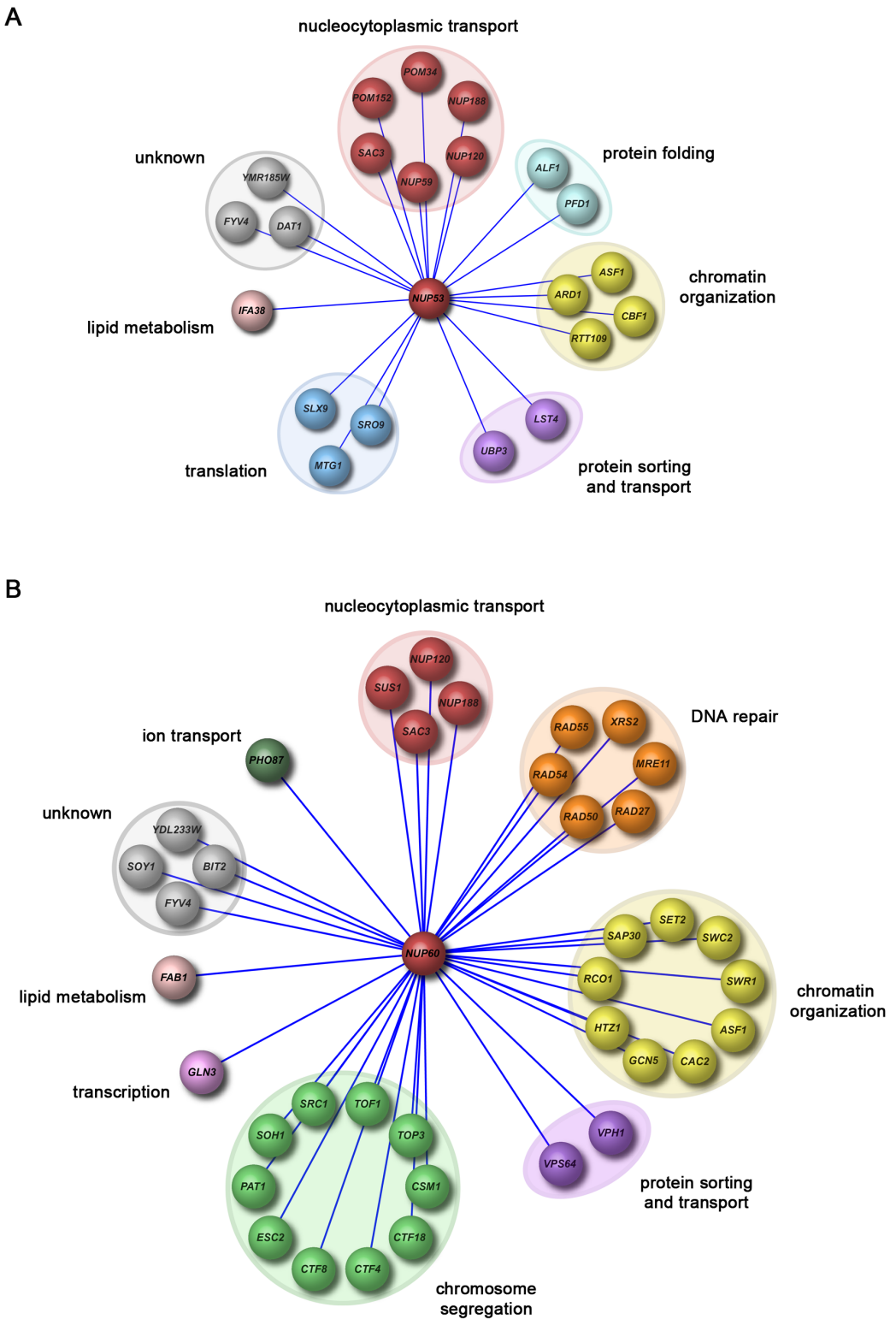

Figure 3-2. *NUP53* and *NUP60* genetic interactions identified by SGA analysis.

Table 3-1. Genetic interactions identified by SGA analysis of *NUP170*, *NUP60*, and *NUP53*.

NUP170	Tetrad analysis	*NUP60*	Tetrad analysis	*NUP53*	Tetrad analysis
APJ1	n.t.	*ASF1**	SL	*ALF1*	n.t.
ARP6	SS	*BIT2*	n.t.	*ARD1*	n.t.
*ARX1**	n.t.	*CAC2*	SS	*ASF1*	n.t.
BRE1	SS	*CSM1**	n.t.	*CBF1*	n.t.
BRE5	n.t.	*CTF4**	n.t.	*DAT1*	n.t.
CTF4	n.t.	*CTF8*	n.t.	*FYV4*	n.t.
CTF18	n.t.	*CTF18**	SSS	*LST4*	n.t.
CTK3	SL	*ESC2**	SSS	*MTG1*	n.t.
DEP1	SSS	*FAB1*	n.t.	*NUP59**	n.t.
ELM1	SSS	*FYV4*	n.t.	*NUP120*	n.t.
FAT1	n.t.	*GCN5*	SL	*NUP188**	n.t.
GEM1	n.t.	*GLN3*	n.t.	*PFD1*	n.t.
HOS2	SSS	*HTZ1**	n.t.	*POM34**	n.t.
HOS4	SS	*MRE11**	SL	*POM152*	n.t.
*HTZ1**	n.t.	*NUP120**	n.t.	*RTT109*	n.t.
HUR1	n.t.	*NUP188**	n.t.	*SAC3*	SS
IPK1	n.t.	*PAT1**	n.t.	*SLX9*	n.t.
ITC1	SS	*PHO87*	n.t.	*SRO9*	n.t.
LGE1	SSS	*RAD27**	SL	*UBP3*	n.t.
LST4	n.t.	*RAD50**	SSS	*IFA38*	n.t.
LTE1	n.t.	*RAD54**	SL	*YMR185W*	n.t.
*MAM1**	n.t.	*RAD55**	SS		
MRE11	n.t.	*RCO1**	SS		
MTC5	n.t.	*SAC3**	SL		
*NUP2**	n.t.	*SAP30*	SS		
NUP42	n.t.	*SET2**	SS		
*NUP53**	n.t.	*SOH1*	n.t.		
*NUP59**	n.t.	*SOY1*	n.t.		
*NUP120**	n.t.	*SRC1**	n.t.		
*NUP133**	n.t.	*SUS1**	SSS		
*NUP188**	n.t.	*SWC2**	SS		
PAT1	n.t.	*SWR1**	SS		
PHO23	SS	*TOF1**	SS		
*POM33**	n.t.	*TOP3*	n.t.		
*POM34**	n.t.	*VPH1*	n.t.		
*POM152**	n.t.	*VPS64*	n.t.		
RAD6	SS	*XRS2**	SL		
RPD3	SS	*YDL233W*	n.t.		
RPP1A	n.t.				
RPS21B	n.t.				

RTT103	SS		
RXT2	SS		
*SAC3**	SL		
*SAP30**	SS		
SCS7	n.t.		
SEC22	n.t.		
SEC28	n.t.		
SET3	SSS		
SIF2	SS		
SIN3	SSS		
SLA1	n.t.		
SNF1	SS		
SNF4	SS		
SNL1	n.t.		
SNT1	n.t.		
SOY1	n.t.		
*SRO9**	n.t.		
STB5	n.t.		
SUR1	n.t.		
SUS1	SS		
SWC2	SSS		
SWC3	SS		
SWC5	SL		
SWC6	SS		
SWR1	SS		
THP1	SL		
UBP3	n.t.		
UBP6	n.t.		
UME1	SS		
UME6	SL		
VIP1	n.t.		
YAF9	SL		

Phenotypes confirmed by tetrad dissection are listed as: SL, synthetic lethality; SSS, severe synthetic sickness; SS, synthetic sickness; n.t., not tested. *, genetic interactions previously identified and annotated in the *Saccharomyces* Genome Database (SGD).

interacting genes did not show similar interactions with various other Nup genes (*NUP188*, *NUP157*, *NUP53,* or *NUP2*) (Table 3-2). Importantly, this role of Nup170p in chromatin organization is unlikely to be linked to nucleocytoplasmic transport, as the *nup170Δ* mutant has no detected defects in active transport (Aitchison et al., 1995a; Scarcelli et al., 2007; Makio et al., 2009), and its previously detected contribution to the NPC diffusion barrier is phenocopied by the *nup188Δ* mutant (Shulga et al., 2000), which did not display a similar genetic interaction profile (Table 3-2).

3.2.2 Nup170p physically interacts with the RSC complex

To evaluate the physical basis for the detected interactions of Nup170p with the chromatin-modifying complexes, we tagged the endogenous *NUP170* ORF at the 3'-end with the coding region for protein A. Nup170-pA was then purified from strains producing GFP-tagged versions of representative members of the genetically interacting complexes. None of the GFP-tagged proteins, however, were detected in association with Nup170-pA, with the exception of low-levels of Rpd3-GFP. By contrast, as previously shown, a robust signal was detected for the Nup170p binding partner Nup53p (Figure 3-3A; Lusk et al., 2002). This result argued against a physical association between Nup170p and its genetically interacting chromatin complexes, and, instead, inferred a role for Nup170p in a functionally overlapping pathway. Such a pathway is predicted to exhibit similar genetic interactions as the *nup170Δ* mutant. Database analysis revealed two chromatin-remodeling complexes, INO80 and RSC, showing similar

Table 3-2 Epistatic interaction profiles of *NUP2*, *NUP53*, *NUP157*, *NUP170*, and *NUP188*.

Mutant genotypes assayed:	*nup170Δ*	*nup157Δ*	*nup188Δ*	*nup53Δ*	*nup2Δ*
Set3C histone deacetylase complex					
hos2Δ	sss	-	-	-	-
hos4Δ	ss	-	-	-	-
set3Δ	sss	-	-	-	-
sif2Δ	ss	-	-	-	-
SWR1 chromatin-remodeling complex					
swc2Δ	sss	-	-	-	-
swc3Δ	ss	-	-	-	-
swc6Δ	ss	-	-	-	n.t.
swc7Δ	-	-	-	-	-
swr1Δ	ss	-	-	-	n.t.
yaf9Δ	sl	-	ss	-	-
Rpd3L histone deacetylase complex					
dep1Δ	sss	-	- [b]	-	n.t.
pho23Δ	ss	-	- [b]	-	-
sap30Δ	ss [a]	-	- [a]	-	-
sin3Δ	sss	-	-	-	n.t.
Rpd3S histone deacetylase complex					
eaf3Δ	-	-	-	-	-
rco1Δ	-	-	-	-	-
set2Δ	-	-	-	-	-
Histone H2BK123 ubiquitination					
bre1Δ	ss	rescue	sl [c]	-	-
rad6Δ	ss	rescue	sl	-	-

- , no affect on growth; sl, synthetic lethality; sss, severe synthetic sickness; ss, synthetic sickness; rescue, suppression of the growth defect of the *bre1Δ* or *rad6Δ* single mutant; n.t., not tested. Interaction with the Rpd3S complex and *nup170Δ* were not detected in the SGA analysis and where used here as a negative control.

[a] Previously identified interaction by high-throughput analysis (Wilmes et al. 2008).

[b] Previously identified interaction by high-throughput analysis (Costanzo et al. 2010).

[c] Previously identified interaction by high-throughput analysis (Pan et al. 2006).

synthetic genetic interactions with the SWR1, Rpd3L, and Set3C complexes (Figure 3-1 and BioGRID; Stark et al., 2006). Nup170-pA showed no interactions with several subunits of the INO80 complex (Figure 3-3A). However, Sth1p, the ATPase subunit of the RSC complex (Figure 3-3B), bound Nup170-pA while showing no interaction with Nup84-pA or Nup188-pA (Figure 3-3D and 3-3E). Reciprocal experiments using Sth1-pA also detected associated Nup170p and its binding partner Nup53p as well as RSC complex members (Figure 3-3F). Notably, Nup53p binding to Sth1-pA was dependent on Nup170p (Figure 3-3H and 3-3I). We conclude from these studies that Nup170p physically associates with the RSC complex, potentially through its binding to Sth1p.

3.2.3 Nup170p is required for silencing of subtelomeric genes

RSC catalyzes nucleosome-restructuring events that play a role in DNA double-strand break repair, telomere structure, and gene expression (Angus-Hill et al., 2001; Askree et al., 2004; Chai et al., 2005; Shim et al., 2005; Ungar et al., 2009). To begin to assess the role of Nup170p in these functions, we examined the consequences of the loss of Nup170p on the cellular transcription profile using DNA microarrays. This analysis revealed specific changes in the transcriptome, with 424 ORFs up-regulated and 59 ORFs down-regulated greater than 2-fold in the *nup170Δ* mutant (Tables 3-3 and 3-4). Strikingly, the up-regulated genes were enriched for ribosomal protein (RP) genes (109 of 137; hypergeometric test, p-value 1.85×10^{-105}) and genes positioned in subtelomeric regions (i.e. within 25 kb of telomeres. The smaller numbers of down-regulated ORFs were randomly

Figure 3-3. Nup170p physically interacts with the RSC chromatin-remodeling complex.

(A) Physical interactions between Nup170p and its genetically interacting chromatin complexes were not detected. The coding region of protein A (pA) was integrated in frame following the last codon of the endogenous *NUP170* ORF in the otherwise wild type haploid yeast strain BY4742. The resulting Nup170-pA strain was mated to haploid strains producing the indicated C-terminally tagged GFP-fusion proteins obtained from the GFP library collection (Huh et al., 2003). Diploid cells synthesizing Nup170-pA and the indicated GFP-fusion protein were grown in YPD medium to mid-logarithmic growth phase, harvested, and flash frozen in liquid nitrogen. Cell lysates were prepared from frozen cells using a planetary ball mill and the Nup170-pA fusion was affinity purified using IgG-conjugated magnetic beads. Bound complexes were washed extensively and then released by step elution of increasing concentrations of $MgCl_2$ (Mg^{2+}) and a final acetic acid elution (AA). Eluted proteins were analyzed by SDS-PAGE and western blotting to detect the indicated proteins. Lanes labeled 'load' and 'wash' contain samples of the total cell lysates and the final wash prior to elution. (B-I) Similar experiments as described in A were performed using haploid yeast strains producing the indicated endogenously C-terminally tagged pA and/or Myc fusion proteins. Asterisks indicate IgG cross-reacting species in the AA fractions. Note, Sth1p failed to interact with Nup84p or Nup188p, while the interaction of Sth1p with Nup53p was lost in the absence of Nup170p.

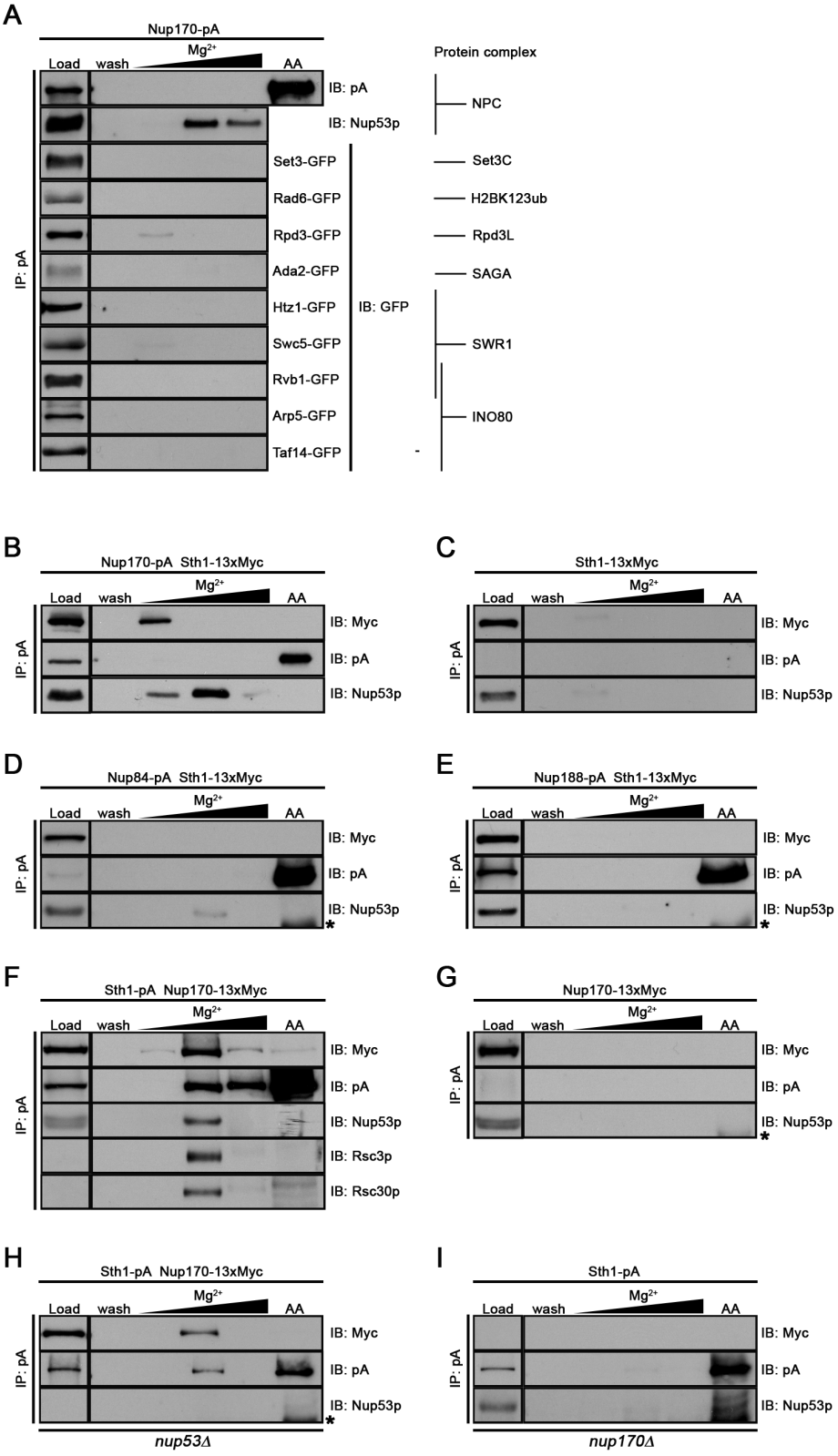

Figure 3-3. Nup170p physically interacts with the RSC chromatin-remodeling complex.

distributed throughout the genome (Figure 3-4A). While housing only ~6% of the total number of ORFs, subtelomeric regions contained ~28% of the genes up-regulated in *nup170Δ* cells (119 of 424; hypergeometric test, p-value 1.94 x 10^{-56}), with ~34% of subtelomeric ORFs (119 of 347) showing alleviated repression. By contrast, no changes in subtelomeric gene expression were detected in *nup157Δ* and *nup188Δ* cells (Figure 3-4A and Table 3-5).

Similar DNA microarray analysis was performed on cells depleted of Sth1p. *STH1* is an essential gene. Thus, to regulate its levels, the endogenous *STH1* promoter was replaced with a repressible *MET3* promoter (P_{MET3}-*STH1*) allowing Sth1p to be rapidly depleted to barely detectable levels 4 h after addition of methionine (Figure 3-4B). We interrogated the transcriptome of P_{MET3}-*STH1* cells 2 h after repression, at which point *STH1* mRNA levels were reduced 4.4-fold (Table 3-7). Similar to *nup170Δ* cells, a pattern of subtelomeric derepression was observed (Figure 3-4C and Tables 3-6 and 3-7). Moreover, subtelomeric gene repression was restored following reinduction of *STH1* (Figure 3-4C and Table 3-8).

Our microarray data are consistent with a role for Nup170p and RSC in subtelomeric gene silencing. This function was further evaluated using cell growth assays that provide a readout for the transcriptional state of two reporter genes, *URA3* and *ADE2*, inserted in subtelomeric regions adjacent to telomeres VII-L (Tel7L) and V-R (Tel5R), respectively (Figure 3-5; Singer et al., 1994). Suppression of these genes in a WT background prevents growth in the absence of uracil and adenine, but allows cells to grow in the presence of 5-FOA.

Figure 3-4. Nup170p and RSC are required for repression of subtelomeric genes.

(A) Gene expression profiles of *nup170Δ*, *nup157Δ*, and *nup188Δ* cells were determined by DNA microarray analysis. RNA was isolated from cells grown to mid-logarithmic growth phase in YPD medium and used in two-color DNA microarrays comparing RNA from i) WT and *nup170Δ* cells, ii) WT and *nup157Δ* cells, and iii) WT and *nup188Δ* cells. Differentially expressed genes were identified by maximum likelihood analysis, lambda ≥ 100 (Ideker et al., 2000; Smith et al., 2002), and ORFs with ≥ 2-fold change in expression were considered significantly affected. To visualize the positions of differentially expressed ORFs, the distances of these ORFs to the nearest telomere was determined and the number of ORFs within 5 kb bins were plotted versus their distance from telomeres. Up-regulated and down-regulated ORFs are represented by red and green histograms, respectively. Shaded histograms (grey) indicate the number of all ORFs within the 5 kb bins displayed at one-third scale. (B) Time course of Sth1p depletion following methionine addition to P_{MET3}-*HA3-STH1* cells. The strain TMY1452 (P_{MET3}-*HA3-STH1*) was grown to early-logarithmic growth phase in SC-medium lacking methionine (SC-met) and Sth1p was depleted by addition of methionine for the indicated times. Following 8 h of depletion cells were washed extensively with SC-met and grown in SC-met for an additional 4 h to reinduce *STH1* expression. Sth1p levels were analyzed by SDS-PAGE and western blotting using anti-HA (HA3-Sth1p) and anti-Gsp1p (load control) antibodies. (C) Subtelomeric genes are derepressed following depletion of Sth1p. Gene expression profiling was performed comparing RNA isolated from cells depleted of Sth1p for 0 h and 2 h and the positions of ORFs exhibiting significant changes in expression were analyzed as described in A. Similar analysis was also performed comparing RNA from cells depleted of Sth1p for 0 h and cells depleted of Sth1p for 8 h followed by reinduction of *STH1* for 4 h (R4). For a complete list of significantly differentially expressed ORFs see Tables 3-3 to 3-8.

* RNA isolation was performed by D.W. Van de Vosse (DWV), cDNA labeling and hybridization was performed by Y. Wan (YW). Data analysis and figure processing were performed by DWV, YW, and W.M. Chen (WMC).

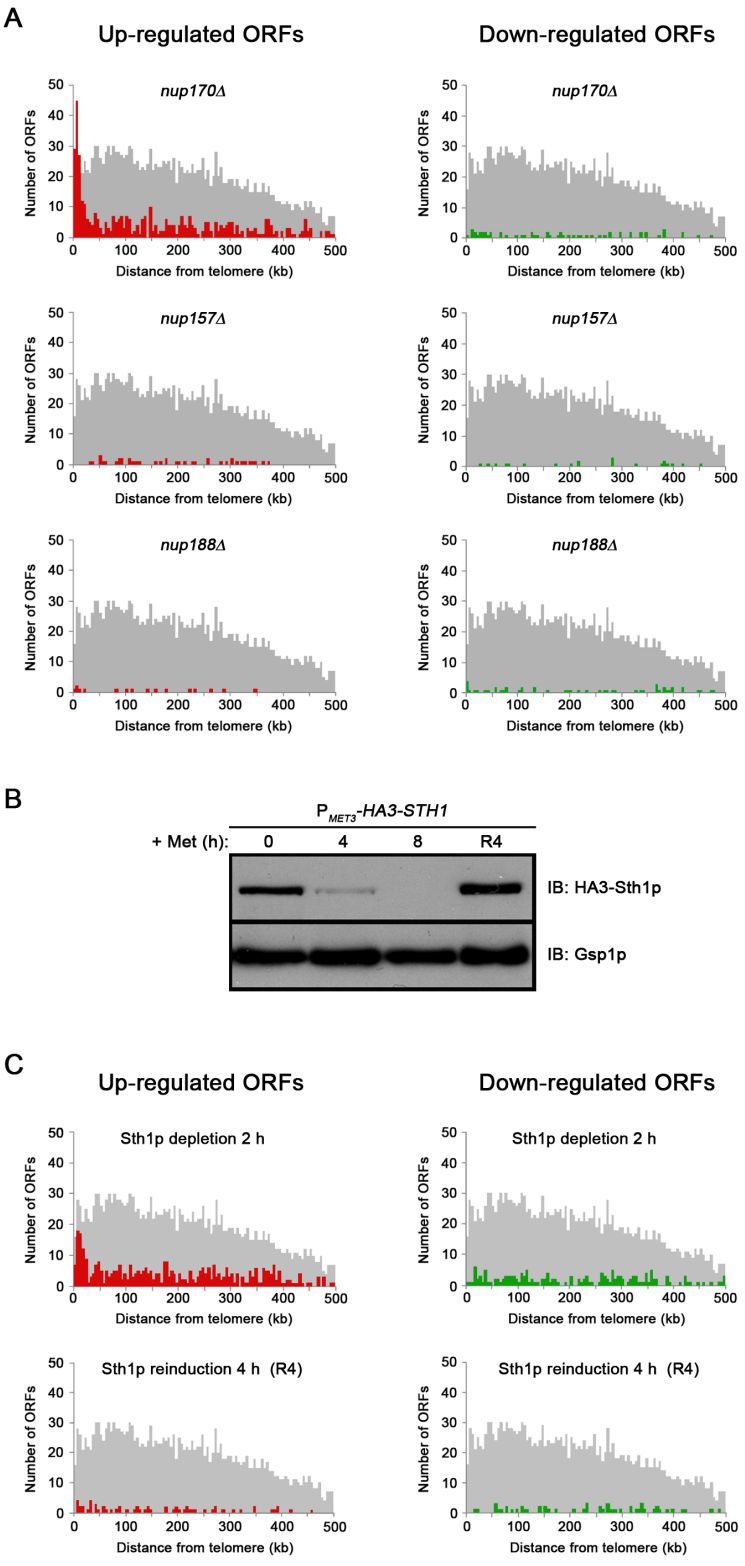

Figure 3-4. Nup170p and RSC are required for repression of subtelomeric genes.

Table 3-3. Up-regulated ORFs in a *MAT*a *nup170Δ* mutant.

Gene name	Fold change	Gene name	Fold change	Gene name	Fold change	Gene name	Fold change
AAD10	2.0	*HAC1*	2.2	*RPL10*	3.0	*RPL7A*	2.7
AAD15	3.9	*HHF1*	2.3	*RPL11A*	2.8	*RPL8B*	2.0
AAD3	2.0	*HHF2*	2.0	*RPL11B*	2.5	*RPL9A*	2.2
ACT1	2.0	*HHT1*	2.4	*RPL12B*	2.7	*RPM2*	2.1
ADH7	3.4	*HHY1*	2.6	*RPL13B*	2.4	*RPP0*	2.1
AHP1	2.5	*HOR7*	3.4	*RPL14A*	2.8	*RPP1A*	2.1
ALD3	2.0	*HPA2*	2.1	*RPL14B*	2.0	*RPP1B*	2.8
ALD4	2.2	*HSP12*	2.4	*RPL15A*	2.0	*RPP2A*	2.2
ARO10	7.4	*HXT11*	2.2	*RPL16A*	2.2	*RPP2B*	2.4
ARO9	2.0	*HXT13*	3.2	*RPL16B*	2.3	*RPS0A*	2.1
ASG7	2.4	*HXT15*	2.7	*RPL17A*	2.0	*RPS10A*	2.4
ATP1	2.4	*HXT16*	2.7	*RPL17B*	2.1	*RPS10B*	2.1
BMH1	2.1	*HXT17*	2.7	*RPL18A*	2.1	*RPS11A*	2.1
BNS1	2.1	*HXT4*	2.3	*RPL19A*	2.7	*RPS11B*	2.3
BSC3	3.7	*HXT6*	3.2	*RPL19B*	3.2	*RPS12*	3.0
BUR6	2.0	*HXT7*	3.4	*RPL1A*	2.0	*RPS14A*	2.9
CAT8	2.2	*HXT9*	2.6	*RPL1B*	2.0	*RPS15*	2.6
CCW12	3.1	*HYP2*	2.1	*RPL20B*	2.2	*RPS16A*	2.0
CLD1	2.5	*ICL1*	2.0	*RPL21B*	2.2	*RPS17A*	2.5
COS1	2.2	*INH1*	2.7	*RPL22A*	2.9	*RPS17B*	2.2
COS12	4.8	*IRC18*	2.0	*RPL23B*	2.6	*RPS18A*	2.3
COS4	2.0	*KRE22*	3.1	*RPL24A*	3.1	*RPS18B*	2.2
COX20	2.3	*LSM3*	2.0	*RPL24B*	4.1	*RPS19A*	2.5
CPR1	2.0	*LSP1*	2.2	*RPL25*	2.4	*RPS19B*	2.3
CRC1	2.2	*MAL12*	2.3	*RPL26A*	2.3	*RPS1B*	2.1
CTS1	2.5	*MAL31*	2.0	*RPL26B*	2.6	*RPS2*	2.1
CWP2	3.1	*MAL32*	2.4	*RPL27A*	2.9	*RPS20*	2.5
CYC7	2.9	*MFα1*	4.9	*RPL27B*	2.0	*RPS21B*	2.1
CYT1	2.4	*MFα2*	3.0	*RPL28*	3.1	*RPS22A*	2.2
DAL1	2.1	*MFA1*	8.9	*RPL29*	3.4	*RPS23A*	2.6
DDI2	2.5	*MFA2*	3.6	*RPL2B*	2.0	*RPS23B*	2.7
DDI3	2.5	*MIG2*	2.5	*RPL3*	2.2	*RPS24A*	2.8
DDR2	6.4	*MND1*	2.0	*RPL30*	2.4	*RPS24B*	2.5
EFB1	2.0	*MRK1*	2.5	*RPL31A*	3.5	*RPS25A*	2.8
EFT1	2.0	*NCA3*	6.3	*RPL31B*	2.2	*RPS26A*	3.9
EFT2	2.1	*NCE102*	2.6	*RPL32*	2.5	*RPS26B*	2.3
EGD2	2.5	*NCE4*	2.0	*RPL33A*	2.2	*RPS27B*	2.9
ERR1	3.1	*NDT80*	2.2	*RPL34A*	2.7	*RPS28A*	2.4
ERR2	3.4	*NHP2*	2.2	*RPL34B*	2.6	*RPS29A*	3.0
ERR3	3.4	*NHP6B*	2.2	*RPL35A*	3.8	*RPS29B*	2.7
FDH1	2.0	*NIP100*	2.0	*RPL35B*	3.5	*RPS30A*	2.5
FLO1	2.0	*NPL3*	2.0	*RPL36A*	2.0	*RPS30B*	2.5
FLO5	2.3	*NQM1*	2.0	*RPL36B*	4.1	*RPS31*	3.1
FLO9	2.7	*NSR1*	2.0	*RPL37A*	2.5	*RPS4A*	2.0
FMP40	2.0	*OM14*	2.1	*RPL37B*	3.0	*RPS4B*	2.0
FRE7	4.8	*PDA1*	2.1	*RPL38*	2.5	*RPS5*	2.2
FUS1	2.6	*PIL1*	2.6	*RPL39*	3.2	*RPS6A*	3.5
FYV15	2.1	*PMA1*	2.6	*RPL40A*	2.3	*RPS6B*	2.8
FYV2	2.0	*PRM10*	2.0	*RPL41A*	2.0	*RPS7B*	2.1
GAL4	2.0	*PTR2*	2.9	*RPL41B*	2.1	*RPS8A*	2.5
GCN4	2.5	*PYK2*	2.2	*RPL42A*	2.7	*RPS8B*	2.2
GEX1	3.5	*QCR2*	2.1	*RPL42B*	2.6	*RPS9B*	2.0
GEX2	3.2	*QCR6*	2.2	*RPL43A*	3.0	*SBP1*	2.0
GIC2	2.8	*QCR7*	2.9	*RPL43B*	2.1	*SCW10*	2.5
GOR1	2.1	*RAD16*	2.0	*RPL4A*	2.5	*SCW4*	3.7
GPH1	3.7	*RDS1*	2.2	*RPL4B*	2.2	*SED1*	2.7
GSY1	2.1	*REE1*	2.1	*RPL5*	2.2	*SFC1*	2.2
GSY2	2.0	*RGM1*	3.1	*RPL6A*	2.2	*SGA1*	2.1

SIK1	2.0	*YCR102W-A*	3.2	*YGR190C*	2.0	*YLR464W*	3.8
SMA1	2.6	*YDL023C*	2.0	*YGR259C*	2.0	*YML007C-A*	2.3
SOM1	2.4	*YDL114W*	2.0	*YGR269W*	2.4	*YML101C-A*	2.2
SPO20	2.3	*YDL114W-A*	2.0	*YGR291C*	2.5	*YML133C*	4.9
SPO22	4.7	*YDL162C*	2.0	*YGR293C*	2.4	*YMR031W-A*	2.0
SPO69	4.0	*YDL196W*	2.0	*YHL049C*	4.5	*YMR086C-A*	2.0
SRL1	2.1	*YDL221W*	2.1	*YHL050C*	3.8	*YMR122C*	2.1
SSS1	2.5	*YDR018C*	2.2	*YHR049C-A*	2.7	*YMR254C*	2.2
STE2	2.3	*YDR048C*	2.0	*YHR212C*	2.6	*YMR304C-A*	3.1
STE6	2.1	*YDR133C*	2.3	*YHR213W*	2.7	*YMR306C-A*	2.1
SUL1	2.0	*YDR154C*	2.2	*YHR214W*	2.3	*YMR326C*	2.5
TDA8	3.7	*YDR203W*	2.2	*YHR217C*	3.2	*YNL017C*	2.3
TEF1	2.7	*YDR526C*	2.2	*YHR218W*	5.0	*YNL019C*	2.1
TEF2	2.5	*YDR535C*	2.1	*YHR219W*	5.0	*YNL033W*	2.2
THI11	2.4	*YDR543C*	2.9	*YIL012W*	2.1	*YNL120C*	2.0
THI12	2.4	*YEL073C*	2.2	*YIL082W*	4.7	*YNL143C*	2.4
THI13	2.6	*YEL074W*	4.4	*YIL100W*	6.3	*YNL190W*	3.2
THI5	2.4	*YEL075C*	3.9	*YIL177C*	5.3	*YNL226W*	2.0
TIR2	2.0	*YEL075W-A*	3.4	*YIR040C*	2.2	*YNL337W*	2.7
UBI4	2.0	*YEL076C*	3.7	*YJL067W*	2.1	*YNR077C*	2.9
UIP4	2.0	*YEL076C-A*	3.8	*YJL127W-A*	2.0	*YOL118C*	2.0
UTH1	3.3	*YEL077C*	5.6	*YJL213W*	2.2	*YOL162W*	2.0
VAM10	2.1	*YER053C-A*	2.7	*YJL218W*	2.7	*YOL166C*	3.0
VBA3	2.1	*YER097W*	2.1	*YJL220W*	2.7	*YOR041C*	2.8
VBA5	2.2	*YER187W*	2.1	*YJL225C*	5.1	*YOR050C*	2.8
VMA10	2.1	*YER188W*	3.2	*YJR018W*	2.0	*YOR139C*	2.1
VPS61	2.3	*YER189W*	3.9	*YJR114W*	2.1	*YOR186W*	2.0
XBP1	3.9	*YFL012W-A*	2.2	*YJR154W*	2.0	*YOR248W*	2.7
YAL064W	2.6	*YFL019C*	2.3	*YJR157W*	3.5	*YOR289W*	2.3
YAL064W-B	2.5	*YFL052W*	3.2	*YJR162C*	2.9	*YOR338W*	3.6
YAL065C	3.1	*YFL063W*	3.2	*YKL111C*	2.7	*YOR343C*	2.5
YAL069W	3.2	*YFL064C*	4.3	*YKL162C-A*	2.1	*YOR392W*	2.1
YAR047C	3.1	*YFL065C*	4.3	*YKL169C*	2.0	*YPL136W*	2.1
YAR053W	2.6	*YFL066C*	5.0	*YKL223W*	2.1	*YPR202W*	4.0
YAR060C	2.5	*YFL067W*	2.5	*YKL225W*	3.1	*YPR203W*	4.5
YAR064W	3.7	*YFL068W*	2.6	*YKR032W*	2.0	*YPR204W*	5.6
YAR066W	2.3	*YFR012W*	2.4	*YLL065W*	2.9	*YPS5*	2.2
YBL012C	2.1	*YFR012W-A*	2.4	*YLL066C*	5.0	*YRA1*	3.1
YBL108W	2.0	*YFR035C*	3.8	*YLL067C*	5.8	*YRF1-1*	4.9
YBL109W	3.7	*YFR056C*	2.1	*YLR156W*	3.7	*YRF1-2*	5.4
YBL111C	4.8	*YGL034C*	2.3	*YLR159W*	3.8	*YRF1-3*	5.6
YBL112C	5.0	*YGL074C*	2.0	*YLR161W*	3.6	*YRF1-4*	4.9
YBL113C	6.1	*YGL109W*	2.3	*YLR279W*	2.9	*YRF1-5*	5.0
YBR032W	5.4	*YGL182C*	2.0	*YLR280C*	2.3	*YRF1-6*	5.4
YBR090C	2.0	*YGL258W-A*	2.0	*YLR312C*	5.9	*YRF1-7*	5.7
YBR300C	2.6	*YGL260W*	2.1	*YLR400W*	2.0	*YRF1-8*	5.0
YCR049C	2.0	*YGL262W*	4.9	*YLR462W*	4.4	*YSY6*	2.0
YCR064C	2.1	*YGR079W*	2.4	*YLR463C*	2.9	*ZEO1*	4.1

Table 3-4. Down-regulated ORFs in a *MAT*a *nup170Δ* mutant.

Gene name	Fold change	Gene name	Fold change	Gene name	Fold change	Gene name	Fold change
ADE12	-2.2	*FIT2*	-4.2	*PHO5*	-8.5	*TKL2*	-2.4
ADE17	-3.7	*FIT3*	-4.0	*PHO8*	-2.5	*VBA1*	-2.0
ADH5	-3.0	*FRE4*	-3.3	*PHO89*	-4.4	*WSC4*	-2.4
ANB1	-2.3	*HEM13*	-2.1	*PLB2*	-3.0	*YDL038C*	-2.3
ARG1	-5.4	*HIS4*	-3.0	*PRM7*	-2.2	*YHB1*	-2.5
ARG3	-2.6	*HO*	-2.6	*RNR3*	-2.1	*YHR140W*	-2.4
ARN2	-3.3	*HSP30*	-5.0	*RPI1*	-2.0	*YKL153W*	-2.3
BNA4	-2.3	*HUG1*	-2.6	*RSN1*	-2.6	*YLR302C*	-3.3
CMK2	-2.6	*IZH4*	-2.0	*SAP4*	-2.0	*YLR346C*	-3.5
CPS1	-2.4	*MET22*	-2.6	*SPL2*	-2.7	*YMR173W-A*	-2.9
DAN1	-3.2	*PCL7*	-2.0	*SSU1*	-2.3	*YNL217W*	-2.1
DDR48	-2.8	*PDR5*	-3.1	*TDH1*	-3.2	*YOL014W*	-3.1
DIA1	-2.5	*PHM6*	-3.6	*TIR1*	-3.1	*YOR385W*	-2.8
FDC1	-2.1	*PHO11*	-3.4	*TIR3*	-2.2	*ZRT1*	-4.9
FIT1	-5.6	*PHO12*	-3.0	*TIS11*	-2.5		

Table 3-5. Differentially expressed ORFs in *NUP157* and *NUP188* null mutant strains.

*MAT***a** *nup157Δ*			
Up-regulated ORFs		Down-regulated ORFs	
Gene name	Fold change	Gene name	Fold change
ALD4	2.1	*ADE17*	-2.2
ASF1	2.0	*ADR1*	-2.6
AUT7	2.1	*AQR1*	-3.5
CDC3	2.1	*ARG1*	-2.0
COX20	2.4	*ARG5,6*	-2.0
DAN1	2.1	*BSC1*	-2.6
DDR2	3.5	*FRE4*	-2.2
EFB1	2.1	*HAC1*	-2.0
EMI2	2.3	*MDH2*	-5.6
FIT2	2.0	*NSR1*	-2.0
FMP43	2.7	*OLE1*	-2.5
GLK1	2.5	*PDR12*	-4.3
GSY1	3.8	*PRM7*	-2.7
MAG1	2.0	*RIB4*	-3.1
MAM1	2.6	*TAT1*	-2.7
MDJ1	2.6	*TPO2*	-3.0
MRP8	2.4	*URA1*	-7.3
MTR2	2.0	*URA2*	-2.4
NHP2	2.0	*URA4*	-2.2
NRG2	2.8	*UTP10*	-2.0
PBP4	2.5	*YDL038C*	-3.0
PRE6	2.6		
PTR2	2.8		
RGI1	3.7		
RHO5	2.0		
RPL24B	2.1		
RPL27A	2.1		
RPS7B	2.2		
SCD6	2.0		
SEM1	2.0		
SMT3	2.0		
SRP21	2.0		
SSS1	2.3		
STF1	2.7		
TIR1	2.8		
TIR3	2.1		
TRS23	2.1		
YAP6	2.4		
YBL028C	2.0		
YER079W	2.1		
YJL049W	2.0		
YKL063C	2.1		
YLR327C	3.3		

MATα nup188Δ			
Up-regulated ORFs		Down-regulated ORFs	
Gene name	Fold change	Gene name	Fold change
ARG4	2.0	*ACO2*	-2.0
COX5B	2.3	*ADE17*	-2.3
CWP1	2.0	*ADE5,7*	-2.1
DDR2	2.2	*ADE6*	-2.0
ECM4	2.0	*BBC1*	-2.2
EMP46	2.2	*BSC1*	-6.1
GEX1	2.6	*COX19*	-2.2
GEX2	2.0	*CVT17*	-2.2
HSP78	2.4	*DBP2*	-2.8
MRP8	2.0	*DED1*	-3.1
NCE103	2.3	*FAS1*	-2.0
TPK1	2.0	*FAS2*	-2.0
YHL044W	2.1	*FRE4*	-2.0
YIR042C	5.3	*GCV2*	-2.1
YJL218W	3.1	*HAC1*	-2.8
YPR158W	2.0	*HSP30*	-2.8
		HXT1	-2.2
		LYS20	-2.0
		MAE1	-2.8
		NAR1	-2.1
		NUP1	-2.7
		OLE1	-2.2
		PDR12	-2.9
		PRM7	-3.6
		PTK1	-2.0
		RPA135	-2.1
		RPA190	-2.0
		RPG1	-2.9
		RRP12	-2.5
		RTG1	-2.0
		SHM2	-2.4
		STP4	-3.5
		SWH1	-3.2
		TPO2	-2.7
		TRM5	-2.7
		UBR2	-2.0
		UTP10	-2.0
		WHI5	-2.5
		YBL111C	-2.3
		YBL112C	-2.4
		YDL038C	-6.1
		YDL109C	-2.0
		YFL066C	-2.7
		YHL050C	-2.0
		YHR218W	-2.3
		YMR317W	-2.0
		YPK2	-3.2
		YPS3	-2.3
		ZRT1	-2.4

Table 3-6. Up-regulated ORFs following Sth1p depletion for 2 h.

Gene name	Fold change	Gene name	Fold change	Gene name	Fold change	Gene name	Fold change
AAP1	2.1	*FRM2*	2.7	*MGR1*	2.9	*TDA8*	2.1
ACO1	2.6	*FYV2*	2.3	*MPD1*	2.4	*TDH2*	2.1
ACP1	2.6	*GAL10*	2.0	*NAT4*	2.1	*THI4*	2.1
ADD37	2.7	*GAL2*	2.0	*NCA3*	2.0	*TIP1*	2.1
ADH1	2.5	*GAT3*	2.4	*NDE2*	2.3	*TIR1*	5.3
ADR1	3.8	*GDB1*	3.0	*NQM1*	2.3	*TIR2*	2.3
AHP1	2.5	*GFA1*	2.3	*OPI3*	2.1	*TKL2*	2.7
AHT1	2.2	*GIT1*	4.0	*OPI7*	2.0	*TOS6*	3.1
AIM26	2.1	*GPH1*	2.5	*OSW1*	2.8	*TSA1*	2.1
ALP1	3.3	*GPM1*	2.2	*OYE3*	17.4	*UBA1*	2.5
AOR1	2.0	*GRE1*	2.0	*PBI2*	2.7	*ULI1*	6.2
APG17	2.2	*GSC2*	2.8	*PCH2*	2.0	*URA3*	2.6
API2	2.1	*HAC1*	2.1	*PCL1*	2.1	*VBA3*	2.5
ARG1	4.9	*HEM13*	3.3	*PDI1*	3.6	*VBA5*	2.6
ARG3	5.7	*HHY1*	3.0	*PGK1*	2.1	*VTC3*	2.1
ASG7	2.3	*HIS3*	2.6	*PHO3*	2.0	*YAL004W*	2.4
AVT6	2.2	*HLR1*	2.9	*PHO89*	2.0	*YAL034C-B*	2.4
BAP2	2.8	*HMRA1*	2.6	*PIM1*	2.1	*YAL065C*	2.0
BAT2	3.5	*HMS1*	2.8	*PMT1*	2.2	*YAL066W*	2.2
BCH2	2.0	*HOP1*	2.0	*POR1*	2.1	*YAR061W*	2.1
BFR1	2.1	*HOR7*	2.2	*PRY1*	4.3	*YAR064W*	2.4
BOP2	2.4	*HSC82*	2.2	*PUS2*	2.2	*YAR069C*	2.0
BUD25	2.2	*HSP10*	2.1	*QDR2*	2.1	*YAR070C*	2.3
BUD26	2.4	*HSP26*	2.5	*RAD23*	2.1	*YBL073W*	2.4
CAT2	2.0	*HSP32*	2.0	*RAD51*	2.1	*YBL107W-A*	2.6
CDC19	2.2	*HSP33*	2.0	*RCK1*	3.5	*YBL108W*	2.8
CDC48	2.1	*HSP60*	2.9	*REC102*	2.0	*YBR012C*	2.7
CIN5	3.1	*HXT10*	2.9	*REC114*	2.1	*YBR032W*	2.0
COX23	2.6	*HXT12*	2.1	*RGI2*	2.4	*YBR051W*	2.3
CPR1	2.3	*HXT12*	2.1	*RNR3*	2.4	*YBR124W*	2.6
CRC1	2.1	*HXT13*	2.2	*RPS9A*	2.1	*YBR144C*	2.0
CSM4	2.1	*HXT14*	2.7	*RRT12*	2.7	*YBR209W*	2.4
CTR3	2.0	*HXT16*	2.0	*RRT16*	2.6	*YBR219C*	2.1
CYM1	2.1	*HXT9*	2.0	*RRT5*	2.3	*YBR232C*	2.1
DAK2	2.0	*ICS2*	2.6	*RRT7*	2.3	*YBR300C*	2.4
DAN1	3.5	*IME4*	2.1	*SAE3*	2.8	*YCL023C*	2.1
DSK2	2.1	*INO1*	3.4	*SED1*	3.0	*YCL042W*	2.2
ECL1	2.3	*IRC13*	2.4	*SIL1*	5.1	*YCL065W*	2.2
ECM11	2.1	*IRC18*	2.0	*SIP18*	5.0	*YCL076W*	2.4
ECM34	2.4	*IRC7*	2.2	*SMA1*	2.8	*YCR001W*	2.3
ECM8	5.0	*KAR2*	5.6	*SMA2*	2.2	*YCR038W-A*	2.0
EGT2	2.6	*KRE21*	2.0	*SNO4*	2.0	*YCR102W-A*	2.2
ENO1	2.1	*KRE24*	2.7	*SOR2*	2.5	*YDL032W*	3.8
ENO2	2.5	*KRE25*	2.1	*SPR28*	3.4	*YDL034W*	2.3
ERO1	2.8	*KRE26*	2.0	*SPS1*	2.2	*YDL068W*	2.2
ERR1	2.2	*LCL1*	2.2	*SPS100*	2.7	*YDL114W*	2.3
ERR2	2.2	*LCL2*	3.2	*SPS2*	2.4	*YDL118W*	2.2
ERR3	2.5	*LEU1*	2.2	*SPS22*	2.8	*YDL124W*	2.5
ERV46	2.2	*LEU2*	2.6	*SPS4*	2.1	*YDL159W-A*	2.2
EUG1	2.1	*LOH1*	2.0	*SPT16*	2.1	*YDL221W*	2.2
EXG1	2.0	*LYS20*	3.0	*SRX1*	2.5	*YDL240C-A*	2.6
FBP1	2.6	*MAL32*	2.2	*SSA2*	2.9	*YDL241W*	2.1
FDH1	2.8	*MAS6*	2.1	*SSC1*	2.2	*YDL242W*	2.4
FDH2	2.7	*MCD4*	2.2	*SSS1*	2.1	*YDR010C*	2.1
FDH2	2.5	*MCH2*	2.4	*SSU1*	2.0	*YDR015C*	2.3
FMP45	3.1	*MEI5*	2.1	*STL1*	2.1	*YDR034C-A*	2.0
FMP52	2.6	*MER1*	2.2	*SWF5*	2.6	*YDR154C*	2.8
FRE5	2.0	*MFa1*	2.4	*TAD2*	2.6	*YDR193W*	2.1

YDR215C	2.5	*YGR164W*	2.5	*YKL097C*	2.0	*YNL067W-A*	2.0
YDR220C	2.4	*YGR176W*	2.1	*YKL102C*	2.7	*YNL184C*	2.6
YDR269C	2.4	*YGR226C*	2.8	*YKL107W*	2.3	*YNL198C*	2.2
YDR278C	2.7	*YGR242W*	2.3	*YKL147C*	2.4	*YNL205C*	2.2
YDR290W	2.2	*YGR290W*	2.4	*YKL223W*	2.7	*YNL324W*	2.5
YDR340W	2.6	*YGR293C*	2.8	*YKR032W*	2.6	*YNR064C*	2.0
YDR401W	2.2	*YHL005C*	2.1	*YKR033C*	2.4	*YOL013W-A*	2.1
YDR442W	2.1	*YHL041W*	2.4	*YLL047W*	2.3	*YOL046C*	2.0
YDR476C	2.0	*YHR033W*	2.3	*YLL065W*	2.1	*YOL085C*	2.4
YDR521W	2.4	*YHR095W*	2.1	*YLR012C*	2.0	*YOL131W*	2.5
YDR537C	2.3	*YHR125W*	2.3	*YLR111W*	2.1	*YOR008C-A*	2.1
YDR544C	2.3	*YIL012W*	2.1	*YLR124W*	2.2	*YOR024W*	3.3
YEL010W	2.1	*YIL025C*	2.4	*YLR235C*	2.3	*YOR029W*	2.6
YER084W	2.8	*YIL032C*	2.3	*YLR236C*	2.1	*YOR050C*	2.0
YER091C-A	4.4	*YIL100W*	2.1	*YLR296W*	2.7	*YOR055W*	2.2
YER135C	2.0	*YIL102C*	2.1	*YLR334C*	2.1	*YOR082C*	2.5
YER138W-A	2.9	*YIL163C*	2.1	*YLR349W*	2.4	*YOR139C*	2.3
YER163C	2.0	*YIL174W*	2.2	*YLR366W*	2.5	*YOR214C*	2.2
YFL012W-A	2.4	*YIR020W-B*	2.2	*YLR374C*	2.0	*YOR268C*	2.3
YFL015C	2.3	*YIR040C*	2.3	*YLR402W*	2.3	*YOR314W*	2.3
YFL032W	2.2	*YJL022W*	2.1	*YLR413W*	2.1	*YOR314W-A*	2.2
YFL040W	2.2	*YJL028W*	2.6	*YLR415C*	2.1	*YOR325W*	2.0
YFL051C	2.2	*YJL043W*	2.4	*YLR416C*	2.7	*YOR376W*	2.5
YFR057W	2.7	*YJL052C-A*	2.8	*YLR458W*	2.4	*YOR392W*	2.0
YGL034C	2.3	*YJL086C*	2.9	*YML047W-A*	2.4	*YPL062W*	2.5
YGL074C	2.1	*YJL135W*	2.2	*YML083C*	2.1	*YPL073C*	2.0
YGL088W	2.7	*YJL150W*	2.1	*YML094C-A*	2.4	*YPL080C*	2.4
YGL118C	2.0	*YJL160C*	2.1	*YML101C-A*	2.1	*YPL261C*	2.7
YGL138C	2.1	*YJL182C*	2.1	*YMR013W-A*	2.1	*YPR014C*	2.3
YGL182C	2.2	*YJL195C*	2.2	*YMR057C*	2.2	*YPR039W*	2.6
YGL188C	2.0	*YJL220W*	2.1	*YMR082C*	2.0	*YPR074W-A*	2.7
YGL260W	2.2	*YJR020W*	2.5	*YMR122C*	2.4	*YPR078C*	2.4
YGL262W	2.4	*YJR037W*	2.2	*YMR135W-A*	2.3	*YPR096C*	3.4
YGR025W	3.2	*YJR038C*	2.6	*YMR158W-A*	2.1	*YPR177C*	2.4
YGR039W	2.0	*YJR120W*	2.3	*YMR324C*	2.7		
YGR051C	2.2	*YJR128W*	2.5	*YMR326C*	2.0		

Table 3-7. Down-regulated ORFs following Sth1p depletion for 2 h.

Gene name	Fold change	Gene name	Fold change	Gene name	Fold change	Gene name	Fold change
ADH5	-2.3	*FDC1*	-2.1	*PHR1*	-2.1	*YBR184W*	-2.1
ADI1	-4.4	*FIN1*	-2.0	*PIC2*	-5.0	*YBR287W*	-2.1
AEP2	-2.2	*FMP48*	-2.1	*PIG2*	-2.5	*YCL049C*	-2.1
AGA1	-3.5	*FUS3*	-2.3	*PRM1*	-2.3	*YCR023C*	-2.4
AGP1	-2.1	*GAC1*	-2.4	*PUS9*	-2.5	*YDR248C*	-2.1
AIM17	-2.1	*GCV1*	-2.9	*PUT1*	-3.5	*YEA4*	-2.6
ALT2	-2.6	*GPM2*	-2.0	*RAD59*	-2.8	*YER053C-A*	-3.5
APC11	-3.6	*GRX8*	-6.2	*REX2*	-2.5	*YER134C*	-2.5
APJ1	-2.1	*GTB1*	-2.1	*RGI1*	-3.4	*YGL039W*	-2.0
ARO3	-2.0	*HOT13*	-2.5	*RIT1*	-2.2	*YGL159W*	-3.5
ATP20	-2.8	*HPA3*	-2.6	*RMD6*	-2.9	*YGR250C*	-3.3
BER1	-2.1	*HRK1*	-2.0	*RME1*	-2.0	*YIH1*	-2.0
BLI1	-2.0	*HSP30*	-3.0	*RPC11*	-2.1	*YIR035C*	-2.4
BNA3	-2.6	*HSP42*	-4.1	*RTS2*	-3.5	*YJL144W*	-3.0
BNA4	-2.2	*HXT4*	-4.7	*RTT10*	-2.1	*YJR129C*	-2.1
BTN2	-4.6	*IML2*	-2.0	*SCM4*	-4.2	*YKL033W-A*	-2.8
CAR1	-2.9	*IRC11*	-3.2	*SEC20*	-2.2	*YKR075C*	-2.2
CMK2	-2.0	*KRE34*	-2.0	*SFK1*	-2.3	*YLR177W*	-2.0
COS7	-2.2	*LCB3*	-2.4	*SNL1*	-2.3	*YLR241W*	-2.2
COX19	-2.3	*LOT6*	-2.3	*SNN1*	-2.1	*YLR326W*	-2.0
CRS5	-2.4	*MDM35*	-2.4	*SPI1*	-2.1	*YMR147W*	-3.1
CSI1	-2.0	*MEP1*	-2.5	*STH1*	-4.4	*YND1*	-2.5
DBP10	-2.7	*MGA1*	-2.3	*SWM1*	-2.0	*YNL144C*	-3.3
DFG10	-2.3	*MMP1*	-4.3	*TDA6*	-2.5	*YNL200C*	-2.3
DIA1	-3.7	*MMS2*	-3.0	*TIM9*	-2.5	*YNR034W-A*	-2.3
DPB11	-2.1	*MPP6*	-2.3	*TMA10*	-6.7	*YOL014W*	-3.4
DSD1	-2.0	*MTH1*	-2.5	*TMA17*	-2.4	*YOL153C*	-2.2
DUG3	-2.4	*MUP3*	-6.6	*TMT1*	-2.1	*YOL163W*	-2.5
DUR1,2	-3.8	*NDE1*	-2.4	*TVP38*	-2.5	*YOR012W*	-2.4
DUR3	-2.9	*NPP1*	-2.3	*UBC5*	-2.1	*YOR338W*	-2.8
DUT1	-2.0	*NPT1*	-2.5	*UBX3*	-2.0	*YOR385W*	-3.5
ELP3	-2.3	*NTF2*	-2.2	*UBX6*	-2.4	*YPK2*	-2.0
ELP4	-2.7	*ODC2*	-4.3	*UIP3*	-2.2	*YPK9*	-2.3
ERG1	-2.3	*OKP1*	-2.0	*UPS3*	-2.4	*YPL071C*	-2.0
ERG26	-2.1	*OPI10*	-2.3	*USV1*	-2.0	*YPR146C*	-2.0
ERG5	-2.0	*PDR11*	-2.0	*VHS1*	-2.4	*ZEO1*	-2.0
ERV1	-2.3	*PGM1*	-2.1	*VID24*	-2.0	*ZPS1*	-3.0

Table 3-8. Differentially expressed ORFs following *STH1* reinduction for 4 h.

Up-regulated ORFs			
Gene name	Fold change	Gene name	Fold change
ADR1	2.4	*PRB1*	2.8
ARE1	2.0	*PRM10*	2.0
AVT6	2.3	*PRM5*	2.4
BAR1	2.1	*PYC1*	2.4
CPR6	2.0	*RNP1*	2.3
CRR1	2.2	*RSC30*	2.1
CSR2	2.0	*SFC1*	2.9
DDR2	2.7	*SGA1*	2.7
DIC1	3.6	*SIT1*	2.2
DLD3	2.8	*SNO4*	3.8
ECM8	2.6	*SOM1*	2.0
FIT2	5.9	*SRL3*	2.3
FIT3	4.5	*SRL4*	2.7
FMP16	2.4	*SSP1*	2.0
FRE1	2.3	*SUT1*	2.1
GDH3	2.7	*THI12*	2.8
GND2	2.7	*TIR2*	2.3
HES1	2.5	*TIS11*	2.5
HSP150	2.3	*ULI1*	2.4
HXT2	2.5	*UTH1*	2.1
HXT5	5.8	*VMR1*	2.3
MAL33	2.8	*VRP1*	2.0
MAM1	2.4	*YAP6*	2.0
MET10	2.0	*YBR284W*	2.4
MET14	2.7	*YCL027C-A*	2.4
MET17	2.6	*YDL038C*	2.2
NCA3	2.0	*YDR042C*	2.1
NCE103	2.9	*YDR476C*	2.0
NQM1	2.0	*YHR054C*	2.0
PAU15	2.1	*YJR128W*	2.2
PAU21	2.5	*YJR157W*	2.5
PAU22	2.4	*YKE4*	2.5
PET117	2.1	*YPS3*	2.1
PIR3	2.8	*ZWF1*	2.9

Down-regulated ORFs			
Gene name	Fold change	Gene name	Fold change
ADE1	-5.2	*LSP1*	-2.1
ADE12	-2.7	*MTD1*	-5.6
ADE13	-5.4	*NCE102*	-2.2
ADE17	-16.6	*PIC2*	-3.9
ADE2	-6.9	*PLB2*	-2.4
ADE4	-3.5	*PSD1*	-2.3
ADE5,7	-4.4	*RGI1*	-7.1
ADE6	-3.3	*SHM2*	-9.0
AGP1	-4.0	*SPI1*	-5.4
ARG4	-2.2	*STF2*	-2.5
CAR1	-2.5	*STP4*	-3.8
CHO1	-2.3	*TDH1*	-3.6
CLB1	-2.3	*TPO2*	-4.3
CMK2	-2.7	*TPO3*	-3.3
DIA1	-2.1	*TYE7*	-2.1
DUR1,2	-2.0	*YDR222W*	-2.7
EIS1	-2.1	*YER130C*	-2.4
GAP1	-2.2	*YGP1*	-2.3
GAS3	-2.1	*YGR250C*	-2.7
GCV1	-11.0	*YKR075C*	-3.5
GCV2	-8.5	*YMR173W-A*	-2.7
GCV3	-3.8	*YPL014W*	-4.6
HAP4	-2.4	*YRO2*	-3.5
HIS4	-4.1	*ZRT1*	-6.3
HIS5	-2.4		
HNM1	-2.5		
HPT1	-2.1		
HSP30	-10.7		
HTB1	-2.0		
HXT1	-2.1		
HXT3	-2.0		
HXT4	-5.4		
HXT6	-3.0		
ICY1	-3.5		

Furthermore, in WT cells repression of *ADE2* results in formation of red colonies. By contrast, the loss of a silencing factor, such as Sir3p (*sir3Δ*), favors derepression of the *URA3* and *ADE2* reporter genes producing white colonies and allowing cell growth on medium lacking adenine and uracil, but rendering them sensitive to 5-FOA (Figure 3-5; Aparicio et al., 1991). An examination of *nup170Δ* cells revealed a similar loss of silencing that could be reversed by addition of an exogenous copy of *NUP170*. Similar silencing defects were not detected in *nup2Δ, nup60Δ*, or *nup188Δ* mutants, however a mild silencing defect was observed in the absence of the Nup170p binding partner Nup53p (Figure 3-5).

We also examined the silencing characteristics of cells lacking components of the RSC complex. While certain subunits of the RSC complex are essential, others are not, allowing us to test the effects of mutations in several RSC components, including *rsc1Δ*, *rsc3Δ*, *rsc7Δ,* and *htl1Δ*, on silencing of the *URA3* and *ADE2* reporter genes. Loss of silencing was most evident and reproducibly detected in the *rsc3Δ* and *htl1Δ* null mutants (Figure 3-5), albeit to a lesser extent than either *nup170Δ* or *sir3Δ*. The milder silencing phenotypes of these *rsc* mutants may be explained by the fact that they do not compromise the essential function of RSC.

Figure 3-5. Nup170p and RSC function in subtelomeric gene silencing.

(A) The indicated gene deletions were introduced into yeast strain UCC3505 encoding *URA3* and *ADE2* integrated adjacent to Tel7L and Tel5R, respectively. Silencing of the subtelomeric reporter genes *URA3* and *ADE2* was examined in the indicated haploid strains containing pRS315 (vector), pHNP170 (p*NUP170*) (*top panel*), or no plasmid (*middle and bottom panels)*. Following overnight growth in non-selective liquid medium, an equal number of cells from each culture were serially diluted and plated onto nonselective (control [SC medium]) and selective conditions (SC medium lacking uracil and adenine [-ura-ade] or SC medium containing 1 mg/mL 5-FOA [5-FOA]) and incubated for 2-5 d at 30˚C. To maintain plasmid selection, strains bearing pRS315 or pHNP170 were plated on SC medium lacking leucine (control), SC-leu-ura-ade (-ura-ade), and SC-leu + 1 mg/mL 5-FOA (5-FOA). (B) Silencing of the subtelomeric reporter gene *ADE2* at Tel5R was examined in the indicated haploid strains. In a WT strain, most cells in the population silence *ADE2* and give rise to red colonies. By contrast, a silencing deficient strain (*sir3Δ*) fails to repress *ADE2*, producing white colonies. To evaluate the efficiency of silencing in various strains, individual red colonies from culture plates were used to inoculate overnight cultures in non-selective YPD medium. In the case of the silencing deficient *sir3Δ* an individual white colony was selected. Cells where then spotted on YPD plates and incubated for 4 d at 30˚C. Red and white colonies indicate repressed and derepressed *ADE2* phenotypes, respectively.

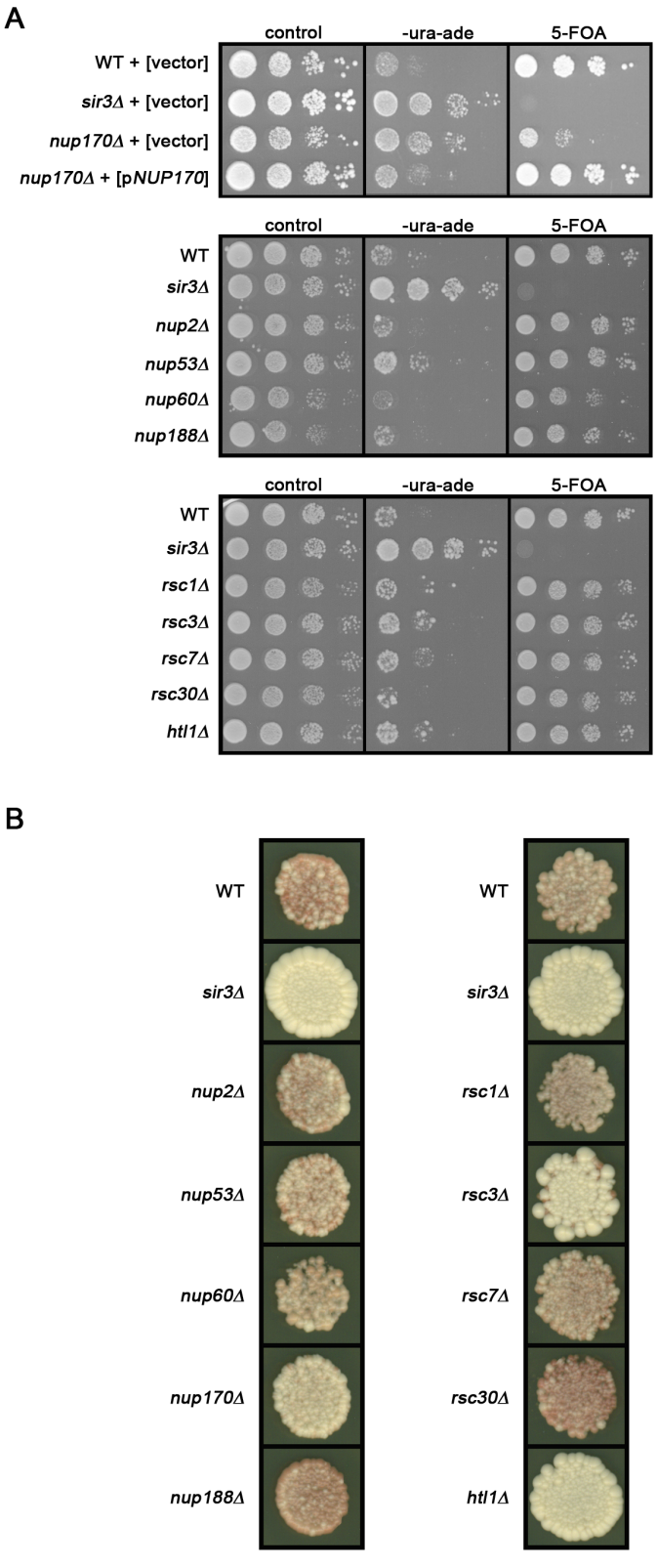

Figure 3-5. Nup170p and RSC function in subtelomeric gene silencing.

3.2.4 Loss of Nup170p alters nucleosome occupancy in subtelomeric chromatin

Nucleosomes in the vicinity of transcriptional start sites (TSS) exhibit a characteristic organization, with a nucleosome free region (NFR) adjacent to the TSS, flanked by a periodic array of upstream and downstream nucleosomes. RSC is an important contributor to this nucleosome pattern (Badis et al., 2008; Parnell et al., 2008; Hartley and Madhani, 2009). Our observations that Nup170p is required for subtelomeric gene silencing led us to hypothesize that Nup170p plays a role in subtelomeric chromatin structure. To test this, we performed genome-wide nucleosome mapping using next-generation DNA sequencing of nuclease-protected chromatin. The positions of nucleosome dyads were estimated at the 5'-end of ORFs and aligned relative to the TSS. We compared nucleosome occupancy in WT and *nup170Δ* strains both genome-wide and in 25 kb segments extending from the ends of chromosomes as transcriptional changes observed in the *nup170Δ* mutant clustered near telomeres. WT cells reveal canonical positioning of the -1 and +1 nucleosomes flanking the NFR followed by periodic phasing of downstream nucleosomes, similar to previous genome-wide studies (Figure 3-6A; Weiner et al., 2010). However, *nup170Δ* cells exhibited a reduction in occupancy of the +1 nucleosome and, to a lesser extent, the -1 nucleosome (Figure 3-6B). Furthermore, the reduction in -1 and +1 nucleosome occupancy was more prominent within subtelomeric regions (0-25 kb), while adjacent regions (25-50 kb) showed no significant differences when compared to the WT control (Figure 3-6C and 3-6D). As with the subtelomeric regions, nucleosome

Figure 3-6. Nup170p is required for nucleosome occupancy in subtelomeric chromatin.

Yeast strains YWY003 (WT) and YWY973 (*nup170Δ*) were grown to mid-logarithmic growth phase and nucleosomes were crosslinked to DNA with 1% formaldehyde for 20 min prior to cell collection. Cells were then permeabilized and treated with micrococcal nuclease to generate mononucleosomal DNA fragments. Next generation sequencing of isolated mononucleosomal DNA permitted the genome-wide identification of nucleosome positions. Nucleosome occupancy at the 5'-end of non-dubious ORFs was analyzed, encompassing the region from -400 bp to +400 bp relative to the transcriptional start site (TSS) of each ORF. (A) Promoter nucleosome occupancy is similar among WT strains. Shown is the mean nucleosome occupancy score at the 5'-end of 5419 non-dubious ORFs aligned based on transcriptional start site (TSS) for WT cells in this study (blue) and WT cells in Weiner et al., 2010 (red). (B-E) TSS-aligned average nucleosome occupancy scores at the 5'-end of 5419 non-dubious ORFs as determined in this study for WT (blue) and *nup170Δ* (red) cells for 5419 ORFs genome wide (B) and ORFs located within regions 0-25 kb (149 ORFs; panel C), and 25-50 kb (343 ORFs; panel D) from chromosome ends. Similar analysis was performed on the 137 ribosomal protein genes (panel E). Note, nucleosome occupancy at the -1 and +1 positions is reduced genome-wide in *nup170Δ* cells with a greater reduction observed within subtelomeric regions (0-25 kb) than within adjacent non-subtelomeric regions (25-50 kb). A similar reduction in nucleosome occupancy was also observed at RP genes in *nup170Δ* cells.

* Experimental procedures involving nucleosome positioning analysis was performed by YW with data analysis performed by WMC. Figure processing was performed by WMC, YW and DWV.

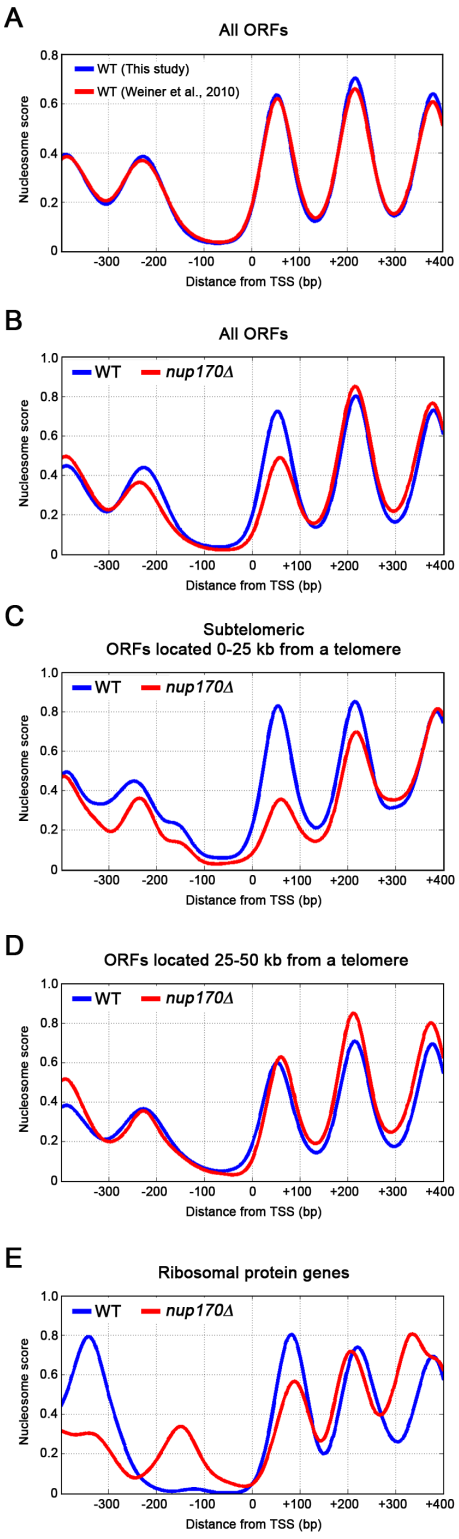

Figure 3-6. Nup170p is required for nucleosome occupancy in subtelomeric chromatin.

profiles were also dramatically altered at RP genes (Figure 3-6E). These data, together with the transcriptional profiles (Figure 3-4), further pointed to a role for Nup170p in defining chromatin structure within subtelomeric regions and RP genes.

3.2.5 Nup170p is enriched at RP genes and subtelomeric DNA

To understand the mechanism by which Nup170p contributes to subtelomeric chromatin structure, we investigated the physical interactions of Nup170p with chromatin. Chromatin immunoprecipitation (ChIP) analysis was performed on strains producing Nup170p tagged with 9xMyc to identify associated DNA. Initially, quantitative, real-time PCR (qPCR) assays were used to assess the interactions of Nup170p with subtelomeric DNA adjacent to a representative telomere (Tel6R). This analysis revealed a significant enrichment of DNA derived from the proximal region of Tel6R associated with Nup170p (Figure 3-7A). These interactions appeared specific for Nup170p, as only background levels of DNA were associated with Nup157p and Nup188p.

The association of Nup170p with chromatin regions proximal to Tel6R prompted a genome-wide analysis to identify DNA regions bound to Nup170p. Using ChIP and DNA microarrays (ChIP-chip), we detected specific regions of the genome enriched in association with Nup170p. Prominent among these were regions of DNA within 10 kb of chromosome ends (DNA enriched with Nup170p significantly bound 117 of 439 probes within 10 kb of a telomere; hypergeometric test, p-value = 1.14×10^{-48}), corresponding to subtelomeric regions of 23 of 32

telomeres, including Tel6R (Figure 3-7B, 3-7C and 3-8A). In addition, we detected most RP genes in association with Nup170p (131 of 137; hypergeometric test, p-value 3.28 x 10^{-112}, and Figure 3-8B). DNA interactions were specific for Nup170p and are not detected when similar experiments were performed on Nup157p (Figure 3-7). Thus, our results are consistent with the physical interaction of Nup170p with regions of chromatin proximal to telomeres and RP genes.

3.2.6 Association of Nup170p with subtelomeric DNA is mediated by Sir4p

Nup170p lacks a detectable DNA binding motif, thus its interactions with specific chromatin regions is likely mediated by a binding partner. Rap1p, together with the yKu70/yKu80 heterodimer and the silent information regulator (SIR) complex (Sir2p, Sir3p, and Sir4p), function in the structural organization of telomeric and subtelomeric chromatin. The positioning and functions of these proteins led us to examine whether they physically interact with Nup170p. Three candidates, Rap1p, yKu70p, and Sir4p, were selected for analysis. In analyzing Nup170-pA purified from cell extracts, we did not detect yKu70-13xMyc or Rap1-13xMyc; however, Sir4-13xMyc was bound to Nup170-pA (Figure 3-9). Moreover, in reciprocal experiments we detected Nup170-13xMyc bound to purified Sir4-pA (Figure 3-9D). The specificity of the Sir4p-Nup170p interaction was also supported by experiments examining the binding of Sir4p to two other Nups, Nup157p and Nup84p. Nup157p is physically associated with Nup170p (Alber et al. 2007b; Amlacher et al., 2011) while Nup84p is a member of a

Figure 3-7. Nup170p is enriched at subtelomeric DNA.

(A) Isogenic yeast strains synthesizing the C-terminal fusion proteins Nup170-9xMyc (red), Nup157-9xMyc (blue), and Nup188-9xMyc (green) were constructed from BY4742 and were grown to mid-logarithmic growth phase. Proteins were crosslinked to their cognate DNA binding sites with 1% formaldehyde for 1 h prior to cell lysis. Following cell disruption, chromatin was sheared and the indicated proteins were immunoprecipitated using an anti-Myc antibody conjugated to magnetic beads. Crosslinks were reversed in both the ChIP and whole cell lysate fractions and samples were analyzed by quantitative real-time PCR (qPCR) using primer sets positioned along a 20 kb subtelomeric region of the right arm of chromosome VI (x-axis). Mean relative enrichment of three independent ChIP experiments is plotted on the y-axis with standard error. (B) To determine the genome-wide binding profile of Nup170-9xMyc, ChIP was performed as described in panel A. However, following removal of crosslinks, the ChIP and whole cell lysate samples were amplified by PCR, labeled, and hybridized to whole-genome tiling arrays. Shown are the binding profiles of Nup170-9xMyc (red) and as a control Nup157-9xMyc (blue) along a representative chromosome (Chromosome VI) as a logarithmic function of their p-value (y-axis; $-\log_{10}$) as determined by ChIP-chip analysis. Statisitical significance (p-value ≤ 0.05) is indicated by a horizontal dashed line while subtelomeric regions are indicated by blue shading. Black rectangles represent ORFs located on the Watson and Crick strands. (C and D) Genome-wide DNA binding profiles of Nup170-9xMyc (C) and Nup157-9xMyc (D), as determined by ChIP-chip analysis. Statistically significant binding sites with p-values ≤ 0.05 are marked by red peaks and statistically insignificant binding sites are marked by green peaks. Peak height is inversely proportional to p-value (y-axis; $-\log_{10}$). Subtelomeric regions are indicated by blue shading.

* ChIP-qPCR experiments and data analysis were performed by YW. ChIP-chip experiments were performed by YW with data analysis by WMC and YW and figure processing by WMC, YW, and DWV.

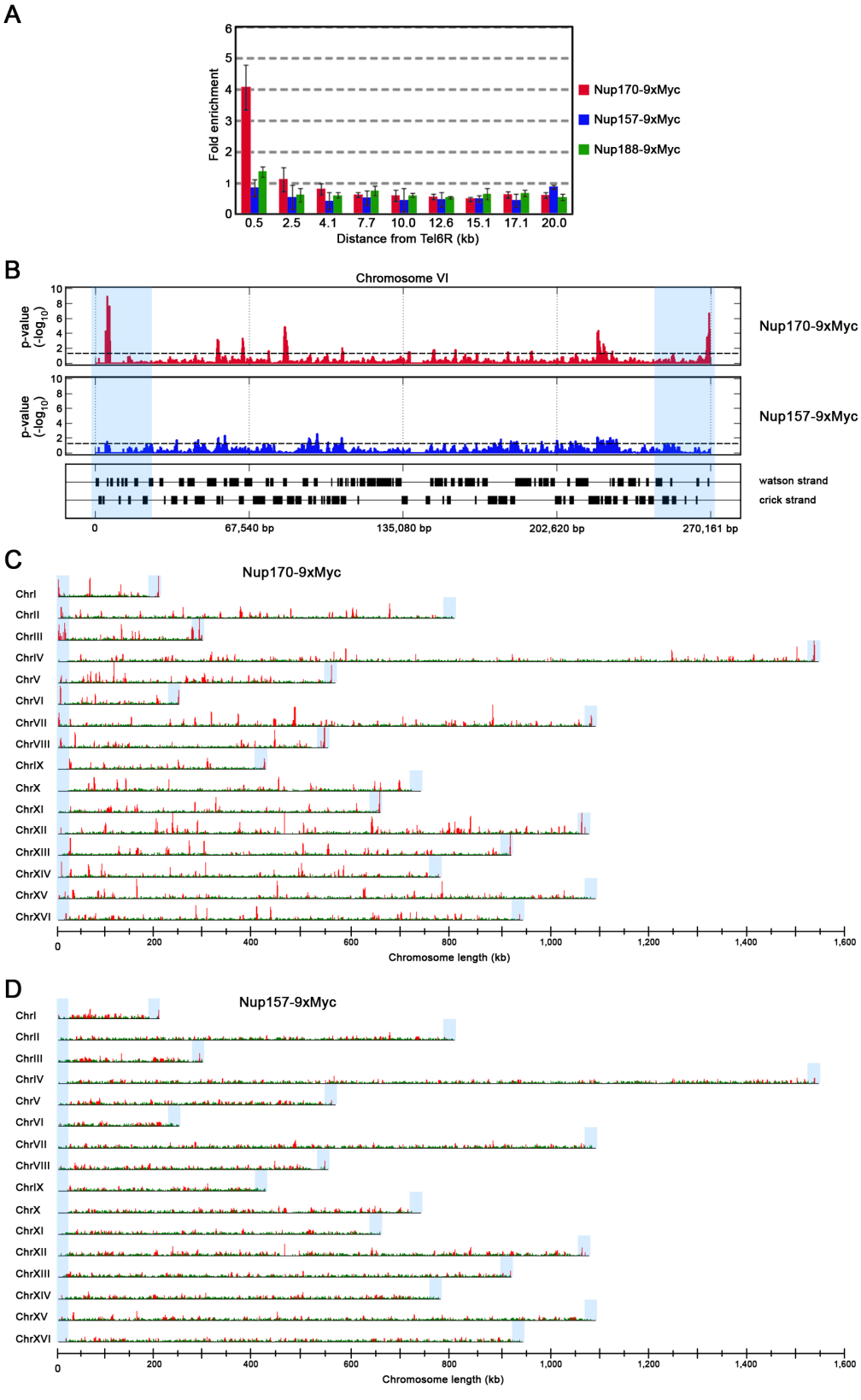

Figure 3-7. Nup170p is enriched at subtelomeric DNA.

Figure 3-8. Nup170p associates with and regulates expression of subtelomeric and ribosomal protein genes.

(A) Visualization of Nup170p binding sites within the 32 subtelomeric regions of the *Saccharomyces cerevisiae* genome using the circular visualization software *Circos* (Krzywinski et al., 2009). Subtelomeric regions are defined as sequences located within 25 kb of a telomere. Nup170p binding sites previously determined by ChIP-chip analysis in Figure 3-7 are color-coded based on percentile-rank score of binding intensity and are located immediately inside the peripheral ring. Up-regulated and down-regulated ORFs in the absence of Nup170p were previously determined in Figure 3-4 and are indicated by red and green lines, respectively, that form the inner-most ring. (B) Comparison of Nup170p DNA binding sites with gene expression changes in the *nup170Δ* mutant. (*left panel*) Changes in gene expression in a *nup170Δ* mutant were determined by microarray analysis (Figure 3-4) and the $\log_2$ expression ratios (*nup170Δ*/WT) for 6193 ORFs are displayed. ORFs are sorted vertically according to Nup170p binding from highest to lowest binding values as indicated in the middle panel. (*middle panel*) Nup170-9xMyc binding sites within the promoter regions (nucleotides -400 to +400 relative to the ATG) of 6193 ORFs as determined by ChIP-chip analysis (Figure 3-7) were aligned relative to the ATG. ORFs are sorted vertically from highest binding (yellow) to lowest binding (blue) according to their rank-sum of $\log_2$ binding ratios and displayed as a heat map. (*right panel*) The location of 109 ribosomal protein genes repressed by Nup170p and the location of 28 ribosomal protein genes whose expression is unaffected by the loss of Nup170p are indicated by blue lines. Note, the location of ribosomal protein genes correlates with high Nup170p DNA binding ratios and increased expression in the absence of Nup170p.

* ChIP-chip and microarray experiments were performed by YW with data analysis performed by WMC, DWV, and YW. Images were processed by WMC and DWV.

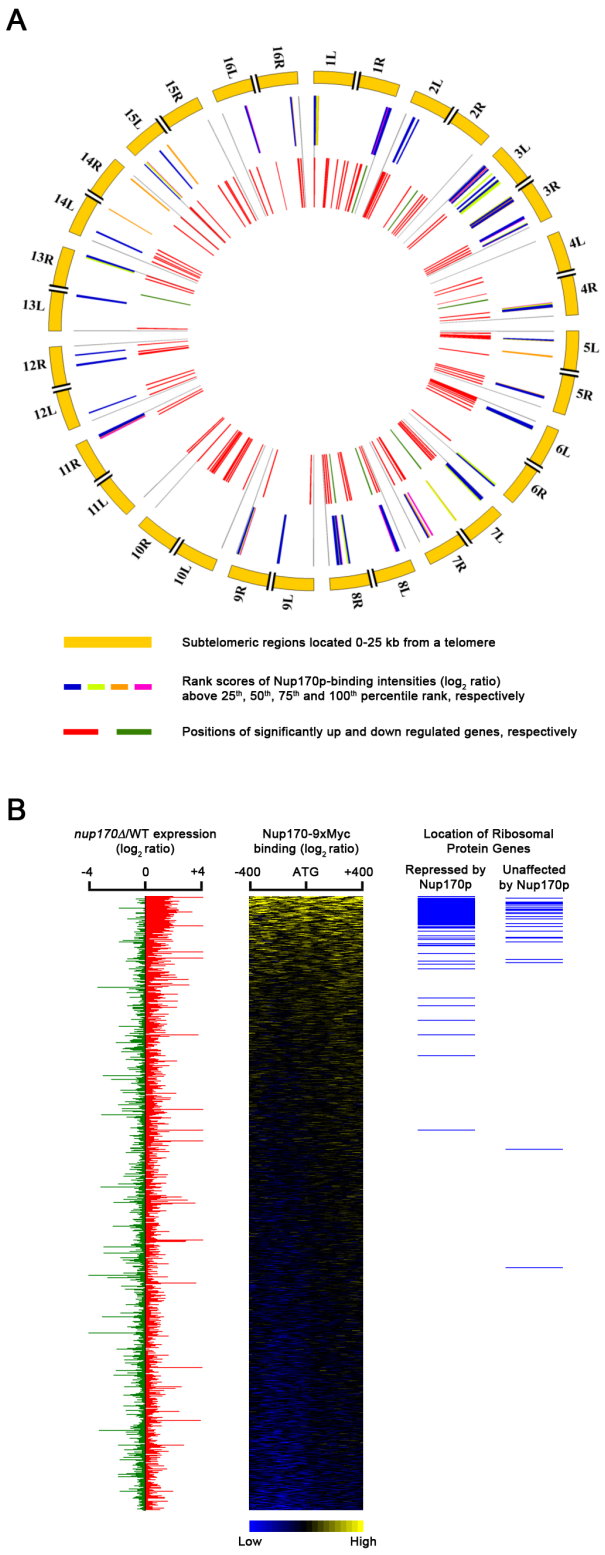

Figure 3-8. Nup170p associates with and regulates expression of subtelomeric and ribosomal protein genes.

distinct NPC subcomplex. Consistent with the interaction of Sir4p with Nup170p, Sir4p was detected in complex with Nup157-pA but not Nup84-pA (Figure 3-9E and 3-9F).

The interactions of Nup170p with Sir4p led us to examine whether the association of Nup170p with subtelomeric regions is dependent on Sir4p. To test this, we performed genome wide ChIP-chip analysis to assess the effects of *sir4Δ* or *yku70Δ* mutations on the binding of Nup170p to chromatin. Loss of Sir4p, but not yKu70p, decreased Nup170p binding to subtelomeric chromatin while showing little affect on Nup170p association with non-subtelomeric DNA (Figure 3-9H and 3-10). By contrast, a *sir2Δ* mutation did not appear to alter the subtelomeric association of Nup170p (Figure 3-9I). Cumulatively, these results are consistent with Sir4p functioning directly or indirectly in facilitating Nup170p binding to subtelomeric chromatin.

3.2.7 Nup170p facilitates Sir4p binding to subtelomeric DNA

We hypothesized that the function of Nup170p in subtelomeric gene silencing is linked to its physical association with Sir4p. Since chromatin association of Sir4p is considered a prerequisite for its role in silencing, we examined the effects of Nup170p loss on the ability of Sir4p to bind a representative telomere, Tel6R. ChIP analysis was performed to assess chromatin association of Sir4-9xMyc in WT and *nup170Δ* cells. As expected, Sir4-9xMyc was significantly enriched at Tel6R in WT cells (Figure 3-11A; Wan et al., 2010). However, in the absence of Nup170p, Sir4-9xMyc association with Tel6R was reduced approximately 4-fold (Figure 3-11A). Concomitant with reduced binding

Figure 3-9. Association of Nup170p with subtelomeric DNA is mediated by Sir4p.

(A-G) Protein A-tagged fusion proteins were affinity purified from cell lysates containing the indicated Myc-tagged proteins as described in Figure 3-3. Cell lysates were prepared from frozen cells using a planetary ball mill and pA-fusion proteins were affinity purified using IgG-conjugated magnetic beads. Bound complexes were released by step elution of increasing concentrations of $MgCl_2$ (Mg^{2+}) and a final acetic acid elution (AA). Eluted proteins were analyzed by SDS-PAGE and western blotting to detect the indicated proteins. Lanes labeled 'load' and 'wash' contain samples of the total cell lysates and the final wash prior to elution. The asterisk indicates an IgG cross-reacting band. (H) Genome-wide DNA binding profiles of Nup170-9xMyc in WT (red), *sir4Δ* (blue), and *yku70Δ* (green) cells were determined by ChIP-chip analysis. Shown is a representative binding profile of Nup170-9xMyc along chromosome VI (x-axis) as a logarithmic function of its p-value (y-axis; $-\log_{10}$). Subtelomeric regions are indicated by blue shading and black rectangles represent ORFs encoded by the Watson and Crick strands. (I) Nup170-9xMyc ChIP samples were derived as from an otherwise WT strain (blue) or a *sir2Δ* strain (red) and analyzed by qPCR using primer sets dispersed along a 20 kb subtelomeric region of the right arm of chromosome VI (x-axis). Mean relative enrichment of three independent ChIP experiments is plotted on the y-axis with standard error. Note, the telomere bound proteins yKu70p and Rap1p failed to interact with Nup170-pA. In contrast, Sir4p interacted with both Nup170-pA as well as an additional subunit of the Nup170 complex, Nup157-pA. Importantly, loss of Sir4p, but not yKu70p or Sir2p, reduced Nup170p binding at subtelomeric DNA.

* Affinity purification experiments were performed by DWV. ChIP experiments were performed by YW with data analysis performed by WMC and YW and image processing by WMC, YW, and DWV.

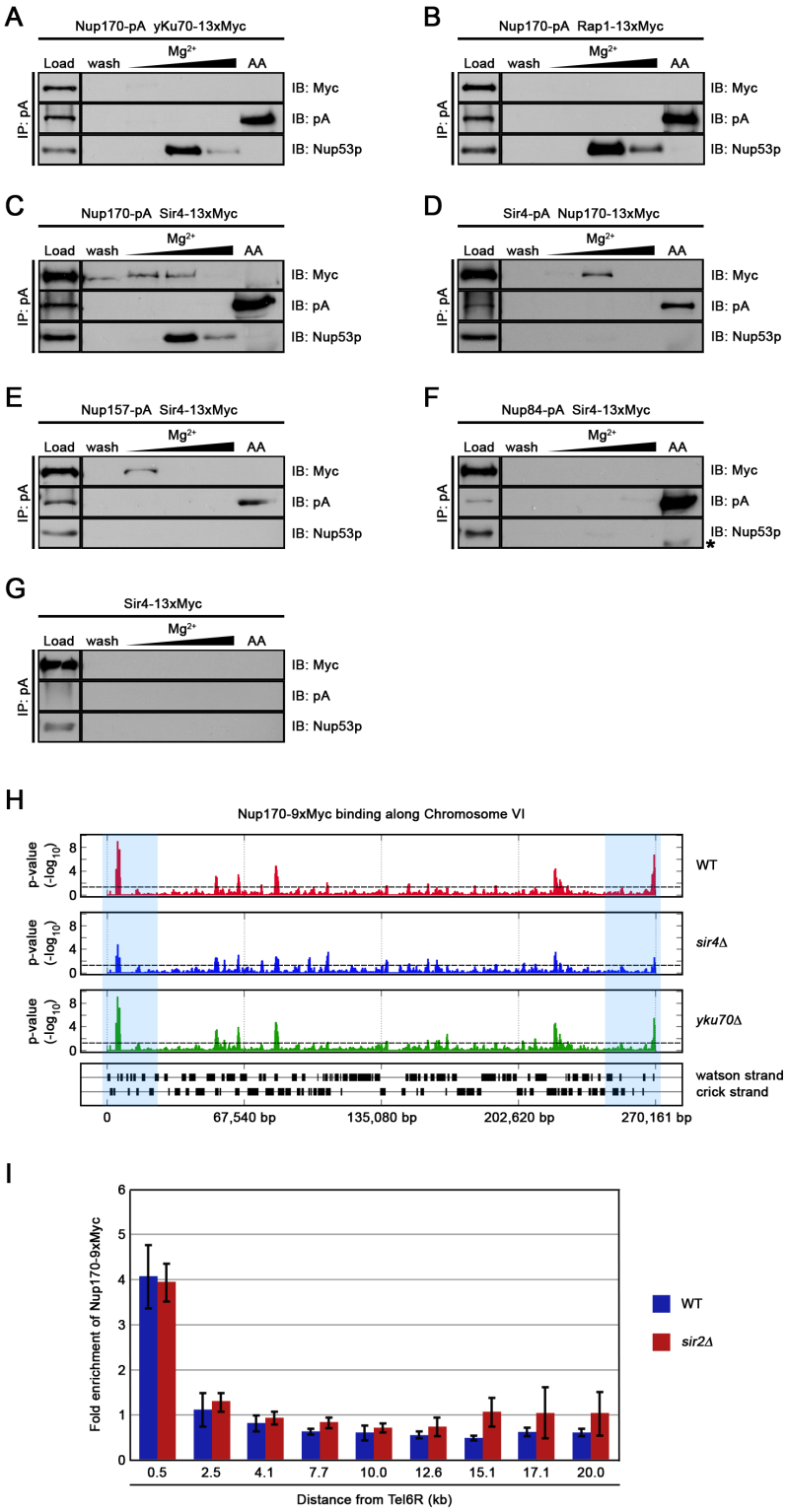

Figure 3-9. Association of Nup170p with subtelomeric DNA is mediated by Sir4p.

Figure 3-10. Association of Nup170p with subtelomeric DNA is mediated by Sir4p while association with non-subtelomeric DNA is Sir4p-independent.

Genome-wide binding profiles of Nup170-9xMyc in WT (A), *sir4Δ* (B), and *yku70Δ* (C) strains as determined by ChIP-chip analysis in Figure 3-8. Statistically significant binding sites with p-values ≤ 0.05 are marked by red peaks, and statistically insignificant binding sites are marked by green peaks. Peak height is inversely proportional to p-value (y-axis; $-\log_{10}$). Subtelomeric regions are shaded blue, while those displaying reduced Nup170p binding in the *sir4Δ* strain relative to WT are shaded magenta (panel B) to aid visual comparison among panels.

* ChIP-chip experiments were performed by YW with data analysis performed by WMC and YW. Images were processed by WMC and DWV.

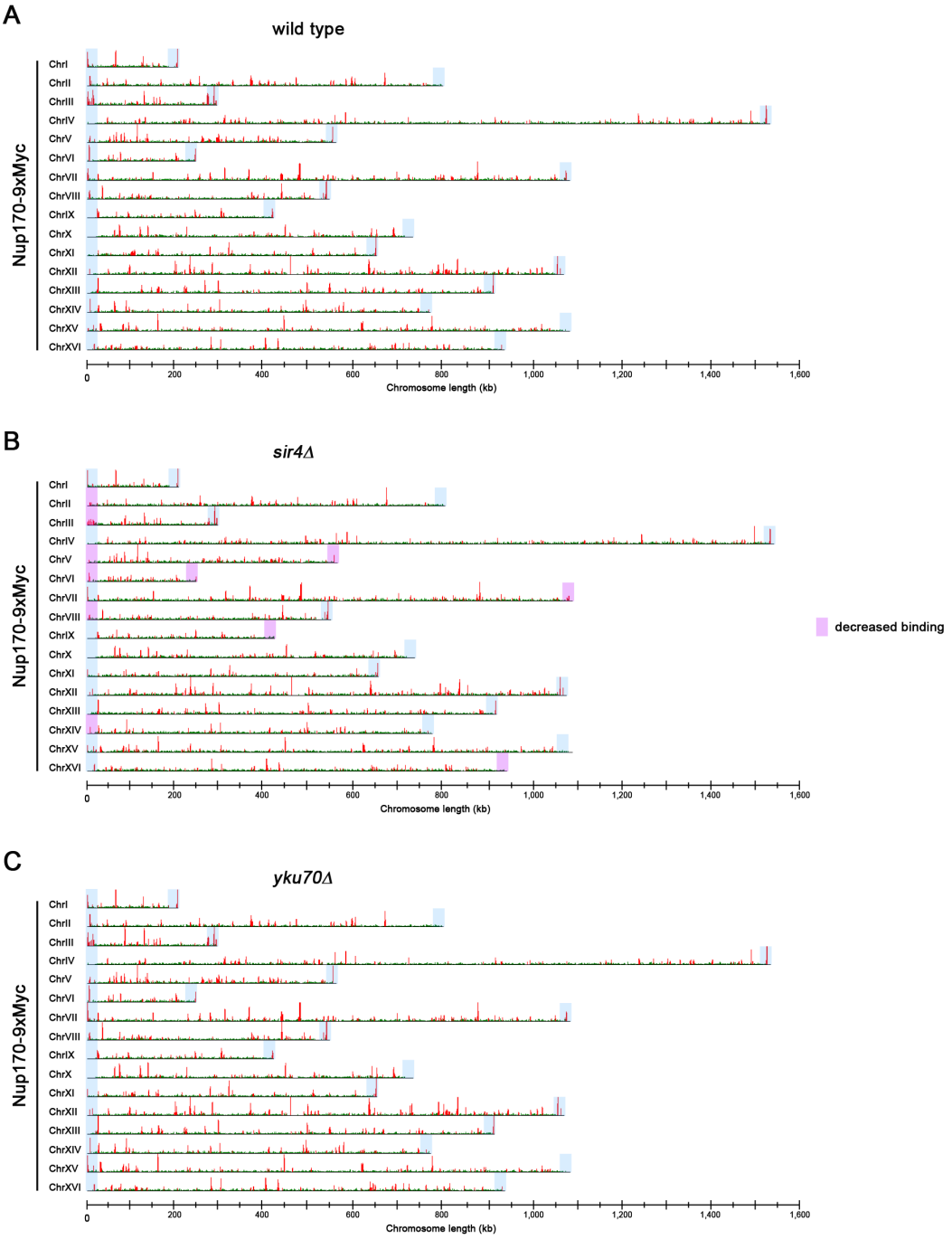

Figure 3-10. Association of Nup170p with subtelomeric DNA is mediated by Sir4p while association with non-subtelomeric DNA is Sir4p-independent.

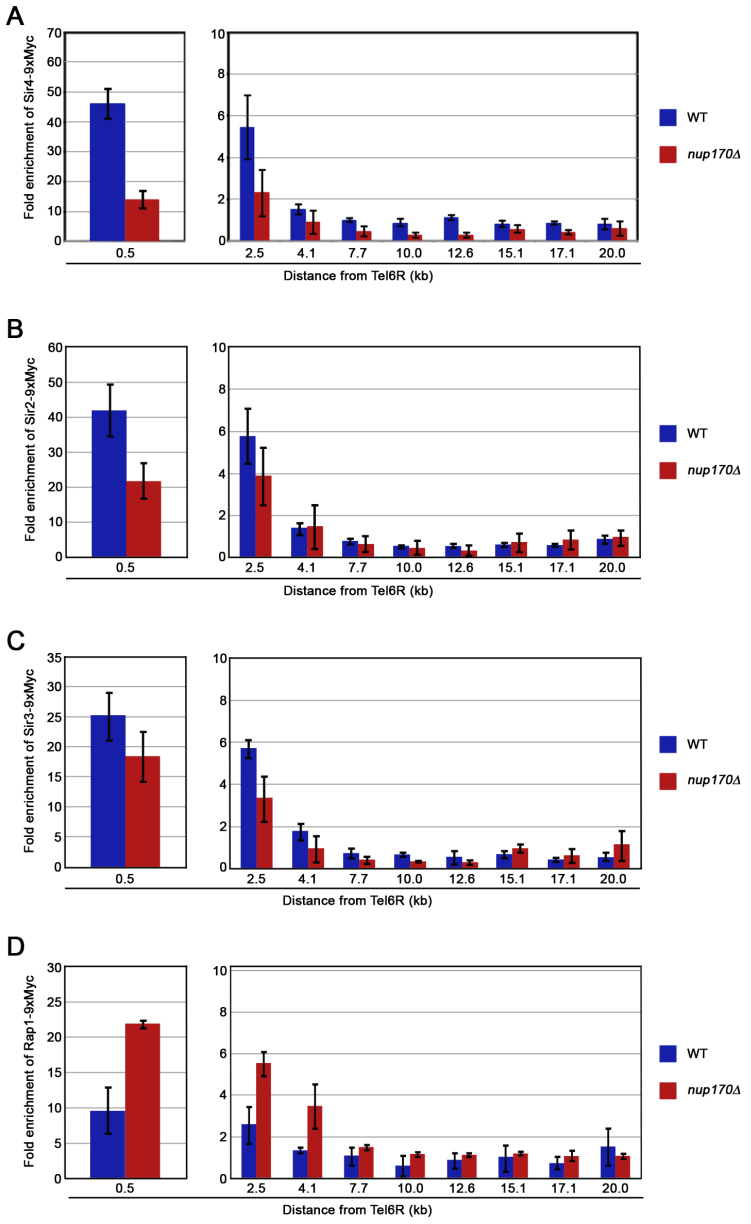

Figure 3-11. Nup170p is required for SIR complex binding to a representative telomere (Tel6R).

The association of Sir4-9xMyc (A), Sir2-9xMyc (B), Sir3-9xMyc (C), and Rap1-9xMyc (D) with subtelomeric DNA was examined in a wild type (blue) and a *nup170Δ* null mutant strain by chromatin immunoprecipitation. ChIP samples were analyzed by qPCR using primer sets dispersed along a 20 kb subtelomeric region of the right arm of chromosome VI (x-axis). Plotted on the y-axis is the mean enrichment and standard error of three independent experiments.
* ChIP-qPCR experiments and data analysis were performed by YW with image processing by YW and DWV.

of Sir4p, its binding partners Sir2-9xMyc and Sir3-9xMyc also showed reduced association with Tel6R (Figure 3-11B and 3-11C), consistent with the established role of Sir4p in facilitating Sir2p and Sir3p binding to chromatin (Strahl-Bosinger et al., 1997; Hoppe et al., 2002; reviewed in Rusche et al., 2003). These observations were in sharp contrast to Rap1p, which showed enhanced binding to Tel6R and subtelomeric regions in the absence of Nup170p (Figure 3-11D). While the basis for the increased binding of Rap1p is unclear, this phenotype further supports the conclusion that Nup170p plays a physiological role at telomeres.

The role of Nup170p in Sir4p localization was also examined by fluorescence microscopy. As a consequence of telomere clustering, Sir4p is generally detected in 6-8 foci positioned along the nuclear periphery in a WT nucleus (Palladino et al., 1993; Gotta et al., 1996). Mutations that reduce Sir4p binding to telomeres impair clustering, resulting in redistribution of foci to the nuclear interior (Cockell et al., 1995; Laroche et al., 1998). We observed 67% of Sir4-GFP foci at the NE in WT cells (Figure 3-12A). By contrast, cells lacking Nup170p exhibited a diffuse intranuclear Sir4-GFP signal and the peripheral localization of Sir4-GFP foci was reduced to 41%, similar to that observed in the tethering deficient *yku70Δ* mutant (Figure 3-12A). This phenotype was observed specifically in *nup170Δ* cells and was not detected in *nup157Δ* cells.

Our results support a model in which Nup170p facilitates the association of Sir4p with binding sites on subtelomeric and telomeric chromatin, including the telomere-associated protein Rap1p. In contrast to Nup170p, the Rap1-

interacting factor, Rif1p, antagonizes Sir4p binding to subtelomeric chromatin by competing with Sir4p for binding to Rap1p (Buck and Shore, 1995; Mishra and Shore, 1999). We, therefore, hypothesized that removing Rif1p and suppressing its antagonistic function would compensate for the loss of Nup170p and restore subtelomeric association and localization of Sir4p. In support of this idea, the introduction of a *rif1Δ* mutation into a *nup170* null mutant (*nup170Δ rif1Δ*) rescued Sir4-GFP localization at the NE to WT levels (Figure 3-12A). In addition, deletion of *RIF1* suppressed the silencing defect of the *nup170Δ* mutant, further linking the loss of silencing phenotype of *nup170Δ* cells to compromised Sir4p function (Figure 3-12B).

3.2.8 Tethering of telomeres at the nuclear envelope requires Nup170p

Sir4p is one of several proteins that function in the tethering of telomeres to the NE, therefore we examined whether the loss of Nup170p altered telomere tethering. Several commonly studied telomeres, Tel6R, Tel8L, and Tel14L, were visualized by tagging a flanking region with an array of 256 *lac* operators (*lacO*) in cells producing the *lacO*-binding protein GFP-LacI (Hediger et al., 2002b). Telomere position relative to the NE marker Sec63-GFP was examined, and foci scored for their localization within three concentric zones of equal area, with zone 1 representing the region immediately underlying the NE (Figure 3-13 and Table 3-9). As previously observed, Tel6R, Tel8L, and Tel14L were enriched in zone 1 (~70% of foci) during G1- and S-phase in WT cells (Figure 3-13 and Table 3-9; Hediger et al., 2002b; Hiraga et al., 2006; Therizols et al., 2006). Similar results

Figure 3-12. Nup170p facilitates Sir4p binding to subtelomeric DNA.

(A) Sir4-GFP is mislocalized from the nuclear envelope in *nup170Δ* cells. The ORF encoding GFP was integrated following the last amino acid codon of the chromosomal copy of *SIR4* in a haploid yeast strain producing Sec63-mCherry. The indicated null mutations were constructed in this strain background and mid-logarithmic cultures of WT, *yku70Δ*, *nup170Δ*, *nup157Δ*, *rif1Δ*, and *rif1Δnup170Δ* cells expressing *SIR4-GFP* and *SEC63-mCHERRY* were analyzed by epifluorescence microscopy. Shown are representative images of a single focal plane taken from a z-stack. To aid visualization of the NE, the Sec63-mCherry signal was deconvolved using an iterative algorithm to remove background signal and reassign blur. Histograms indicate the percentage of Sir4-GFP foci localized at the nuclear periphery in interphase cells. For each experiment > 400 foci were counted per strain. The mean percentage and standard error of three independent experiments are shown. The statistical significance of the difference between nup170Δ and WT cells is indicated (Student's t-Test). Scale bar, 2 μm. (B) Deletion of *RIF1* restores subtelomeric silencing in a *nup170Δ* mutant. Silencing of the subtelomeric reporter gene *ADE2* at Tel5R was evaluated in the indicated null mutant strains derived from UCC3505. In this background WT cells repress the *ADE2* gene giving rise to red colonies, while silencing deficient cells fail to repress *ADE2* and produce white colonies. To evaluate the efficiency of silencing in various strains, individual red colonies from culture plates were used to inoculate overnight cultures in non-selective YPD medium. For the *sir3Δ* strain an individual white colony was selected. Cells where then spotted on YPD plates and incubated for 4 d at 30˚C. Note, deletion of the *RIF1* gene restored both Sir4-GFP localization at the nuclear periphery and subtelomeric silencing of *ADE2* in the *nup170Δ* mutant.

* Fluorescence microscopy and subsequent quantitation were performed by DWV in which DL imaged and quantified *rif1Δ* and *rif1Δnup170Δ* strains. DL performed the silencing assay.

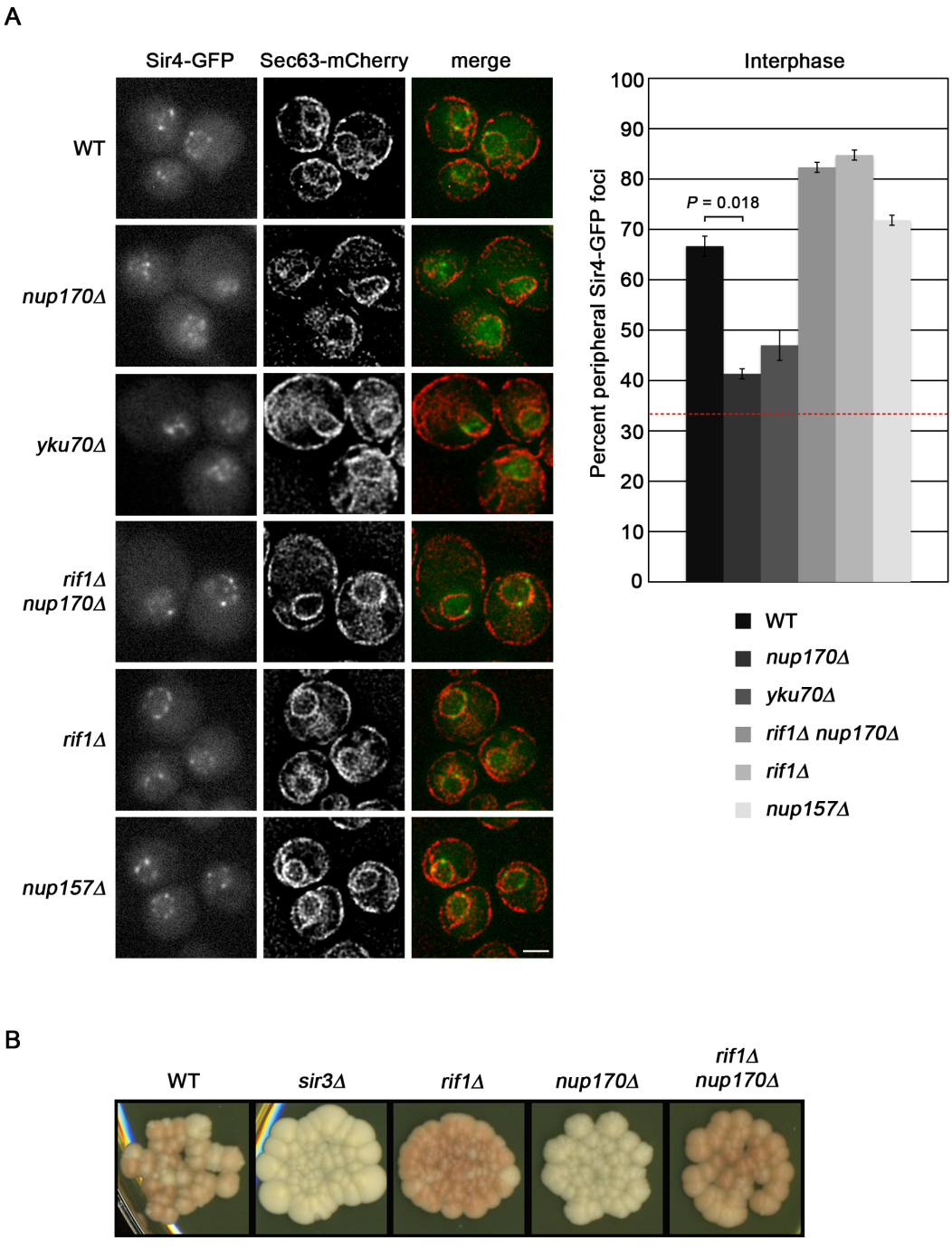

Figure 3-12. Nup170p facilitates Sir4p binding to subtelomeric DNA.

Figure 3-13. Telomere tethering is disrupted in the absence of Nup170p.

Telomere positioning was analyzed in asynchronous cultures of WT, *nup170Δ, sir4Δ, yku70Δ*, *nup157Δ*, and *nup2Δ* cells. To visualize telomeres in live cells ~256 tandem repeats of the *Escherichia coli* lactose operator (*lacO*) were integrated ~14 kb from Tel6R, ~8 kb from Tel8L, or ~21 kb from Tel14L into a yeast strain producing N-terminally GFP-tagged lactose repressor (GFP-LacI). To aid visualization of the nuclear envelope the ORF encoding GFP was integrated in frame with the C-terminus of *SEC63* to produce Sec63-GFP. The indicated null mutations were then generated within these strains backgrounds (W303). Cells were grown to mid-logarithmic growth phase in YPD medium supplemented with 40 μg/mL adenine to reduce autofluorescence, washed twice with SC medium, immobilized on agarose pads containing SC medium supplemented with 40 μg/mL adenine and imaged by epifluorescence microscopy. (A) The subnuclear position of GFP foci in a single focal plane was determined relative to the NE marker Sec63-GFP and assigned to one of three concentric nucleoplasmic zones of equal area (schematic, *left*; representative single focal plane images, *right*). Scale bar, 1 μm. (B) The subnuclear position of 100 foci for Tel14L and 50 foci for Tel6R and Tel8L were determined in unbudded (G1-phase; *left histograms*) and small budded (S-phase; *right histograms*) cells. The mean percentages of telomere foci localized in zone 1 and the standard error between three independent experiments are shown. A random-distribution is indicated by a red dashed-line at 33%. The statistical significance of the difference between *nup170Δ* and WT in zone 1 of G1-phase cells is indicated (Student's t-Test). For a complete list of telomere localization values see Table 3-9.

* Strains were constructed by DWV. Fluorescence microscopy and data analysis were performed by DL. Figure processing was performed by DWV.

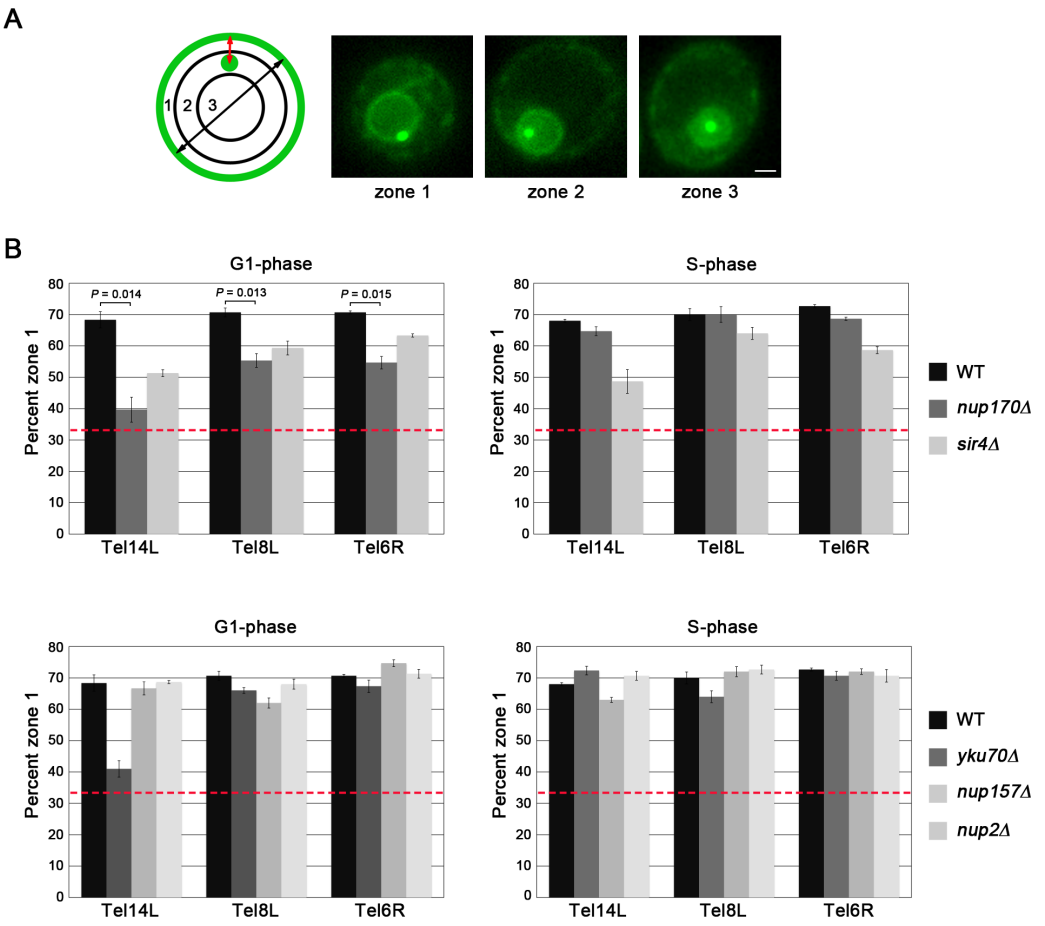

Figure 3-13. Telomere tethering is disrupted in the absence of Nup170p.

Table 3-9. Localization of *lacO*-tagged telomere loci.

		WT	*nup170Δ*	*sir4Δ*	*yku70Δ*	*nup157Δ*	*nup2Δ*
Tel14L							
G1-phase	zone 1	68.3 ±2.6	39.7 ±4.0	51.3 ±1.1	41.0 ±2.6	66.7 ±2.1	68.7 ±0.5
	zone 2	17.3 ±1.9	24.7 ±2.4	24.7 ±1.1	39.7 ±2.6	18.0 ±1.6	15.0 ±0.5
	zone 3	14.3 ±2.0	35.7 ±1.8	24.0 ±1.9	19.3 ±2.1	15.3 ±1.2	16.0 ±0.9
S-phase	zone 1	68.0 ±0.5	64.7 ±1.4	48.7 ±3.8	72.3 ±1.4	63.0 ±0.8	70.7 ±1.4
	zone 2	18.7 ±1.8	17.3 ±1.9	24.7 ±2.0	14.0 ±0.5	17.7 ±1.1	15.3 ±2.0
	zone 3	14.3 ±1.4	18.0 ±0.5	26.7 ±2.0	13.7 ±1.2	19.3 ±1.0	14.0 ±1.6
Tel8L							
G1-phase	zone 1	70.7 ±1.4	55.3 ±2.2	59.3 ±2.2	66.0 ±0.9	62.0 ±1.6	68.0 ±1.6
	zone 2	16.0 ±0.9	22.0 ±3.3	19.3 ±1.4	18.7 ±0.5	12.8 ±1.4	16.7 ±2.0
	zone 3	13.3 ±1.1	22.7 ±2.9	21.3 ±2.4	15.3 ±1.1	25.3 ±0.5	15.3 ±2.2
S-phase	zone 1	70.0 ±1.9	70.0 ±2.5	64.0 ±1.9	64.0 ±1.9	72.0 ±1.6	72.7 ±1.4
	zone 2	16.0 ± 0 *	16.0 ±2.5	17.3 ±0.5	18.0 ±1.9	15.3 ±0.5	12.7 ±1.4
	zone 3	14.0 ±1.9	14.0 ± 0 *	18.7 ±1.4	18.0 ±1.9	13.3 ±1.4	14.7 ±1.4
Tel6R							
G1-phase	zone 1	70.7 ±0.5	54.7 ±2.0	63.3 ±0.5	67.3 ±2.0	74.7 ±1.1	71.3 ±1.4
	zone 2	16.0 ±2.5	20.7 ±0.5	15.3 ±0.5	16.0 ±1.6	14.0 ± 0 *	11.3 ±1.1
	zone 3	13.3 ±2.6	24.7 ±1.4	21.3 ±0.5	16.7 ±2.2	11.3 ±1.1	17.3 ±0.5
S-phase	zone 1	72.7 ±0.5	68.7 ±0.5	58.7 ±1.1	70.7 ±1.4	72.0 ±0.9	70.7 ±2.0
	zone 2	13.3 ±0.5	14.7 ±1.1	18.0 ±0.9	18.7 ±0.5	12.0 ±0.9	18.0 ±1.6
	zone 3	14.0 ±0.9	16.7 ±1.4	23.3 ±1.4	10.0 ±0.9	16.0 ± 0 *	11.3 ±0.5

Percentage of telomere loci localized in zones 1-3 with standard error. Values represent the average of three independent experiments, with n = 100 (Tel14L), and n = 50 (Tel6R, Tel8L). *, identical values were obtained in three separate experiments.

were obtained using the *nup2Δ* or *nup157Δ* mutants. However, the NE association of all three telomeres was compromised in *nup170Δ* cells during G1-phase. This loss of tethering was most pronounced for Tel14L, with its localization (~39% of foci in zone 1) suggestive of a near random positioning within the nucleoplasm. Defects in G1-phase telomere localization were also detected in strains lacking yKu70p and Sir4p similar to previous reports (Hediger et al., 2002b; Hiraga et al., 2008). The *nup170Δ* cells, however, showed no defects in telomere localization in S-phase cells. Thus, we conclude that Nup170p plays an essential role in telomere localization during G1-phase of the cell cycle.

Sir4p-mediated telomere tethering occurs through interactions with the inner nuclear membrane associated proteins Mps3p and Esc1p (Taddei et al., 2004; Bupp et al., 2007). Since Nup170p may play a role in targeting some proteins to the inner nuclear membrane (King et al., 2006), we examined the localization of Mps3-RFP and Esc1-GFP in WT and *nup170Δ* cells (Figure 3-14). Localization of either protein was similar in the presence or absence of Nup170p, suggesting that the defects in telomere localization are not due to an altered localization of these tethering factors at the NE.

Having shown that Esc1p is targeted appropriately to the NE in *nup170Δ* cells, we examined whether Esc1p remained competent to interact with Sir4p at the NE in the absence of Nup170p. To test this, four *lexA* operators (*lexA*^{op}) were linked to ~256 *lacO* repeats and integrated at an otherwise randomly positioned locus near ARS607 (referred to as Chr6^{int}) in cells producing GFP-LacI and either LexA, LexA-Sir4^{PAD}, or LexA-Esc1^{C} (Taddei et al., 2004). Sir4^{PAD} is a C-terminal

Figure 3-14. Esc1p remains competent to interact with Sir4p at the NE in the absence of Nup170p.

The subcellular localization of Esc1-GFP (A) and Mps3-RFP (B) was examined in WT and *nup170Δ* cells. Cells were grown to mid-logarithmic growth phase and immobilized on agarose pads containing SC medium and imaged by epifluorescence microscopy. Shown are representative single focal plane images taken from a z-stack. Scale bars, 2 μm. (C) To assess whether Esc1p retains its ability to interact with Sir4p at the NE four *lexA* operators (*lexA*^{op}) were linked to ~256 *lacO* repeats and integrated at an otherwise randomly positioned locus (ARS607; referred to as Chr6^{int}) on chromosome VI. Expression of *GFP-lacI* permitted visualization of the locus in live cells. Plasmids encoding *lexA*, *lexA-SIR4*^{PAD}, and *lexA-ESC1*^{C} were introduced into WT, *nup170Δ*, and *esc1Δ* strains and the ability of the LexA-fusion proteins to tether Chr6^{int} to the NE was assessed. Cells were grown to mid-logarithmic growth phase in SC medium lacking tryptophan to maintain plasmid selection, immobilized on agarose pads and imaged using fluorescence microscopy. The subnuclear position of GFP foci in a single focal plane was determined relative to the NE marker Sec63-GFP and assigned to one of three concentric nucleoplasmic zones of equal area, with zone 1 representing the nuclear periphery. For each strain the subnuclear position of 50 GFP-foci were determined in unbudded (G1-phase; *left histogram*) and small budded (S-phase; *right histogram*) cells. The mean percentages of Chr6^{int} foci localized in zone 1 and the standard error between three independent experiments are shown. A random-distribution is indicated by a red dashed-line at 33%. Note, Sir4^{PAD} is a C-terminal fragment of Sir4p (aa 960-1262) that contains an Esc1p interaction domain but lacks interaction domains for Mps3p or other members of the SIR complex. Esc1^{C} requires homodimerization with endogenous Esc1p for its NE targeting.

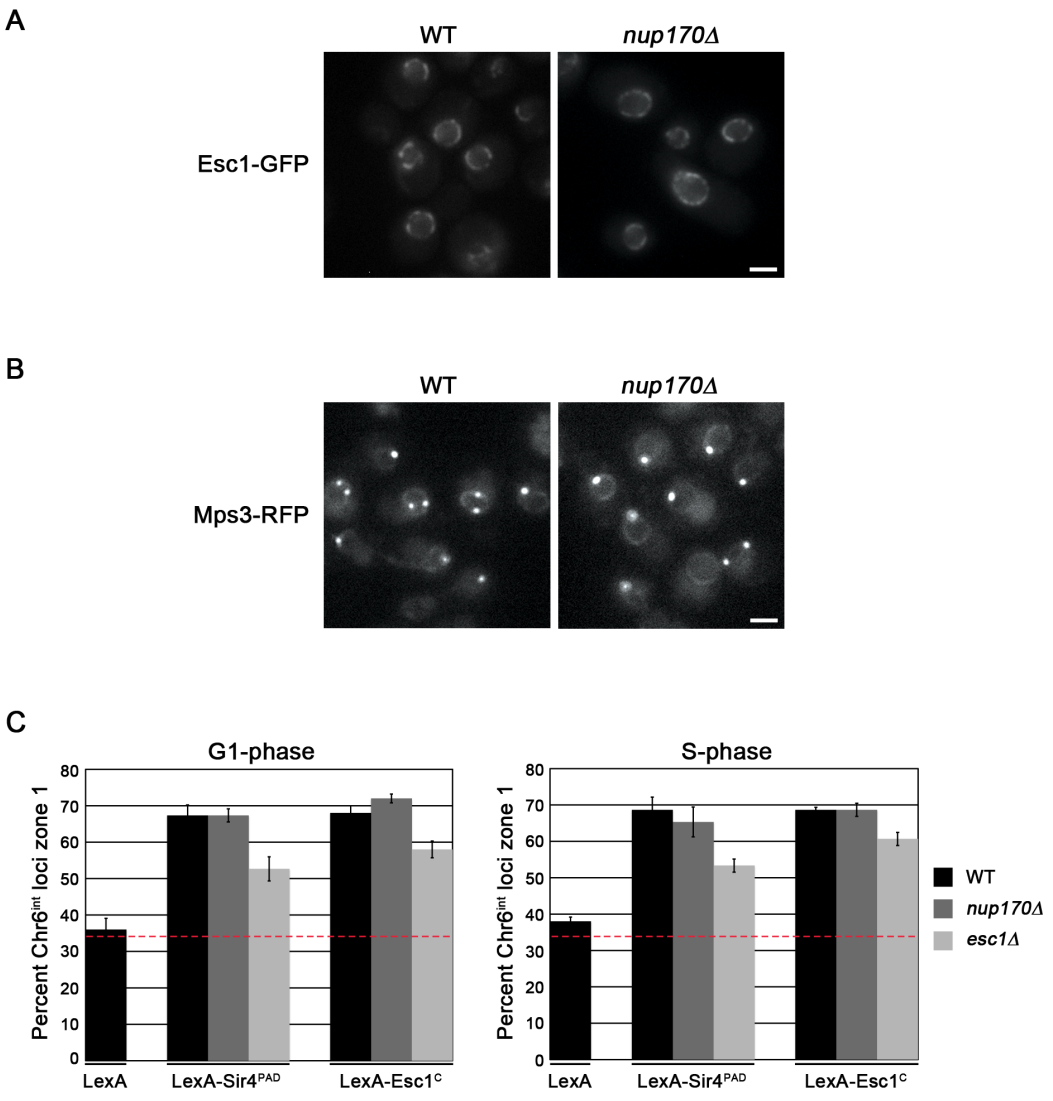

Figure 3-14. Esc1p remains competent to interact with Sir4p at the NE in the absence of Nup170p.

fragment (aa 960-1262) that contains an Esc1p interaction domain, but is unable to interact with Mps3p or other members of the SIR complex. The C-terminal 540 residues of Esc1p ($Esc1^{C}$) contain a Sir4p interaction domain and a homodimerization domain that requires endogenous Esc1p for NE targeting (Taddei et al., 2004). Thus expresssion of *lexA-SIR4*^{PAD} or *lexA-ESC1*^{C} relocates $Chr6^{int}$ to the NE via an Esc1p-Sir4p interaction. To assess the tethering function of Esc1p, the subnuclear position of $Chr6^{int}$ in unbudded cells (G1-phase) was determined relative to the NE marker Sec63-GFP in WT, *nup170Δ* and *esc1Δ* cells (Figure 3-14C). As previously documented (Taddei et al., 2004), in WT cells $Chr6^{int}$ was randomly positioned in nuclei of cells expressing *lexA* alone (30% of foci in zone 1). However, it was effectively targeted to the NE in cells producing LexA-$Sir4^{PAD}$ or LexA-$Esc1^{C}$ (>60% of foci in zone 1). The NE targeting of either fusion protein however was sensitive to loss of Esc1p, consistent with previous results (Taddei et al., 2004). By contrast, in *nup170Δ* cells both fusion proteins relocated $Chr6^{int}$ to the NE at levels comparable to WT, indicating that, in the absence of Nup170p, Esc1p retains its ability to interact with Sir4p and tether a locus at the NE.

3.2.9 Sir4p and subtelomeric DNA are recruited to NPCs during mitosis

Following replication of subtelomeric DNA in late S-phase, telomeres and Sir4p are largely dislodged from the NE until late mitosis (i.e. telophase) when telomere tethering at the NE is re-established (Laroche et al., 2000; Ebrahimi and Donaldson, 2008). Moreover, silencing is re-established in cells arrested in

telophase but not metaphase, indicating a requirement for passage through mitosis (Lau et al., 2002; Martins-Taylor et al., 2004). On the basis of these results and our observations that Nup170p plays an essential role in telomere association with the NE during G1-phase, we speculated that Nup170p may facilitate Sir4p binding to subtelomeric DNA and the re-establishment of telomere tethering to the NE during the latter stages of mitosis. To investigate this possibility, we examined the physical relationship between Sir4-GFP foci and NPCs (labeled with Nup60-mCherry) during various stages of the cell cycle. In unbudded (G1-phase) and small-budded (S-phase) cells, Sir4-GFP foci showed limited colocalization with NPCs (~20%; Figure 3-15). This degree of colocalization was similar to that previously observed between Sir4p and the telomere-tethering factor Esc1p (Taddei et al., 2004). Examination of large-budded (G2/M-phase) cells, however, revealed a nearly 2-fold increase in colocalization of Sir4p with NPCs when compared to interphase cells (36%; Figure 3-15), suggesting Sir4p was positioned at, or adjacent to, NPCs during mitosis.

Given our identification of Sir4p and Nup170p as interacting partners and the enrichment of Sir4-GFP with NPCs during mitosis, we examined whether the Sir4p-Nup170p interaction was occurring preferentially at specific points in the cell cycle. To examine this possibility, we assessed the ability of Sir4p to interact with Nup170p in cells arrested in G1-, S-, or G2/M-phase of the cell cycle. Purification of Nup170-pA from cell lysates derived from strains producing Sir4-13xMyc and arrested in G1-phase or S-phase failed to detect Sir4p in association with Nup170-pA (Figure 3-16A and 3-16B). By contrast, Sir4-13xMyc was

Figure 3-15. Sir4p colocalizes with NPCs during mitosis.

To examine the localization of Sir4p in relation to NPCs in live cells, the yeast strain DVY2032 synthesizing Sir4-GFP and Nup60-mCherry from their endogenous promoters was grown to mid-logarithmic phase and imaged by epifluorescence microscopy. Immediately prior to imaging, asynchronous cells were collected, washed twice with SC medium and immoblilized on agarose pads. Shown are representative images of a single focal plane taken from a z-stack depicting cells in G1 (unbudded), S (small budded), and G2/M (defined as large budded with the nucleus either positioned at the bud neck or undergoing division) phases of the cell cycle. In the merged images cells are outlined in white and arrows indicate Sir4-GFP foci that colocalize with Nup60-mCherry. The percentage of Sir4-GFP foci that colocalize with Nup60-mCherry was determined for cells in G1, S, and G2/M phases of the cell cycle and displayed as a histogram. For each foci, a single focal plane was chosen where the GFP signal was most intense. An overlap of ~50% with the Nup60-mCherry signal was the threshold for assigning colocalization. The number of Sir4-GFP foci counted for each stage of the cell cycle is indicated (n). Scale bar, 2 μm.

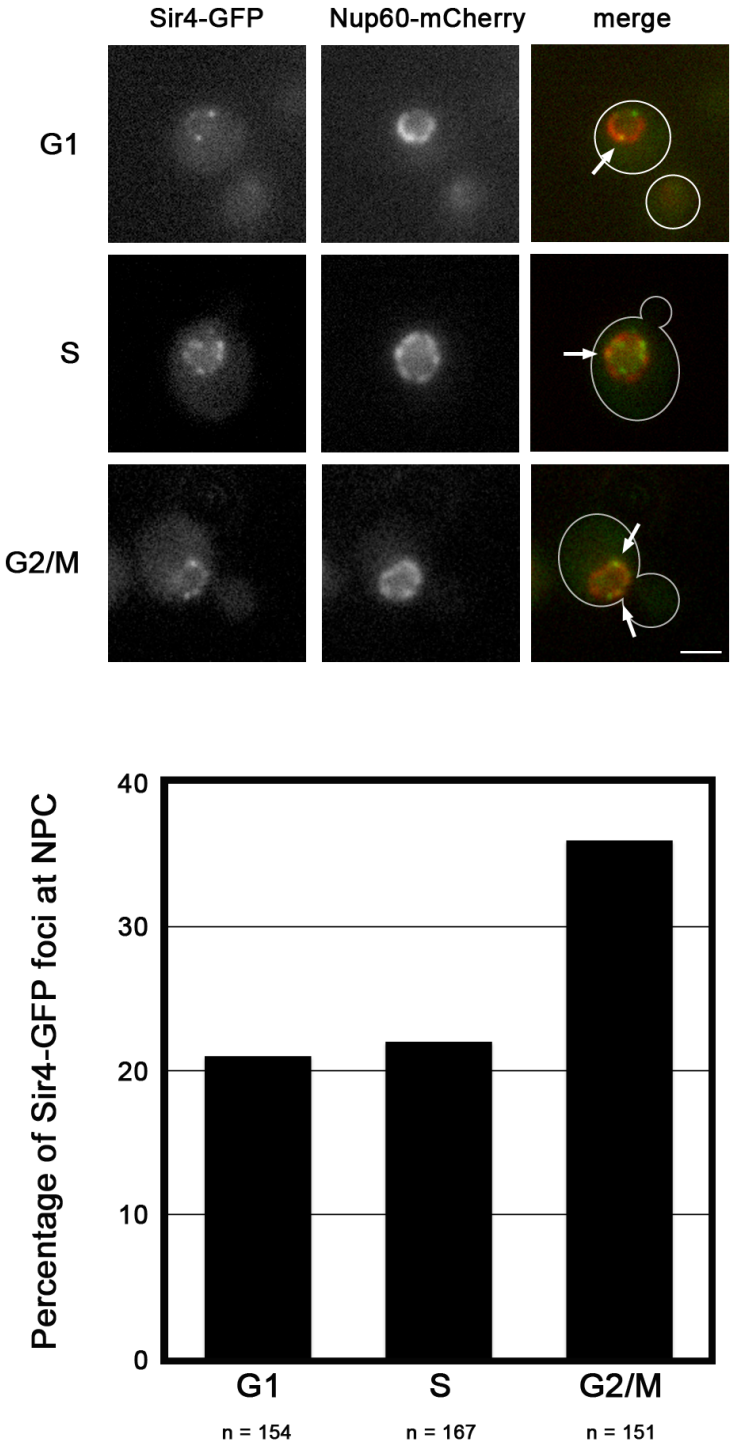

Figure 3-15. Sir4p colocalizes with NPCs during mitosis.

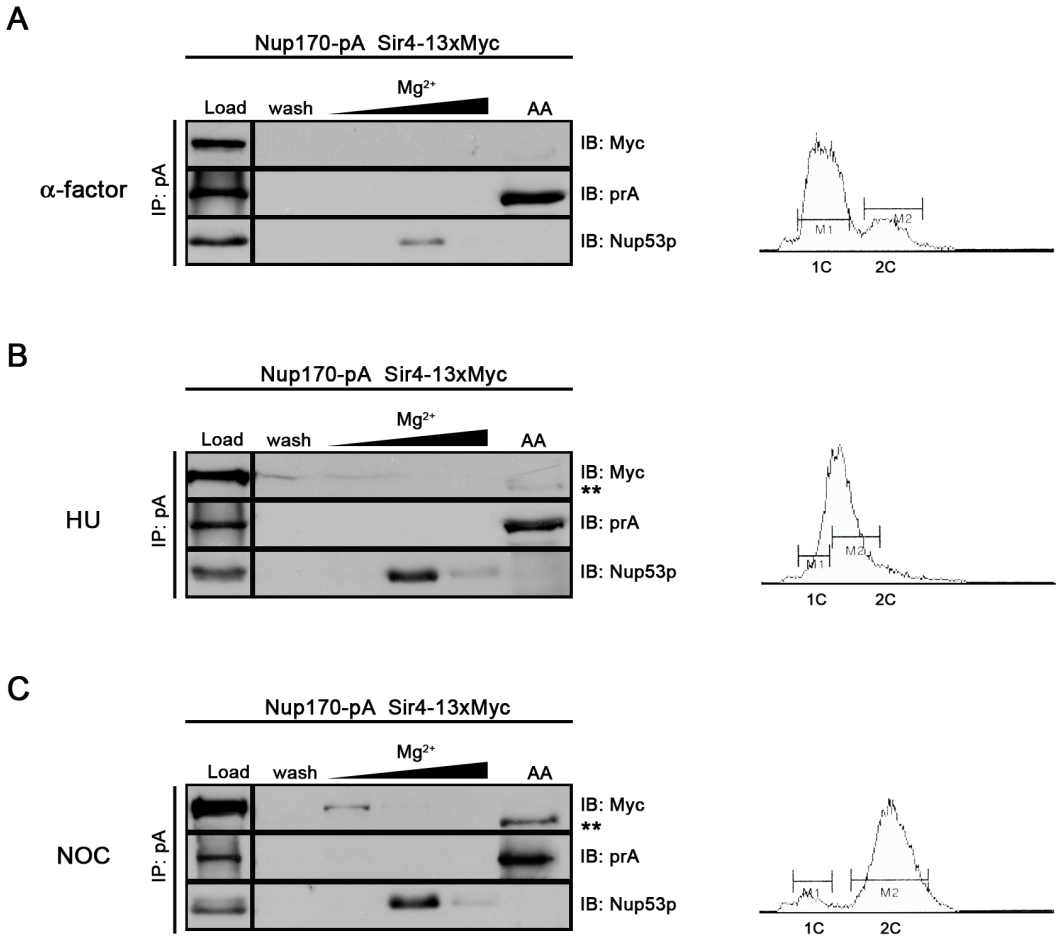

Figure 3-16. Nup170p and Sir4p physically interact during mitosis.

Cell cultures of a *bar1Δ* strain producing Nup170-pA and Sir4-13xMyc were grown to an OD_{600} of ~0.5 phase and treated for 2.5 h at 23˚C with 50 ng/mL α-factor to arrest in G1-phase (α-factor), 200 mM hydroxyurea to arrest in S-phase (HU), or 15 mg/mL nocodazole to arrest in G2/M-phase (NOC). Cell cycle arrests were monitored microscopically for cell morphology and DNA content was assessed by FACS analysis (*right panels*). Nup170-pA was affinity purified from cell lysates using IgG-conjugated magnetic beads as described in Figure 3-3. Protein samples were analyzed by SDS-PAGE and western blotting using antibodies to detect the indicated proteins. The asterisk indicates a pA cross-reactive band in the AA fraction. Note, interaction of Sir4p with Nup170-pA was only detected in G2/M-phase arrested cells.

* Affinity purifications were performed by DWV and FACS analysis was performed by DL. Figure processing was performed by DWV.

bound to Nup170-pA in lysates of G2/M-phase arrested cells (Figure 3-16C). Cumulatively, these results suggest that Nup170p recruits Sir4p to NPCs during mitosis.

Based on our hypothesis that Nup170p mediates the post-mitotic re-establishment of subtelomeric silencing and telomere tethering, we predicted that the association of Nup170p with subtelomeric chromatin would also occur during the latter stages of mitosis or perhaps early in G1-phase. To test this possibility, we arrested cells in G1-phase with α-factor and examined DNA associated with Nup170-9xMyc by ChIP-chip analysis at various times following release from α-factor arrest. Cell cycle progression was monitored by FACS analysis and ChIP-chip analysis was performed at times following release that corresponded with a population of cells primarily in G1-, S-, or M-phase (Figure 3-17A). Enrichment of subtelomeric DNA with Nup170-9xMyc was greatest in G1-arrested cells, significantly reduced in S-phase cells, and increased in both M-phase and the subsequent G1-phase (Figure 3-17B). The increased association of subtelomeric DNA with Nup170p during M- and G1-phase is consistent with the observed mitotic interaction of Nup170p with Sir4p, and the subsequent loss of telomere tethering in *nup170Δ* cells during G1-phase. Based on these results, we conclude that Nup170p recruits both Sir4p and subtelomeric DNA to NPCs during mitosis.

Figure 3-17. Nup170p preferentially associates with subtelomeric DNA during mitosis.

The association of Nup170p with subtelomeric DNA was analyzed throughout the cell cycle by ChIP-chip. A *NUP170-9xMYC bar1Δ* strain (YWY1066) was grown to mid-logarithmic growth phase in YPD medium and arrested in G1-phase with 50 ng/mL α-factor for 2.5 h at 25˚C. G1-arrest was released by transferring cells to YPD medium, and at the indicated times samples were taken for ChIP-chip analysis. (A) Cell cycle progression following release from α-factor arrest was monitored by FACS analysis. Time points used in ChIP-chip analyses are highlighted in color with 0 min (green), 40 min (aquamarine), 80 min (blue), and 120 min (gold) samples containing cells in G1-, S-, M,- and re-entry into G1-phase, respectively. (B) Shown are the binding profiles of Nup170-9xMyc as determined by ChIP-chip analysis within the subtelomeric regions of a representative chromosome (Chromosome I) obtained 0 min (G1-phase; green), 40 min (S-phase; aquamarine), 80 min (M-phase; blue), and 120 min (re-entry into G1; gold) following release from α-factor arrest. Nup170p binding is plotted as a logarithmic function of its p-value (y-axis; $-\log_{10}$). The threshold of statistical significance (p-value ≤ 0.05) is indicated by a horizontal dashed line. Black rectangles represent the position of ORFs located on the Watson and Crick strands.

* ChIP-chip experiments and FACS analysis were performed by YW with data analysis performed by YW and WMC. Figure processing was performed by WMC, YW, and DWV.

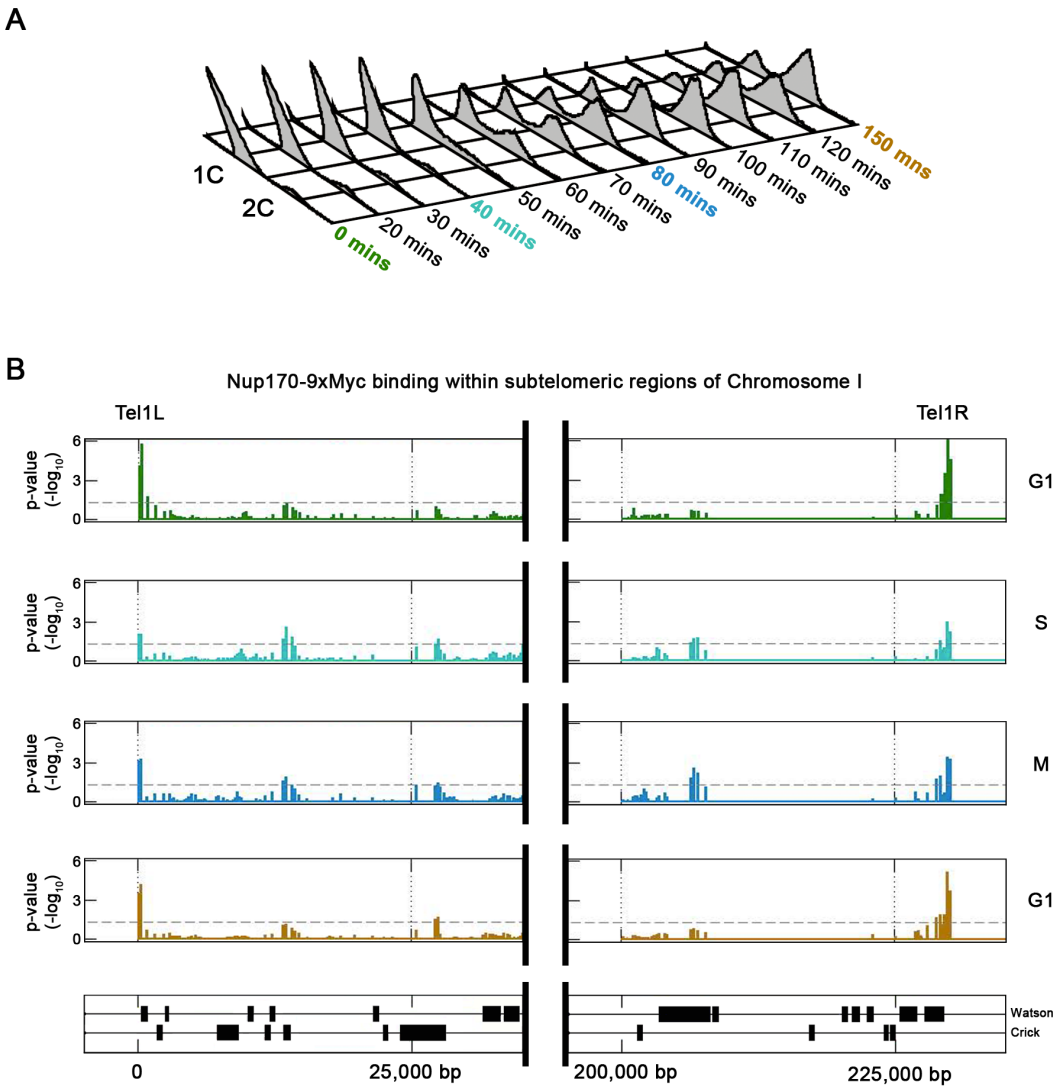

Figure 3-17. Nup170p preferentially associates with subtelomeric DNA during mitosis.

3.3 Discussion

The NE creates a diverse landscape for interactions with chromatin. The inner nuclear membrane in most cell types interacts with chromatin that is condensed and/or silenced. By contrast, NPCs are associated with decondensed and often transcriptionally active euchromatin. Studies in yeast and metazoan cells have established functional links between Nups and transcriptionally active genes (Casolari et al., 2004; Mendjan et al., 2006; Taddei et al., 2006; Cabal et al., 2006; Luthra et al., 2007; Ahmed et al., 2010). Thus, the regions between NPCs and the inner nuclear membrane are likely dynamic, transitional zones between these two chromatin states. We have uncovered physical and functional interactions between the NPC component Nup170p and chromatin domains that generally reside adjacent to the NE, including subtelomeric and telomeric regions. We propose that during the latter stages of mitosis Nup170p establishes a platform at the NPC that interacts with these chromatin regions and, through its interactions with the RSC complex and the silencing protein Sir4p, facilitates the assembly of subtelomeric heterochromatin and its reassociation with the inner nuclear membrane following cellular division.

Key to uncovering the relationship between Nup170p and chromatin structure was the identification of functional links between Nup170p and various chromatin-modifying factors. Our data lead us to conclude that Nup170p contributes to a distinct, but related, function to that of its genetically interacting partners, including transcriptional repression and heterochromatin assembly. Set3C and Rpd3L are histone deacetylase complexes (HDACs) with roles in

silencing (Rundlett et al., 1996; Ehrentraut et al., 2010), and the E3 ubiquitin ligase Bre1p and its interactors mediate silencing through their downstream effects on histone H3 methylation (Sun and Allis, 2002). The SWR1 complex also contributes to silencing by defining heterochromatin regions through its ability to exchange canonical histone H2A for the histone variant H2A.Z (Htz1p), and, notably, to regulate genes enriched near telomeres (Krogan et al., 2003; Mizuguchi et al., 2004). Cumulatively, the annotated functions of these genetically interacting complexes support the conclusion of a parallel function for Nup170p in heterochromatin formation and the regulation of gene silencing.

This concept was supported by results establishing a role for Nup170p in the organization of nucleosomes *in vivo* (Figure 3-6), the first such indication that a Nup functions in this capacity. Genome-wide analysis of the *nup170Δ* mutant revealed changes in nucleosome structure that are most evident in nucleosomes flanking the NFR with both a decrease in -1 and +1 nucleosome occupancy, as well as a broadening of the NFR. Examination of chromosomal regions revealed these changes were nonrandom and most prominent in subtelomeric chromatin and at RP genes. While the mechanistic role of Nup170p in nucleosome occupancy is unclear, we suggest it is likely linked to its interaction with RSC, or an as yet unidentified chromatin modifier. Consistent with the former, loss of RSC activity also leads to aberrant -1 and +1 nucleosome occupancy and changes in the size of the NFR (Badis et al., 2008; Hartley and Madhani, 2009).

In addition to its role in promoting transcription (Carey et al. 2006; Badis et al., 2008; Hartley and Madhani et al., 2009), reports also suggest RSC plays a

role in transcriptional repression (Angus-Hill et al., 2001; Badis et al., 2008). Notably, loss of Rsc30p function leads to a strong up-regulation of RP genes (Angus-Hill et al., 2001), a result strikingly similar to that observed in the *nup170Δ* mutant (Figure 3-8 and Table 3-3). Moreover, RSC components are required for normal telomere length (Rsc2p, Rsc4p, Rsc14p, and Htl1p; Askree et al., 2004), Rap1 localization (Rsc1p and Rsc2p; Hiraga et al., 2008), and, as we have shown, the depletion of Sth1p derepresses multiple subtelomeric genes and alters interactions of Nup170p with subtelomeric chromatin (Figures 3-4 and 7-12). These varied functions underscore what are likely context-dependent roles of RSC, defined by its subunits and accessory binding factors such as Nup170p. Nup170p could direct RSC function by altering its remodeling activity and/or by positioning RSC at defined locations, both on chromatin and spatially within the nucleus.

Nup170p interacts with essentially all RP genes (Figure 3-8). Consistent with this conclusion, NPCs appear to interact with RP genes (Casolari et al., 2004; Yoshida et al., 2010). Interestingly, Harata and colleagues showed that the association of the *RPL9A* gene with NPCs is sensitive to the loss of Arp6p, a component of the SWR1 complex that functionally interacts with Nup170p (Figure 3-1). Moreover, the loss of *ARP6* leads to up-regulation of 21 RP genes. These results, and our observations of the *nup170Δ* mutant, are consistent with a model in which NPCs function to dampen or attenuate RP gene expression.

Our ChIP-chip data also provide direct evidence for a physical interaction of Nup170p with subtelomeric regions of one or both ends of 15 of 16

chromosomes (Figure 3-7 and 3-8). The idea that NPCs interact with telomeres has been previously suggested but has remained a controversial topic because data supporting this claim have been indirect. A protein that contributes to the nuclear basket of the NPC, Mlp2p, appears to interact with the telomere binding protein yKu70p, and this interaction is suggested to play a role in anchoring telomeres to the NE and repression of telomere proximal genes (Galy et al., 2000; Feuerbach et al. 2002). However, others have failed to detect these functions for the Mlp proteins (Hediger et al., 2002a and 2002b). More recently, mutations in members of a distinct NPC subcomplex, the Nup84 complex, were shown to alter the NE association of Tel11L and Sir3p, as well as suppress subtelomeric silencing (Therizols et al., 2006). However, the mechanistic link between the Nup84 complex and telomeres is unclear, and the interpretation of these observations are confounded by pleiotropic effects of mutations in members of the Nup84 complex on NPC structure and function (Doye et al., 1994; Atichison et al., 1995b). By comparison, loss of Nup170p does not alter NE structure and no defects in active transport have been reported (Aitchison et al., 1995a; Scarcelli et al., 2007; Makio et al., 2009).

Our analysis of Nup170p has provided a mechanistic basis for the observed role of the NPC in subtelomeric gene silencing. On the basis of ChIP-chip analysis, we propose that Nup170p forms a binding platform for telomeric and subtelomeric chromatin at the NPC (Figure 3-7). Moreover, the Nup170p/Sir4p association appears critical for the binding of both proteins to subtelomeric chromatin. In the absence of Sir4p, binding of Nup170p to regions

of chromatin proximal to telomeres was reduced (Figure 3-9 and 3-10). Similarly, cells lacking Nup170p exhibited a decrease in NE-associated Sir4p foci and reduced levels of Sir4p were detected bound to a representative telomere, Tel6R (Figure 3-11 and 3-12). These effects do not appear to be caused by changes in the NE localization of either Esc1p or Mps3p, two known inner membrane-binding partners of Sir4p (Figure 3-14). Deletion of *NUP170* also did not impair the ability of an exogenous LexA-Sir4^{PAD} fusion protein to artificially tether an intranuclear locus at the NE in G1-phase (Figure 3-14), suggesting that Nup170p is not required for Sir4p binding to Esc1p. However, Nup53p, a Nup170p binding partner, may contribute to Sir4p binding to Msp3p, as the *Schizosaccharomyces pombe* counterparts of Nup53p and Mps3p, Nup40 and Sad1, physically interact (Miki et al., 2004).

Sir4p and the yKu70/yKu80 heterodimer play key roles in facilitating telomere binding to the NE (Hediger et al., 2002b; Taddei et al., 2004; Schober et al., 2009; reviewed in Taddei et al., 2010) during G1- and S-phase. After DNA replication in late S-phase, the NE localization of telomeres and Sir4p decreases and telomeres are more generally dispersed throughout the nucleoplasm until the latter stages of mitosis (Laroche et al., 2000; Hediger et al., 2002b; Ebrahimi and Donaldson, 2008). Sir4p and yKu70p have distinct roles in telomere anchoring during the cell cycle. For example, loss of Sir4p has moderate effects on telomere localization during G1 and more dramatic consequences during S-phase (Hediger et al., 2002b; Taddei et al., 2004; Figure 3-13). Similarly, in the absence of Nup170p, the telomeres examined (Tel6R, Tel8L, and Tel14L) showed decreased

levels of NE localization specifically during G1-phase (Figure 3-13). These results are consistent with Nup170p contributing to the repositioning of telomeres at the NE in the latter stages of mitosis or G1-phase. Interestingly, this role for Nup170p would coincide with mitotic events proposed to establish silencing of subtelomeric regions (Martins-Taylor et al., 2004; Matecic et al., 2006; Martins-Taylor et al., 2011; reviewed in: Young and Kirchmaier, 2012). Intriguingly, telomeres exhibit limited colocalization with NPCs when asynchronous cell populations are examined by fluorescence microscopy (Taddei et al., 2004; Figure 3-15). However, this is also true of the telomere tethering factors Esc1p and Mps3p, with the bulk of Esc1p failing to colocalize with Sir4p and appearing in regions of the NE free of telomeres (Taddei et al., 2004), and Mps3p being present predominantly at spindle pole bodies (Jaspersen et al., 2002; Nishikawa et al., 2003). These observations may reflect the ability of telomeres to sample multiple binding sites along the NE. Consistent with this idea, telomere binding to the NE, in general, appears transient, with resident times ranging from seconds to several minutes separated by periods of diffusive movement within the nucleoplasm (Heun et al., 2001; Hediger et al., 2002b; Hiraga et al., 2006; Ebrahimi and Donaldson, 2008). With this in mind, we predicted that the Nup170p platform interacts transiently with Sir4p and subtelomeric chromatin, perhaps during periods of Sir4p assembly onto chromatin or at specific points in the cell-cycle. Indeed, upon examination throughout the cell cycle, the previously observed physical interaction between Nup170p and Sir4p was specific to G2/M-phase cells (Figure 3-16) and coincided with a ~2-fold increase in colocalization

of Sir4-GFP with NPCs (Figure 3-15). Furthermore, association of Nup170p with subtelomeric DNA was greatest during M- and G1-phase (Figure 3-17). We envisage a model in which Nup170p generates a binding platform within the NPC that, during the latter stages of mitosis, recruits Sir4p and subtelomeric DNA to NPCs to promote Sir4p binding to subtelomeric chromatin. In doing so, Nup170p functions to re-establish a repressive subtelomeric chromatin structure and facilitate its re-association with the NE following exit from mitosis (Figure 3-18).

The interactions of Nup170p with chromatin, Sir4p, and the RSC complex provide a physical basis for one of what are likely, multiple NPC platforms capable of interfacing with functionally distinct chromatin domains. While Nup170p contributes to gene silencing and heterochromatin structure, other Nups interface with activated genes to augment transcription, mRNA export, and facilitate transcriptional memory (Rodriguez-Navarro et al., 2004; Cabal et al., 2006; Taddei et al., 2006; Brickner et al., 2007; Luthra et al., 2007; Kohler et al., 2008; Light et al., 2010; reviewed in Taddei et al., 2010; Van de Vosse et al., 2011). Still other Nups appear to function in establishing boundaries between silenced and transcriptionally active chromatin (i.e. Nup2p; Ishii et al., 2002; Dilworth et al., 2005) or have been linked to DNA double-strand break repair (the Nup84 complex; Therizols et al., 2006). Our analysis of Nup170p and its physical interaction with the RSC complex highlights the ability of the NPC to recruit and potentially regulate chromatin modifiers that are predicted to influence local chromatin structure. Less clear, but equally intriguing, are the roles chromatin and chromatin modifiers play in NPC structure. For example, recent evidence suggest

Figure 3-18. A role for Nup170p in the formation of silent, subtelomeric chromatin and its association with the nuclear envelope.

(*top panel*) During interphase, telomeres are tethered at the nuclear envelope (NE) through two redundant pathways involving Sir4p and the yKu70p/yKu80p heterodimer (yKu). Sir4p-mediated telomere tethering occurs through direct interaction with the inner nuclear membrane (INM) associated proteins Esc1p and Mps3p. In addition, Mps3p tethers telomeres at the NE through a direct interaction with telomerase, which also interacts with yKu. Both yKu and Sir4p are sumoylated by the SUMO-E3 ligase Siz2p, which is required for telomere tethering at the NE throughout interphase (Ferreira et al., 2011). At the NPC, the RSC chromatin-remodeling complex associates with Nup170p throughout the cell cycle (D.W. Van de Vosse and R.W. Wozniak, personal communication). (*middle panel*) Following DNA replication in late S-phase, yKu-mediated tethering is inhibited, resulting in a loss of telomere tethering at the NE. The molecular mechanism that disrupts telomere tethering remains unknown. However, it is possible that the NPC-associated SUMO-deconjugating enzyme Ulp1p may desumoylate Sir4p and/or yKu to facilitate detachment of telomeres from the NE during the early stages of mitosis. During this stage of the cell cycle, loss of telomere tethering alleviates telomerase inhibition and, therefore, promotes telomere extension. Concomitantly, the accessibility of a repressed subtelomeric promoter to a transcription factor is increased during G2/M-phase (Aparicio and Gottschling, 1994), suggesting that subtelomeric chromatin structure is partially disrupted. Moreover, the association of Sir4p with NPCs and its interaction with Nup170p is enriched during mitosis. (*bottom panel*) We propose that the Sir4p-Nup170p interaction mediates the association of Nup170p with subtelomeric DNA during the latter stages of mitosis at which point Nup170p facilitates Sir4p binding to subtelomeric DNA and the re-establishment of silent, subtelomeric chromatin. Furthermore, Nup170p associates with the SUMO-E3 ligase Siz2p (D. Lapetina and R.W. Wozniak, personal communication), suggesting that telomere recruitment to NPCs during mitosis also provides an opportunity for NPC-associated Siz2p to sumoylate Sir4p and yKu in order to re-establish telomere anchoring at the NE during the latter stages of mitosis. As a result, the NPC generates a platform in which Nup170p, through its interactions with Sir4p, subtelomeric DNA, Siz2p, and the RSC chromatin-remodeling complex, facilitates the formation of silent subtelomeric chromatin and its association with the NE following exit from mitosis.

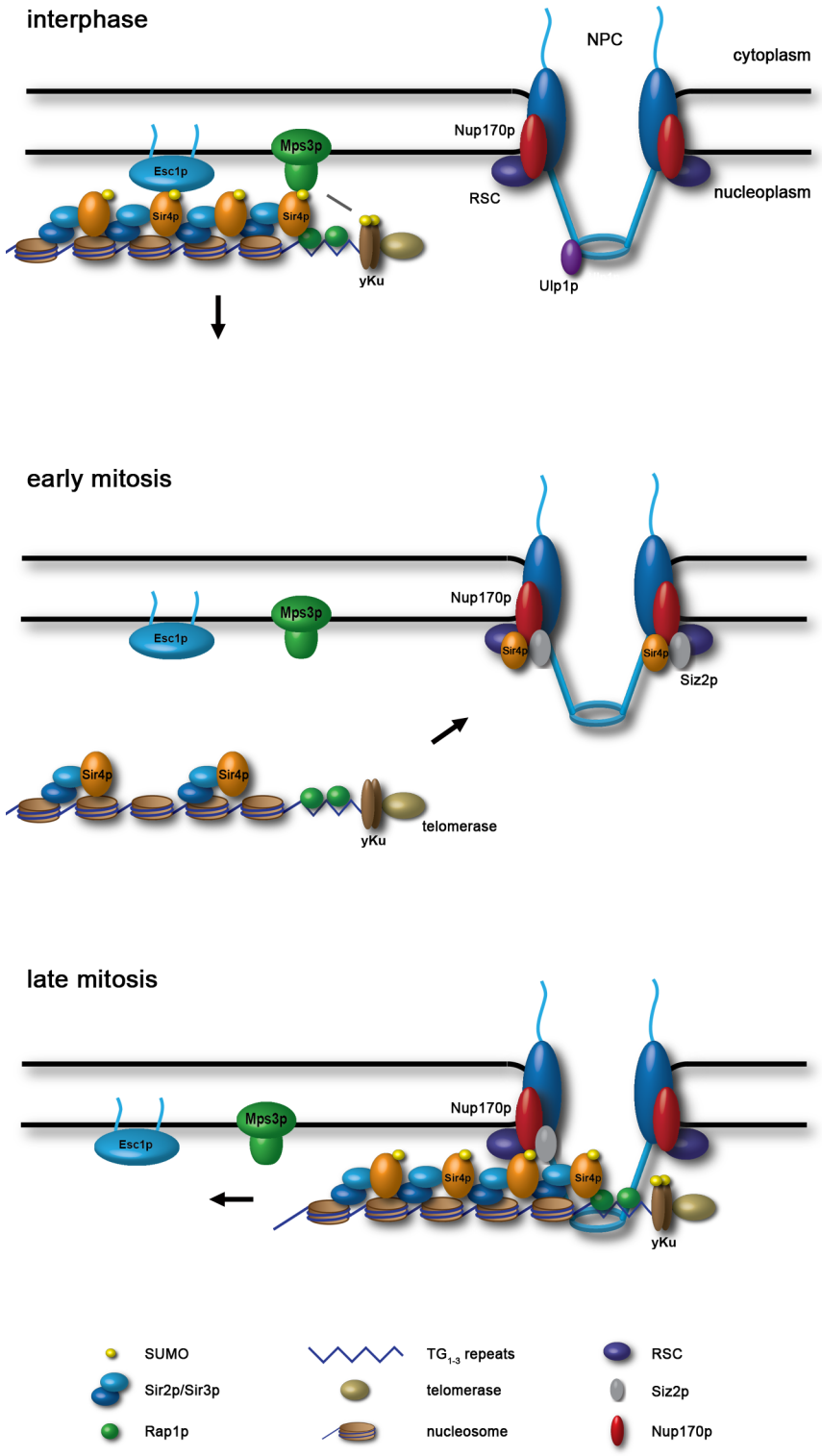

Figure 3-18. A role for Nup170p in the formation of silent, subtelomeric chromatin and its association with the nuclear envelope.

that RSC and other chromatin modifiers contribute to the structural organization of the NPC (Figures 7-9 and 7-10; Titus et al., 2010).

The molecular interactions we have described here between the yeast Nup170p-containing complex and Sir4p, as well as the interactions of Sir4p with Mps3p, may be conserved at the interface between NPCs and heterochromatin in higher eukaryotes. Intriguingly, Sun1, a mammalian protein that shares homology with Mps3p, localizes to the inner nuclear membrane and NPCs (Liu et al., 2007) where it interacts with heterochromatin and, in cells undergoing meiotic division, contributes to telomere tethering at the NE (Ding et al., 2007). At the NPC, Sun1 appears to interact with Pom121 (Talamas and Hetzer, 2011), which would place Sun1 in close proximity to another binding partner of Pom121, Nup155 (the mammalian counterpart of Nup170p; Mitchell et al, 2010). Strikingly Sun1, Nup155 and Nup53 all interact with nuclear lamins, with these Nups proposed to sit at the interface between the NPC and the nuclear lamina (Hawryluk-Gara et al., 2005; Crisp et al., 2006; J.M. Mitchell and R.W. Wozniak personal communication). The apparent outlying components when comparing the yeast and vertebrate complexes, is the presence of Sir4p in yeast and the lamins in vertebrates. However, these proteins may, in fact, share similar functions. Over two decades ago Diffley and Stillman (1989) reported on structural similarities between Sir4p and lamin A/C. While the similarities between these proteins lie within coiled-coil motifs common to a number of proteins, the conserved nature of their binding partners, their association with the inner nuclear membrane, and their links to silencing suggest Sir4p and the lamins share, at least a subset, of

functional properties. Finally, the conserved nature of these complexes also lead us to conclude that Nup155 may function as a chromatin binding platform similar to Nup170p, an idea consistent with a reported interaction between Nup155 and the histone deacetylase HDAC4 (Kehat et al., 2011).

Chapter IV: *Cell-type-dependent repression of a-specific genes requires Nup170p*

4.1 Overview

The nuclear envelope (NE) is an important mediator of genome positioning. Through reversible interactions with the underlying chromatin, the NE facilitates nuclear compartmentalization and the formation of transcriptionally distinct chromatin domains. In most cell types, the inner nuclear membrane associates with transcriptionally silenced chromatin (Deniaud and Bickmore, 2009). By contrast, nuclear pore complexes (NPCs) embedded in the NE generally associate with transcriptionally active chromatin (Casolari et al., 2004; Taddei, 2007). Despite this, however, NPCs have also been implicated in the regulation of transcriptionally silenced chromatin. The functional role NPCs play in the organization and regulation of these transcriptionally distinct chromatin domains remains unclear. In Chapter III, data were presented that suggest the NPC component Nup170p functions in the structure of silenced, subtelomeric chromatin. In expanding the analysis of the role of Nup170p in silenced chromatin structure, we have uncovered a role for Nup170p in the organization of chromatin structure at additional transcriptionally repressed loci. In particular, we demonstrate that Nup170p functions in gene silencing at *HML* and *HMR*, and is required for full repression of **a**-specific genes. In the absence of Nup170p, nucleosome occupancy within **a**-specific gene promoters is disrupted leading to partial derepression of **a**-specific genes and the appearance of cell-type-dependent alterations in cellular morphology. These results further establish a role for NPCs in the structural organization of transcripitonally repressed chromatin.

4.2 Results

4.2.1 *nup170Δ* cells display cell-type-dependent alterations in cellular morphology.

An increasing body of work has established functional interactions of NPCs and their components (Nups) with chromatin, most notably in processes that regulate gene expression and DNA repair (Casolari et al., 2004; Loeillet et al., 2005; Cabal et al., 2006; Taddei et al., 2006; Therizols et al., 2006; Palancade et al., 2007; Nagai et al., 2008; Ahmed et al., 2010). To gain a better understanding of the molecular basis for these interactions, we previously undertook a genetic approach to identify proteins and pathways whose functions are linked to several Nups previously implicated in chromatin structure and function (see Chapter III). This analysis identified genetic interactions between *NUP170* and numerous chromatin complexes, consistent with the observation that *nup170* null mutants exhibit defects in centromeric chromatin structure (Kerscher et al., 2001). Moreover, counterparts of Nup170p in higher eukaryotes have been linked to chromatin structure through their physical association with chromatin-modifying complexes (Mendjan et al., 2006; Kehat et al., 2011).

In characterizing the function of Nup170p in chromatin structure, we observed alterations in cellular morphology of a *NUP170* null mutant of the α-mating type (Figure 4-1A). These morphological alterations were characterized by cellular elongation often originating at the bud selection site and were not present in *nup170Δ* cells of the **a**-mating type. Moreover, these alterations were a consequence of loss of Nup170p and not a second site mutation as expression of

exogenous *NUP170* prevented elongation, reverting *MAT*α *nup170Δ* cells to a wild type morphology.

Loss of Nup170p has been previously associated with reduced fitness (Aitchison et al., 1995a; Kenna et al., 1996). To discern whether the observed morphological changes correlated with reduced fitness, we assessed the growth rates of a WT and *nup170Δ* strain of both mating types at a range of temperatures (Figure 4-1B). At both low and high temperatures, 16˚C and 37˚C, the growth rates of WT and *nup170Δ* strains were similar, however a mild growth defect was observed for the *nup170Δ* mutant at 23˚C, becoming more pronounced at 30˚C. Despite dramatic differences in morphology, the growth rates of haploid *NUP170* null mutant strains were similar to one another regardless of mating type or temperature tested, arguing that these two phenotypes are independent.

4.2.2 *nup170Δ* cells of the a-mating type secrete both mating pheromones.

Yeast cells of **a**-mating type produce and secrete the mating pheromone **a**-factor, while cells of the α-mating type secrete α-factor. Mating pheromones induce cell-cycle arrest and stimulate the mating response in cells of the opposite mating type (i.e. *MAT***a** cells are responsive to α-factor but not **a**-factor). In response to pheromone, stimulated cells produce a mating projection, often referred to as a shmoo, to facilitate conjugation. Since the morphology of *nup170Δ* cells of the α-mating type was reminiscent of cells forming a mating projection, we examined pheromone secretion in haploid WT and *nup170Δ* strains of both mating types. Secretion of **a**-factor and α-factor was monitored using a

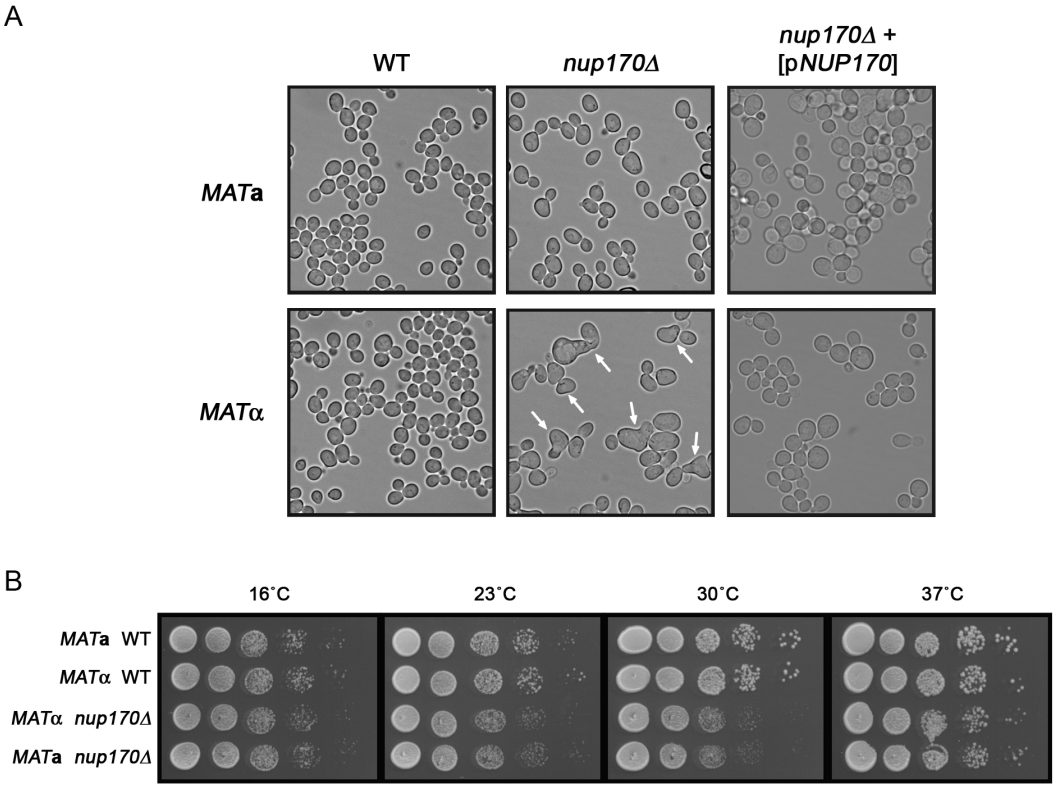

Figure 4-1. *nup170Δ* cells display cell-mating-type specific alterations in cellular morphology.

(A) *MAT*α *nup170Δ* cells display a cellular morphology indicative of a mating pheromone response. The cellular morphology of WT and *nup170Δ* cells of the *MAT***a** and *MAT*α mating types were examined by bright field microscopy in the presence or absence of an exogenous copy of *NUP170* (pRS316A-NUP170; p*NUP170*). Arrows highlight cells with a cellular morphology resembling a shmoo-like phenotype. (B) Four isogenic strains of the indicated genotypes were isolated by tetrad dissection of a diploid strain heterozygous for a *nup170* null mutation (DVY1160). To assess growth rates, equal numbers of cells from overnight cultures were serially diluted ten-fold and spotted onto YPD plates for 2-3 d at the indicated temperatures.

halo assay and strains hypersensitive to **a**-factor (*MAT*α *sst2Δ ste3*^{L194Q}) and α-factor (*MAT***a** *bar1Δ*) (Figure 4-2; Sprague and Herskowitz, 1981; Chan and Otte, 1982a and 1982b; Boone et al., 1993). In this assay, secretion of mating pheromones into the surrounding media by the strain of interest induces cell-cycle arrest and growth inhibition dependent on the pheromone sensitivity of the underlying lawn. As expected, a zone of growth inhibition (i.e. a halo) formed around the WT strain of **a**-mating type when plated onto a cell lawn hypersensitive to **a**-factor (*MAT*α cells), but not when plated onto a lawn hypersensitive to α-factor (*MAT***a**) (Figure 4-2A). This indicated the appropriate secretion of **a**-factor by the *MAT***a** WT strain. For a *MAT*α WT strain the reciprocal was true, indicating secretion of α-factor. By contrast, analysis of the *nup170Δ* mutants revealed secretion of **a**-factor by cells of both mating types (Figure 4-2A). However, secretion of α-factor by *MAT*α *nup170Δ* cells was not detectable. In an effort to evaluate this phenotype of *MAT*α *nup170Δ* cells more closely, we deleted the α-factor protease, *BAR1*. Indeed, upon deletion of *BAR1* in the *MAT*α *nup170Δ* mutant, secretion of α-factor was readily detectable (Figure 4-2B), indicating that these cells, produce both mating pheromones. Importantly, similar to the alterations in cellular morphology, expression of exogenous *NUP170* restored appropriate pheromone secretion to these mutants.

Figure 4-2. *MAT*α *nup170Δ* cells secrete both mating pheromones.

(A) Secretion of the mating pheromones **a**-factor and α-factor from haploid strains harboring either pRS316 (empty vector) or pRS316A-NUP170 (p*NUP170*) was examined using halo assays. Cells hypersensitive to either **a**-factor (*MAT*α *sst2Δ ste3*^{L194Q}*;* DVY1190) or α-factor (*MAT***a** *bar1Δ*; DVY1191) were spread evenly over the surface of YPD plates. The indicated strains were then streaked onto the plates and incubated for 2-3 d at 30˚C. In this assay, secretion of **a**-factor by the strain of interest leads to a halo of growth inhibition of the surrounding lawn of *MAT*α cells but not *MAT***a** cells. Conversely, secretion of α-factor is indicated by a halo of growth inhibition of the *MAT***a** lawn but not the *MAT*α lawn. For each panel the pheromone to which the underlying cell lawn is hypersensitive to is indicated. In a WT strain *MAT***a** cells secrete **a**-factor while *MAT*α cells secrete α-factor. Note, *MAT*α *nup170Δ* cells inhibit growth of *MAT*α *sst2Δ ste3*^{L194Q} suggesting they adherently secrete **a**-factor. This phenotype is suppressed by an exogenous copy of *NUP170*. (B) To examine whether *MAT*α *nup170Δ* cells produce α-factor, halo assays were performed as described in A with the exception that *BAR1* was additionally deleted in a *MAT*α *nup170Δ* mutant. Note, secretion of α-factor in the *MAT*α *nup170Δ* strain was detected only in the absence of the α-factor protease, Bar1p.

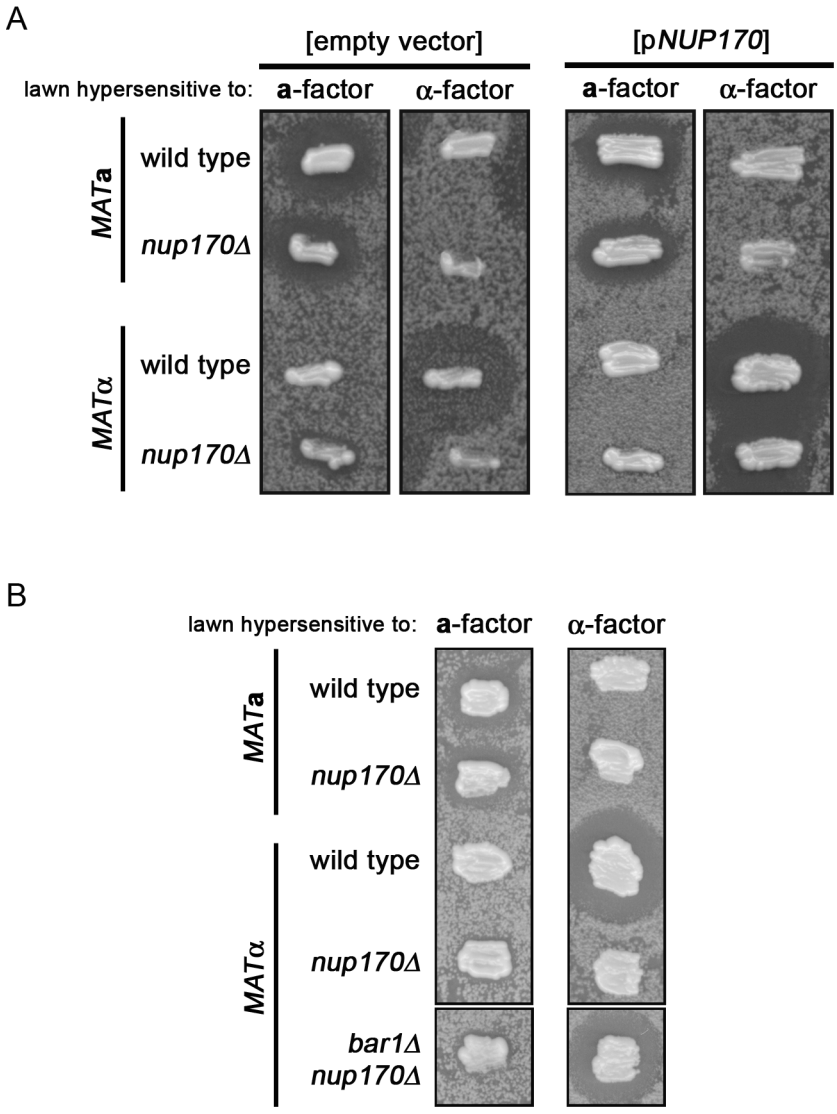

Figure 4-2. *MATα nup170Δ* cells secrete both mating pheromones.

4.2.3 Cell-type-specific morphology defects are not observed in other *nup* mutants

The *Saccharomyces cerevisiae* genome contains ~551 duplicate gene pairs (Scannell et al., 2007). One of these gene pairs consists of the nucleoporin genes *NUP170* and *NUP157* (Aitchison et al., 1995a). Consequently, Nup170p and Nup157p perform similar functions (Aitchison et al., 1995a; Makio et al., 2009) but, despite these similarities, it is clear that that they perform distinct functions (see Chapter III; Kerscher et al., 2001). With this in mind we examined whether a *nup157Δ* mutant exhibited similar cell-type-specific defects in cell morphology as the *nup170Δ* mutant. Microscopy analysis of *nup157Δ* cells of either mating type revealed no alterations in cell morphology and, in fact, no cell-type-specific defects in morphology were detected in several other *nup* null mutants tested including *nup2Δ*, *nup60Δ*, and *nup188Δ* (Figure 4-3A). Moreover, pheromone secretion as evaluated using halo assays of various *nup* mutants, including *nup188Δ*, *nup157Δ*, *nup60Δ*, *nup53Δ*, and *nup2Δ* (Figure 4-3B) revealed normal pheromone secretion (Figure 4-3B).

In the absence of Nup170p targeting of the integral membrane protein Heh1p to the INM is impaired and Heh1p accumulates at the ONM (King et al., 2006). To determine whether the cell-type-dependent defects observed in the *nup170Δ* mutant arise from a loss of Heh1p at the INM, we examined pheromone secretion in *heh1Δ* strains. In these mutants pheromone secretion was similar to wild type strains (Figure 4-3B), suggesting the defect observed in the *nup170Δ* mutant is independent of Heh1p. Importantly, the cell-type-specific defects of the

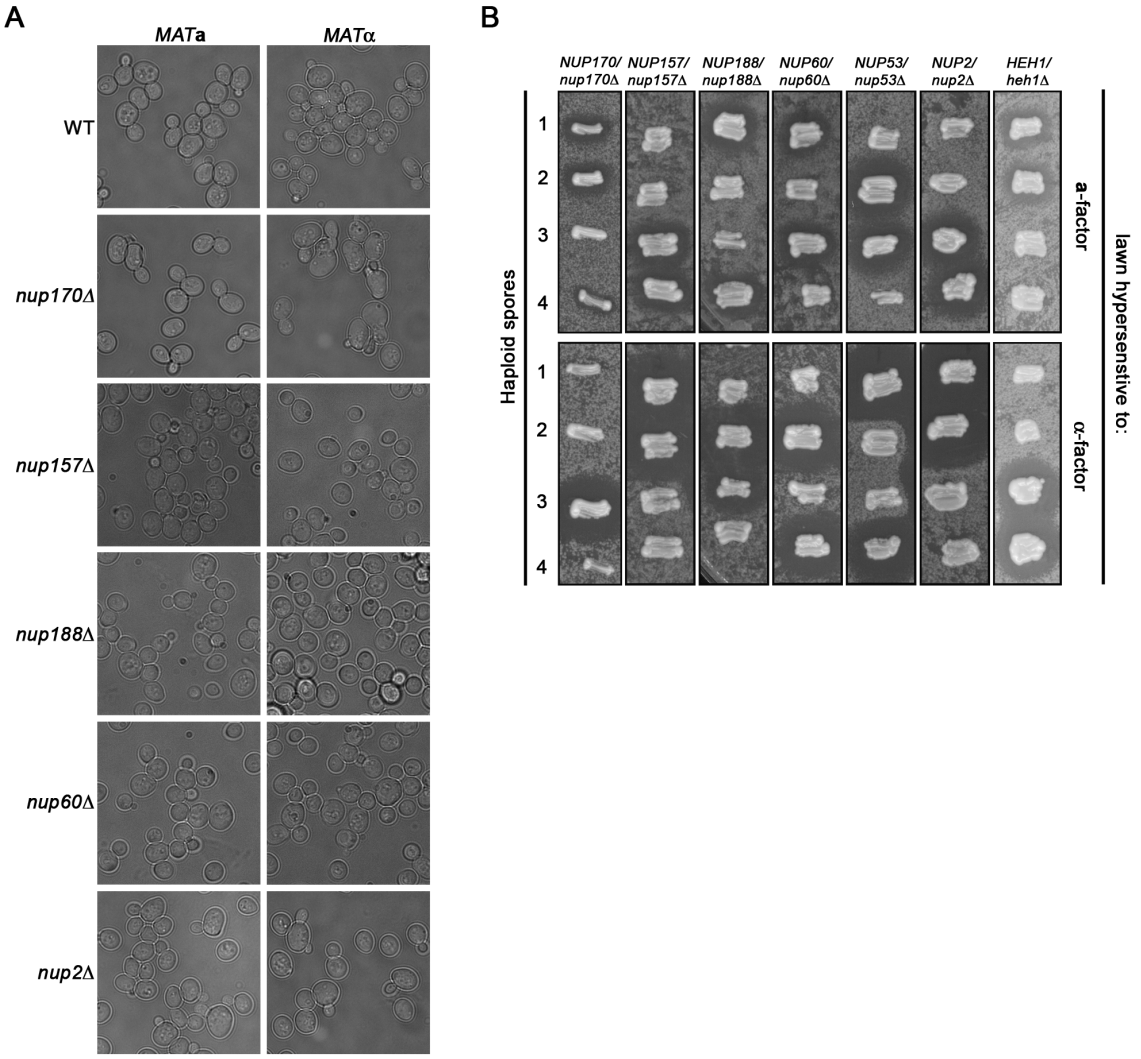

Figure 4-3. Aberrant mating pheromone secretion does not occur in other Nup null mutants tested.

(A) Cellular morphology was examined in *MAT***a** and *MAT*α mating types of WT, *nup2Δ*, *nup60Δ*, *nup157Δ*, *nup170Δ*, and *nup188Δ* strains. Cells were grown in YPD medium to mid-logarithmic growth phase and imaged by light microscopy. Shown are representative bright field images. (B) Heterozygous null mutations of *NUP2*, *NUP53*, *NUP60*, *NUP170*, *NUP157*, *NUP188,* and *HEH1* were constructed in the diploid strain (BY4743). From each diploid strain, meiotic progeny were obtained by tetrad dissection, and mating pheromone secretion of each set of haploid spores (labeled 1-4) was evaluated using halo assays described in Figure 4-2. For each panel, the pheromone to which the underlying cell lawn is hypersensitive to is indicated. Halos of growth inhibition present in the top panels indicate secretion of **a**-factor and halos present in the bottom panels indicate secretion of α-factor. Note, in the heterozygous *nup170* mutant progeny **a**-factor secretion segregates 3:1 whereas **a**-factor secretion segregates 2:2 in all other mutants tested.

nup170Δ mutant are unlikely to be linked to alterations in nucleocytoplasmic transport, as the *nup170Δ* mutant has no detected defects in active transport (Aitchison et al., 1995a; Makio et al., 2009). Furthermore, the previously described defect in the *nup170*Δ mutant to maintain the NPC diffusion barrier was similarly described in the *nup188Δ* mutant (Shulga et al., 2003), which did not display alterations in cell morphology or pheromone secretion (Figure 4-3).

4.2.4 Nup170p is required for repression of a-specific genes.

Inhibition of **a**-factor secretion in cells of α-mating type occurs at the level of transcription. In this cell type, similar to other **a**-specific genes, the genes encoding **a**-factor, *MFA1* and *MFA2*, are repressed. The production and secretion of **a**-factor in *MATα nup170Δ* cells suggests that *MFA1* and/or *MFA2* as well as *STE6,* an **a**-specific gene encoding the transporter required for **a**-factor secretion (McGrath and Varshavsky, 1989), are derepressed in the absence of Nup170p. Moreover, detection of α-factor secretion only upon deletion of *BAR1*, an **a**-specific gene encoding the α-factor protease Bar1p (Mackay et al., 1988), further argued that repression of **a**-specific genes is alleviated in the absence of Nup170p. To test this possibility, we evaluated the expression levels of **a**-specific genes in WT and *nup170Δ* cells of both mating types using semi-quantitative reverse transcription PCR (RT-PCR) analysis (Figure 4-4A). As expected, in a WT background transcripts of the **a**-specific genes *ASG7* (required for attenuation of the pheromone response; Roth et al., 2000; Rivers and Sprague, 2003), *BAR1, STE2* (encoding a transmembrane receptor of α-factor; Blumer et al., 1988), and

STE6 were readily detected in *MAT***a** but not *MAT*α cells, with the exception of trace levels of *STE6* transcripts present in the α-mating type. Conversely, transcripts of the α-specific genes *STE3* and *HML*α*2* were detected in *MAT*α, but not *MAT***a** cells. In the *nup170Δ* background, however, transcripts of all four **a**-specific genes were detected in both *MAT***a** and *MAT*α cells, albeit *STE6* transcripts were only slightly increased in *MAT*α *nup170Δ* cells compared to their WT counterpart. Nevertheless, these results clearly support a role for Nup170p in repression of **a**-specific genes.

The extent of derepression of **a**-specific genes in the absence of Nup170p was also revealed by DNA microarrays of the cellular transcriptional profile of *MAT*α *nup170Δ* cells. This analysis identified 396 ORFs up-regulated and 98 ORFs down-regulated greater than two-fold in a *nup170Δ* mutant of α-mating type (Tables 4-1 and 4-2). Up-regulated ORFs were enriched for genes encoding ribosomal protein genes (129 of 137) and genes located within subtelomeric regions (107 of 347), consistent with the up-regulation of RP and subtelomeric genes observed in a *nup170Δ* mutant of the opposite mating type (see Chapter III, Tables 3-3 and 3-4). Gene ontology (GO) analysis of up-regulated ORFs using a hypergeometric distribution test identified enrichment of genes involved in conjugation (27 genes; p-value 6.9×10^{-9}), sexual reproduction (33 genes; p-value 1.2×10^{-5}), response to mating pheromone (21 genes; p-value 2.6×10^{-5}), cytogamy (6 genes; p-value 4.4×10^{-3}), and agglutination (4 genes; p-value 0.02). Consistent with the previous RT-PCR analysis, the **a**-specific genes *ASG7, BAR1, MFA1*, *MFA2*, and *STE2* were all among the most significantly up-regulated ORFs, while

STE6 displayed no significant change in expression (Figure 4-4B). Interestingly, expression of several α-specific genes was also increased which could, in part, arise from the observed two-fold increase in expression of the *α1* gene (Figure 4-4B), encoding a transcriptional activator of α-specific genes (Hagen et al., 1993). Taken together these results are consistent with a role for Nup170p in repression of **a**-specific genes.

4.2.5 Nup170p is required for silencing at *HML* and *HMR* loci.

In cells of α-mating type the *α1* gene is present in two alleles, located at the mating type locus *MAT* and the silent mating type locus *HML*. The *α1* allele present at *MAT* (*MATα1)* is transcriptionally active, whereas the *α1* allele present at *HML* (*HMLα1*) is transcriptionally silenced. Considering the function of Nup170p in subtelomeric gene silencing (see Chapter III, Figure 3-5) and that much of the silencing machinery is conserved between telomeres and the mating type loci, we hypothesized that the two-fold up-regulation of *α1* observed in the *nup170Δ* mutant resulted from loss of silencing at *HML*. To test this, *HML* silencing was evaluated using cell growth assays that reflect the transcriptional status of the reporter genes *URA3* and *ADE2* inserted within the *HML* locus (Figure 4-5A; Ishii et al., 2002; Dilworth et al., 2005). In this background, WT cells favor repression of *URA3* and *ADE2;* however, a mutation within the I-silencer causes partial derepression of *URA3* and *ADE2* (Mahoney and Broach, 1989), permitting modest growth in the absence of uracil and adenine and growth in the presence of 5-FOA. In addition, repression of *ADE2* in WT cells produces

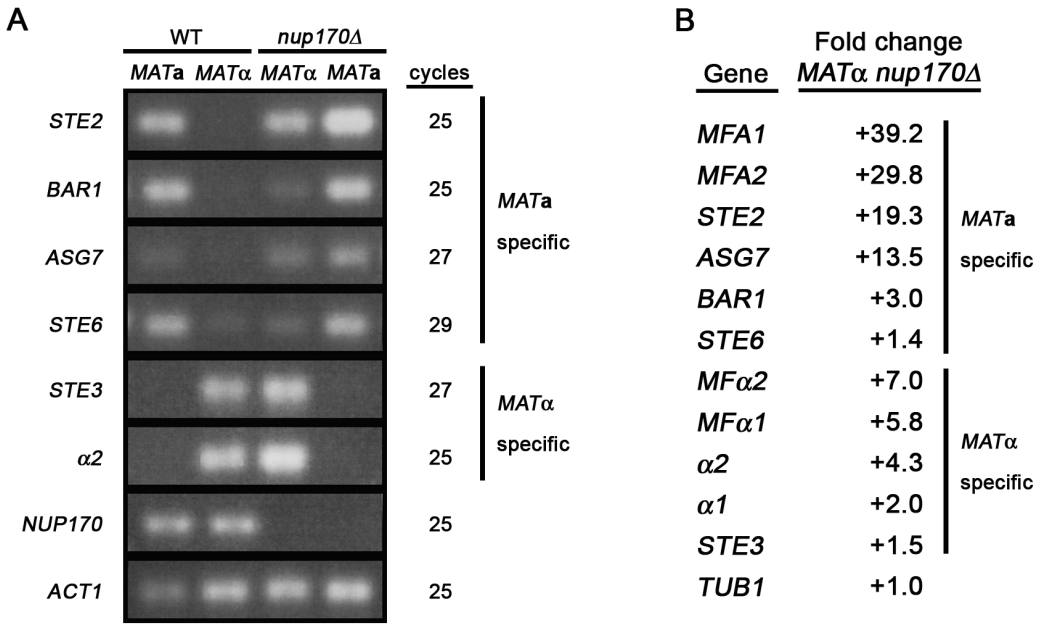

Figure 4-4. a-specific genes are derepressed in the absence of Nup170p.

Repression of **a**- and α-specific genes was assessed in wild type and *nup170Δ* haploid cells. Total RNA was isolated from WT and *nup170Δ* cells of the indicated mating types and expression of **a**-specific genes (*STE2*, *BAR1*, *ASG7*, and *STE6*) and α-specific genes (*STE3* and *HMLα2*) were determined by semi-quantitative reverse-transcription PCR (RT-PCR) using primer sets specific to each target cDNA. *ACT1* served as a loading control and *NUP170* served as confirmation of gene deletion. The number of PCR cycles used for amplification of each target cDNA is indicated. (B) Two-color DNA microarray analysis was performed comparing RNA isolated from *MATα* WT and *MATα nup170Δ* cells. Shown are the fold-changes in gene expression of a subset of **a**-specific and α-specific genes in *MATα nup170Δ* cells. Genes up-regulated ≥ 2-fold were also identified as being differentially expressed by maximum-likelihood analysis (lambda ≥ 100). *TUB1* served as a control. For a complete list of significantly differentially expressed ORFs see Tables 4-1 and 4-2. Note, *MFA1* and *MFA2* both encode **a**-factor.

* RT-PCR was performed by DWV. RNA isolation for microarray analysis was performed by DWV and cDNA labeling and hybridization was performed by YW. Data analysis was performed by WMC and DWV.

Table 4-1. Up-regulated ORFs in a *MATα nup170Δ* mutant.

Gene name	Fold change	Gene name	Fold change	Gene name	Fold change	Gene name	Fold change
AAD15	3.0	*GUA1*	2.4	*RPL11B*	2.9	*RPL4B*	2.8
ACT1	3.0	*HAC1*	2.3	*RPL12A*	2.9	*RPL5*	2.9
ADO1	2.8	*HHF1*	2.1	*RPL12B*	3.2	*RPL6A*	3.1
AFR1	2.5	*HHT1*	2.0	*RPL13A*	2.4	*RPL6B*	2.1
AGA1	11.7	*HHY1*	2.3	*RPL13B*	2.7	*RPL7A*	3.8
AGA2	31.6	*HMLα1*	2.0	*RPL14A*	4.0	*RPL8B*	2.6
ARF1	2.3	*HMLα2*	4.3	*RPL14B*	2.8	*RPL9A*	2.5
ASG7	13.5	*HMRA1*	3.8	*RPL16A*	2.8	*RPP0*	2.4
ASP3-2	2.0	*HMRA2*	4.2	*RPL16B*	3.0	*RPP1A*	3.4
ASP3-3	2.2	*HMS1*	3.2	*RPL17A*	2.3	*RPP1B*	4.0
ASP3-4	2.1	*HXT11*	2.4	*RPL17B*	2.4	*RPP2A*	3.0
ATP1	2.5	*HXT12*	2.9	*RPL18A*	3.0	*RPP2B*	3.0
BAR1	3.0	*HXT13*	3.2	*RPL19A*	3.5	*RPS0A*	2.6
BAT1	2.6	*HXT15*	2.2	*RPL19B*	3.5	*RPS0B*	2.3
BGL2	2.2	*HXT16*	2.3	*RPL1A*	2.6	*RPS10A*	2.9
BSC3	3.2	*HXT17*	2.6	*RPL1B*	2.8	*RPS10B*	2.8
BSC4	3.9	*HXT9*	3.2	*RPL20B*	2.7	*RPS11A*	3.1
BUR6	2.3	*HYP2*	2.7	*RPL21B*	2.5	*RPS11B*	2.9
CBF5	3.1	*IMD4*	2.3	*RPL22A*	3.7	*RPS12*	3.6
CCW12	3.9	*IME4*	3.8	*RPL23A*	2.9	*RPS13*	2.3
CDA1	2.2	*INH1*	2.9	*RPL23B*	3.1	*RPS14A*	3.8
CIS3	2.7	*IRC18*	2.7	*RPL24A*	4.0	*RPS15*	3.5
CLN3	2.2	*KAR4*	5.8	*RPL24B*	5.0	*RPS16A*	2.5
COS1	2.4	*KAR5*	3.0	*RPL25*	3.2	*RPS16B*	2.6
COS12	5.2	*KRE22*	3.4	*RPL26A*	3.6	*RPS17A*	3.1
COS4	2.1	*LIF1*	2.8	*RPL26B*	3.3	*RPS17B*	2.9
CPR1	2.5	*MATA2*	4.2	*RPL27A*	3.5	*RPS18A*	2.7
CTS1	3.2	*MFα1*	5.8	*RPL27B*	2.5	*RPS18B*	2.6
CUP1-1	2.5	*MFα2*	7.0	*RPL28*	3.8	*RPS19A*	2.7
CUP1-2	2.6	*MFA1*	39.2	*RPL29*	4.7	*RPS19B*	2.9
CWP2	3.7	*MFA2*	29.8	*RPL2A*	2.4	*RPS1A*	2.1
DAL1	2.2	*MIR1*	2.3	*RPL2B*	2.2	*RPS1B*	2.5
DCV1	2.3	*MOS1*	2.3	*RPL3*	2.7	*RPS2*	2.8
DDI2	2.2	*NCA3*	2.3	*RPL30*	3.2	*RPS20*	2.6
DDI3	2.5	*NHP2*	2.8	*RPL31A*	4.2	*RPS21A*	2.4
EFB1	3.1	*NHP6B*	2.1	*RPL31B*	2.2	*RPS21B*	2.7
EFT1	2.7	*NIP100*	2.1	*RPL32*	3.2	*RPS22A*	3.1
EFT2	2.5	*NOP10*	2.1	*RPL33A*	3.0	*RPS23A*	3.1
EGD1	2.3	*NPL3*	2.1	*RPL33B*	2.8	*RPS23B*	3.2
EGD2	3.2	*NSR1*	2.8	*RPL34A*	3.4	*RPS24A*	3.4
ERR1	4.5	*PDA1*	2.3	*RPL34B*	3.4	*RPS24B*	2.7
ERR2	3.9	*PET9*	2.4	*RPL35A*	4.7	*RPS25A*	3.3
ERR3	4.9	*PEX34*	2.2	*RPL35B*	4.4	*RPS25B*	2.3
FAR1	3.7	*PHO3*	2.4	*RPL36A*	2.5	*RPS26A*	4.7
FAS2	2.2	*PMA1*	3.1	*RPL36B*	5.0	*RPS26B*	2.6
FIG1	42.9	*POT1*	2.2	*RPL37A*	3.1	*RPS27A*	2.2
FIG2	10.2	*PRM1*	11.8	*RPL37B*	3.3	*RPS27B*	3.9
FLO9	2.1	*PRM2*	14.9	*RPL38*	3.4	*RPS28A*	3.8
FUS1	4.7	*PRM3*	17.7	*RPL39*	3.5	*RPS29A*	3.9
FUS2	6.6	*PRM6*	15.9	*RPL40A*	3.1	*RPS29B*	3.5
FUS3	3.1	*PRM8*	3.4	*RPL40B*	2.3	*RPS3*	2.2
GCN4	2.5	*PRY2*	2.8	*RPL41A*	3.0	*RPS30A*	3.2
GEX1	2.5	*PXR1*	2.1	*RPL41B*	2.9	*RPS30B*	3.4
GEX2	2.6	*QCR6*	2.1	*RPL42A*	3.7	*RPS31*	4.1
GIC2	4.3	*QCR7*	2.6	*RPL42B*	3.4	*RPS4A*	2.7
GIM4	2.2	*RGM1*	2.6	*RPL43A*	3.8	*RPS4B*	2.6
GPA1	2.9	*RPL10*	3.1	*RPL43B*	2.7	*RPS5*	2.9
GSP1	2.4	*RPL11A*	3.5	*RPL4A*	3.1	*RPS6A*	4.0

RPS6B	3.7	*YAL064W*	2.2	*YER188W*	2.5	*YLR161W*	3.9
RPS7B	2.8	*YAL064W-B*	2.4	*YER189W*	2.8	*YLR279W*	2.5
RPS8A	3.3	*YAL065C*	3.4	*YFL063W*	2.8	*YLR280C*	2.2
RPS8B	2.9	*YAL069W*	2.7	*YFL064C*	3.1	*YLR302C*	7.4
RPS9B	2.7	*YAR030C*	2.2	*YFL065C*	3.0	*YLR312C*	2.7
RRT5	2.6	*YAR047C*	2.8	*YFL066C*	3.3	*YLR434C*	2.5
SAG1	8.4	*YAR053W*	2.6	*YFL067W*	2.3	*YLR462W*	3.0
SBP1	2.1	*YAR060C*	2.1	*YFL068W*	2.4	*YLR463C*	3.0
SCW10	3.4	*YAR061W*	3.1	*YFR012W-A*	2.2	*YLR464W*	2.5
SCW4	4.8	*YAR062W*	2.5	*YGL052W*	3.2	*YML007C-A*	2.6
SIK1	2.6	*YAR064W*	3.5	*YGL109W*	2.7	*YML133C*	3.3
SMA1	2.4	*YAR066W*	2.3	*YGL262W*	8.1	*YMR122W-A*	3.1
SML1	2.4	*YBL109W*	2.8	*YGR269W*	2.4	*YMR304C-A*	3.8
SOM1	3.1	*YBL111C*	3.4	*YGR291C*	2.5	*YMR326C*	2.1
SPO22	4.5	*YBL112C*	3.4	*YGR293C*	2.4	*YNL143C*	2.1
SPO69	2.9	*YBL113C*	3.7	*YHL049C*	3.1	*YNL190W*	4.9
SSS1	3.1	*YBR032W*	9.8	*YHL050C*	2.5	*YNL337W*	2.2
SST2	3.1	*YBR116C*	2.1	*YHR033W*	2.1	*YNR077C*	2.5
STE2	19.3	*YBR300C*	2.2	*YHR212C*	2.3	*YOL162W*	2.6
TDA8	3.4	*YCL076W*	37.7	*YHR213W*	2.6	*YOL163W*	2.4
TEC1	2.3	*YCR038W-A*	2.1	*YHR214W*	2.3	*YOL166C*	2.2
TEF1	2.3	*YCR041W*	2.1	*YHR217C*	2.6	*YOR050C*	3.2
TEF2	2.8	*YCR064C*	2.1	*YHR218W*	3.4	*YOR248W*	2.7
TEF4	2.5	*YCR097W-A*	2.0	*YHR219W*	3.2	*YOR343C*	7.9
TFP1	2.3	*YCR102W-A*	3.1	*YIL082W*	76.9	*YPL025C*	2.5
THI11	2.8	*YDL071C*	2.1	*YIL082W-A*	25.5	*YPR202W*	2.6
THI12	2.5	*YDL152W*	2.3	*YIL100W*	4.7	*YPR203W*	3.0
THI13	2.9	*YDR124W*	5.2	*YIL177C*	3.3	*YPR204W*	3.5
THI5	2.6	*YDR133C*	2.5	*YIR040C*	2.2	*YPT1*	2.0
TIF1	2.2	*YDR134C*	2.5	*YIR042C*	4.7	*YRA1*	3.3
TIF2	2.4	*YDR154C*	2.5	*YJL220W*	3.0	*YRF1-1*	3.1
TIP1	2.8	*YDR535C*	2.1	*YJL225C*	3.2	*YRF1-2*	3.4
TKL1	2.0	*YDR543C*	2.6	*YJR157W*	3.0	*YRF1-3*	3.4
TMA23	2.1	*YEF3*	2.6	*YJR162C*	2.5	*YRF1-4*	3.2
TMA7	2.3	*YEL074W*	3.5	*YKL223W*	2.1	*YRF1-5*	3.4
TYS1	2.3	*YEL075C*	2.8	*YKL225W*	2.6	*YRF1-6*	3.4
UTH1	4.5	*YEL075W-A*	3.0	*YLL065W*	2.4	*YRF1-7*	3.7
UTR2	2.1	*YEL076C*	2.7	*YLL066C*	3.2	*YRF1-8*	3.5
VMA10	2.6	*YEL076C-A*	2.4	*YLL067C*	3.8	*YSY6*	2.2
VPS61	2.2	*YEL077C*	4.0	*YLR156W*	4.1	*ZEO1*	4.0
XBP1	2.6	*YER187W*	2.3	*YLR159W*	4.3	*ZUO1*	2.0

Table 4-2. Down-regulated ORFs in a *MATα nup170Δ* mutant.

Gene name	Fold change	Gene name	Fold change	Gene name	Fold change	Gene name	Fold change
ADH5	-2.7	*FIT2*	-10.0	*PHO12*	-3.8	*VHS1*	-2.0
AIM17	-3.7	*FIT3*	-8.0	*PHO5*	-10.6	*VMR1*	-2.5
ARE2	-2.1	*FMP23*	-3.0	*PHO8*	-3.1	*VTC3*	-3.7
ARG1	-4.3	*FRE1*	-3.6	*PHO81*	-2.4	*VTC4*	-2.6
ARG3	-2.3	*FRE4*	-3.9	*PHO84*	-3.1	*YDC1*	-2.6
ARN1	-2.6	*FTR1*	-2.3	*PHO89*	-8.6	*YDL241W*	-2.2
ARN2	-4.1	*GRE2*	-2.6	*RGI1*	-6.6	*YGR035C*	-2.6
BAG7	-3.3	*GTO3*	-2.6	*RMD6*	-2.0	*YHB1*	-3.8
BNA4	-2.4	*HEM3*	-2.2	*RNR3*	-2.3	*YHR140W*	-3.8
CCC2	-2.3	*HO*	-2.7	*RSB1*	-2.7	*YJL012C-A*	-2.4
CHA1	-2.4	*HSP26*	-3.2	*RTS3*	-2.2	*YJL144W*	-2.6
CIT2	-2.3	*HSP30*	-9.3	*SAM2*	-2.2	*YLR108C*	-3.1
CMK2	-3.8	*HSP42*	-3.0	*SAP4*	-2.9	*YLR194C*	-2.1
CPS1	-3.6	*HSP78*	-2.7	*SIT1*	-5.1	*YLR346C*	-3.4
CTF19	-2.8	*ICY2*	-2.2	*SPL2*	-9.0	*YMR102C*	-2.1
CTR1	-3.1	*LYS20*	-2.2	*SSU1*	-2.4	*YMR173W-A*	-3.3
CWP1	-2.8	*MAM33*	-2.2	*TDA1*	-2.5	*YMR317W*	-2.9
DAN1	-4.3	*MET22*	-2.8	*TDA10*	-2.6	*YNL217W*	-2.4
DDR48	-3.0	*MGA1*	-2.3	*TDH1*	-2.4	*YOL014W*	-3.1
DIA1	-2.5	*OYE3*	-2.3	*TIR1*	-2.5	*YOR385W*	-2.5
DIP5	-3.2	*PDR5*	-3.7	*TIS11*	-7.9	*YPL014W*	-2.9
EMI2	-2.4	*PGM2*	-2.7	*TMA10*	-4.9	*YTP1*	-2.4
ENB1	-3.4	*PHD1*	-2.3	*TPO4*	-3.0	*ZRT1*	-4.8
FET4	-2.4	*PHM6*	-8.3	*TPS2*	-2.7		
FIT1	-5.5	*PHO11*	-3.4	*VBA1*	-2.1		

red colonies. By contrast, a silencing deficient strain (*sir3Δ*) favors derepression of *URA3* and *ADE2*, producing white colonies, rendering cells sensitive to 5-FOA, and permitting enhanced growth on medium lacking adenine and uracil as compared to WT cells (Figure 4-5A; Aparicio et al., 1991). Examination of *nup170Δ* cells revealed a loss of silencing similar to a *sir3Δ* mutant. Silencing was restored to the *nup170Δ* mutant following addition of exogenous *NUP170*. Similar defects in silencing were not detected in either *nup2Δ* or *nup60Δ* mutants (Figure 4-5A).

Similar cell growth assays were performed to assess silencing of the *HMR* locus, using a single reporter gene, *URA3,* integrated between the silencer elements *HMR*-E and *HMR*-I (Donze et al., 1999). As was the case for *HML*, silencing of *HMR* was also reduced in the absence of Nup170p, and could be restored by addition of exogenous *NUP170* (Figure 4-5B). Loss of silencing at *HMR* did not appear to be as substantial as that observed at *HML*. The differential effect on silencing at the mating type loci may reflect a more significant role for Nup170p at *HML,* or, more likely, may result from a combinatorial effect due to loss of Nup170p and partial impairment of I-silencer function.

Previous analysis of the genome-wide DNA binding profile of Nup170p revealed binding within both *HML* and *HMR* (see Chapter III, Figure 3-7), consistent with its role in silencing at these loci. Nup170p binding at *HMR* was further supported by ChIP of Nup170-9xMyc in conjunction with qPCR analysis using primer sets adjacent to and within *HMR* (Figure 4-5C). By contrast, ChIP-qPCR analyses performed with Nup157-9xMyc or Nup188-9xMyc (other

members of the Nup170 subcomplex) did not reveal similar levels of enrichment of the *HMR* locus (Figure 4-5C; Alber et al., 2007b; Amlacher et al., 2011). Although for both of these Nups multiple primer sets displayed enrichments above background at or near the significant cut-off (≥2-fold), likely reflecting the presence of these proteins in the Nup170 complex (Alber et al., 2007b; Amlacher et al., 2011). From these results we conclude that Nup170p associates with *HML* and *HMR*.

Association of Nup170p with the silent mating type loci led us to examine whether it functions in silencing at these loci through a mechanism similar to its previously described role in recruiting Sir proteins to subtelomeric DNA (Chapter III; Figures 3-11 and 3-12). To assess this possibility, ChIP of Sir2-9xMyc and Sir3-9xMyc in conjunction with qPCR analysis was performed using primer sets immediately adjacent to and within *HMR* in WT and *nup170Δ* strains (Figure 4-6A and 4-6B). Surprisingly, binding of Sir2p and Sir3p within *HMR* was not affected by deletion of *NUP170*, suggesting that the function of Nup170p in silencing at the mating type loci is distinct from its silencing function at telomeres.

Over-expression of Sir4p disrupts silencing (including at *HMR*) through a dominant negative effect (Cockell et al., 1995; Singer et al., 1998). With this in mind, we hypothesized that the silencing defect at the mating type loci in *nup170Δ* cells may also arise from a dominant negative effect in which dispersal of Sir4p from subtelomeric DNA (Chapter III; Figure 3-11) results in an increase

Figure 4-5. Silencing at the *HMR* and *HML* loci is lost in the absence of Nup170p.

The indicated gene deletions were introduced into the yeast strains KIY54, encoding *URA3* and *ADE2* integrated between the *E* and *I* silencer elements of the *HML* locus (A), and ROY648, encoding *URA3* integrated between the *E* and *I* silencer elements of the *HMR* locus (B) as shown. Silencing of the reporter genes was examined in the indicated haploid strains containing no plasmid, pRS315 (vector), or pHNP170 (p*NUP170*). Following overnight growth in non-selective liquid medium, an equal number of cells from each culture were serially diluted and plated onto nonselective (control) and selective conditions (SC medium lacking uracil [-ura], SC medium lacking uracil and adenine [-ura-ade], or SC medium containing 1 mg/mL 5-FOA [5-FOA]) and incubated for 2-5 d at 30˚C. To maintain plasmid selection, strains bearing pRS315 or pHNP170 were plated on SC medium lacking leucine (control), SC-leu-ura-ade (-ura-ade), and SC-leu + 1 mg/mL 5-FOA (5-FOA). Note, red and white colonies indicate repressed and derepressed *ADE2* phenotypes, respectively. Growth on 5-FOA indicates a repressed *URA3* state. (C) Cells producing Nup170-9xMyc (blue), Nup157-9xMyc (red), and Nup188-9xMyc (green) were grown to mid-logarithmic growth phase and association of the Myc-tagged fusion proteins with the silent mating type locus *HMR* was determined by ChIP-qPCR analysis. Primer sets were positioned within *HMR* (primers B to E) and adjacent to *HMR* (primers A, F, and G) as indicated. Mean relative enrichment of three independent ChIP experiments is plotted on the y-axis with standard error.

* Silencing and mating assays were performed by DWV. ChIP-qPCR analysis was performed by YW. Figure processing was performed by YW and DWV.

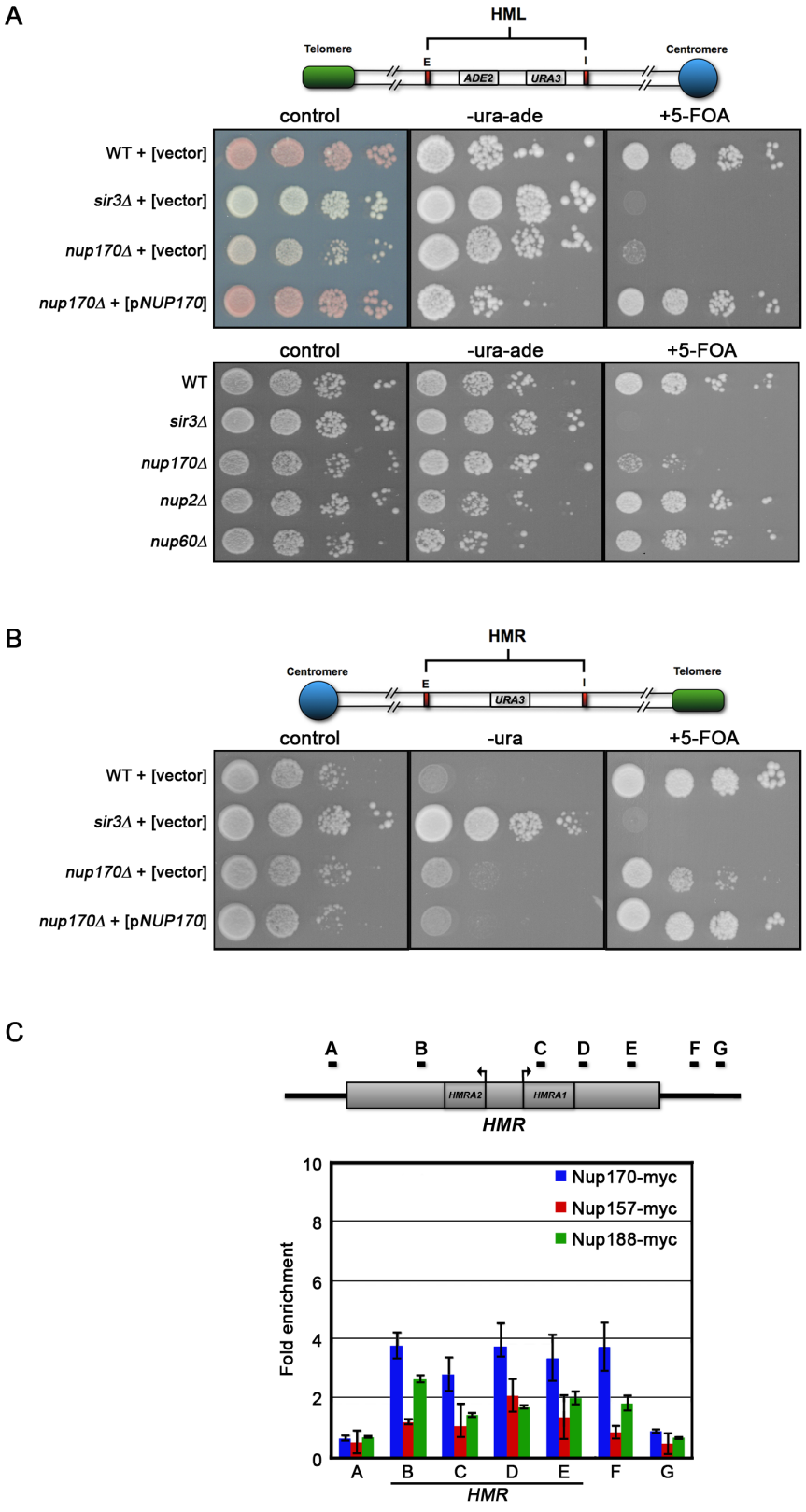

Figure 4-5. Silencing at the *HMR* and *HML* loci is lost in the absence of Nup170p.

in Sir4p association at *HMR* such that the stoichiometry of the SIR complex is altered. In support of this hypothesis, binding of Sir4p within *HMR* was significantly increased in the absence of Nup170p (Figure 4-6C). Sir4p binding was particularly enhanced near the Rap1p binding site of the *HMR*-E silencer. Together these results suggest that, in the absence of Nup170p, additional Sir4p is recruited to *HMR* in what is likely to be a Rap1p-dependent manner. Here increased levels of Sir4p may function to inhibit silencing by disrupting the stoichiometry of the SIR complex.

Derepression of the silent mating type loci, regardless of mating type, leads to expression of both *HMLα2* (encoding a repressor of **a-**specific genes; Herschbach et al., 1994) and *HMRA1* (encoding a co-repressor of haploid specific genes; Goutte et al., 1988) resulting in repression of haploid specific genes and sterility (reviewed in: Klar, 2010; Haber, 2012). With this in mind, non-quantitative mating assays were performed to determine the mating ability of *nup170Δ* strains. In this assay, *nup170Δ* strains of **a**- and α-mating type were crossed to WT strains of similar or opposing mating type and then plated on medium to select for growth of diploid cells. As indicated in Figure 4-7 by growth on diploid selection media, *nup170Δ* strains successfully diploidized when mated with a WT strain of the opposing mating type. This result demonstrates that, despite the observed reduction in silencing at *HML* and *HMR, nup170Δ* strains are mating competent and, in agreement with the transcriptome profiling data, continue to express haploid specific genes.

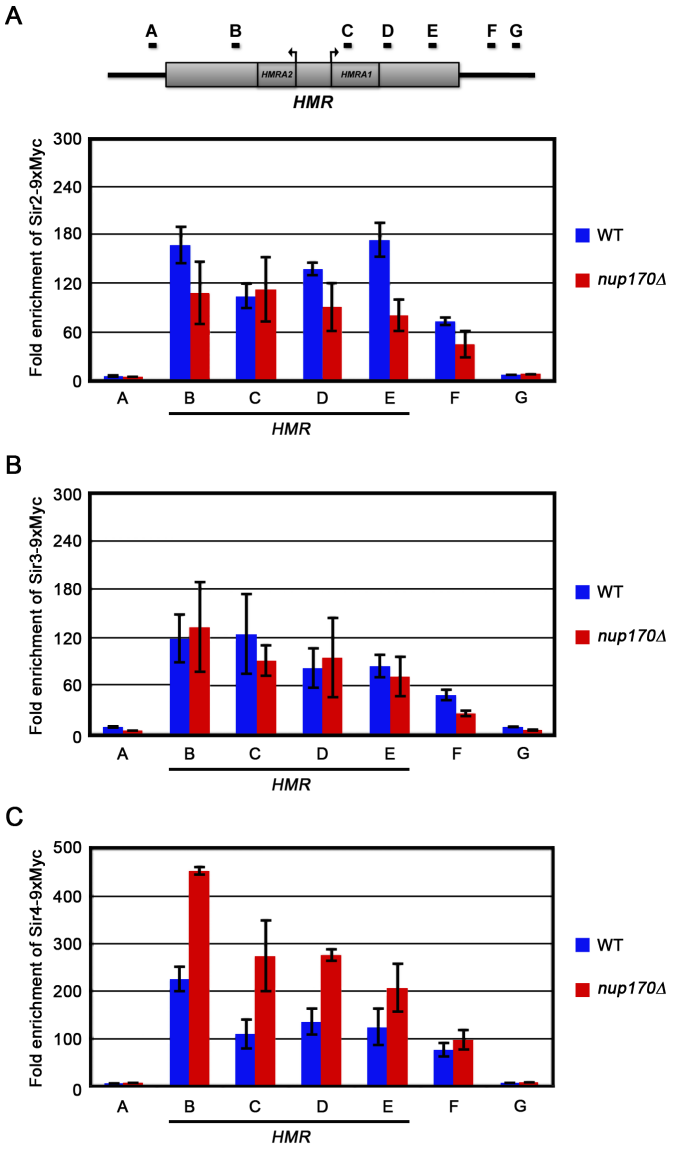

Figure 4-6. Deletion of *NUP170* enhances the association of Sir4p with the *HMR* locus.

Association of Sir2-9xMyc (A), Sir3-9xMyc (B), and Sir4-9xMyc (C) with *HMR* was examined in wild type (blue) and *nup170Δ* (red) cells by chromatin immunoprecipitation. ChIP samples were analyzed by qPCR using primer sets positioned within *HMR* (primers B to E) and flanking *HMR* (primers A, F, and G) as indicated. Plotted on the y-axis is the mean enrichment and standard error of three independent experiments. Note, association of Sir4-9xMyc, but not Sir2-9xMyc or Sir3-9xMyc, with the *HMR* locus is enhanced in the *nup170Δ* mutant with a biased distribution in favor of the Rap1p binding site located at *HMR*-E.
* ChIP-qPCR analysis was performed by YW. Figure processing was performed by YW and DWV.

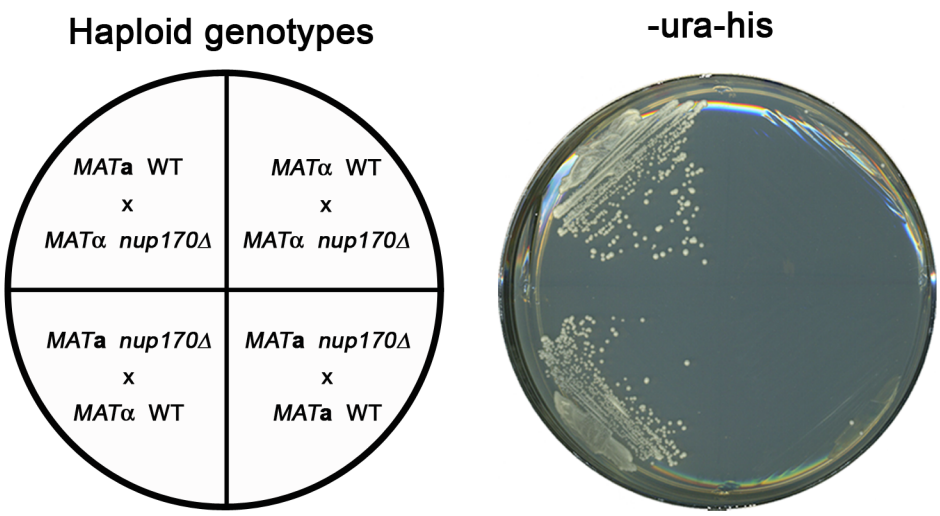

Figure 4-7. *nup170Δ* cells are competent for mating.

*MAT***a** and *MATα nup170Δ* cells containing pRS316 (*URA3*) were mixed with WT cells of the opposite mating type containing pRS315 (*HIS3*) on YPD medium overnight to facilitate mating. Cells were then streaked on SC medium lacking uracil and histidine to select for growth of diploid cells and incubated for 3 d at 30˚C. The genotypes and positions of the haploid strains used in each mating are indicated.

4.2.6 *NUP170* functionally interacts with *ITC1*, encoding a subunit of the ISW2 chromatin-remodeling complex required for a-specific gene repression

Itc1p is a subunit of the ISW2 chromatin-remodeling complex required for repression of **a**-specific genes (Gelbart et al., 2001; Ruiz et al., 2003; Trachtulcova et al., 2004). In *MAT*α cells disruption of *ITC1* produces similar phenotypes as deletion of *NUP170*, including: a shmoo-like cell morphology, aberrant secretion of **a**-factor, and derepression of **a**-specific genes (Sugiyama et al., 2001; Ruiz et al., 2003). We identified *ITC1* in a genetic screen for null mutations that in combination with a *NUP170* deletion led to a synthetic fitness defect (see Chapter III, Table 3-1). Furthermore, cell growth assays of isogenic haploid strains revealed a reproducible growth defect in the *itc1Δ nup170Δ* double mutant strain not observed in either single deletion mutant (Figure 4-8A). Strikingly, upon microscopic examination the *MAT*α *itc1Δ nup170Δ* double mutant exhibited a pronounced enhancement of the shmoo-like phenotype (Figure 4-8B). Additionally, aberrant secretion of **a**-factor from *MAT*α cells was weakly detected in the *itc1Δ* strain and was more readily detected in the *nup170Δ* strain; however, **a**-factor secretion was greatest in the *MAT*α *itc1Δ nup170Δ* double mutant (Figure 4-8C). Taken together, these results indicate a functional interaction between Nup170p and Itc1p and further argue for a role of Nup170p in **a**-specific gene repression.

Figure 4-8. Nup170p functions in a parallel manner to Itc1p.

Heterozygous null mutations in *NUP170* and *ITC1* were sequentially inserted into the diploid yeast strain BY4743 and meiotic progeny obtained by tetrad dissection. The resulting haploid strains were grown in YPD medium to mid-logarithmic growth phase and an equal number of cells from each culture were serially diluted and spotted onto YPD medium for 3 d at 30˚C. The growth rate of the *itc1Δ nup170Δ* double null mutant was compared to both single deletion mutants and a WT strain in both *MAT***a** (left panel) and *MAT*α (right panel) backgrounds. (B) Cellular morphology of the haploid strains described in panel A was examined using light microscopy. Shown are representative bright field images of the indicated haploid strains. Note, individual deletion of either *ITC1* or *NUP170* in *MAT*α cells results in a shmoo-like phenotype, which is enhanced in *MAT*α *itc1Δ nup170Δ* cells. (C) WT, *itc1Δ*, *nup170Δ*, and *itc1Δ nup170Δ* strains of both mating types were assayed for **a**-factor secretion using halo assays. Cells hypersensitive to **a**-factor (*MAT*α *sst2Δ* $ste3^{L194Q}$) were spread evenly over the surface of YPD plates and *MAT***a** (left panel) or *MAT*α (right panel) strains of the indicated genotypes were spotted onto the plates and incubated for 2-3 d at 30˚C. Note, halos of growth inhibition indicate secretion of **a**-factor.

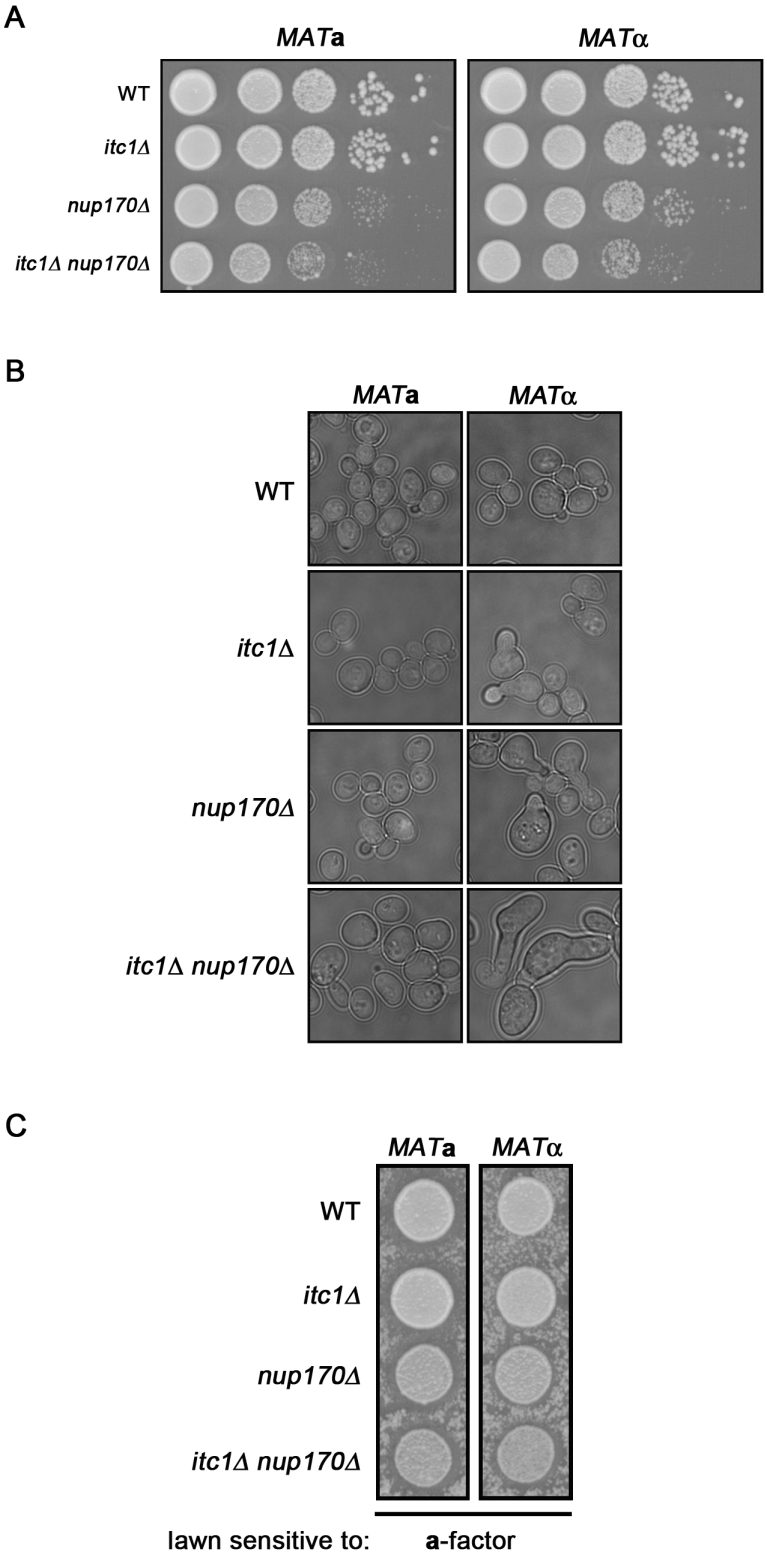

Figure 4-8. Nup170p functions in a parallel manner to Itc1p.

4.2.7 Nup170p is required for nucleosome occupancy at a-specific gene promoters.

Repression of **a**-specific genes by the ISW2 complex occurs through its effects on nucleosome positioning within **a**-specific gene promoters (Zhang et al., 2004; Morohashi et al., 2006). ISW2-mediated chromatin-remodeling within the *BAR1* promoter places a well-positioned nucleosome such that the TATA box is occluded in *MAT*α cells (Morohashi et al., 2006). In the absence of ISW2 activity, nucleosome positioning is disrupted, exposing the TATA box and leading to partial derepression and low-levels of transcriptional activity. Having shown that Nup170p physically interacts with a member of the Swi/Snf family of chromatin-remodelers (i.e. RSC, Chapter III, Figure 3-3), functionally interacts with the ISW2 complex (Figure 4-8), and is required for chromatin structure (Chapter III, Figure 3-6), we examined whether the cell-type-specific phenotypes of the *nup170Δ* mutant could be linked to altered nucleosome positioning within **a**-specific gene promoters. To test this idea, we examined the genome-wide nucleosome mapping results presented in Chapter III (Figure 3-6), which by design were obtained from *MAT*α cells, to assess nucleosome positioning surrounding the **a**-specific genes *BAR1*, *STE6*, *STE2*, and *ASG7*. As shown in Figure 4-9, in WT cells of the α-mating type nucleosomes were positioned throughout the promoter and coding regions of the four genes examined. In addition, three of the four promoters examined contain a TATA box, and each of these were occluded by an appropriately-positioned nucleosome. By contrast, in the *nup170Δ* mutant, in general, nucleosomes were not detected within the

promoter regions, consequently, the TATA box was not occluded by a well-positioned nucleosome (Figure 4-7). Chromatin structure, in general, was also altered in many of the regions surrounding the **a**-specific genes examined. This indicates that, in addition to its function in nucleosome occupancy at **a**-specific genes, Nup170p is also required for genome-wide chromatin structure, two functions which have also been attributed to the ISW2 complex (Morohashi et al., 2006; Whitehouse et al., 2007; Gkikopoulos et al., 2011).

4.3 Discussion

NPCs play an important role in transcriptional regulation at the NE, as certain yeast genes are recruited to NPCs following gene activation (Taddei et al., 2006; Ahmed et al., 2010). In addition, NPC components have been implicated in the organization and regulation of silent chromatin domains at the NE (Galy et al., 2000; Feuerbach et al., 2002; Dilworth et al., 2005; Therizols et al., 2006; Ruben et al., 2011). Nup170p is particularly important in the organization of transcriptionally silenced subtelomeric chromatin as its association with these regions promotes chromatin structure and transcriptional silencing (Chapter III). Here we have further analyzed the role of Nup170p in silent chromatin structure and have uncovered additional functions for Nup170p at transcriptionally repressed loci. Specifically, Nup170p associates with, and is required for, silencing at the mating type loci as well as defining the chromatin structure at transcriptionally repressed **a**-specific genes. Thus further implicating NPCs in chromatin organization and transcriptional regulation.

Figure 4-9. Promoter nucleosome occupancy is reduced in *MATα nup170Δ* cells.

WT (red) and *nup170Δ* (blue) strains of the α-mating type were grown to mid-logarithmic growth phase and mononucleosomal DNA was isolated. Next generation sequencing of isolated mononucleosomal DNA permitted the genome-wide identification of nucleosome positions. Data previously generated in Chapter III (Figure 3-5) were further evaluated to assess the chromatin structure within 10 kb regions surrounding the **a**-specific genes *BAR1* (A), *STE6* (B), *STE2* (C), and *ASG7* (D). Nucleosome occupancy is plotted on the x-axis (bp) as a function of its occupancy score (y-axis). **a**-specific genes are highlighted in green with black arrows indicating transcriptional orientation. The position of a TATA box within each **a**-specific gene promoter is indicated by a red "T". Promoter nucleosomes are highlighted by pink rectangles. Black rectangles represent ORFs located on the Watson and Crick strands. Note, under repressive conditions (WT; red) the TATA box within **a**-specific gene promoters is generally concealed within a precisely positioned nucleosome; however, in the *nup170Δ* strain (blue) promoter nucleosomes are primarily absent.

* Nucleosome positioning analysis was performed by YW with data analysis performed by WMC. Figure processing was performed by WMC, YW and DWV.

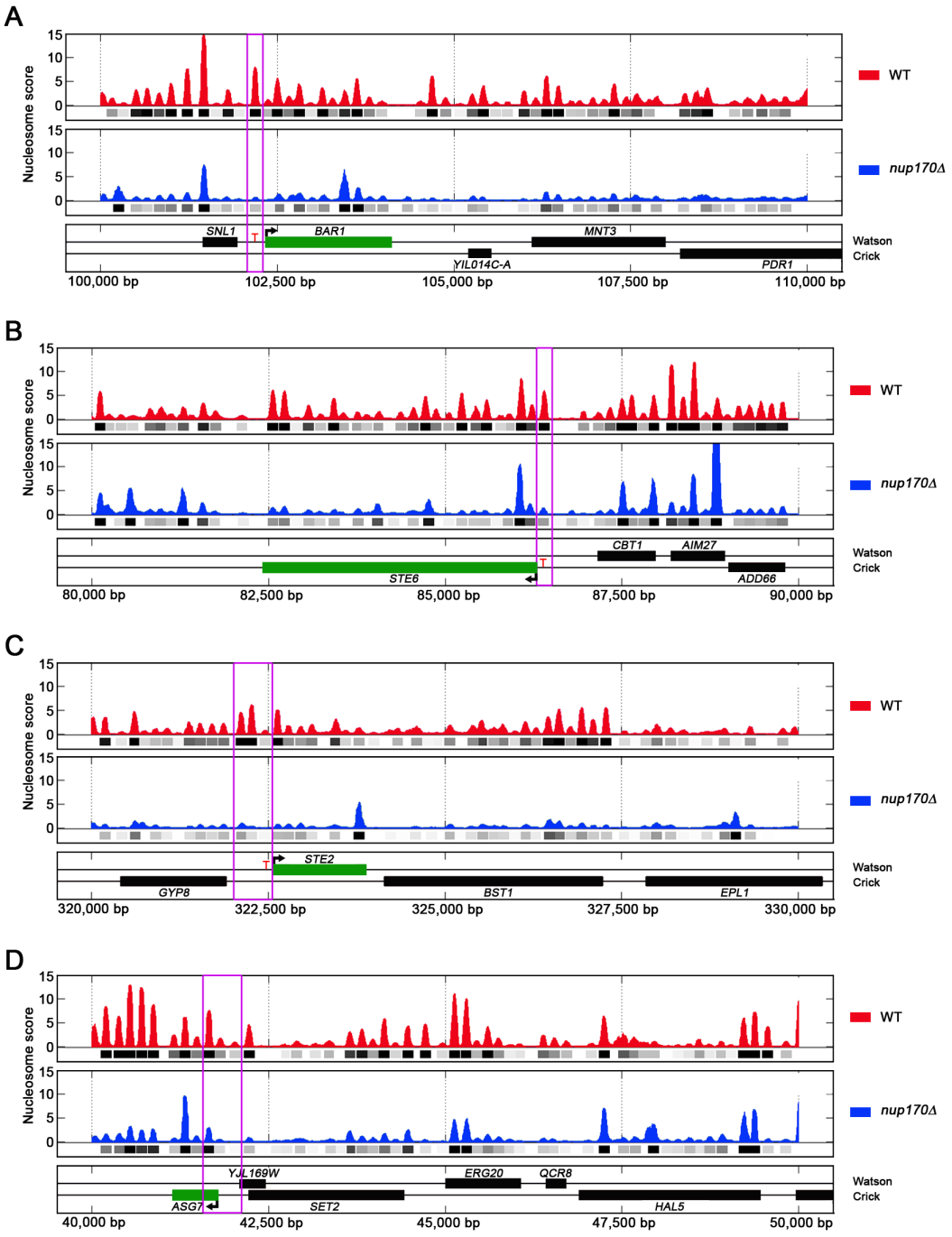

Figure 4-9. Promoter nucleosome occupancy is reduced in *MATα nup170Δ* cells.

Initial characterization of the *NUP170* null mutant revealed a cell-type-dependent morphology defect in *MAT*α cells (Figure 4-1). The cellular morphology of these cells was highly reminiscent of the mating projection formed by cells arrested in G1-phase of the cell cycle in response to the presence of a mating pheromone. However, despite the appearance of these shmoo-like projections, a *MAT*α *nup170*Δ strain did not exhibit a reduced growth rate compared to a comparable isogenic *MAT***a** strain (Figure 4-1). Nevertheless, the altered cellular morphology suggested that these cells were aberrantly producing and secreting **a**-factor. Indeed, pheromone secretion assays reproducibly detected secretion of **a**-factor in *MAT*α *nup170Δ* strains (Figure 4-2A). A more drastic phenotype is observed in the *tup1* mutant (Trachtulcova et al., 2004). Tup1p is a co-repressor of **a**-specific genes, and in its absence **a**-specific genes are fully derepressed leading to similar levels of **a**-factor secretion in both *MAT***a** and *MAT*α *tup1* mutants (Fujita et al. 1992; Trachtulcova et al., 2004). The limited amount of **a**-factor secretion detected in the *nup170Δ* mutant is therefore indicative of only partial derepression of **a**-specific genes, consistent with the overall low percentage of cells exhibiting the shmoo-like phenotype.

A defect in **a**-specific gene repression was further indicated by the detection of α-factor secretion in *MAT*α *nup170*Δ cells only upon further deletion of the **a**-specific gene *BAR1* (Figure 4-2B), which encodes a protease that degrades α-factor (Manney, 1983; MacKay et al., 1988). From this result we conclude that aberrant expression of the **a**-specific gene *BAR1* in *MAT*α *nup170*Δ cells resulted in proteolysis and inactivation of α-factor, leading to the inability to

detect secretion of α-factor by these cells. This concept is further supported by results of gene expression analyses that revealed a role for Nup170p in repression of multiple **a**-specific genes including *BAR1* (Figure 4-4). Surprisingly, DNA micorarray analysis of a *nup170Δ* strain did not reveal increased expression of *STE6,* the plasma membrane transporter required for **a**-factor secretion (McGrath et al., 1989; Kuchler et al., 1989). However, partial derepression of *STE6* was observed by RT-PCR analysis (Figure 4-4A), which is likely sufficient to mediate **a**-factor secretion. Cumulatively, these results support the conclusion that Nup170p functions in repression of **a**-specific genes.

In Chapter III data were presented indicating that Nup170p has an important role in defining chromatin structure at transcriptionally repressed loci, and we predict that Nup170p performs a similar function at **a**-specific genes. A re-examination of the nucleosome positioning data presented in Chapter III (Figure 3-6) revealed a role for Nup170p in defining the repressive chromatin structure at **a**-specific gene promoters (Figure 4-9). Specifically, in the absence of Nup170p, nucleosomes were, for the most part, absent from these regions. Consequently, promoter sequences such as the TATA-box were exposed. This presumably leads to recruitment of the transcriptional machinery and low levels of expression of a-specific genes. Repression of **a**-specific genes is mediated by binding of the α2 co-repressor to its operator sequence followed by the α2-medated recruitment of the Tup1-Cyc8 corepressor (Komachi et al., 1994; Smith et al., 1995). In turn, Tup1-Cyc8 recruits multiple chromatin-modifying complexes required to generate a repressive chromatin structure at **a**-specific genes (Ruiz et al., 2003;

Trachtulcova et al., 2004; Morohashi et al., 2006). These include the Itc1p containing ISW2 chromatin-remodeling complex and the histone deacetylase complex Set3C (Watson et al., 2000; Ruiz et al., 2003; Trachtulcova et al., 2004; Morohashi et al., 2006), both of which functionally interact with *NUP170* (Figure 3-1 and Figure 4-6).

The finding that Nup170p is required for chromatin structure at **a**-specific genes is consistent with our previous finding that chromatin structure at subtelomeric and RP genes is altered in the absence of Nup170p (Chapter III). Unlike its role at subtelomeric and RP genes, however, with the exception of *BAR1* we did not detect Nup170p binding at **a**-specific genes, we cannot exclude the possibility that the association of Nup170p with these loci is a transient event and, therefore, less susceptible to chromatin immunoprecipitation than other Nup170p-DNA interactions. Similarly, transient interactions with chromatin have been proposed to account for the low enrichment levels previously observed for ChIP-chip analysis of RSC complex subunits as well as TFIIIC (Roberts et al., 2003; Parnell et al., 2008; Badis et al., 2008). Alternatively, **a**-specific genes could be recruited to NPCs independently of Nup170p through interactions with other Nups.

The concept that **a**-specific genes associate with NPCs, whether transiently or stably, is an appealing hypothesis. An NPC interaction would place these loci in close proximity to both NPC-associated chromatin modifying complexes and adjacent transcriptionally repressive chromatin domains. Intriguingly, Nup170p plays an important role in both the NPC-association of chromatin complexes and

the establishment of silent chromatin domains at the NE. For instance, Nup170p and its homologs in higher eukaryotes have been detected in association with chromatin-modifying complexes including HDAC4 in mammals (Kehat et al. 2011), the dosage compensation complex in Drosophila (Mendjan et al., 2006), and the RSC complex in yeast (Chapter III). Furthermore, Nup170p is required for the establishment of silent chromatin domains at the NE (Chapter III). Thus, certain chromatin-modifying complexes are present at NPCs and perturbations to Nup170p could potentially disrupt the function of one or more of these complexes, resulting in the observed alterations in chromatin structure of **a**-specific genes. Support for this idea comes from the observation that RNAi knockdown of Nup155, the mammalian homolog of Nup170p, abrogated the association of HDAC4 with NPCs, leading to misregulation of HDAC4-target genes. Precisely how chromatin-modifying complexes in yeast are affected by the loss of Nup170p remains unclear. Future studies will be necessary to distinguish whether chromatin-modifying complexes functioning at **a**-specific genes are affected by the loss of Nup170p or, alternatively, whether the loss of Nup170p alters the localization of **a**-specific genes.

In addition to its function in repression of **a**-specific genes, we also identified a requirement for Nup170p in transcriptional repression at the silent mating type loci, *HML* and *HMR* (Figure 4-5A and 4-5B). These results are consistent with a previously indentified role for Nup170p in subtelomeric gene silencing (Chapter III; Figure 3-5). Furthermore, previous ChIP-chip studies that detected Nup170p in association with subtelomeric DNA also detected Nup170p

in association with both *HML* and *HMR* (Chapter III; Figure 3-7C). In support of this observation, ChIP-qPCR experiments further confirmed Nup170p binding within the *HMR* locus (Figure 4-5C). Importantly, similar levels of *HMR* enrichment were not detected with other members of the Nup170 subcomplex (Nup157p and Nup188p; Figure 4-5C) and the low levels of enrichment that were detected likely occur indirectly through association with Nup170p.

Surprisingly, association of Nup170p with *HMR* was not required for Sir4p binding at *HMR* (Figure 4-6). This is in stark contrast to the role of Nup170p in promoting Sir4p binding within subtelomeric regions (Chapter III), suggesting that Nup170p has distinct roles in transcriptional silencing at telomeres and the silent mating type loci. This idea is exemplified by the observation that Sir4p association with *HMR* was, in fact, enhanced in the absence of Nup170p (Figure 4-6). Interestingly, overexpression of Sir4p leads to loss of silencing at the mating type loci (Cockell et al., 1995; Singer et al., 1998). This latter result suggests that the silencing defect observed at *HMR* in the *nup170Δ* mutant could arise indirectly from the loss of Sir4p binding at telomeres and its redistribution to additional Sir4p-target loci (i.e. *HMR*). In support of this hypothesis the loss of telomere tethering results in dispersion of silencing factors (i.e. Sir4p) to ectopic sites throughout the genome (Taddei et al., 2009). Alternatively, Nup170p may have a direct role in silencing at the mating type loci independent of Sir4p recruitment and related to its functional interactions with multiple chromatin complexes involved in gene silencing (Chapter III; Figure 3-1).

The idea that NPCs interact with the silent mating type loci has previously been suggested but the functional significance of these interactions has been confounded by contrary results. Our finding that the *HMR* locus interacts with NPCs through Nup170p is congruent with a recent finding that *HMR* is tethered at the NE by the nuclear basket components Nup2p and Nup60p (Ruben et al., 2011). Unlike the *nup170Δ* mutant, however, deletion of *NUP2* or *NUP60* had no affect on silencing within the *HMR* locus (Ruben et al., 2011). Moreover, contrary to the previously identified role of Nup2p and Nup60p in mediating boundary activity (Ishii et al., 2002; Dilworth et al., 2005; Valenzuela et al., 2008), loss of either Nup did not affect the activity of an *HMR*-adjacent boundary element (Ruben et al., 2011). An additional nuclear basket protein, Mlp1p, has been proposed to interact with *HML* and *HMR* (Casolari et al., 2004; Casolari et al., 2005), and loss of Mlp1p was reported to disrupt both silencing and the NE localization of silent domains (Galy et al., 2000; Feuerbach et al., 2002). However, the role of Mlp1p in these processes remains unclear, as others failed to detect similar functions for Mlp1p (Hediger et al., 2002a and 2002b). Whether Nup170p has a similar function in localizing *HML* and *HMR* at the NE remains to be established, though it is quite probable considering Nup170p associates with *HMR* (Figure 4-5) and functions in telomere tethering (Chapter III; Figure 3-13). Recruitment of the silent mating type loci to NPCs would place these loci in close proximity to several NPC-mediated transcriptional activities. Here they would be subject to the silencing functions of Nup170p, and possibly Mlp1p, as well as the boundary activities of Nup2p and the RSC chromatin-remodeling complex

(Dhillon et al., 2009). Thus, recruitment to the NPC would provide a platform for the establishment and/or maintenance of silent chromatin at the NE.

Chapter V: *Perspectives*

5.1 Synopsis

In most eukaryotic cell types condensed, transcriptionally silent heterochromatin preferentially associates at the NE, while transcriptionally active euchromatin predominates the nuclear interior (Deniaud and Bickmore, 2009; Peric-Hupkes and van Steensel, 2010). This is true for the budding yeast *Saccharomyces cerevisiae* where transcriptionally silent heterochromatin-like domains are tethered at the NE (Taddei et al., 2010). Several NE-associated proteins have been implicated in peripheral targeting of chromosomal loci including NPC proteins. Through interactions with both transcriptionally active and silenced chromatin, in addition to the boundaries between these regions, NPCs have been postulated to assist in the transition of chromatin between transcriptional states (Galy et al., 2000; Feuerbach et al., 2002; Ishii et al., 2002; Dilworth et al., 2005). However, the mechanisms involved in this process are unclear. Here we have defined genetic and physical interactions implicating Nup170p in chromatin organization. We have shown that Nup170p associates with, and regulates the expression of, subtelomeric and ribosomal protein genes. Moreover, we have demonstrated that Nup170p is required for proper nucleosome occupancy at these loci, in what is believed to be the first report of such a requirement for a Nup. Additionally, we have shown that Nup170p, through its interaction with the silencing factor Sir4p, promotes the formation of silent chromatin at subtelomeric regions and their association at the NE in a cell-cycle-dependent manner. In this chapter, I discuss the implications of our results on telomere biology, as well as other nuclear processes influenced by NPCs. In

particular, I speculate on how NPCs may influence these processes by providing a scaffold for chromatin modifiers to access peripheral chromatin domains.

5.2 NPCs at the interface between chromatin domains

In the decades since early electron micrographs first revealed attachment of chromatin fibres to the NE through annuli it has become evident that NPCs not only regulate nucleocytoplasmic trafficking but can also influence gene expression through their association with chromatin (DuPraw, 1965; Comings, 1970; Ahmed and Brickner, 2007; Capelson et al., 2010; Kohler and Hurt, 2010; Van de Vosse et al., 2011). Several lines of evidence suggest that following activation certain yeast genes, including *INO1, GAL1*, and *HXK1* among others, are recruited to the nuclear periphery in a Nup-dependent manner (Dieppois et al., 2006; Taddei et al., 2006; Brickner et al. 2007) and, at least in the case of the *HXK1* gene, NPC-mediated targeting is required for full transcriptional activity (Taddei et al., 2006). For many of these genes, transcriptional activity is induced in response to environmental cues, stress conditions, or changes in nutritional status, and tethering at the NPC may couple transcription with efficient mRNA export as first proposed in the "gene gating hypothesis" (Blobel, 1985) and supported by more recent studies (reviewed in: Rodriguez-Navarro and Hurt, 2011; Garcia-Oliver et al., 2012). Interestingly, upon repression of *GAL1* and *INO1* both genes remain associated with the NE for multiple generations and NPC components have been implicated in this process, with nuclear basket Nups mediating targeting of both active and newly repressed *INO1*, whereas members

of the Nup84 complex appear specific to the targeting of newly repressed *INO1* (Brickner et al., 2007; Light et al., 2010). This raises the possibility that following repression Nup-*INO1* interactions are remodeled such that the locus is no longer associated with the nuclear basket and instead interacts with components of the outer ring. Here, repressed *INO1* would be positioned near the INM and in close proximity to an adjacent silent chromatin domain, which may promote further repression. Upon reinduction, *INO1* could rapidly be repositioned to the nuclear basket to access the transcriptional machinery. The extent to which interactions between *INO1* and the NPC are restructured in response to transcriptional changes remains to be determined, however the association of at least two Nups with *INO1* are differentially altered in response to changes in *INO1* expression (Light et al., 2010). It is worth noting that many subtelomeric genes, including *HXK1*, are induced in response to stress conditions and positioning of these genes at the NE may not only facilitate transcriptional repression but may also promote efficient activation in response to stress stimuli by positioning them in close proximity to transcriptionally active domains at NPCs. Future work will be needed to determine whether additional subtelomeric genes associate with NPCs when activated.

Live-cell imaging suggests that silent domains and NPCs form distinct regions at the NE (Andrulis et al., 2002; Hediger et al., 2002b; Taddei et al., 2004; Taddei et al., 2009; Taddei et al., 2010). However, it is also evident from these studies that the two domains are juxtaposed and, as suggested above, chromosomal loci are likely to transition from one to the other in response to

transcriptional stimuli. In addition, their close proximity suggests that they are likely to influence one another. Indeed, assembly of the nuclear basket is disrupted in the absence of Esc1p (Lewis et al., 2007), an INM-associated protein that tethers telomeres at the NE and displays limited overlap with NPCs (Andrulis et al., 2002; Taddei et al., 2004). Conversely, targeting of the inner membrane protein Heh1p, required for NE tethering of silent rDNA, but not subtelomeric DNA, is NPC-dependent (King et al., 2006; Grund et al., 2008; Mekhail et al., 2008). Furthermore, the NE association of Sir4p and telomeres is disrupted in the absence of Nup170p (Figures 3-12 and 3-13). Thus the structural organization of either domain is dependent on the other. This idea is further supported by the finding that Sun1, a mammalian INM protein that interacts with heterochromatin and tethers meiotic telomeres at the NE (Ding et al., 2007), interacts with Pom121, and is required for NPC assembly (Liu et al., 2007; Talamas and Hetzer, 2011). Similarly, the yeast INM protein Mps3p shares homology with Sun1, tethers telomeres at the NE, and co-purifies with the NPC-associated protein Mlp2p (Keck et al., 2011). Athough Mps3p and Mlp2p presumably interact at spindle pole bodies (Jaspersen et al., 2002; Niepel et al., 2005), the *Schizosaccharomyces pombe* counterpart of Mps3p, Sad1, interacts with the NPC protein Nup40 (the counterpart of *S.cerevisiae* Nup53p), suggesting that the Mps3p-Mlp2p interaction may also occur at NPCs in budding yeast (Miki et al., 2004). Perhaps the strongest evidence of the physical association between NPCs and silent domains comes from the finding that both Sir4p and subtelomeric DNA associate with Nup170p (Figures 3-7 and 3-9). Cumulatively, these findings imply

that the NE scaffolds of active and silent domains are structurally interdependent and physical interactions between the two, whether stable or transient, further complicate the distinction between these domains.

5.3 The NPC as a scaffold for chromatin modifiers to gain access to peripheral chromatin domains

Exactly how silent and active domains are established and maintained at the NE is unclear. However, NPCs are ideally situated at the interface between these domains and, through interactions with both active and silent chromatin, they have been postulated to facilitate the transition of chromatin between activity states (Ishii et al., 2002; Dilworth et al., 2005). Precisely how NPCs facilitate the transition between these chromatin states remains unknown. Such a transition would likely involve a wide-range of chromatin remodeling activities such as post-translational histone modifications, repositioning and eviction of nucleosomes, histone exchange, and for certain genes subnuclear repositioning. A growing body of evidence suggests that some of the factors responsible for these remodeling events can associate with NPCs and are discussed in the following sections. In agreement with this, genetic analysis of *NUP170* revealed functional interactions with numerous chromatin-modifying and chromatin-remodeling complexes (Figure 3-1 and Tables 3-1 and 3-2). Furthermore, a physical interaction was observed between Nup170p and the RSC chromatin-remodeling complex (Figure 3-3). Thus, NPCs could be viewed as a binding platform for chromatin-modifying complexes, which, when NPC-associated, acquire access to

NE-associated chromatin. Considering essentially all DNA metabolic processes require some form of chromatin remodeling, it is not surprising that NPC components have been implicated in many of these processes, several of which are discussed in the following sections.

5.3.1 NPCs and centromeric chromatin structure

The underlying chromatin structure at centromeres is critical for proper kinetochore function and pertubations in centromeric chromatin lead to defects in chromosome segregation (Schulman and Bloom, 1991; Sullivan, 2001). Essential to this process is the RSC complex. The RSC complex constitutively associates with centromeres where it functions to maintain nucleosome positioning. In the absence of RSC complex function sister chromatids are missegregated (Tsuchiya et al., 1998; Hsu et al., 2003). Intriguingly, defects in chromosome segregation and kinetochore integrity have also been reported in a *NUP170* null mutant (Kersher et al., 2001), and our finding that the RSC complex physically interacts with Nup170p (Figure 3-3) potentially links these two observations. Moreover, we have identified several Nups in association with centromeric DNA (Figure 7-4), including Nup170p, whose centromeric association is Sth1p-dependent (Figure 7-5). Taken together, these results suggest a direct function for Nup170p at centromeres, which is likely mediated through its association with the RSC chromatin-remodeling complex. It is unclear how Nup170p promotes chromatin structure at centromeres, though it is possible that Nup170p may modulate RSC complex activity or facilitate RSC complex binding. It is also possible that

association with Nup170p, whether stable or transient, promotes centromeric chromatin structure through the activity of additional NPC-associated complexes.

5.3.2 NPC-associated DNA repair

Following the formation of a DNA double-strand break (DSB) nucleosomes within the vicinity of the DSB can be modified, remodeled, or evicted to facilitate recruitment and function of DNA repair proteins. Upon completion of DNA repair, the chromatin structure must be restored to turn off checkpoint signaling and permit a return to the pre-existing transcriptional state. Implicated in this process are several histone post-translational modifications and the ATP-dependent chromatin remodeling complexes SWR1, INO80, SWI/SNF, and RSC (Chai et al., 2005; Shim et al., 2005; Morrison and Shen, 2009; Huertas et al., 2009). Although DSB repair occurs predominantly in the nuclear interior, irreparable DSBs localize to NPCs (Nagai et al. 2008). Moreover, critically short telomeres are recognized as DSBs and relocate to NPCs (Khadaroo et al., 2009). Presumably, relocation to NPCs provides access to NPC-associated DNA repair pathways such as the SUMO-deconjugating enzyme Ulp1p and the SUMO-dependent ubiquitin ligases Slx5p/Slx8p (Li et al., 2003; Panse et al., 2003; Makhnevych et al., 2007; Nagai et al., 2008). In the case of Ulp1p, targeting to the NPC is critical for its function in DNA repair as mutations in the Nup84 complex or nuclear basket proteins, Nup60p, Mlp1p or Mlp2p, fail to target Ulp1p to the NPC, confer sensitivity to DNA damaging agents, exhibit genetic interactions with DNA repair genes, and display reduced DNA repair efficiencies

(Galy et al., 2000; Loeillet et al., 2005; Palancade et al., 2007). In agreement with a previous report, our genetic analysis of *NUP60* is supportive of a role for Nup60p in DNA repair (Figure 3-2 and Table 3-1; Palancade et al., 2007).

Localization of irreparable DSBs to NPCs would not only provide access to enzymes involved in desumoylation and ubiquitination but would also provide access to Nup170p-associated RSC complex (Figure 3-3) and potentially other chromatin-modifying complexes involved in DNA repair. For example, INO80 is implicated in eviction of histone γH2AX-containing nucleosomes at DSBs (van Attikum et al., 2007) and the INO80 subunits Rvb1p and Rvb2p copurify with Nup2p (Dilworth et al., 2005), although the dynamic association of Nup2p with NPCs suggests this interaction may not necessarily occur at NPCs. Interestingly, given that the nuclear periphery appears to be refractory to recombination (Therizols et al., 2006; Oza et al., 2009; Schober et al., 2009), localizing a DSB to NPCs could be a potential mechanism to shift the balance away from homologous recombination and favor alternative recombination pathways or non-homologous end joining (NHEJ). Consistent with this interpretation, *nup60*, *ulp1p*, and Nup84 complex mutants exhibit increased rates of spontaneous homologous recombination and decreased NHEJ efficiency (Palancade et al., 2007). In addition, recruitment of the DNA-end binding yKu70/80 heterodimer to DSB promotes NHEJ and is facilitated by the RSC complex (Shim et al., 2005; Shim et al., 2007), further strengthening the hypothesis that DSBs are targeted to NPCs to access distinct DNA repair pathways. Further experiments will be needed to

determine the specific functions of the NPC-associated RSC complex in DNA repair.

5.3.3 NPCs and transcriptional activation

Perhaps the strongest evidence to support the role of NPCs as platforms for chromatin organization stems from their functions in transcriptional activation. Tethering active genes at NPCs positions these loci in close proximity to nuclear import complexes and likely increases their availability to newly imported transcriptional factors. For example, import of the TATA-binding protein (TBP) is mediated by Kap114p and dissociation of the TBP/Kap114p complex is stimulated by TATA-containing DNA, suggesting that Kap114p mediates targeting of TBP to its target promoters (Pemberton et al., 1999). Conveniently, some of these promoters may be tethered at NPCs. When transcriptionally active the TATA-containing *GAL1/10* promoter is tethered at NPCs through an interaction between Mlp1p and the SAGA complex (Luthra et al., 2007). It is worth noting that, in addition to its histone acetyltransferase activity, SAGA also contains a TBP-binding module that facilitates recruitment of TBP to promoters (Dudley et al., 1999). Thus, tethering of the *GAL* genes to NPCs positions them in close proximity to multiple aspects of transcriptional activation. In a similar fashion, the transcriptional activator complex Rap1/Gcr1/Gcr2 associates with NPCs and tethering a reporter gene to the Nup84 complex was sufficient to promote Gcr1-dependent transcriptional activation (Menon et al., 2005), further indicating that NPCs are a nexus for transcriptional regulation.

Studies in *Drosphila melanogaster* have provided an additional example of a chromatin-modifying complex required for transcriptional activation in association with NPCs. Several Nups, including the Drosophila Nup170p homolog, Nup154, physically interact with the dosage compensation complex (DCC) required for hypertranscription of the male X chromosome, and RNAi knockdown of some of these Nups alters DCC localization and alleviates dosage compensation (Mendjan et al., 2006). In yeast, a role for Nup170p in transcriptional activation has not been demonstrated, and, in fact, transcriptome profiling of a *nup170* mutant argues for a repressive role for Nup170p at subtelomeric, RP, and **a**-specific genes (Figures 3-4, 3-8, and 4-4). However, in the absence of Nup170p, 59 genes exhibited a decrease in expression (Table 3-4), the significance of which is unclear.

5.3.4 NPCs and transcriptional repression

In mammalian cardiomyocytes the chromatin modifier and transcriptional repressor, HDAC4, interacts with Nup155 and is targeted to NPCs (Kehat et al., 2010). Similarly, several of our results indicate that the yeast homolog of Nup155 performs a similar function. Initially, SGA analysis revealed *NUP170* exhibits multiple genetic interactions with chromatin complexes involved in gene silencing (Figure 3-1 and Table 3-1). Importantly, Nup170p is targeted to RP and subtelomeric genes where it is required for repression (Figures 3-4, 3-7, and 3-8). The repressive function of Nup170p is likely performed through the promotion of a repressive chromatin structure as demonstrated at the promoter regions of **a**-

specific genes (Figure 4-9). Similarly, changes in chromatin structure were identified in RP and subtelomeric gene promoters in the absence of Nup170p (Figure 3-6). Exactly how Nup170p influences chromatin structure is unclear, though we envisage that the affects occur through the association of Nup170p with specific regions of the genome and chromatin modifiers (i.e. the RSC complex and potentially other modifiers discussed above) creating a distinct environment to modulate chromatin structure including, for example subtelomeric chromatin. Here, Nup170p binding is required for efficient recruitment of Sir4p and the downstream silencing factors that generate a compact heavily nucleated chromatin structure that is transcriptionally silent (Figures 3-7 and 3-11, and 3-12).

5.4 Establishment and association of silent domains at the NE

The yeast nuclear periphery is a transcriptionally repressive environment believed to result from the sequestration of Sir proteins through the anchoring and clustering of telomeres at the NE (reviewed in: Taddei et al., 2010). Two partially redundant pathways using yKu and Sir4p to tether telomeres at the NE have been extensively studied. Significantly less is understood regarding the regulatory mechanisms that promote or inhibit telomere tethering. Such regulatory mechanisms would be critical for the detachment of telomeres from the NE following DNA replication in late S-phase and the re-establishment of tethering in G1-phase.

Subtelomeric origins-of-replication are late firing. Consequently, replication of telomeric DNA occurs in late S-phase and has a pivotal role in dislodging telomeres from the NE. For instance, mutations that delay DNA replication result in a similar delay in telomere detachment from the NE (Ebrahimi and Donaldson, 2008). Additionally, fluorescently tagged telomeres have been observed to increase in fluorescence intensity nearly 2-fold prior to disengaging from the NE, indicating replication of telomeric DNA occurs at the NE and precedes telomere detachment (Hediger et al., 2002b; Ebrahimi and Donaldson, 2008). Precisely how DNA replication inhibits telomere tethering is not clear. It has been proposed that passage of the replication fork may physically disrupt the association of tethering factors with chromatin (Laroche et al., 2000). Alternatively, tethering factors may remain associated with telomeres but DNA replication may alter their interactions with NE-associated anchors. Consistent with this latter hypothesis, binding of yKu to chromosome ends is unaffected by DNA replication, however yKu-mediated tethering is inhibited following DNA replication (Ebrahimi and Donaldson, 2008). A telomere-tethering pathway likely to be disrupted by DNA replication is the yKu80p-telomerase-Mps3p pathway since telomerase activity is inhibited at the nuclear periphery and stimulated by DNA replication (Gilson and Geli, 2007; Ferreira et al., 2011).

A recent study has implicated the SUMO E3 ligase Siz2p in telomere tethering (Ferreira et al., 2011). Specifically, Sir4p, yKu70p, and yKu80p are sumoylated in a Siz2p-dependent manner and, importantly, loss of Siz2p impairs yKu80p-mediated tethering specifically in S-phase. Thus a potential model

emerges whereby desumoylation of yKu80p following DNA replication would disrupt the yKu80p-telomerease-Mps3p interaction, suppressing yKu tethering and releasing telomeres from the NE as well as stimulating activation of telomerase. Two key aspects of this model remain untested. First, is the sumoylation status of yKu cell-cycle regulated. And, second, which of the SUMO-deconjugating enzymes are involved, Ulp1p or Ulp2p. Ulp1p is an attractive candidate, as it is associated with NPCs (Panse et al., 2003; Makhnevych et al., 2007) and telomere association with NPCs increases during G2/M-phase precisely when desumoylation would be predicted to occur (Figures 3-15, 3-16, and 3-17). In addition, this model predicts that sumoylation of yKu would re-establish tethering in G1-phase (discussed below).

Our current understanding of how telomeres are initially targeted to the NE is limited. It has been proposed that yKu facilitates initial NE attachment and promotes telomere clustering. In turn, clustered telomeres promote subtelomeric silencing by concentrating silencing factors at the NE which reinforces tethering through Sir4p-mediated mechanisms (Gasser et al., 2004). However, the regulatory mechanism that initiates yKu tethering in a cell-cycle-dependent manner is unclear. If telomeres are detached from the NE by desumoylation of yKu then, presumably, tethering is restored in the latter stages of mitosis or early G1-phase whereby sumoylation of yKu would facilitate interaction with NE anchors. Re-establishment of telomere tethering could occur through a retention model in which the random movements of dislodged telomeres lead to contact with NE anchors and subsequent retention. In support of this model, time-lapse

imaging of dislodged telomeres during G2/M-phase demonstrated a series of random, oscillating movements over short distances of 150-300 nm, that were interspersed with larger movements covering distances >0.5 μm in a short period of time, ~10 sec (Hediger et al., 2002b). This implies that such movements are likely sufficient for telomeres to access the NE in a timely fashion following nuclear division. A prediction of a random movement and retention model is that telomeres would initially associate with random regions of the NE prior to attachment. Alternatively, telomeres may be recruited to specific regions of the NE to promote reassociation. In agreement with this idea, association of subtelomeric DNA and the tethering component Sir4p with NPCs peaks during mitosis (Figures 3-15 and 3-17). Moreover, levels of detectable Sir4p-Nup170p complexes are greatest in G2/M-phase (Figure 3-16). These results spatially and temporally position Sir4p and telomeres at NPCs concomitant with both the re-establishment of subtelomeric silencing (Martins-Taylor et al., 2004; Young and Kirchmaier, 2011) and reassociation of telomeres at the NE (Laroche et al., 2000; Hediger et al., 2002b; Ebrahimi and Donaldson, 2008). Consistent with this hypothesis, loss of Nup170p results in an initial defect in telomere tethering in G1-phase that is compensated for by additional mechanisms functioning in S-phase (Figure 3-13 and Table 3-9). Given the many enzymatic activities associated with NPCs, we cannot rule out the possibility that an NPC association is required for sumoylation of yKu and the re-stablishment of tethering. Support for this hypothesis comes from the observation that loss of Nup170p leads to an accumulation of SUMO foci and alterations in global sumoylation patterns, but

does not affect Ulp1p localization (C. Ptak and R.W. Wozniak, personal communication), implicating Nup170p in SUMO regulation independent of Ulp1p. Moreover, Siz2p has been identified as a Nup170p interacting partner (D. Lapetina and R.W. Wozniak, personal communication), placing both Siz2p and Ulp1p at NPCs. Thus, there appears to be a competition between sumoylation and desumoylation events at NPCs. Curiously, Ulp1p appears to become mobile and a portion of Ulp1p is targeted to the septin ring during cytokinesis (Makhnevych et al., 2007). These events may tip the balance in favor of Siz2p-mediated sumoylation during the latter stages of mitosis when telomeres reassociate at the NE. Further experiments will be required to determine how sumoylation affects telomere tethering and what role NPCs, and Nup170p in particular, play in regulating the sumoylation status of telomeric proteins.

5.5 NPC assembly and chromatin organization are interdependent

In higher eukaryotes, NPCs assemble into an intact NE throughout interphase and reform from disassembled precursors in the absence of the NE at the end of mitosis (reviewed in: Fernandez-Martinez and Rout, 2009; Doucet and Hetzer, 2010). Conversely, NPC assembly in yeast occurs solely into an intact NE due to a closed mitosis (Winey et al., 1997). Considering certain cell types form extensive NE-associated heterochromatin, and that euchromatic channels have been observed penetrating the peripheral heterochromatin subjacent to NPCs, it is reasonable to postulate that substantial remodeling of the underlying chromatin must occur within the vicinity of assembling NPCs in order to maintain this

organization. Consequently, numerous questions arise regarding how this remodeling may occur. Does assembly of the nuclear basket physically exclude heterochromatin and thereby force it to adjacent NE regions? If so, how do NPCs establish connections with euchromatin channels? Does initiation of nuclear transport through a newly assembled NPC establish connections with chromatin? Is chromatin remodeled prior to, during, or following NPC assembly? To date these questions remain largely unanswered, however a recent study in *S. cerevisiae* demonstrated that the RSC chromatin-remodeling complex is required for NPC structure (Titus et al., 2010). Importantly, the authors did not identify transcriptional changes in genes involved in NPC assembly, leading to the conclusion that the RSC complex itself functions in NPC assembly. In agreement with this conclusion, we observed electron dense proteinaceous structures of similar size to NPCs attached to the INM along with a decrease in NPC number following depletion of Sth1p (T. Makio and R.W. Wozniak, personal communication), indicative of a defect in NPC assembly. Furthermore, our finding that the RSC complex interacts with Nup170p potentially positions this complex at NPC assembly sites (Figure 3-3).

Additional support of a role for chromatin complexes in interphase NPC assembly comes from the finding that null mutants exhibiting reduced growth rates in combination with a *NUP170* deletion mutant also display defects in NPC structure in the absence of Nup170p (Figures 7-9 and 7-10). More specifically, this analysis implicated the SWR1, Set3C, Rpd3L, and the Rad6/Bre1 chromatin modifiers in NPC assembly, arguing for a function for these complexes either

prior to or during NPC assembly. It is possible that remodeling of the underlying chromatin marks future sites of NPC assembly or that chromatin remodeling prevents heterochromatin from sterically hindering NPC formation and/or nuclear transport. In general these results are supportive of our hypothesis that NPCs form a scaffold for chromatin complexes to bind and facilitate chromatin organization at the NE and future studies will be required to determine the temporal order of these events with respect to NPC assembly.

Since budding yeast lack extensive heterochromatin, NPC assembly in yeast may not be as constrained by NE-associated chromatin as interphase NPC assembly in higher eukaryotes. Despite this, the results reported in chapter III suggest NPCs are important factors in organizing silent chromatin domains at the NE. Consequently, defects in NPC assembly or a dramatic reduction in NPC number would be predicted to alter the organization and transcriptional status of these domains. Consistent with this prediction, deletion of *APQ12*, an integral INM protein linked to NPC biogenesis (Scarcelli et al., 2007), exhibited derepression of subtelomeric genes (Figure 7-11) and a *nup170* null mutant was shown to have reduced NPC numbers (Figure 7-8). Although the precise role for chromatin remodelers in NPC assembly remains to be determined, we conclude that NPC assembly and chromatin organization are not separable events, but are, in fact, highly intertwined such that chromatin organization requires NPC assembly and NPC assembly requires chromatin remodeling.

Our studies have revealed that Nup170p functionally and physically interacts with chromatin complexes and functions as a repressor at specific

chromosomal loci by influencing local chromatin structure. In particular, Nup170p associates with subtelomeric DNA during mitosis to promote silent chromatin formation and its association at the NE. We have suggested that NPCs may provide a scaffold to which chromatin complexes bind and acquire access to the distinct transcriptional domains located at the nuclear periphery. Our studies suggest that NPCs perform a pivotal role in modulating gene expression through the spatial and temporal organization of chromatin. Additional studies will be required to further address the role of NPCs in the association of silent chromatin with the NE. Of particular importance will be the determination of the molecular events as well as the regulatory mechanisms responsible for the cell-cycle-dependent manner in which telomeres detach and subsequently reassociate with the NE.

Chapter VI: *References*

Abraham, J., K.A. Nasmyth, J.N. Strathern, A.J. Klar, and J.B. Hicks. 1984. Regulation of mating-type information in yeast. Negative control requiring sequences both 5' and 3' to the regulated region. *J Mol Biol*. 176:307-31.

Aebi, M., M.W. Clark, U. Vijayraghavan, and J. Abelson. 1990. A yeast mutant, PRP20, altered in mRNA metabolism and maintenance of the nuclear structure, is defective in a gene homologous to the human gene RCC1 which is involved in the control of chromosome condensation. *Mol Gen Genet*. 224:72-80.

Ahmed, S., and J.H. Brickner. 2007. Regulation and epigenetic control of transcription at the nuclear periphery. *Trends Genet*. 23:396-402.

Ahmed, S., D.G. Brickner, W.H. Light, I. Cajigas, M. McDonough, A.B. Froyshteter, T. Volpe, and J.H. Brickner. 2010. DNA zip codes control an ancient mechanism for gene targeting to the nuclear periphery. *Nat Cell Biol*. 12:111-8.

Aitchison, J.D., M.P. Rout, M. Marelli, G. Blobel, and R.W. Wozniak. 1995a. Two novel related yeast nucleoporins Nup170p and Nup157p: complementation with the vertebrate homologue Nup155p and functional interactions with the yeast nuclear pore-membrane protein Pom152p. *J Cell Biol*. 131:1133-48.

Aitchison, J.D., G. Blobel, and M.P. Rout. 1995b. Nup120p: a yeast nucleoporin required for NPC distribution and mRNA transport. *J Cell Biol*. 131:1659-75.

Aitchison, J.D., and M.P. Rout. 2012. The yeast nuclear pore complex and transport through it. *Genetics*. 190:855-83.

Akey, C.W., and M. Radermacher. 1993. Architecture of the Xenopus nuclear pore complex revealed by three-dimensional cryo-electron microscopy. *J Cell Biol*. 122:1-19.

Alber, F., S. Dokudovskaya, L.M. Veenhoff, W. Zhang, J. Kipper, D. Devos, A. Suprapto, O. Karni-Schmidt, R. Williams, B.T. Chait, M.P. Rout, and A. Sali. 2007a. Determining the architectures of macromolecular assemblies. *Nature*. 450:683-94.

Alber, F., S. Dokudovskaya, L.M. Veenhoff, W. Zhang, J. Kipper, D. Devos, A. Suprapto, O. Karni-Schmidt, R. Williams, B.T. Chait, A. Sali, and M.P. Rout. 2007b. The molecular architecture of the nuclear pore complex. *Nature*. 450:695-701.

Alcazar-Roman, A.R., E.J. Tran, S. Guo, and S.R. Wente. 2006. Inositol hexakisphosphate and Gle1 activate the DEAD-box protein Dbp5 for nuclear mRNA export. *Nat Cell Biol*. 8:711-6.

Allfrey, V.G., R. Faulkner, and A.E. Mirsky. 1964. Acetylation and Methylation of Histones and Their Possible Role in the Regulation of Rna Synthesis. *Proc Natl Acad Sci U S A*. 51:786-94.

Almer, A., H. Rudolph, A. Hinnen, and W. Horz. 1986. Removal of positioned nucleosomes from the yeast PHO5 promoter upon PHO5 induction releases additional upstream activating DNA elements. *EMBO J*. 5:2689-96.

Amlacher, S., P. Sarges, D. Flemming, V. van Noort, R. Kunze, D.P. Devos, M. Arumugam, P. Bork, and E. Hurt. 2011. Insight into structure and assembly of the nuclear pore complex by utilizing the genome of a eukaryotic thermophile. *Cell*. 146:277-89.

Andrulis, E.D., A.M. Neiman, D.C. Zappulla, and R. Sternglanz. 1998. Perinuclear localization of chromatin facilitates transcriptional silencing. *Nature*. 394:592-5.

Andrulis, E.D., D.C. Zappulla, A. Ansari, S. Perrod, C.V. Laiosa, M.R. Gartenberg, and R. Sternglanz. 2002. Esc1, a nuclear periphery protein required for Sir4-based plasmid anchoring and partitioning. *Mol Cell Biol*. 22:8292-301.

Angus-Hill, M.L., A. Schlichter, D. Roberts, H. Erdjument-Bromage, P. Tempst, and B.R. Cairns. 2001. A Rsc3/Rsc30 zinc cluster dimer reveals novel roles for the chromatin remodeler RSC in gene expression and cell cycle control. *Mol Cell*. 7:741-51.

Antonin, W., C. Franz, U. Haselmann, C. Antony, and I.W. Mattaj. 2005. The integral membrane nucleoporin pom121 functionally links nuclear pore complex assembly and nuclear envelope formation. *Mol Cell*. 17:83-92.

Aparicio, O.M., B.L. Billington, and D.E. Gottschling. 1991. Modifiers of position effect are shared between telomeric and silent mating-type loci in S. cerevisiae. *Cell*. 66:1279-87.

Arnaoutov, A., Y. Azuma, K. Ribbeck, J. Joseph, Y. Boyarchuk, T. Karpova, J. McNally, and M. Dasso. 2005. Crm1 is a mitotic effector of Ran-GTP in somatic cells. *Nat Cell Biol*. 7:626-32.

Askree, S.H., T. Yehuda, S. Smolikov, R. Gurevich, J. Hawk, C. Coker, A. Krauskopf, M. Kupiec, and M.J. McEachern. 2004. A genome-wide screen

for Saccharomyces cerevisiae deletion mutants that affect telomere length. *Proc Natl Acad Sci U S A*. 101:8658-63.

Axelrod, J.D., M.S. Reagan, and J. Majors. 1993. GAL4 disrupts a repressing nucleosome during activation of GAL1 transcription in vivo. *Genes Dev*. 7:857-69.

Babiarz, J.E., J.E. Halley, and J. Rine. 2006. Telomeric heterochromatin boundaries require NuA4-dependent acetylation of histone variant H2A.Z in Saccharomyces cerevisiae. *Genes Dev*. 20:700-10.

Badis, G., E.T. Chan, H. van Bakel, L. Pena-Castillo, D. Tillo, K. Tsui, C.D. Carlson, A.J. Gossett, M.J. Hasinoff, C.L. Warren, M. Gebbia, S. Talukder, A. Yang, S. Mnaimneh, D. Terterov, D. Coburn, A. Li Yeo, Z.X. Yeo, N.D. Clarke, J.D. Lieb, A.Z. Ansari, C. Nislow, and T.R. Hughes. 2008. A library of yeast transcription factor motifs reveals a widespread function for Rsc3 in targeting nucleosome exclusion at promoters. *Mol Cell*. 32:878-87.

Bailey, D., and P. O'Hare. 2004. Characterization of the localization and proteolytic activity of the SUMO-specific protease, SENP1. *J Biol Chem*. 279:692-703.

Bannister, A.J., and T. Kouzarides. 2011. Regulation of chromatin by histone modifications. *Cell Res*. 21:381-95.

Bastos, R., L. Ribas de Pouplana, M. Enarson, K. Bodoor, and B. Burke. 1997. Nup84, a novel nucleoporin that is associated with CAN/Nup214 on the cytoplasmic face of the nuclear pore complex. *J Cell Biol*. 137:989-1000.

Belgareh, N., C. Snay-Hodge, F. Pasteau, S. Dagher, C.N. Cole, and V. Doye. 1998. Functional characterization of a Nup159p-containing nuclear pore subcomplex. *Mol Biol Cell*. 9:3475-92.

Berger, A.B., G.G. Cabal, E. Fabre, T. Duong, H. Buc, U. Nehrbass, J.C. Olivo-Marin, O. Gadal, and C. Zimmer. 2008. High-resolution statistical mapping reveals gene territories in live yeast. *Nat Methods*. 5:1031-7.

Berke, I.C., T. Boehmer, G. Blobel, and T.U. Schwartz. 2004. Structural and functional analysis of Nup133 domains reveals modular building blocks of the nuclear pore complex. *J Cell Biol*. 167:591-7.

Bernad, R., H. van der Velde, M. Fornerod, and H. Pickersgill. 2004. Nup358/RanBP2 attaches to the nuclear pore complex via association with Nup88 and Nup214/CAN and plays a supporting role in CRM1-mediated nuclear protein export. *Mol Cell Biol*. 24:2373-84.

Bianchi, A., and D. Shore. 2007. Increased association of telomerase with short telomeres in yeast. *Genes Dev*. 21:1726-30.

Bianchi, A., and D. Shore. 2008. How telomerase reaches its end: mechanism of telomerase regulation by the telomeric complex. *Mol Cell*. 31:153-65.

Bischoff, F.R., and H. Ponstingl. 1991. Catalysis of guanine nucleotide exchange on Ran by the mitotic regulator RCC1. *Nature*. 354:80-2.

Bischoff, F.R., C. Klebe, J. Kretschmer, A. Wittinghofer, and H. Ponstingl. 1994. RanGAP1 induces GTPase activity of nuclear Ras-related Ran. *Proc Natl Acad Sci U S A*. 91:2587-91.

Blackburn, E.H., and K. Collins. 2011. Telomerase: an RNP enzyme synthesizes DNA. *Cold Spring Harb Perspect Biol*. 3.

Blobel, G. 1985. Gene gating: a hypothesis. *Proc Natl Acad Sci U S A*. 82:8527-9.

Blumer, K.J., J.E. Reneke, and J. Thorner. 1988. The STE2 gene product is the ligand-binding component of the alpha-factor receptor of Saccharomyces cerevisiae. *J Biol Chem*. 263:10836-42.

Boeger, H., J. Griesenbeck, J.S. Strattan, and R.D. Kornberg. 2003. Nucleosomes unfold completely at a transcriptionally active promoter. *Mol Cell*. 11:1587-98.

Boeke, J.D., J. Trueheart, G. Natsoulis, and G.R. Fink. 1987. 5-Fluoroorotic acid as a selective agent in yeast molecular genetics. *Methods Enzymol*. 154:164-75.

Bolzer, A., G. Kreth, I. Solovei, D. Koehler, K. Saracoglu, C. Fauth, S. Muller, R. Eils, C. Cremer, M.R. Speicher, and T. Cremer. 2005. Three-dimensional maps of all chromosomes in human male fibroblast nuclei and prometaphase rosettes. *PLoS Biol*. 3:e157.

Boone, C., N.G. Davis, and G.F. Sprague, Jr. 1993. Mutations that alter the third cytoplasmic loop of the a-factor receptor lead to a constitutive and hypersensitive phenotype. *Proc Natl Acad Sci U S A*. 90:9921-5.

Brachmann, C.B., A. Davies, G.J. Cost, E. Caputo, J. Li, P. Hieter, and J.D. Boeke. 1998. Designer deletion strains derived from Saccharomyces cerevisiae S288C: a useful set of strains and plasmids for PCR-mediated gene disruption and other applications. *Yeast*. 14:115-32.

Brand, A.H., L. Breeden, J. Abraham, R. Sternglanz, and K. Nasmyth. 1985. Characterization of a "silencer" in yeast: a DNA sequence with properties opposite to those of a transcriptional enhancer. *Cell*. 41:41-8.

Brickner, J.H., and P. Walter. 2004. Gene recruitment of the activated INO1 locus to the nuclear membrane. *PLoS Biol*. 2:e342.

Brickner, D.G., I. Cajigas, Y. Fondufe-Mittendorf, S. Ahmed, P.C. Lee, J. Widom, and J.H. Brickner. 2007. H2A.Z-mediated localization of genes at the nuclear periphery confers epigenetic memory of previous transcriptional state. *PLoS Biol*. 5:e81.

Brickner, J.H. 2009. Transcriptional memory at the nuclear periphery. *Curr Opin Cell Biol*. 21:127-33.

Brohawn, S.G., J.R. Partridge, J.R. Whittle, and T.U. Schwartz. 2009. The nuclear pore complex has entered the atomic age. *Structure*. 17:1156-68.

Brown, C.R., C.J. Kennedy, V.A. Delmar, D.J. Forbes, and P.A. Silver. 2008. Global histone acetylation induces functional genomic reorganization at mammalian nuclear pore complexes. *Genes Dev*. 22:627-39.

Buchberger, J.R., M. Onishi, G. Li, J. Seebacher, A.D. Rudner, S.P. Gygi, and D. Moazed. 2008. Sir3-nucleosome interactions in spreading of silent chromatin in Saccharomyces cerevisiae. *Mol Cell Biol*. 28:6903-18.

Buck, S.W., and D. Shore. 1995. Action of a RAP1 carboxy-terminal silencing domain reveals an underlying competition between HMR and telomeres in yeast. *Genes Dev*. 9:370-84.

Bupp, J.M., A.E. Martin, E.S. Stensrud, and S.L. Jaspersen. 2007. Telomere anchoring at the nuclear periphery requires the budding yeast Sad1-UNC-84 domain protein Mps3. *J Cell Biol*. 179:845-54.

Burge, S., G.N. Parkinson, P. Hazel, A.K. Todd, and S. Neidle. 2006. Quadruplex DNA: sequence, topology and structure. *Nucleic Acids Res*. 34:5402-15.

Cabal, G.G., A. Genovesio, S. Rodriguez-Navarro, C. Zimmer, O. Gadal, A. Lesne, H. Buc, F. Feuerbach-Fournier, J.C. Olivo-Marin, E.C. Hurt, and U. Nehrbass. 2006. SAGA interacting factors confine sub-diffusion of transcribed genes to the nuclear envelope. *Nature*. 441:770-3.

Cairns, B.R., Y. Lorch, Y. Li, M. Zhang, L. Lacomis, H. Erdjument-Bromage, P. Tempst, J. Du, B. Laurent, and R.D. Kornberg. 1996. RSC, an essential, abundant chromatin-remodeling complex. *Cell*. 87:1249-60.

Callan, H.G., and S.G. Tomlin. 1950. Experimental studies on amphibian oocyte nuclei. I. Investigation of the structure of the nuclear membrane by means of the electron microscope. *Proc R Soc Lond B Biol Sci*. 137:367-78.

Campbell, M.S., G.K. Chan, and T.J. Yen. 2001. Mitotic checkpoint proteins HsMAD1 and HsMAD2 are associated with nuclear pore complexes in interphase. *J Cell Sci*. 114:953-63.

Capelson, M., Y. Liang, R. Schulte, W. Mair, U. Wagner, and M.W. Hetzer. 2010. Chromatin-bound nuclear pore components regulate gene expression in higher eukaryotes. *Cell*. 140:372-83.

Carey, M., B. Li, and J.L. Workman. 2006. RSC exploits histone acetylation to abrogate the nucleosomal block to RNA polymerase II elongation. *Mol Cell*. 24:481-7.

Carrozza, M.J., B. Li, L. Florens, T. Suganuma, S.K. Swanson, K.K. Lee, W.J. Shia, S. Anderson, J. Yates, M.P. Washburn, and J.L. Workman. 2005. Histone H3 methylation by Set2 directs deacetylation of coding regions by Rpd3S to suppress spurious intragenic transcription. *Cell*. 123:581-92.

Casolari, J.M., C.R. Brown, S. Komili, J. West, H. Hieronymus, and P.A. Silver. 2004. Genome-wide localization of the nuclear transport machinery couples transcriptional status and nuclear organization. *Cell*. 117:427-39.

Casolari, J.M., C.R. Brown, D.A. Drubin, O.J. Rando, and P.A. Silver. 2005. Developmentally induced changes in transcriptional program alter spatial organization across chromosomes. *Genes Dev*. 19:1188-98.

Chadrin, A., B. Hess, M. San Roman, X. Gatti, B. Lombard, D. Loew, Y. Barral, B. Palancade, and V. Doye. 2010. Pom33, a novel transmembrane nucleoporin required for proper nuclear pore complex distribution. *J Cell Biol*. 189:795-811.

Chai, B., J. Huang, B.R. Cairns, and B.C. Laurent. 2005. Distinct roles for the RSC and Swi/Snf ATP-dependent chromatin remodelers in DNA double-strand break repair. *Genes Dev*. 19:1656-61.

Chan, R.K., and C.A. Otte. 1982a. Isolation and genetic analysis of Saccharomyces cerevisiae mutants supersensitive to G1 arrest by a factor and alpha factor pheromones. *Mol Cell Biol*. 2:11-20.

Chan, R.K., and C.A. Otte. 1982b. Physiological characterization of Saccharomyces cerevisiae mutants supersensitive to G1 arrest by a factor and alpha factor pheromones. *Mol Cell Biol*. 2:21-9.

Chatel, G., and B. Fahrenkrog. 2012. Dynamics and diverse functions of nuclear pore complex proteins. *Nucleus*. 3.

Chial, H.J., M.P. Rout, T.H. Giddings, and M. Winey. 1998. Saccharomyces cerevisiae Ndc1p is a shared component of nuclear pore complexes and spindle pole bodies. *J Cell Biol*. 143:1789-800.

Chien, C.T., S. Buck, R. Sternglanz, and D. Shore. 1993. Targeting of SIR1 protein establishes transcriptional silencing at HM loci and telomeres in yeast. *Cell*. 75:531-41.

Chook, Y.M., and G. Blobel. 2001. Karyopherins and nuclear import. *Curr Opin Struct Biol*. 11:703-15.

Clapier, C.R., and B.R. Cairns. 2009. The biology of chromatin remodeling complexes. *Annu Rev Biochem*. 78:273-304.

Cockell, M., F. Palladino, T. Laroche, G. Kyrion, C. Liu, A.J. Lustig, and S.M. Gasser. 1995. The carboxy termini of Sir4 and Rap1 affect Sir3 localization: evidence for a multicomponent complex required for yeast telomeric silencing. *J Cell Biol*. 129:909-24.

Comings, D.E., and T.A. Okada. 1970. Association of chromatin fibers with the annuli of the nuclear membrane. *Exp Cell Res*. 62:293-302.

Cordes, V.C., S. Reidenbach, H.R. Rackwitz, and W.W. Franke. 1997. Identification of protein p270/Tpr as a constitutive component of the nuclear pore complex-attached intranuclear filaments. *J Cell Biol*. 136:515-29.

Crisp, M., Q. Liu, K. Roux, J.B. Rattner, C. Shanahan, B. Burke, P.D. Stahl, and D. Hodzic. 2006. Coupling of the nucleus and cytoplasm: role of the LINC complex. *J Cell Biol*. 172:41-53.

Croft, J.A., J.M. Bridger, S. Boyle, P. Perry, P. Teague, and W.A. Bickmore. 1999. Differences in the localization and morphology of chromosomes in the human nucleus. *J Cell Biol*. 145:1119-31.

Cronshaw, J.M., A.N. Krutchinsky, W. Zhang, B.T. Chait, and M.J. Matunis. 2002. Proteomic analysis of the mammalian nuclear pore complex. *J Cell Biol*. 158:915-27.

Cubizolles, F., F. Martino, S. Perrod, and S.M. Gasser. 2006. A homotrimer-heterotrimer switch in Sir2 structure differentiates rDNA and telomeric silencing. *Mol Cell*. 21:825-36.

D'Angelo, M.A., and M.W. Hetzer. 2008. Structure, dynamics and function of nuclear pore complexes. *Trends Cell Biol*. 18:456-66.

Damelin, M., I. Simon, T.I. Moy, B. Wilson, S. Komili, P. Tempst, F.P. Roth, R.A. Young, B.R. Cairns, and P.A. Silver. 2002. The genome-wide localization of Rsc9, a component of the RSC chromatin-remodeling complex, changes in response to stress. *Mol Cell*. 9:563-73.

de Bruin, D., S.M. Kantrow, R.A. Liberatore, and V.A. Zakian. 2000. Telomere folding is required for the stable maintenance of telomere position effects in yeast. *Mol Cell Biol*. 20:7991-8000.

Debler, E.W., Y. Ma, H.S. Seo, K.C. Hsia, T.R. Noriega, G. Blobel, and A. Hoelz. 2008. A fence-like coat for the nuclear pore membrane. *Mol Cell*. 32:815-26.

Dechat, T., K. Pfleghaar, K. Sengupta, T. Shimi, D.K. Shumaker, L. Solimando, and R.D. Goldman. 2008. Nuclear lamins: major factors in the structural organization and function of the nucleus and chromatin. *Genes Dev*. 22:832-53.

Delphin, C., T. Guan, F. Melchior, and L. Gerace. 1997. RanGTP targets p97 to RanBP2, a filamentous protein localized at the cytoplasmic periphery of the nuclear pore complex. *Mol Biol Cell*. 8:2379-90.

Deniaud, E., and W.A. Bickmore. 2009. Transcription and the nuclear periphery: edge of darkness? *Curr Opin Genet Dev*. 19:187-91.

Denning, D., B. Mykytka, N.P. Allen, L. Huang, B. Al, and M. Rexach. 2001. The nucleoporin Nup60p functions as a Gsp1p-GTP-sensitive tether for Nup2p at the nuclear pore complex. *J Cell Biol*. 154:937-50.

Denning, D.P., V. Uversky, S.S. Patel, A.L. Fink, and M. Rexach. 2002. The Saccharomyces cerevisiae nucleoporin Nup2p is a natively unfolded protein. *J Biol Chem*. 277:33447-55.

Denning, D.P., S.S. Patel, V. Uversky, A.L. Fink, and M. Rexach. 2003. Disorder in the nuclear pore complex: the FG repeat regions of nucleoporins are natively unfolded. *Proc Natl Acad Sci U S A*. 100:2450-5.

Devos, D., S. Dokudovskaya, F. Alber, R. Williams, B.T. Chait, A. Sali, and M.P. Rout. 2004. Components of coated vesicles and nuclear pore complexes share a common molecular architecture. *PLoS Biol*. 2:e380.

Devos, D., S. Dokudovskaya, R. Williams, F. Alber, N. Eswar, B.T. Chait, M.P. Rout, and A. Sali. 2006. Simple fold composition and modular architecture of the nuclear pore complex. *Proc Natl Acad Sci U S A*. 103:2172-7.

Dhalluin, C., J.E. Carlson, L. Zeng, C. He, A.K. Aggarwal, and M.M. Zhou. 1999. Structure and ligand of a histone acetyltransferase bromodomain. *Nature*. 399:491-6.

Dhillon, N., J. Raab, J. Guzzo, S.J. Szyjka, S. Gangadharan, O.M. Aparicio, B. Andrews, and R.T. Kamakaka. 2009. DNA polymerase epsilon, acetylases and remodellers cooperate to form a specialized chromatin structure at a tRNA insulator. *EMBO J*. 28:2583-600.

Dieppois, G., N. Iglesias, and F. Stutz. 2006. Cotranscriptional recruitment to the mRNA export receptor Mex67p contributes to nuclear pore anchoring of activated genes. *Mol Cell Biol*. 26:7858-70.

Diffley, J.F., and B. Stillman. 1989. Transcriptional silencing and lamins. *Nature*. 342:24.

Dilworth, D.J., A. Suprapto, J.C. Padovan, B.T. Chait, R.W. Wozniak, M.P. Rout, and J.D. Aitchison. 2001. Nup2p dynamically associates with the distal regions of the yeast nuclear pore complex. *J Cell Biol*. 153:1465-78.

Dilworth, D.J., A.J. Tackett, R.S. Rogers, E.C. Yi, R.H. Christmas, J.J. Smith, A.F. Siegel, B.T. Chait, R.W. Wozniak, and J.D. Aitchison. 2005. The mobile nucleoporin Nup2p and chromatin-bound Prp20p function in endogenous NPC-mediated transcriptional control. *J Cell Biol*. 171:955-65.

Ding, X., R. Xu, J. Yu, T. Xu, Y. Zhuang, and M. Han. 2007. SUN1 is required for telomere attachment to nuclear envelope and gametogenesis in mice. *Dev Cell*. 12:863-72.

Dingwall, C., J. Robbins, S.M. Dilworth, B. Roberts, and W.D. Richardson. 1988. The nucleoplasmin nuclear location sequence is larger and more complex than that of SV-40 large T antigen. *J Cell Biol*. 107:841-9.

Donze, D., C.R. Adams, J. Rine, and R.T. Kamakaka. 1999. The boundaries of the silenced HMR domain in Saccharomyces cerevisiae. *Genes Dev*. 13:698-708.

Donze, D., and R.T. Kamakaka. 2001. RNA polymerase III and RNA polymerase II promoter complexes are heterochromatin barriers in Saccharomyces cerevisiae. *EMBO J*. 20:520-31.

Doucet, C.M., and M.W. Hetzer. 2010. Nuclear pore biogenesis into an intact nuclear envelope. *Chromosoma*. 119:469-77.

Dover, J., J. Schneider, M.A. Tawiah-Boateng, A. Wood, K. Dean, M. Johnston, and A. Shilatifard. 2002. Methylation of histone H3 by COMPASS requires ubiquitination of histone H2B by Rad6. *J Biol Chem*. 277:28368-71.

Doye, V., R. Wepf, and E.C. Hurt. 1994. A novel nuclear pore protein Nup133p with distinct roles in poly(A)+ RNA transport and nuclear pore distribution. *EMBO J*. 13:6062-75.

Dreger, M., L. Bengtsson, T. Schoneberg, H. Otto, and F. Hucho. 2001. Nuclear envelope proteomics: novel integral membrane proteins of the inner nuclear membrane. *Proc Natl Acad Sci U S A*. 98:11943-8.

Drubin, D.A., A.M. Garakani, and P.A. Silver. 2006. Motion as a phenotype: the use of live-cell imaging and machine visual screening to characterize transcription-dependent chromosome dynamics. *BMC Cell Biol*. 7:19.

Dudley, A.M., C. Rougeulle, and F. Winston. 1999. The Spt components of SAGA facilitate TBP binding to a promoter at a post-activator-binding step in vivo. *Genes Dev*. 13:2940-5.

Dultz, E., E. Zanin, C. Wurzenberger, M. Braun, G. Rabut, L. Sironi, and J. Ellenberg. 2008. Systematic kinetic analysis of mitotic dis- and reassembly of the nuclear pore in living cells. *J Cell Biol*. 180:857-65.

Dupraw, E.J. 1965. The Organization of Nuclei and Chromosomes in Honeybee Embryonic Cells. *Proc Natl Acad Sci U S A*. 53:161-8.

Ebrahimi, H., and A.D. Donaldson. 2008. Release of yeast telomeres from the nuclear periphery is triggered by replication and maintained by suppression of Ku-mediated anchoring. *Genes Dev*. 22:3363-74.

Ehrentraut, S., J.M. Weber, J.N. Dybowski, D. Hoffmann, and A.E. Ehrenhofer-Murray. 2010. Rpd3-dependent boundary formation at telomeres by removal of Sir2 substrate. *Proc Natl Acad Sci U S A*. 107:5522-7.

Ekwall, K. 2005. Genome-wide analysis of HDAC function. *Trends Genet*. 21:608-15.

Fahrenkrog, B., E.C. Hurt, U. Aebi, and N. Pante. 1998. Molecular architecture of the yeast nuclear pore complex: localization of Nsp1p subcomplexes. *J Cell Biol*. 143:577-88.

Fang, G., and T.R. Cech. 1993. The beta subunit of Oxytricha telomere-binding protein promotes G-quartet formation by telomeric DNA. *Cell*. 74:875-85.

Fasken, M.B., M. Stewart, and A.H. Corbett. 2008. Functional significance of the interaction between the mRNA-binding protein, Nab2, and the nuclear pore-associated protein, Mlp1, in mRNA export. *J Biol Chem*. 283:27130-43.

Fernandez-Martinez, J., and M.P. Rout. 2009. Nuclear pore complex biogenesis. *Curr Opin Cell Biol*. 21:603-12.

Ferreira, H.C., B. Luke, H. Schober, V. Kalck, J. Lingner, and S.M. Gasser. 2011. The PIAS homologue Siz2 regulates perinuclear telomere position and telomerase activity in budding yeast. *Nat Cell Biol*. 13:867-74.

Feuerbach, F., V. Galy, E. Trelles-Sticken, M. Fromont-Racine, A. Jacquier, E. Gilson, J.C. Olivo-Marin, H. Scherthan, and U. Nehrbass. 2002. Nuclear architecture and spatial positioning help establish transcriptional states of telomeres in yeast. *Nat Cell Biol*. 4:214-21.

Field, M.C., and J.B. Dacks. 2009. First and last ancestors: reconstructing evolution of the endomembrane system with ESCRTs, vesicle coat proteins, and nuclear pore complexes. *Curr Opin Cell Biol*. 21:4-13.

Field, M.C., A. Sali, and M.P. Rout. 2011. Evolution: On a bender--BARs, ESCRTs, COPs, and finally getting your coat. *J Cell Biol*. 193:963-72.

Fischer, T., K. Strasser, A. Racz, S. Rodriguez-Navarro, M. Oppizzi, P. Ihrig, J. Lechner, and E. Hurt. 2002. The mRNA export machinery requires the novel Sac3p-Thp1p complex to dock at the nucleoplasmic entrance of the nuclear pores. *EMBO J*. 21:5843-52.

Fiserova, J., S.A. Richards, S.R. Wente, and M.W. Goldberg. 2010. Facilitated transport and diffusion take distinct spatial routes through the nuclear pore complex. *J Cell Sci*. 123:2773-80.

Fisher, T.S., A.K. Taggart, and V.A. Zakian. 2004. Cell cycle-dependent regulation of yeast telomerase by Ku. *Nat Struct Mol Biol*. 11:1198-205.

Fornerod, M., M. Ohno, M. Yoshida, and I.W. Mattaj. 1997. CRM1 is an export receptor for leucine-rich nuclear export signals. *Cell*. 90:1051-60.

Fourel, G., E. Revardel, C.E. Koering, and E. Gilson. 1999. Cohabitation of insulators and silencing elements in yeast subtelomeric regions. *EMBO J*. 18:2522-37.

Frey, S., R.P. Richter, and D. Gorlich. 2006. FG-rich repeats of nuclear pore proteins form a three-dimensional meshwork with hydrogel-like properties. *Science*. 314:815-7.

Frey, S., and D. Gorlich. 2007. A saturated FG-repeat hydrogel can reproduce the permeability properties of nuclear pore complexes. *Cell*. 130:512-23.

Frey, S., and D. Gorlich. 2009. FG/FxFG as well as GLFG repeats form a selective permeability barrier with self-healing properties. *EMBO J*. 28:2554-67.

Frosst, P., T. Guan, C. Subauste, K. Hahn, and L. Gerace. 2002. Tpr is localized within the nuclear basket of the pore complex and has a role in nuclear protein export. *J Cell Biol*. 156:617-30.

Fujita, A., Y. Misumi, Y. Ikehara, and H. Kobayashi. 1992. The yeast SFL2 gene may be necessary for mating-type control. *Gene*. 112:85-90.

Funabiki, H., I. Hagan, S. Uzawa, and M. Yanagida. 1993. Cell cycle-dependent specific positioning and clustering of centromeres and telomeres in fission yeast. *J Cell Biol*. 121:961-76.

Gall, J.G. 1967. Octagonal nuclear pores. *J Cell Biol*. 32:391-9.

Galy, V., J.C. Olivo-Marin, H. Scherthan, V. Doye, N. Rascalou, and U. Nehrbass. 2000. Nuclear pore complexes in the organization of silent telomeric chromatin. *Nature*. 403:108-12.

Galy, V., O. Gadal, M. Fromont-Racine, A. Romano, A. Jacquier, and U. Nehrbass. 2004. Nuclear retention of unspliced mRNAs in yeast is mediated by perinuclear Mlp1. *Cell*. 116:63-73.

Gao, H., T.B. Toro, M. Paschini, B. Braunstein-Ballew, R.B. Cervantes, and V. Lundblad. 2010. Telomerase recruitment in Saccharomyces cerevisiae is not dependent on Tel1-mediated phosphorylation of Cdc13. *Genetics*. 186:1147-59.

Garcia-Oliver, E., V. Garcia-Molinero, and S. Rodriguez-Navarro. 2012. mRNA export and gene expression: The SAGA-TREX-2 connection. *Biochim Biophys Acta*. 1819:555-65.

Gasser, S.M., F. Hediger, A. Taddei, F.R. Neumann, and M.R. Gartenberg. 2004. The function of telomere clustering in yeast: the circe effect. *Cold Spring Harb Symp Quant Biol*. 69:327-37.

Gelbart, M.E., T. Rechsteiner, T.J. Richmond, and T. Tsukiyama. 2001. Interactions of Isw2 chromatin remodeling complex with nucleosomal arrays: analyses using recombinant yeast histones and immobilized templates. *Mol Cell Biol*. 21:2098-106.

Gietz, R.D., and R.A. Woods. 2002. Transformation of yeast by lithium acetate/single-stranded carrier DNA/polyethylene glycol method. *Methods Enzymol*. 350:87-96.

Gilson, E., M. Roberge, R. Giraldo, D. Rhodes, and S.M. Gasser. 1993. Distortion of the DNA double helix by RAP1 at silencers and multiple telomeric binding sites. *J Mol Biol*. 231:293-310.

Gilson, E., and V. Geli. 2007. How telomeres are replicated. *Nat Rev Mol Cell Biol*. 8:825-38.

Giraldo, R., and D. Rhodes. 1994. The yeast telomere-binding protein RAP1 binds to and promotes the formation of DNA quadruplexes in telomeric DNA. *EMBO J*. 13:2411-20.

Gkikopoulos, T., P. Schofield, V. Singh, M. Pinskaya, J. Mellor, M. Smolle, J.L. Workman, G.J. Barton, and T. Owen-Hughes. 2011. A role for Snf2-related nucleosome-spacing enzymes in genome-wide nucleosome organization. *Science*. 333:1758-60.

Goldberg, M.W., and T.D. Allen. 1996. The nuclear pore complex and lamina: three-dimensional structures and interactions determined by field emission in-lens scanning electron microscopy. *J Mol Biol*. 257:848-65.

Goldfarb, D.S., A.H. Corbett, D.A. Mason, M.T. Harreman, and S.A. Adam. 2004. Importin alpha: a multipurpose nuclear-transport receptor. *Trends Cell Biol*. 14:505-14.

Gorlich, D., N. Pante, U. Kutay, U. Aebi, and F.R. Bischoff. 1996. Identification of different roles for RanGDP and RanGTP in nuclear protein import. *EMBO J*. 15:5584-94.

Gotta, M., T. Laroche, A. Formenton, L. Maillet, H. Scherthan, and S.M. Gasser. 1996. The clustering of telomeres and colocalization with Rap1, Sir3, and Sir4 proteins in wild-type Saccharomyces cerevisiae. *J Cell Biol*. 134:1349-63.

Gottschling, D.E., O.M. Aparicio, B.L. Billington, and V.A. Zakian. 1990. Position effect at S. cerevisiae telomeres: reversible repression of Pol II transcription. *Cell*. 63:751-62.

Goutte, C., and A.D. Johnson. 1988. a1 protein alters the DNA binding specificity of alpha 2 repressor. *Cell*. 52:875-82.

Govind, C.K., H. Qiu, D.S. Ginsburg, C. Ruan, K. Hofmeyer, C. Hu, V. Swaminathan, J.L. Workman, B. Li, and A.G. Hinnebusch. 2010. Phosphorylated Pol II CTD recruits multiple HDACs, including Rpd3C(S), for methylation-dependent deacetylation of ORF nucleosomes. *Mol Cell*. 39:234-46.

Grandi, P., V. Doye, and E.C. Hurt. 1993. Purification of NSP1 reveals complex formation with 'GLFG' nucleoporins and a novel nuclear pore protein NIC96. *EMBO J*. 12:3061-71.

Gravel, S., M. Larrivee, P. Labrecque, and R.J. Wellinger. 1998. Yeast Ku as a regulator of chromosomal DNA end structure. *Science*. 280:741-4.

Green, D.M., C.P. Johnson, H. Hagan, and A.H. Corbett. 2003. The C-terminal domain of myosin-like protein 1 (Mlp1p) is a docking site for heterogeneous nuclear ribonucleoproteins that are required for mRNA export. *Proc Natl Acad Sci U S A*. 100:1010-5.

Greider, C.W., and E.H. Blackburn. 1985. Identification of a specific telomere terminal transferase activity in Tetrahymena extracts. *Cell*. 43:405-13.

Gross, D.S., C.C. Adams, S. Lee, and B. Stentz. 1993. A critical role for heat shock transcription factor in establishing a nucleosome-free region over the TATA-initiation site of the yeast HSP82 heat shock gene. *EMBO J*. 12:3931-45.

Grund, S.E., T. Fischer, G.G. Cabal, O. Antunez, J.E. Perez-Ortin, and E. Hurt. 2008. The inner nuclear membrane protein Src1 associates with subtelomeric genes and alters their regulated gene expression. *J Cell Biol*. 182:897-910.

Guan, T., R.H. Kehlenbach, E.C. Schirmer, A. Kehlenbach, F. Fan, B.E. Clurman, N. Arnheim, and L. Gerace. 2000. Nup50, a nucleoplasmically oriented nucleoporin with a role in nuclear protein export. *Mol Cell Biol*. 20:5619-30.

Guillemette, B., A.R. Bataille, N. Gevry, M. Adam, M. Blanchette, F. Robert, and L. Gaudreau. 2005. Variant histone H2A.Z is globally localized to the

promoters of inactive yeast genes and regulates nucleosome positioning. *PLoS Biol*. 3:e384.

Haber, J.E. 2012. Mating-Type Genes and MAT Switching in Saccharomyces cerevisiae. *Genetics*. 191:33-64.

Hagen, D.C., L. Bruhn, C.A. Westby, and G.F. Sprague, Jr. 1993. Transcription of alpha-specific genes in Saccharomyces cerevisiae: DNA sequence requirements for activity of the coregulator alpha 1. *Mol Cell Biol*. 13:6866-75.

Hahn, S., and E.T. Young. 2011. Transcriptional regulation in Saccharomyces cerevisiae: transcription factor regulation and function, mechanisms of initiation, and roles of activators and coactivators. *Genetics*. 189:705-36.

Hang, J., and M. Dasso. 2002. Association of the human SUMO-1 protease SENP2 with the nuclear pore. *J Biol Chem*. 277:19961-6.

Hanna, J.S., E.S. Kroll, V. Lundblad, and F.A. Spencer. 2001. Saccharomyces cerevisiae CTF18 and CTF4 are required for sister chromatid cohesion. *Mol Cell Biol*. 21:3144-58.

Hartley, P.D., and H.D. Madhani. 2009. Mechanisms that specify promoter nucleosome location and identity. *Cell*. 137:445-58.

Hawryluk-Gara, L.A., E.K. Shibuya, and R.W. Wozniak. 2005. Vertebrate Nup53 interacts with the nuclear lamina and is required for the assembly of a Nup93-containing complex. *Mol Biol Cell*. 16:2382-94.

Hecht, A., S. Strahl-Bolsinger, and M. Grunstein. 1996. Spreading of transcriptional repressor SIR3 from telomeric heterochromatin. *Nature*. 383:92-6.

Hediger, F., K. Dubrana, and S.M. Gasser. 2002a. Myosin-like proteins 1 and 2 are not required for silencing or telomere anchoring, but act in the Tel1 pathway of telomere length control. *J Struct Biol*. 140:79-91.

Hediger, F., F.R. Neumann, G. Van Houwe, K. Dubrana, and S.M. Gasser. 2002b. Live imaging of telomeres: yKu and Sir proteins define redundant telomere-anchoring pathways in yeast. *Curr Biol*. 12:2076-89.

Heitz, E. 1928. Das Heterochromatin der Moose. *Jahrb Wiss Bot*. 69:762-818.

Herschbach, B.M., M.B. Arnaud, and A.D. Johnson. 1994. Transcriptional repression directed by the yeast alpha 2 protein in vitro. *Nature*. 370:309-11.

Heun, P., T. Laroche, K. Shimada, P. Furrer, and S.M. Gasser. 2001. Chromosome dynamics in the yeast interphase nucleus. *Science*. 294:2181-6.

Hinshaw, J.E., and R.A. Milligan. 2003. Nuclear pore complexes exceeding eightfold rotational symmetry. *J Struct Biol*. 141:259-68.

Hiraga, S., E.D. Robertson, and A.D. Donaldson. 2006. The Ctf18 RFC-like complex positions yeast telomeres but does not specify their replication time. *EMBO J*. 25:1505-14.

Hiraga, S., S. Botsios, and A.D. Donaldson. 2008. Histone H3 lysine 56 acetylation by Rtt109 is crucial for chromosome positioning. *J Cell Biol*. 183:641-51.

Hirano, Y., K. Fukunaga, and K. Sugimoto. 2009. Rif1 and rif2 inhibit localization of tel1 to DNA ends. *Mol Cell*. 33:312-22.

Hoelz, A., E.W. Debler, and G. Blobel. 2011. The structure of the nuclear pore complex. *Annu Rev Biochem*. 80:613-43.

Hoppe, G.J., J.C. Tanny, A.D. Rudner, S.A. Gerber, S. Danaie, S.P. Gygi, and D. Moazed. 2002. Steps in assembly of silent chromatin in yeast: Sir3-independent binding of a Sir2/Sir4 complex to silencers and role for Sir2-dependent deacetylation. *Mol Cell Biol*. 22:4167-80.

Hopper, A.K., H.M. Traglia, and R.W. Dunst. 1990. The yeast RNA1 gene product necessary for RNA processing is located in the cytosol and apparently excluded from the nucleus. *J Cell Biol*. 111:309-21.

Hsia, K.C., P. Stavropoulos, G. Blobel, and A. Hoelz. 2007. Architecture of a coat for the nuclear pore membrane. *Cell*. 131:1313-26.

Hsu, J.M., J. Huang, P.B. Meluh, and B.C. Laurent. 2003. The yeast RSC chromatin-remodeling complex is required for kinetochore function in chromosome segregation. *Mol Cell Biol*. 23:3202-15.

Huang, H., A. Kahana, D.E. Gottschling, L. Prakash, and S.W. Liebman. 1997. The ubiquitin-conjugating enzyme Rad6 (Ubc2) is required for silencing in Saccharomyces cerevisiae. *Mol Cell Biol*. 17:6693-9.

Huang, J., J.M. Hsu, and B.C. Laurent. 2004. The RSC nucleosome-remodeling complex is required for Cohesin's association with chromosome arms. *Mol Cell*. 13:739-50.

Huang, S., H. Zhou, J. Tarara, and Z. Zhang. 2007. A novel role for histone chaperones CAF-1 and Rtt106p in heterochromatin silencing. *EMBO J*. 26:2274-83.

Huertas, D., R. Sendra, and P. Munoz. 2009. Chromatin dynamics coupled to DNA repair. *Epigenetics*. 4:31-42.

Hurwitz, M.E., C. Strambio-de-Castillia, and G. Blobel. 1998. Two yeast nuclear pore complex proteins involved in mRNA export form a cytoplasmically oriented subcomplex. *Proc Natl Acad Sci U S A*. 95:11241-5.

Ideker, T., V. Thorsson, A.F. Siegel, and L.E. Hood. 2000. Testing for differentially-expressed genes by maximum-likelihood analysis of microarray data. *J Comput Biol*. 7:805-17.

Imai, S., C.M. Armstrong, M. Kaeberlein, and L. Guarente. 2000. Transcriptional silencing and longevity protein Sir2 is an NAD-dependent histone deacetylase. *Nature*. 403:795-800.

Iouk, T., O. Kerscher, R.J. Scott, M.A. Basrai, and R.W. Wozniak. 2002. The yeast nuclear pore complex functionally interacts with components of the spindle assembly checkpoint. *J Cell Biol*. 159:807-19.

Ishii, K., G. Arib, C. Lin, G. Van Houwe, and U.K. Laemmli. 2002. Chromatin boundaries in budding yeast: the nuclear pore connection. *Cell*. 109:551-62.

Janke, C., M.M. Magiera, N. Rathfelder, C. Taxis, S. Reber, H. Maekawa, A. Moreno-Borchart, G. Doenges, E. Schwob, E. Schiebel, and M. Knop. 2004. A versatile toolbox for PCR-based tagging of yeast genes: new fluorescent proteins, more markers and promoter substitution cassettes. *Yeast*. 21:947-62.

Jarnik, M., and U. Aebi. 1991. Toward a more complete 3-D structure of the nuclear pore complex. *J Struct Biol*. 107:291-308.

Jaspersen, S.L., T.H. Giddings, Jr., and M. Winey. 2002. Mps3p is a novel component of the yeast spindle pole body that interacts with the yeast centrin homologue Cdc31p. *J Cell Biol*. 159:945-56.

Jeudy, S., and T.U. Schwartz. 2007. Crystal structure of nucleoporin Nic96 reveals a novel, intricate helical domain architecture. *J Biol Chem*. 282:34904-12.

Jhunjhunwala, S., M.C. van Zelm, M.M. Peak, and C. Murre. 2009. Chromatin architecture and the generation of antigen receptor diversity. *Cell*. 138:435-48.

Jin, Q., E. Trelles-Sticken, H. Scherthan, and J. Loidl. 1998. Yeast nuclei display prominent centromere clustering that is reduced in nondividing cells and in meiotic prophase. *J Cell Biol*. 141:21-9.

Kalderon, D., B.L. Roberts, W.D. Richardson, and A.E. Smith. 1984. A short amino acid sequence able to specify nuclear location. *Cell*. 39:499-509.

Kalverda, B., Pickersgill, H, Shloma, VV, Fornerod, M. 2010. Nucleoporins Directly Stimulate Expression of Developmental and Cell-Cycle Genes Inside the Nucleoplasm. *Cell*. 140:360-371.

Kampmann, M., and G. Blobel. 2009. Three-dimensional structure and flexibility of a membrane-coating module of the nuclear pore complex. *Nat Struct Mol Biol*. 16:782-8.

Kaplan, N., I.K. Moore, Y. Fondufe-Mittendorf, A.J. Gossett, D. Tillo, Y. Field, E.M. LeProust, T.R. Hughes, J.D. Lieb, J. Widom, and E. Segal. 2009. The DNA-encoded nucleosome organization of a eukaryotic genome. *Nature*. 458:362-6.

Kasten, M., H. Szerlong, H. Erdjument-Bromage, P. Tempst, M. Werner, and B.R. Cairns. 2004. Tandem bromodomains in the chromatin remodeler RSC recognize acetylated histone H3 Lys14. *EMBO J*. 23:1348-59.

Keck, J.M., M.H. Jones, C.C. Wong, J. Binkley, D. Chen, S.L. Jaspersen, E.P. Holinger, T. Xu, M. Niepel, M.P. Rout, J. Vogel, A. Sidow, J.R. Yates, 3rd, and M. Winey. 2011. A cell cycle phosphoproteome of the yeast centrosome. *Science*. 332:1557-61.

Kehat, I., F. Accornero, B.J. Aronow, and J.D. Molkentin. 2011. Modulation of chromatin position and gene expression by HDAC4 interaction with nucleoporins. *J Cell Biol*. 193:21-9.

Kenna, M.A., J.G. Petranka, J.L. Reilly, and L.I. Davis. 1996. Yeast N1e3p/Nup170p is required for normal stoichiometry of FG nucleoporins within the nuclear pore complex. *Mol Cell Biol*. 16:2025-36.

Kerscher, O., P. Hieter, M. Winey, and M.A. Basrai. 2001. Novel role for a Saccharomyces cerevisiae nucleoporin, Nup170p, in chromosome segregation. *Genetics*. 157:1543-53.

Khadaroo, B., M.T. Teixeira, P. Luciano, N. Eckert-Boulet, S.M. Germann, M.N. Simon, I. Gallina, P. Abdallah, E. Gilson, V. Geli, and M. Lisby. 2009. The DNA damage response at eroded telomeres and tethering to the nuclear pore complex. *Nat Cell Biol*. 11:980-7.

Kim, T., and S. Buratowski. 2009. Dimethylation of H3K4 by Set1 recruits the Set3 histone deacetylase complex to 5' transcribed regions. *Cell*. 137:259-72.

Kimura, A., T. Umehara, and M. Horikoshi. 2002. Chromosomal gradient of histone acetylation established by Sas2p and Sir2p functions as a shield against gene silencing. *Nat Genet*. 32:370-7.

King, M.C., C.P. Lusk, and G. Blobel. 2006. Karyopherin-mediated import of integral inner nuclear membrane proteins. *Nature*. 442:1003-7.

Klar, A.J. 2010. The yeast mating-type switching mechanism: a memoir. *Genetics*. 186:443-9.

Klebe, C., F.R. Bischoff, H. Ponstingl, and A. Wittinghofer. 1995. Interaction of the nuclear GTP-binding protein Ran with its regulatory proteins RCC1 and RanGAP1. *Biochemistry*. 34:639-47.

Kobor, M.S., S. Venkatasubrahmanyam, M.D. Meneghini, J.W. Gin, J.L. Jennings, A.J. Link, H.D. Madhani, and J. Rine. 2004. A protein complex containing the conserved Swi2/Snf2-related ATPase Swr1p deposits histone variant H2A.Z into euchromatin. *PLoS Biol*. 2:E131.

Kohler, A., M. Schneider, G.G. Cabal, U. Nehrbass, and E. Hurt. 2008. Yeast Ataxin-7 links histone deubiquitination with gene gating and mRNA export. *Nat Cell Biol*. 10:707-15.

Kohler, A., and E. Hurt. 2010. Gene regulation by nucleoporins and links to cancer. *Mol Cell*. 38:6-15.

Korber, P., T. Luckenbach, D. Blaschke, and W. Horz. 2004. Evidence for histone eviction in trans upon induction of the yeast PHO5 promoter. *Mol Cell Biol*. 24:10965-74.

Kosak, S.T., J.A. Skok, K.L. Medina, R. Riblet, M.M. Le Beau, A.G. Fisher, and H. Singh. 2002. Subnuclear compartmentalization of immunoglobulin loci during lymphocyte development. *Science*. 296:158-62.

Krishnan, V.V., E.Y. Lau, J. Yamada, D.P. Denning, S.S. Patel, M.E. Colvin, and M.F. Rexach. 2008. Intramolecular cohesion of coils mediated by

phenylalanine--glycine motifs in the natively unfolded domain of a nucleoporin. *PLoS Comput Biol*. 4:e1000145.

Krogan, N.J., M.C. Keogh, N. Datta, C. Sawa, O.W. Ryan, H. Ding, R.A. Haw, J. Pootoolal, A. Tong, V. Canadien, D.P. Richards, X. Wu, A. Emili, T.R. Hughes, S. Buratowski, and J.F. Greenblatt. 2003. A Snf2 family ATPase complex required for recruitment of the histone H2A variant Htz1. *Mol Cell*. 12:1565-76.

Krull, S., J. Thyberg, B. Bjorkroth, H.R. Rackwitz, and V.C. Cordes. 2004. Nucleoporins as components of the nuclear pore complex core structure and Tpr as the architectural element of the nuclear basket. *Mol Biol Cell*. 15:4261-77.

Krull, S., J. Dorries, B. Boysen, S. Reidenbach, L. Magnius, H. Norder, J. Thyberg, and V.C. Cordes. 2010. Protein Tpr is required for establishing nuclear pore-associated zones of heterochromatin exclusion. *EMBO J*. 29:1659-73.

Kuchler, K., R.E. Sterne, and J. Thorner. 1989. Saccharomyces cerevisiae STE6 gene product: a novel pathway for protein export in eukaryotic cells. *EMBO J*. 8:3973-84.

Kundu, S., P.J. Horn, and C.L. Peterson. 2007. SWI/SNF is required for transcriptional memory at the yeast GAL gene cluster. *Genes Dev*. 21:997-1004.

Kurshakova, M.M., A.N. Krasnov, D.V. Kopytova, Y.V. Shidlovskii, J.V. Nikolenko, E.N. Nabirochkina, D. Spehner, P. Schultz, L. Tora, and S.G. Georgieva. 2007. SAGA and a novel Drosophila export complex anchor efficient transcription and mRNA export to NPC. *EMBO J*. 26:4956-65.

Kvam, E., and D.S. Goldfarb. 2006. Structure and function of nucleus-vacuole junctions: outer-nuclear-membrane targeting of Nvj1p and a role in tryptophan uptake. *J Cell Sci*. 119:3622-33.

Laine, J.P., B.N. Singh, S. Krishnamurthy, and M. Hampsey. 2009. A physiological role for gene loops in yeast. *Genes Dev*. 23:2604-9.

Laroche, T., S.G. Martin, M. Gotta, H.C. Gorham, F.E. Pryde, E.J. Louis, and S.M. Gasser. 1998. Mutation of yeast Ku genes disrupts the subnuclear organization of telomeres. *Curr Biol*. 8:653-6.

Laroche, T., S.G. Martin, M. Tsai-Pflugfelder, and S.M. Gasser. 2000. The dynamics of yeast telomeres and silencing proteins through the cell cycle. *J Struct Biol*. 129:159-74.

Lau, A., H. Blitzblau, and S.P. Bell. 2002. Cell-cycle control of the establishment of mating-type silencing in S. cerevisiae. *Genes Dev*. 16:2935-45.

Lee, A., R. Tam, P. Belhumeur, T. DiPaolo, and M.W. Clark. 1993. Prp20, the Saccharomyces cerevisiae homolog of the regulator of chromosome condensation, RCC1, interacts with double-stranded DNA through a multi-component complex containing GTP-binding proteins. *J Cell Sci*. 106 (Pt 1):287-98.

Lee, G.W., F. Melchior, M.J. Matunis, R. Mahajan, Q. Tian, and P. Anderson. 1998. Modification of Ran GTPase-activating protein by the small ubiquitin-related modifier SUMO-1 requires Ubc9, an E2-type ubiquitin-conjugating enzyme homologue. *J Biol Chem*. 273:6503-7.

Lee, C.K., Y. Shibata, B. Rao, B.D. Strahl, and J.D. Lieb. 2004. Evidence for nucleosome depletion at active regulatory regions genome-wide. *Nat Genet*. 36:900-5.

Lee, W., D. Tillo, N. Bray, R.H. Morse, R.W. Davis, T.R. Hughes, and C. Nislow. 2007. A high-resolution atlas of nucleosome occupancy in yeast. *Nat Genet*. 39:1235-44.

Levy, D.L., and E.H. Blackburn. 2004. Counting of Rif1p and Rif2p on Saccharomyces cerevisiae telomeres regulates telomere length. *Mol Cell Biol*. 24:10857-67.

Lewis, A., R. Felberbaum, and M. Hochstrasser. 2007. A nuclear envelope protein linking nuclear pore basket assembly, SUMO protease regulation, and mRNA surveillance. *J Cell Biol*. 178:813-27.

Li, S.J., and M. Hochstrasser. 2000. The yeast ULP2 (SMT4) gene encodes a novel protease specific for the ubiquitin-like Smt3 protein. *Mol Cell Biol*. 20:2367-77.

Li, S.J., and M. Hochstrasser. 2003. The Ulp1 SUMO isopeptidase: distinct domains required for viability, nuclear envelope localization, and substrate specificity. *J Cell Biol*. 160:1069-81.

Li, B., M. Carey, and J.L. Workman. 2007a. The role of chromatin during transcription. *Cell*. 128:707-19.

Li, B., M. Gogol, M. Carey, S.G. Pattenden, C. Seidel, and J.L. Workman. 2007b. Infrequently transcribed long genes depend on the Set2/Rpd3S pathway for accurate transcription. *Genes Dev*. 21:1422-30.

Li, S., S. Makovets, T. Matsuguchi, J.D. Blethrow, K.M. Shokat, and E.H. Blackburn. 2009. Cdk1-dependent phosphorylation of Cdc13 coordinates telomere elongation during cell-cycle progression. *Cell*. 136:50-61.

Liang, Y., and M.W. Hetzer. 2011. Functional interactions between nucleoporins and chromatin. *Curr Opin Cell Biol*. 23:65-70.

Light, W.H., D.G. Brickner, V.R. Brand, and J.H. Brickner. 2010. Interaction of a DNA zip code with the nuclear pore complex promotes H2A.Z incorporation and INO1 transcriptional memory. *Mol Cell*. 40:112-25.

Lim, R.Y., N.P. Huang, J. Koser, J. Deng, K.H. Lau, K. Schwarz-Herion, B. Fahrenkrog, and U. Aebi. 2006. Flexible phenylalanine-glycine nucleoporins as entropic barriers to nucleocytoplasmic transport. *Proc Natl Acad Sci U S A*. 103:9512-7.

Lim, R.Y., B. Fahrenkrog, J. Koser, K. Schwarz-Herion, J. Deng, and U. Aebi. 2007. Nanomechanical basis of selective gating by the nuclear pore complex. *Science*. 318:640-3.

Liou, G.G., J.C. Tanny, R.G. Kruger, T. Walz, and D. Moazed. 2005. Assembly of the SIR complex and its regulation by O-acetyl-ADP-ribose, a product of NAD-dependent histone deacetylation. *Cell*. 121:515-27.

Liu, Q., N. Pante, T. Misteli, M. Elsagga, M. Crisp, D. Hodzic, B. Burke, and K.J. Roux. 2007. Functional association of Sun1 with nuclear pore complexes. *J Cell Biol*. 178:785-98.

Loeillet, S., B. Palancade, M. Cartron, A. Thierry, G.F. Richard, B. Dujon, V. Doye, and A. Nicolas. 2005. Genetic network interactions among replication, repair and nuclear pore deficiencies in yeast. *DNA Repair (Amst)*. 4:459-68.

Louis, E.J. 1995. The chromosome ends of Saccharomyces cerevisiae. *Yeast*. 11:1553-73.

Luger, K., T.J. Rechsteiner, A.J. Flaus, M.M. Waye, and T.J. Richmond. 1997. Characterization of nucleosome core particles containing histone proteins made in bacteria. *J Mol Biol*. 272:301-11.

Luo, K., M.A. Vega-Palas, and M. Grunstein. 2002. Rap1-Sir4 binding independent of other Sir, yKu, or histone interactions initiates the assembly of telomeric heterochromatin in yeast. *Genes Dev*. 16:1528-39.

Lusk, C.P., T. Makhnevych, M. Marelli, J.D. Aitchison, and R.W. Wozniak. 2002. Karyopherins in nuclear pore biogenesis: a role for Kap121p in the assembly of Nup53p into nuclear pore complexes. *J Cell Biol*. 159:267-78.

Lusk, C.P., G. Blobel, and M.C. King. 2007. Highway to the inner nuclear membrane: rules for the road. *Nat Rev Mol Cell Biol*. 8:414-20.

Luthra, R., S.C. Kerr, M.T. Harreman, L.H. Apponi, M.B. Fasken, S. Ramineni, S. Chaurasia, S.R. Valentini, and A.H. Corbett. 2007. Actively transcribed GAL genes can be physically linked to the nuclear pore by the SAGA chromatin modifying complex. *J Biol Chem*. 282:3042-9.

Lutzmann, M., R. Kunze, A. Buerer, U. Aebi, and E. Hurt. 2002. Modular self-assembly of a Y-shaped multiprotein complex from seven nucleoporins. *EMBO J*. 21:387-97.

Ma, J., and W. Yang. 2010. Three-dimensional distribution of transient interactions in the nuclear pore complex obtained from single-molecule snapshots. *Proc Natl Acad Sci U S A*. 107:7305-10.

MacKay, V.L., S.K. Welch, M.Y. Insley, T.R. Manney, J. Holly, G.C. Saari, and M.L. Parker. 1988. The Saccharomyces cerevisiae BAR1 gene encodes an exported protein with homology to pepsin. *Proc Natl Acad Sci U S A*. 85:55-9.

Madrid, A.S., J. Mancuso, W.Z. Cande, and K. Weis. 2006. The role of the integral membrane nucleoporins Ndc1p and Pom152p in nuclear pore complex assembly and function. *J Cell Biol*. 173:361-71.

Mahajan, R., C. Delphin, T. Guan, L. Gerace, and F. Melchior. 1997. A small ubiquitin-related polypeptide involved in targeting RanGAP1 to nuclear pore complex protein RanBP2. *Cell*. 88:97-107.

Mahoney, D.J., and J.R. Broach. 1989. The HML mating-type cassette of Saccharomyces cerevisiae is regulated by two separate but functionally equivalent silencers. *Mol Cell Biol*. 9:4621-30.

Maillet, L., C. Boscheron, M. Gotta, S. Marcand, E. Gilson, and S.M. Gasser. 1996. Evidence for silencing compartments within the yeast nucleus: a role for telomere proximity and Sir protein concentration in silencer-mediated repression. *Genes Dev*. 10:1796-811.

Makhnevych, T., C. Ptak, C.P. Lusk, J.D. Aitchison, and R.W. Wozniak. 2007. The role of karyopherins in the regulated sumoylation of septins. *J Cell Biol*. 177:39-49.

Makio, T., L.H. Stanton, C.C. Lin, D.S. Goldfarb, K. Weis, and R.W. Wozniak. 2009. The nucleoporins Nup170p and Nup157p are essential for nuclear pore complex assembly. *J Cell Biol*. 185:459-73.

Manney, T.R. 1983. Expression of the BAR1 gene in Saccharomyces cerevisiae: induction by the alpha mating pheromone of an activity associated with a secreted protein. *J Bacteriol*. 155:291-301.

Mansfeld, J., S. Guttinger, L.A. Hawryluk-Gara, N. Pante, M. Mall, V. Galy, U. Haselmann, P. Muhlhausser, R.W. Wozniak, I.W. Mattaj, U. Kutay, and W. Antonin. 2006. The conserved transmembrane nucleoporin NDC1 is required for nuclear pore complex assembly in vertebrate cells. *Mol Cell*. 22:93-103.

Marcand, S., D. Wotton, E. Gilson, and D. Shore. 1997. Rap1p and telomere length regulation in yeast. *Ciba Found Symp*. 211:76-93; discussion 93-103.

Marelli, M., J.D. Aitchison, and R.W. Wozniak. 1998. Specific binding of the karyopherin Kap121p to a subunit of the nuclear pore complex containing Nup53p, Nup59p, and Nup170p. *J Cell Biol*. 143:1813-30.

Marelli, M., C.P. Lusk, H. Chan, J.D. Aitchison, and R.W. Wozniak. 2001. A link between the synthesis of nucleoporins and the biogenesis of the nuclear envelope. *J Cell Biol*. 153:709-24.

Martins-Taylor, K., M.L. Dula, and S.G. Holmes. 2004. Heterochromatin spreading at yeast telomeres occurs in M phase. *Genetics*. 168:65-75.

Martins-Taylor, K., U. Sharma, T. Rozario, and S.G. Holmes. 2011. H2A.Z (Htz1) controls the cell-cycle-dependent establishment of transcriptional silencing at Saccharomyces cerevisiae telomeres. *Genetics*. 187:89-104.

Matecic, M., K. Martins-Taylor, M. Hickman, J. Tanny, D. Moazed, and S.G. Holmes. 2006. New alleles of SIR2 define cell-cycle-specific silencing functions. *Genetics*. 173:1939-50.

Matunis, M.J., E. Coutavas, and G. Blobel. 1996. A novel ubiquitin-like modification modulates the partitioning of the Ran-GTPase-activating protein RanGAP1 between the cytosol and the nuclear pore complex. *J Cell Biol*. 135:1457-70.

Matunis, M.J., J. Wu, and G. Blobel. 1998. SUMO-1 modification and its role in targeting the Ran GTPase-activating protein, RanGAP1, to the nuclear pore complex. *J Cell Biol*. 140:499-509.

McGrath, J.P., and A. Varshavsky. 1989. The yeast STE6 gene encodes a homologue of the mammalian multidrug resistance P-glycoprotein. *Nature*. 340:400-4.

Mekhail, K., J. Seebacher, S.P. Gygi, and D. Moazed. 2008. Role for perinuclear chromosome tethering in maintenance of genome stability. *Nature*. 456:667-70.

Melcak, I., A. Hoelz, and G. Blobel. 2007. Structure of Nup58/45 suggests flexible nuclear pore diameter by intermolecular sliding. *Science*. 315:1729-32.

Mellad, J.A., D.T. Warren, and C.M. Shanahan. 2011. Nesprins LINC the nucleus and cytoskeleton. *Curr Opin Cell Biol*. 23:47-54.

Meluh, P.B., P. Yang, L. Glowczewski, D. Koshland, and M.M. Smith. 1998. Cse4p is a component of the core centromere of Saccharomyces cerevisiae. *Cell*. 94:607-13.

Mendjan, S., M. Taipale, J. Kind, H. Holz, P. Gebhardt, M. Schelder, M. Vermeulen, A. Buscaino, K. Duncan, J. Mueller, M. Wilm, H.G. Stunnenberg, H. Saumweber, and A. Akhtar. 2006. Nuclear pore components are involved in the transcriptional regulation of dosage compensation in Drosophila. *Mol Cell*. 21:811-23.

Meneghini, M.D., M. Wu, and H.D. Madhani. 2003. Conserved histone variant H2A.Z protects euchromatin from the ectopic spread of silent heterochromatin. *Cell*. 112:725-36.

Menon, B.B., N.J. Sarma, S. Pasula, S.J. Deminoff, K.A. Willis, K.E. Barbara, B. Andrews, and G.M. Santangelo. 2005. Reverse recruitment: the Nup84 nuclear pore subcomplex mediates Rap1/Gcr1/Gcr2 transcriptional activation. *Proc Natl Acad Sci U S A*. 102:5749-54.

Miao, M., K.J. Ryan, and S.R. Wente. 2006. The integral membrane protein Pom34p functionally links nucleoporin subcomplexes. *Genetics*. 172:1441-57.

Miki, F., A. Kurabayashi, Y. Tange, K. Okazaki, M. Shimanuki, and O. Niwa. 2004. Two-hybrid search for proteins that interact with Sad1 and Kms1, two membrane-bound components of the spindle pole body in fission yeast. *Mol Genet Genomics*. 270:449-61.

Mishra, K., and D. Shore. 1999. Yeast Ku protein plays a direct role in telomeric silencing and counteracts inhibition by rif proteins. *Curr Biol*. 9:1123-6.

Mitchell, J.M., J. Mansfeld, J. Capitanio, U. Kutay, and R.W. Wozniak. 2010. Pom121 links two essential subcomplexes of the nuclear pore complex core to the membrane. *J Cell Biol*. 191:505-21.

Mizuguchi, G., X. Shen, J. Landry, W.H. Wu, S. Sen, and C. Wu. 2004. ATP-driven exchange of histone H2AZ variant catalyzed by SWR1 chromatin remodeling complex. *Science*. 303:343-8.

Mondoux, M.A., J.G. Scaife, and V.A. Zakian. 2007. Differential nuclear localization does not determine the silencing status of Saccharomyces cerevisiae telomeres. *Genetics*. 177:2019-29.

Montpetit, B., N.D. Thomsen, K.J. Helmke, M.A. Seeliger, J.M. Berger, and K. Weis. 2011. A conserved mechanism of DEAD-box ATPase activation by nucleoporins and InsP6 in mRNA export. *Nature*. 472:238-42.

Moretti, P., K. Freeman, L. Coodly, and D. Shore. 1994. Evidence that a complex of SIR proteins interacts with the silencer and telomere-binding protein RAP1. *Genes Dev*. 8:2257-69.

Moretti, P., and D. Shore. 2001. Multiple interactions in Sir protein recruitment by Rap1p at silencers and telomeres in yeast. *Mol Cell Biol*. 21:8082-94.

Morohashi, N., Y. Yamamoto, S. Kuwana, W. Morita, H. Shindo, A.P. Mitchell, and M. Shimizu. 2006. Effect of sequence-directed nucleosome disruption on cell-type-specific repression by alpha2/Mcm1 in the yeast genome. *Eukaryot Cell*. 5:1925-33.

Morrison, A.J., and X. Shen. 2009. Chromatin remodelling beyond transcription: the INO80 and SWR1 complexes. *Nat Rev Mol Cell Biol*. 10:373-84.

Nagai, S., K. Dubrana, M. Tsai-Pflugfelder, M.B. Davidson, T.M. Roberts, G.W. Brown, E. Varela, F. Hediger, S.M. Gasser, and N.J. Krogan. 2008. Functional targeting of DNA damage to a nuclear pore-associated SUMO-dependent ubiquitin ligase. *Science*. 322:597-602.

Ng, H.H., F. Robert, R.A. Young, and K. Struhl. 2002. Genome-wide location and regulated recruitment of the RSC nucleosome-remodeling complex. *Genes Dev*. 16:806-19.

Niepel, M., C. Strambio-de-Castillia, J. Fasolo, B.T. Chait, and M.P. Rout. 2005. The nuclear pore complex-associated protein, Mlp2p, binds to the yeast spindle pole body and promotes its efficient assembly. *J Cell Biol*. 170:225-35.

Nishikawa, S., Y. Terazawa, T. Nakayama, A. Hirata, T. Makio, and T. Endo. 2003. Nep98p is a component of the yeast spindle pole body and essential for nuclear division and fusion. *J Biol Chem*. 278:9938-43.

O'Sullivan, J.M., S.M. Tan-Wong, A. Morillon, B. Lee, J. Coles, J. Mellor, and N.J. Proudfoot. 2004. Gene loops juxtapose promoters and terminators in yeast. *Nat Genet*. 36:1014-8.

Ohtsubo, M., H. Okazaki, and T. Nishimoto. 1989. The RCC1 protein, a regulator for the onset of chromosome condensation locates in the nucleus and binds to DNA. *J Cell Biol*. 109:1389-97.

Oki, M., and R.T. Kamakaka. 2005. Barrier function at HMR. *Mol Cell*. 19:707-16.

Onischenko, E., L.H. Stanton, A.S. Madrid, T. Kieselbach, and K. Weis. 2009. Role of the Ndc1 interaction network in yeast nuclear pore complex assembly and maintenance. *J Cell Biol*. 185:475-91.

Owen, D.J., P. Ornaghi, J.C. Yang, N. Lowe, P.R. Evans, P. Ballario, D. Neuhaus, P. Filetici, and A.A. Travers. 2000. The structural basis for the recognition of acetylated histone H4 by the bromodomain of histone acetyltransferase gcn5p. *EMBO J*. 19:6141-9.

Oza, P., S.L. Jaspersen, A. Miele, J. Dekker, and C.L. Peterson. 2009. Mechanisms that regulate localization of a DNA double-strand break to the nuclear periphery. *Genes Dev*. 23:912-27.

Paine, P.L., L.C. Moore, and S.B. Horowitz. 1975. Nuclear envelope permeability. *Nature*. 254:109-14.

Palancade, B., X. Liu, M. Garcia-Rubio, A. Aguilera, X. Zhao, and V. Doye. 2007. Nucleoporins prevent DNA damage accumulation by modulating Ulp1-dependent sumoylation processes. *Mol Biol Cell*. 18:2912-23.

Palladino, F., T. Laroche, E. Gilson, A. Axelrod, L. Pillus, and S.M. Gasser. 1993. SIR3 and SIR4 proteins are required for the positioning and integrity of yeast telomeres. *Cell*. 75:543-55.

Panse, V.G., B. Kuster, T. Gerstberger, and E. Hurt. 2003. Unconventional tethering of Ulp1 to the transport channel of the nuclear pore complex by karyopherins. *Nat Cell Biol*. 5:21-7.

Pante, N., and M. Kann. 2002. Nuclear pore complex is able to transport macromolecules with diameters of about 39 nm. *Mol Biol Cell*. 13:425-34.

Parnell, T.J., J.T. Huff, and B.R. Cairns. 2008. RSC regulates nucleosome positioning at Pol II genes and density at Pol III genes. *EMBO J*. 27:100-10.

Passarge, E. 1979. Emil Heitz and the concept of heterochromatin: longitudinal chromosome differentiation was recognized fifty years ago. *Am J Hum Genet*. 31:106-15.

Patel, S.S., B.J. Belmont, J.M. Sante, and M.F. Rexach. 2007. Natively unfolded nucleoporins gate protein diffusion across the nuclear pore complex. *Cell*. 129:83-96.

Patterton, H.G., C.C. Landel, D. Landsman, C.L. Peterson, and R.T. Simpson. 1998. The biochemical and phenotypic characterization of Hho1p, the putative linker histone H1 of Saccharomyces cerevisiae. *J Biol Chem*. 273:7268-76.

Pedroso, I.M., W. Hayward, and T.M. Fletcher. 2009. The effect of the TRF2 N-terminal and TRFH regions on telomeric G-quadruplex structures. *Nucleic Acids Res*. 37:1541-54.

Pemberton, L.F., J.S. Rosenblum, and G. Blobel. 1999. Nuclear import of the TATA-binding protein: mediation by the karyopherin Kap114p and a possible mechanism for intranuclear targeting. *J Cell Biol*. 145:1407-17.

Pemberton, L.F., and B.M. Paschal. 2005. Mechanisms of receptor-mediated nuclear import and nuclear export. *Traffic*. 6:187-98.

Pennock, E., K. Buckley, and V. Lundblad. 2001. Cdc13 delivers separate complexes to the telomere for end protection and replication. *Cell*. 104:387-96.

Peric-Hupkes, D., and B. van Steensel. 2010. Role of the nuclear lamina in genome organization and gene expression. *Cold Spring Harb Symp Quant Biol*. 75:517-24.

Peters, R. 2005. Translocation through the nuclear pore complex: selectivity and speed by reduction-of-dimensionality. *Traffic*. 6:421-7.

Peters, R. 2009. Translocation through the nuclear pore: Kaps pave the way. *Bioessays*. 31:466-77.

Pichler, A., A. Gast, J.S. Seeler, A. Dejean, and F. Melchior. 2002. The nucleoporin RanBP2 has SUMO1 E3 ligase activity. *Cell*. 108:109-20.

Pryde, F.E., and E.J. Louis. 1999. Limitations of silencing at native yeast telomeres. *EMBO J*. 18:2538-50.

Ptak, C., A.M. Anderson, R.J. Scott, D. Van de Vosse, R.S. Rogers, Y. Sydorskyy, J.D. Aitchison, and R.W. Wozniak. 2009. A role for the karyopherin Kap123p in microtubule stability. *Traffic*. 10:1619-34.

Radu, A., G. Blobel, and M.S. Moore. 1995a. Identification of a protein complex that is required for nuclear protein import and mediates docking of import substrate to distinct nucleoporins. *Proc Natl Acad Sci U S A*. 92:1769-73.

Radu, A., M.S. Moore, and G. Blobel. 1995b. The peptide repeat domain of nucleoporin Nup98 functions as a docking site in transport across the nuclear pore complex. *Cell*. 81:215-22.

Ragoczy, T., M.A. Bender, A. Telling, R. Byron, and M. Groudine. 2006. The locus control region is required for association of the murine beta-globin locus with engaged transcription factories during erythroid maturation. *Genes Dev*. 20:1447-57.

Raisner, R.M., P.D. Hartley, M.D. Meneghini, M.Z. Bao, C.L. Liu, S.L. Schreiber, O.J. Rando, and H.D. Madhani. 2005. Histone variant H2A.Z marks the 5' ends of both active and inactive genes in euchromatin. *Cell*. 123:233-48.

Rando, O.J., and F. Winston. 2012. Chromatin and transcription in yeast. *Genetics*. 190:351-87.

Reddy, K.L., J.M. Zullo, E. Bertolino, and H. Singh. 2008. Transcriptional repression mediated by repositioning of genes to the nuclear lamina. *Nature*. 452:243-7.

Reichelt, R., A. Holzenburg, E.L. Buhle, Jr., M. Jarnik, A. Engel, and U. Aebi. 1990. Correlation between structure and mass distribution of the nuclear pore complex and of distinct pore complex components. *J Cell Biol*. 110:883-94.

Rexach, M., and G. Blobel. 1995. Protein import into nuclei: association and dissociation reactions involving transport substrate, transport factors, and nucleoporins. *Cell*. 83:683-92.

Ribbeck, K., and D. Gorlich. 2002. The permeability barrier of nuclear pore complexes appears to operate via hydrophobic exclusion. *EMBO J*. 21:2664-71.

Rivers, D.M., and G.F. Sprague, Jr. 2003. Autocrine activation of the pheromone response pathway in matalpha2- cells is attenuated by SST2- and ASG7-dependent mechanisms. *Mol Genet Genomics*. 270:225-33.

Robert, F., D.K. Pokholok, N.M. Hannett, N.J. Rinaldi, M. Chandy, A. Rolfe, J.L. Workman, D.K. Gifford, and R.A. Young. 2004. Global position and recruitment of HATs and HDACs in the yeast genome. *Mol Cell*. 16:199-209.

Rodriguez-Navarro, S., T. Fischer, M.J. Luo, O. Antunez, S. Brettschneider, J. Lechner, J.E. Perez-Ortin, R. Reed, and E. Hurt. 2004. Sus1, a functional component of the SAGA histone acetylase complex and the nuclear pore-associated mRNA export machinery. *Cell*. 116:75-86.

Rodriguez-Navarro, S., and E. Hurt. 2011. Linking gene regulation to mRNA production and export. *Curr Opin Cell Biol*. 23:302-9.

Roth, A.F., B. Nelson, C. Boone, and N.G. Davis. 2000. Asg7p-Ste3p inhibition of pheromone signaling: regulation of the zygotic transition to vegetative growth. *Mol Cell Biol*. 20:8815-25.

Roth, P., N. Xylourgidis, N. Sabri, A. Uv, M. Fornerod, and C. Samakovlis. 2003. The Drosophila nucleoporin DNup88 localizes DNup214 and CRM1 on the nuclear envelope and attenuates NES-mediated nuclear export. *J Cell Biol*. 163:701-6.

Rout, M.P., and G. Blobel. 1993. Isolation of the yeast nuclear pore complex. *J Cell Biol*. 123:771-83.

Rout, M.P., J.D. Aitchison, A. Suprapto, K. Hjertaas, Y. Zhao, and B.T. Chait. 2000. The yeast nuclear pore complex: composition, architecture, and transport mechanism. *J Cell Biol*. 148:635-51.

Rout, M.P., J.D. Aitchison, M.O. Magnasco, and B.T. Chait. 2003. Virtual gating and nuclear transport: the hole picture. *Trends Cell Biol*. 13:622-8.

Roy, R., B. Meier, A.D. McAinsh, H.M. Feldmann, and S.P. Jackson. 2004. Separation-of-function mutants of yeast Ku80 reveal a Yku80p-Sir4p interaction involved in telomeric silencing. *J Biol Chem*. 279:86-94.

Ruben, G.J., J.G. Kirkland, T. Macdonough, M. Chen, R.N. Dubey, M.R. Gartenberg, and R.T. Kamakaka. 2011. Nucleoporin Mediated Nuclear Positioning and Silencing of HMR. *PLoS One*. 6:e21923.

Ruiz, C., V. Escribano, E. Morgado, M. Molina, and M.J. Mazon. 2003. Cell-type-dependent repression of yeast a-specific genes requires Itc1p, a subunit of the Isw2p-Itc1p chromatin remodelling complex. *Microbiology*. 149:341-51.

Rundlett, S.E., A.A. Carmen, R. Kobayashi, S. Bavykin, B.M. Turner, and M. Grunstein. 1996. HDA1 and RPD3 are members of distinct yeast histone deacetylase complexes that regulate silencing and transcription. *Proc Natl Acad Sci U S A*. 93:14503-8.

Rusche, L.N., A.L. Kirchmaier, and J. Rine. 2003. The establishment, inheritance, and function of silenced chromatin in Saccharomyces cerevisiae. *Annu Rev Biochem*. 72:481-516.

Sabourin, M., and V.A. Zakian. 2008. ATM-like kinases and regulation of telomerase: lessons from yeast and mammals. *Trends Cell Biol*. 18:337-46.

Saitoh, H., R. Pu, M. Cavenagh, and M. Dasso. 1997. RanBP2 associates with Ubc9p and a modified form of RanGAP1. *Proc Natl Acad Sci U S A*. 94:3736-41.

Santisteban, M.S., T. Kalashnikova, and M.M. Smith. 2000. Histone H2A.Z regulats transcription and is partially redundant with nucleosome remodeling complexes. *Cell*. 103:411-22.

Scannell, D.R., G. Butler, and K.H. Wolfe. 2007. Yeast genome evolution--the origin of the species. *Yeast*. 24:929-42.

Scarcelli, J.J., C.A. Hodge, and C.N. Cole. 2007. The yeast integral membrane protein Apq12 potentially links membrane dynamics to assembly of nuclear pore complexes. *J Cell Biol*. 178:799-812.

Schirmer, E.C., L. Florens, T. Guan, J.R. Yates, 3rd, and L. Gerace. 2003. Nuclear membrane proteins with potential disease links found by subtractive proteomics. *Science*. 301:1380-2.

Schmid, M., G. Arib, C. Laemmli, J. Nishikawa, T. Durussel, and U.K. Laemmli. 2006. Nup-PI: the nucleopore-promoter interaction of genes in yeast. *Mol Cell*. 21:379-91.

Schmitt, C., C. von Kobbe, A. Bachi, N. Pante, J.P. Rodrigues, C. Boscheron, G. Rigaut, M. Wilm, B. Seraphin, M. Carmo-Fonseca, and E. Izaurralde. 1999. Dbp5, a DEAD-box protein required for mRNA export, is recruited to the cytoplasmic fibrils of nuclear pore complex via a conserved interaction with CAN/Nup159p. *EMBO J*. 18:4332-47.

Schober, H., H. Ferreira, V. Kalck, L.R. Gehlen, and S.M. Gasser. 2009. Yeast telomerase and the SUN domain protein Mps3 anchor telomeres and repress subtelomeric recombination. *Genes Dev*. 23:928-38.

Schulman, I., and K.S. Bloom. 1991. Centromeres: an integrated protein/DNA complex required for chromosome movement. *Annu Rev Cell Biol*. 7:311-36.

Scott, R.J., C.P. Lusk, D.J. Dilworth, J.D. Aitchison, and R.W. Wozniak. 2005. Interactions between Mad1p and the nuclear transport machinery in the yeast Saccharomyces cerevisiae. *Mol Biol Cell*. 16:4362-74.

Scott, R.J., L.V. Cairo, D.W. Van de Vosse, and R.W. Wozniak. 2009. The nuclear export factor Xpo1p targets Mad1p to kinetochores in yeast. *J Cell Biol*. 184:21-9.

Shampay, J., and E.H. Blackburn. 1988. Generation of telomere-length heterogeneity in Saccharomyces cerevisiae. *Proc Natl Acad Sci U S A*. 85:534-8.

Shannon, P., A. Markiel, O. Ozier, N.S. Baliga, J.T. Wang, D. Ramage, N. Amin, B. Schwikowski, and T. Ideker. 2003. Cytoscape: a software environment for integrated models of biomolecular interaction networks. *Genome Res*. 13:2498-504.

Shia, W.J., B. Li, and J.L. Workman. 2006. SAS-mediated acetylation of histone H4 Lys 16 is required for H2A.Z incorporation at subtelomeric regions in Saccharomyces cerevisiae. *Genes Dev*. 20:2507-12.

Shilatifard, A. 2006. Chromatin modifications by methylation and ubiquitination: implications in the regulation of gene expression. *Annu Rev Biochem*. 75:243-69.

Shim, E.Y., J.L. Ma, J.H. Oum, Y. Yanez, and S.E. Lee. 2005. The yeast chromatin remodeler RSC complex facilitates end joining repair of DNA double-strand breaks. *Mol Cell Biol*. 25:3934-44.

Shim, E.Y., S.J. Hong, J.H. Oum, Y. Yanez, Y. Zhang, and S.E. Lee. 2007. RSC mobilizes nucleosomes to improve accessibility of repair machinery to the damaged chromatin. *Mol Cell Biol*. 27:1602-13.

Shimi, T., K. Pfleghaar, S. Kojima, C.G. Pack, I. Solovei, A.E. Goldman, S.A. Adam, D.K. Shumaker, M. Kinjo, T. Cremer, and R.D. Goldman. 2008. The A- and B-type nuclear lamin networks: microdomains involved in chromatin organization and transcription. *Genes Dev*. 22:3409-21.

Shivaswamy, S., A. Bhinge, Y. Zhao, S. Jones, M. Hirst, and V.R. Iyer. 2008. Dynamic remodeling of individual nucleosomes across a eukaryotic genome in response to transcriptional perturbation. *PLoS Biol*. 6:e65.

Shulga, N., N. Mosammaparast, R. Wozniak, and D.S. Goldfarb. 2000. Yeast nucleoporins involved in passive nuclear envelope permeability. *J Cell Biol*. 149:1027-38.

Shulga, N., and D.S. Goldfarb. 2003. Binding dynamics of structural nucleoporins govern nuclear pore complex permeability and may mediate channel gating. *Mol Cell Biol*. 23:534-42.

Sikorski, R.S., and P. Hieter. 1989. A system of shuttle vectors and yeast host strains designed for efficient manipulation of DNA in Saccharomyces cerevisiae. *Genetics*. 122:19-27.

Simms, T.A., S.L. Dugas, J.C. Gremillion, M.E. Ibos, M.N. Dandurand, T.T. Toliver, D.J. Edwards, and D. Donze. 2008. TFIIIC binding sites function as both heterochromatin barriers and chromatin insulators in Saccharomyces cerevisiae. *Eukaryot Cell*. 7:2078-86.

Singer, M.S., and D.E. Gottschling. 1994. TLC1: template RNA component of Saccharomyces cerevisiae telomerase. *Science*. 266:404-9.

Singer, M.S., A. Kahana, A.J. Wolf, L.L. Meisinger, S.E. Peterson, C. Goggin, M. Mahowald, and D.E. Gottschling. 1998. Identification of high-copy disruptors of telomeric silencing in Saccharomyces cerevisiae. *Genetics*. 150:613-32.

Siniossoglou, S., M. Lutzmann, H. Santos-Rosa, K. Leonard, S. Mueller, U. Aebi, and E. Hurt. 2000. Structure and assembly of the Nup84p complex. *J Cell Biol*. 149:41-54.

Siomi, H., and G. Dreyfuss. 1995. A nuclear localization domain in the hnRNP A1 protein. *J Cell Biol*. 129:551-60.

Smith, J.J., M. Marelli, R.H. Christmas, F.J. Vizeacoumar, D.J. Dilworth, T. Ideker, T. Galitski, K. Dimitrov, R.A. Rachubinski, and J.D. Aitchison. 2002. Transcriptome profiling to identify genes involved in peroxisome assembly and function. *J Cell Biol*. 158:259-71.

Smith, J.J., S.A. Ramsey, M. Marelli, B. Marzolf, D. Hwang, R.A. Saleem, R.A. Rachubinski, and J.D. Aitchison. 2007. Transcriptional responses to fatty acid are coordinated by combinatorial control. *Mol Syst Biol*. 3:115.

Smogorzewska, A., and T. de Lange. 2004. Regulation of telomerase by telomeric proteins. *Annu Rev Biochem*. 73:177-208.

Smythe, C., H.E. Jenkins, and C.J. Hutchison. 2000. Incorporation of the nuclear pore basket protein nup153 into nuclear pore structures is dependent upon lamina assembly: evidence from cell-free extracts of Xenopus eggs. *EMBO J*. 19:3918-31.

Snay-Hodge, C.A., H.V. Colot, A.L. Goldstein, and C.N. Cole. 1998. Dbp5p/Rat8p is a yeast nuclear pore-associated DEAD-box protein essential for RNA export. *EMBO J*. 17:2663-76.

Spencer, F., S.L. Gerring, C. Connelly, and P. Hieter. 1990. Mitotic chromosome transmission fidelity mutants in Saccharomyces cerevisiae. *Genetics*. 124:237-49.

Sprague, G.F., Jr., and I. Herskowitz. 1981. Control of yeast cell type by the mating type locus. I. Identification and control of expression of the a-specific gene BAR1. *J Mol Biol*. 153:305-21.

Stade, K., C.S. Ford, C. Guthrie, and K. Weis. 1997. Exportin 1 (Crm1p) is an essential nuclear export factor. *Cell*. 90:1041-50.

Stark, C., B.J. Breitkreutz, T. Reguly, L. Boucher, A. Breitkreutz, and M. Tyers. 2006. BioGRID: a general repository for interaction datasets. *Nucleic Acids Res*. 34:D535-9.

Stellwagen, A.E., Z.W. Haimberger, J.R. Veatch, and D.E. Gottschling. 2003. Ku interacts with telomerase RNA to promote telomere addition at native and broken chromosome ends. *Genes Dev*. 17:2384-95.

Stelter, P., R. Kunze, D. Flemming, D. Hopfner, M. Diepholz, P. Philippsen, B. Bottcher, and E. Hurt. 2007. Molecular basis for the functional interaction of dynein light chain with the nuclear-pore complex. *Nat Cell Biol*. 9:788-96.

Strahl, B.D., and C.D. Allis. 2000. The language of covalent histone modifications. *Nature*. 403:41-5.

Strahl-Bolsinger, S., A. Hecht, K. Luo, and M. Grunstein. 1997. SIR2 and SIR4 interactions differ in core and extended telomeric heterochromatin in yeast. *Genes Dev*. 11:83-93.

Strahm, Y., B. Fahrenkrog, D. Zenklusen, E. Rychner, J. Kantor, M. Rosbach, and F. Stutz. 1999. The RNA export factor Gle1p is located on the cytoplasmic fibrils of the NPC and physically interacts with the FG-nucleoporin Rip1p, the DEAD-box protein Rat8p/Dbp5p and a new protein Ymr 255p. *EMBO J*. 18:5761-77.

Strambio-de-Castillia, C., G. Blobel, and M.P. Rout. 1999. Proteins connecting the nuclear pore complex with the nuclear interior. *J Cell Biol*. 144:839-55.

Strawn, L.A., T. Shen, N. Shulga, D.S. Goldfarb, and S.R. Wente. 2004. Minimal nuclear pore complexes define FG repeat domains essential for transport. *Nat Cell Biol*. 6:197-206.

Sugiyama, M., and J. Nikawa. 2001. The Saccharomyces cerevisiae Isw2p-Itc1p complex represses INO1 expression and maintains cell morphology. *J Bacteriol*. 183:4985-93.

Suka, N., K. Luo, and M. Grunstein. 2002. Sir2p and Sas2p opposingly regulate acetylation of yeast histone H4 lysine16 and spreading of heterochromatin. *Nat Genet*. 32:378-83.

Sukegawa, J., and G. Blobel. 1993. A nuclear pore complex protein that contains zinc finger motifs, binds DNA, and faces the nucleoplasm. *Cell*. 72:29-38.

Sun, Z.W., and M. Hampsey. 1999. A general requirement for the Sin3-Rpd3 histone deacetylase complex in regulating silencing in Saccharomyces cerevisiae. *Genetics*. 152:921-32.

Sun, Z.W., and C.D. Allis. 2002. Ubiquitination of histone H2B regulates H3 methylation and gene silencing in yeast. *Nature*. 418:104-8.

Sun, J.Q., A. Hatanaka, and M. Oki. 2011. Boundaries of transcriptionally silent chromatin in Saccharomyces cerevisiae. *Genes Genet Syst*. 86:73-81.

Tackett, A.J., D.J. Dilworth, M.J. Davey, M. O'Donnell, J.D. Aitchison, M.P. Rout, and B.T. Chait. 2005. Proteomic and genomic characterization of chromatin complexes at a boundary. *J Cell Biol*. 169:35-47.

Taddei, A., F. Hediger, F.R. Neumann, C. Bauer, and S.M. Gasser. 2004. Separation of silencing from perinuclear anchoring functions in yeast Ku80, Sir4 and Esc1 proteins. *EMBO J*. 23:1301-12.

Taddei, A., G. Van Houwe, F. Hediger, V. Kalck, F. Cubizolles, H. Schober, and S.M. Gasser. 2006. Nuclear pore association confers optimal expression levels for an inducible yeast gene. *Nature*. 441:774-8.

Taddei, A. 2007. Active genes at the nuclear pore complex. *Curr Opin Cell Biol*. 19:305-10.

Taddei, A., G. Van Houwe, S. Nagai, I. Erb, E. van Nimwegen, and S.M. Gasser. 2009. The functional importance of telomere clustering: global changes in gene expression result from SIR factor dispersion. *Genome Res*. 19:611-25.

Taddei, A., H. Schober, and S.M. Gasser. 2010. The budding yeast nucleus. *Cold Spring Harb Perspect Biol*. 2:a000612.

Talamas, J.A., and M.W. Hetzer. 2011. POM121 and Sun1 play a role in early steps of interphase NPC assembly. *J Cell Biol*. 194:27-37.

Tan, M., H. Luo, S. Lee, F. Jin, J.S. Yang, E. Montellier, T. Buchou, Z. Cheng, S. Rousseaux, N. Rajagopal, Z. Lu, Z. Ye, Q. Zhu, J. Wysocka, Y. Ye, S. Khochbin, B. Ren, and Y. Zhao. 2011. Identification of 67 histone marks and histone lysine crotonylation as a new type of histone modification. *Cell*. 146:1016-28.

Tan-Wong, S.M., J.D. French, N.J. Proudfoot, and M.A. Brown. 2008. Dynamic interactions between the promoter and terminator regions of the mammalian BRCA1 gene. *Proc Natl Acad Sci U S A*. 105:5160-5.

Tan-Wong, S.M., H.D. Wijayatilake, and N.J. Proudfoot. 2009. Gene loops function to maintain transcriptional memory through interaction with the nuclear pore complex. *Genes Dev*. 23:2610-24.

Tanner, K.G., J. Landry, R. Sternglanz, and J.M. Denu. 2000. Silent information regulator 2 family of NAD- dependent histone/protein deacetylases generates a unique product, 1-O-acetyl-ADP-ribose. *Proc Natl Acad Sci U S A*. 97:14178-82.

Tanny, J.C., G.J. Dowd, J. Huang, H. Hilz, and D. Moazed. 1999. An enzymatic activity in the yeast Sir2 protein that is essential for gene silencing. *Cell*. 99:735-45.

Tcheperegine, S.E., M. Marelli, and R.W. Wozniak. 1999. Topology and functional domains of the yeast pore membrane protein Pom152p. *J Biol Chem*. 274:5252-8.

Teixeira, M.T., M. Arneric, P. Sperisen, and J. Lingner. 2004. Telomere length homeostasis is achieved via a switch between telomerase- extendible and -nonextendible states. *Cell*. 117:323-35.

Tham, W.H., and V.A. Zakian. 2002. Transcriptional silencing at Saccharomyces telomeres: implications for other organisms. *Oncogene*. 21:512-21.

Therizols, P., C. Fairhead, G.G. Cabal, A. Genovesio, J.C. Olivo-Marin, B. Dujon, and E. Fabre. 2006. Telomere tethering at the nuclear periphery is essential for efficient DNA double strand break repair in subtelomeric region. *J Cell Biol*. 172:189-99.

Titus, L.C., T.R. Dawson, D.J. Rexer, K.J. Ryan, and S.R. Wente. 2010. Members of the RSC chromatin-remodeling complex are required for maintaining proper nuclear envelope structure and pore complex localization. *Mol Biol Cell*. 21:1072-87.

Tompa, R., and H.D. Madhani. 2007. Histone H3 lysine 36 methylation antagonizes silencing in Saccharomyces cerevisiae independently of the Rpd3S histone deacetylase complex. *Genetics*. 175:585-93.

Tong, A.H., M. Evangelista, A.B. Parsons, H. Xu, G.D. Bader, N. Page, M. Robinson, S. Raghibizadeh, C.W. Hogue, H. Bussey, B. Andrews, M. Tyers, and C. Boone. 2001. Systematic genetic analysis with ordered arrays of yeast deletion mutants. *Science*. 294:2364-8.

Tong, A.H., G. Lesage, G.D. Bader, H. Ding, H. Xu, X. Xin, J. Young, G.F. Berriz, R.L. Brost, M. Chang, Y. Chen, X. Cheng, G. Chua, H. Friesen, D.S. Goldberg, J. Haynes, C. Humphries, G. He, S. Hussein, L. Ke, N. Krogan, Z. Li, J.N. Levinson, H. Lu, P. Menard, C. Munyana, A.B. Parsons, O. Ryan, R. Tonikian, T. Roberts, A.M. Sdicu, J. Shapiro, B. Sheikh, B. Suter, S.L. Wong, L.V. Zhang, H. Zhu, C.G. Burd, S. Munro, C. Sander, J. Rine, J. Greenblatt, M. Peter, A. Bretscher, G. Bell, F.P. Roth, G.W. Brown, B. Andrews, H. Bussey, and C. Boone. 2004. Global mapping of the yeast genetic interaction network. *Science*. 303:808-13.

Trachtulcova, P., I. Frydlova, I. Janatova, and J. Hasek. 2004. The absence of the Isw2p-Itc1p chromatin-remodelling complex induces mating type-specific and Flo11p-independent invasive growth of Saccharomyces cerevisiae. *Yeast*. 21:389-401.

Triolo, T., and R. Sternglanz. 1996. Role of interactions between the origin recognition complex and SIR1 in transcriptional silencing. *Nature*. 381:251-3.

Tseng, S.F., J.J. Lin, and S.C. Teng. 2006. The telomerase-recruitment domain of the telomere binding protein Cdc13 is regulated by Mec1p/Tel1p-dependent phosphorylation. *Nucleic Acids Res*. 34:6327-36.

Tsuchiya, E., T. Hosotani, and T. Miyakawa. 1998. A mutation in NPS1/STH1, an essential gene encoding a component of a novel chromatin-remodeling complex RSC, alters the chromatin structure of Saccharomyces cerevisiae centromeres. *Nucleic Acids Res*. 26:3286-92.

Turner, B.M. 1993. Decoding the nucleosome. *Cell*. 75:5-8.

Turner, B.M. 2000. Histone acetylation and an epigenetic code. *Bioessays*. 22:836-45.

Ungar, L., N. Yosef, Y. Sela, R. Sharan, E. Ruppin, and M. Kupiec. 2009. A genome-wide screen for essential yeast genes that affect telomere length maintenance. *Nucleic Acids Res*. 37:3840-9.

Valenzuela, L., N. Dhillon, R.N. Dubey, M.R. Gartenberg, and R.T. Kamakaka. 2008. Long-range communication between the silencers of HMR. *Mol Cell Biol*. 28:1924-35.

van Attikum, H., O. Fritsch, and S.M. Gasser. 2007. Distinct roles for SWR1 and INO80 chromatin remodeling complexes at chromosomal double-strand breaks. *EMBO J*. 26:4113-25.

Van de Vosse, D.W., Y. Wan, R.W. Wozniak, and J.D. Aitchison. 2011. Role of the nuclear envelope in genome organization and gene expression. *Wiley Interdiscip Rev Syst Biol Med*. 3:147-66.

van Leeuwen, F., P.R. Gafken, and D.E. Gottschling. 2002. Dot1p modulates silencing in yeast by methylation of the nucleosome core. *Cell*. 109:745-56.

Vaquerizas, J.M., R. Suyama, J. Kind, K. Miura, N.M. Luscombe, and A. Akhtar. 2010. Nuclear pore proteins nup153 and megator define transcriptionally active regions in the Drosophila genome. *PLoS Genet*. 6:e1000846.

Vassileva, M.T., and M.J. Matunis. 2004. SUMO modification of heterogeneous nuclear ribonucleoproteins. *Mol Cell Biol*. 24:3623-32.

Vasu, S., S. Shah, A. Orjalo, M. Park, W.H. Fischer, and D.J. Forbes. 2001. Novel vertebrate nucleoporins Nup133 and Nup160 play a role in mRNA export. *J Cell Biol*. 155:339-54.

Walde, S., and R.H. Kehlenbach. 2010. The Part and the Whole: functions of nucleoporins in nucleocytoplasmic transport. *Trends Cell Biol*. 20:461-9.

Walther, T.C., A. Alves, H. Pickersgill, I. Loiodice, M. Hetzer, V. Galy, B.B. Hulsmann, T. Kocher, M. Wilm, T. Allen, I.W. Mattaj, and V. Doye. 2003. The conserved Nup107-160 complex is critical for nuclear pore complex assembly. *Cell*. 113:195-206.

Wan, Y., R.A. Saleem, A.V. Ratushny, O. Roda, J.J. Smith, C.H. Lin, J.H. Chiang, and J.D. Aitchison. 2009. Role of the histone variant H2A.Z/Htz1p in TBP recruitment, chromatin dynamics, and regulated expression of oleate-responsive genes. *Mol Cell Biol*. 29:2346-58.

Wan, Y., J.H. Chiang, C.H. Lin, C.E. Arens, R.A. Saleem, J.J. Smith, and J.D. Aitchison. 2010. Histone chaperone Chz1p regulates H2B ubiquitination and subtelomeric anti-silencing. *Nucleic Acids Res*.

Watson, M.L. 1955. The nuclear envelope; its structure and relation to cytoplasmic membranes. *J Biophys Biochem Cytol*. 1:257-70.

Watson, M.L. 1959. Further observations on the nuclear envelope of the animal cell. *J Biophys Biochem Cytol*. 6:147-56.

Watson, J.D. 1972. Origin of concatemeric T7 DNA. *Nat New Biol*. 239:197-201.

Watson, A.D., D.G. Edmondson, J.R. Bone, Y. Mukai, Y. Yu, W. Du, D.J. Stillman, and S.Y. Roth. 2000. Ssn6-Tup1 interacts with class I histone deacetylases required for repression. *Genes Dev*. 14:2737-44.

Weiner, A., A. Hughes, M. Yassour, O.J. Rando, and N. Friedman. 2010. High-resolution nucleosome mapping reveals transcription-dependent promoter packaging. *Genome Res*. 20:90-100.

Weirich, C.S., J.P. Erzberger, J.M. Berger, and K. Weis. 2004. The N-terminal domain of Nup159 forms a beta-propeller that functions in mRNA export by tethering the helicase Dbp5 to the nuclear pore. *Mol Cell*. 16:749-60.

Weirich, C.S., J.P. Erzberger, J.S. Flick, J.M. Berger, J. Thorner, and K. Weis. 2006. Activation of the DExD/H-box protein Dbp5 by the nuclear-pore protein Gle1 and its coactivator InsP6 is required for mRNA export. *Nat Cell Biol*. 8:668-76.

Wellinger, R.J. 2010. When the caps fall off: responses to telomere uncapping in yeast. *FEBS Lett*. 584:3734-40.

Wente, S.R., and M.P. Rout. 2010. The nuclear pore complex and nuclear transport. *Cold Spring Harb Perspect Biol*. 2:a000562.

Werner, A., A. Flotho, and F. Melchior. 2012. The RanBP2/RanGAP1(*)SUMO1/Ubc9 Complex Is a Multisubunit SUMO E3 Ligase. *Mol Cell*. 46:287-98.

Whitehouse, I., O.J. Rando, J. Delrow, and T. Tsukiyama. 2007. Chromatin remodelling at promoters suppresses antisense transcription. *Nature*. 450:1031-5.

Wiblin, A.E., W. Cui, A.J. Clark, and W.A. Bickmore. 2005. Distinctive nuclear organisation of centromeres and regions involved in pluripotency in human embryonic stem cells. *J Cell Sci*. 118:3861-8.

Williams, R.R., V. Azuara, P. Perry, S. Sauer, M. Dvorkina, H. Jorgensen, J. Roix, P. McQueen, T. Misteli, M. Merkenschlager, and A.G. Fisher. 2006. Neural induction promotes large-scale chromatin reorganisation of the Mash1 locus. *J Cell Sci*. 119:132-40.

Winey, M., M.A. Hoyt, C. Chan, L. Goetsch, D. Botstein, and B. Byers. 1993. NDC1: a nuclear periphery component required for yeast spindle pole body duplication. *J Cell Biol*. 122:743-51.

Winey, M., D. Yarar, T.H. Giddings, Jr., and D.N. Mastronarde. 1997. Nuclear pore complex number and distribution throughout the Saccharomyces cerevisiae cell cycle by three-dimensional reconstruction from electron micrographs of nuclear envelopes. *Mol Biol Cell*. 8:2119-32.

Winzeler, E.A., D.D. Shoemaker, A. Astromoff, H. Liang, K. Anderson, B. Andre, R. Bangham, R. Benito, J.D. Boeke, H. Bussey, A.M. Chu, C. Connelly, K. Davis, F. Dietrich, S.W. Dow, M. El Bakkoury, F. Foury, S.H. Friend, E. Gentalen, G. Giaever, J.H. Hegemann, T. Jones, M. Laub, H. Liao, N. Liebundguth, D.J. Lockhart, A. Lucau-Danila, M. Lussier, N. M'Rabet, P. Menard, M. Mittmann, C. Pai, C. Rebischung, J.L. Revuelta, L. Riles, C.J. Roberts, P. Ross-MacDonald, B. Scherens, M. Snyder, S. Sookhai-Mahadeo, R.K. Storms, S. Veronneau, M. Voet, G. Volckaert, T.R. Ward, R. Wysocki, G.S. Yen, K. Yu, K. Zimmermann, P. Philippsen, M. Johnston, and R.W. Davis. 1999. Functional characterization of the S. cerevisiae genome by gene deletion and parallel analysis. *Science*. 285:901-6.

Wolfe, K.H., and D.C. Shields. 1997. Molecular evidence for an ancient duplication of the entire yeast genome. *Nature*. 387:708-13.

Wood, A., J. Schneider, J. Dover, M. Johnston, and A. Shilatifard. 2003. The Paf1 complex is essential for histone monoubiquitination by the Rad6-Bre1 complex, which signals for histone methylation by COMPASS and Dot1p. *J Biol Chem*. 278:34739-42.

Wool, I.G., Y.L. Chan, and A. Gluck. 1995. Structure and evolution of mammalian ribosomal proteins. *Biochem Cell Biol*. 73:933-47.

Wozniak, R.W., G. Blobel, and M.P. Rout. 1994. POM152 is an integral protein of the pore membrane domain of the yeast nuclear envelope. *J Cell Biol*. 125:31-42.

Wozniak, R.W., M.P. Rout, and J.D. Aitchison. 1998. Karyopherins and kissing cousins. *Trends Cell Biol*. 8:184-8.

Wu, J., M.J. Matunis, D. Kraemer, G. Blobel, and E. Coutavas. 1995. Nup358, a cytoplasmically exposed nucleoporin with peptide repeats, Ran-GTP binding sites, zinc fingers, a cyclophilin A homologous domain, and a leucine-rich region. *J Biol Chem*. 270:14209-13.

Yamada, J., J.L. Phillips, S. Patel, G. Goldfien, A. Calestagne-Morelli, H. Huang, R. Reza, J. Acheson, V.V. Krishnan, S. Newsam, A. Gopinathan, E.Y. Lau, M.E. Colvin, V.N. Uversky, and M.F. Rexach. 2010. A bimodal distribution of two distinct categories of intrinsically disordered structures with separate functions in FG nucleoporins. *Mol Cell Proteomics*. 9:2205-24.

Yang, Q., M.P. Rout, and C.W. Akey. 1998. Three-dimensional architecture of the isolated yeast nuclear pore complex: functional and evolutionary implications. *Mol Cell*. 1:223-34.

Yoshida, T., K. Shimada, Y. Oma, V. Kalck, K. Akimura, A. Taddei, H. Iwahashi, K. Kugou, K. Ohta, S.M. Gasser, and M. Harata. 2010. Actin-related protein Arp6 influences H2A.Z-dependent and -independent gene expression and links ribosomal protein genes to nuclear pores. *PLoS Genet*. 6:e1000910.

Young, T.J., and A.L. Kirchmaier. 2011. Cell cycle regulation of silent chromatin formation. *Biochim Biophys Acta*.

Yuan, G.C., Y.J. Liu, M.F. Dion, M.D. Slack, L.F. Wu, S.J. Altschuler, and O.J. Rando. 2005. Genome-scale identification of nucleosome positions in S. cerevisiae. *Science*. 309:626-30.

Zaug, A.J., E.R. Podell, and T.R. Cech. 2005. Human POT1 disrupts telomeric G-quadruplexes allowing telomerase extension in vitro. *Proc Natl Acad Sci U S A*. 102:10864-9.

Zawadzki, K.A., A.V. Morozov, and J.R. Broach. 2009. Chromatin-dependent transcription factor accessibility rather than nucleosome remodeling predominates during global transcriptional restructuring in Saccharomyces cerevisiae. *Mol Biol Cell*. 20:3503-13.

Zeng, L., and M.M. Zhou. 2002. Bromodomain: an acetyl-lysine binding domain. *FEBS Lett*. 513:124-8.

Zhang, H., H. Saitoh, and M.J. Matunis. 2002a. Enzymes of the SUMO modification pathway localize to filaments of the nuclear pore complex. *Mol Cell Biol*. 22:6498-508.

Zhang, Z., M.K. Hayashi, O. Merkel, B. Stillman, and R.M. Xu. 2002b. Structure and function of the BAH-containing domain of Orc1p in epigenetic silencing. *EMBO J*. 21:4600-11.

Zhang, Z., and J.C. Reese. 2004. Ssn6-Tup1 requires the ISW2 complex to position nucleosomes in Saccharomyces cerevisiae. *EMBO J*. 23:2246-57.

Zhang, H., D.N. Roberts, and B.R. Cairns. 2005. Genome-wide dynamics of Htz1, a histone H2A variant that poises repressed/basal promoters for activation through histone loss. *Cell*. 123:219-31.

Zhou, J., B.O. Zhou, B.A. Lenzmeier, and J.Q. Zhou. 2009. Histone deacetylase Rpd3 antagonizes Sir2-dependent silent chromatin propagation. *Nucleic Acids Res*. 37:3699-713.

Zuleger, N., N. Korfali, and E.C. Schirmer. 2008. Inner nuclear membrane protein transport is mediated by multiple mechanisms. *Biochem Soc Trans*. 36:1373-7.

Chapter VII: *Appendix*

Contained within this chapter are the results of several unpublished experiments that are not part of the previous chapters and were performed in conjunction with Y. Wan (Figures 7-4, 7-5, 7-11, and 7-12). The first figure, Figure 7-1, presents verification that Nup60p is required for chromosome segregation, a result initially suggested by genetic analysis of *NUP60* (Figure 3-2 and Table 3-1). Figure 7-2 shows the severe fitness defect and altered cellular morphology observed in *elm1Δ nup170Δ* double null mutants, which can be partially rescued by the C-terminus of Nup170p (aa 1000-1502). Figure 7-3 indicates that, among the *nup* mutants tested, derepression of subtelomeric genes is specific to the *nup170Δ* mutant. Figure 7-4 shows the association of Nup157p, Nup170p, and Nup188p with centromeric DNA. The results shown in Figure 7-5 indicate that in the absence of Sth1p, Nup170p binding at centromeric DNA is reduced whereas Nup170p binding at the *HMR* locus is enhanced. In Figure 7-6 the colocalization between two Nups located within a subcomplex (Nup170-GFP and Nup53-mCherry) or two distinct subcomplexes (Nup159-RFP and Nup170-GFP) were determined. This analysis revealed similar, but lower than expected, levels of colocalization amongst Nups (~50%) that was independent of Nup position within the NPC. Figure 7-7 shows that an asynchronous population of *nup170Δ* cells contains a disproportionate number of G1-phase cells as compared to a wild type population. In Figure 7-8 the linear density of NPCs was determined in WT and *nup170Δ* cells, revealing a reduction in the number of NPCs per micron of NE in comparison to WT cells. Figure 7-9, TEM analysis suggests that the genetic interactions identified between *NUP170* and genes

involved in chromatin organization may, in part, arise from defects in NE morphology and NPC assembly. In Figure 7-10 localization of the cytoplasmic Nups Gle1-GFP, Nup82-GFP, and Nup159-GFP was examined in deletion mutants displaying reduced fitness in combination with *nup170Δ*, revealing that chromatin remodeling complexes are required for proper NPC structure. In Figure 7-11 we examined the genome-wide transcriptional profile of two conditional mutants, *apq12Δ* and P_{MET3}-*HA3-STH1*, that result in defects in NPC assembly under non-permissive conditions, 23˚C and presence of methionine, respectively. This analysis revealed that, when shifted to the non-permissive condition, subtelomeric genes are derepressed in both mutants. Figure 7-12 shows both ChIP-qPCR and ChIP-chip experiments suggesting that association of Nup170p with subtelomeric DNA is increased in the absence of Sth1p. Lastly, in Figure 7-13 expression of the **a**-specific genes *BAR1* and *STE2* were examined in two conditional mutants, *apq12Δ* and *nup157Δ* P_{MET3}-*HA3-NUP170*, that result in defects in NPC assembly under non-permissive conditions, 23˚C and the presence of methionine, respectively. WT and *nup170Δ* strains served as controls. This analysis suggests that **a**-specific genes are derepressed in both NPC assembly mutants when shifted to the non-permissive condition.

Figure 7-1. Nup60p functions in chromosome segregation.

(A) Chromosome stability was examined in WT and homozygous *NUP60* and *NUP170* null mutant diploid strains containing two copies of the ochre allele *ade2-101* and a single copy of the non-essential chromosome fragment CFVII (*RAD2.d.YPH277*) carrying the ochre suppressor tRNA gene *SUP11*. Cells were grown to an OD_{600} ~1.0 and plated to single colonies on YPD medium for 2-4 d at 30˚C. In WT cells a single copy of *SUP11* in *ade2-101* homozygous diploid cells results in partial suppression of the ochre alleles, resulting in pink colonies. Mutations that affect genome stability (i.e. *nup170Δ*) can also produce red colonies arising from loss of *SUP11* (chromosome loss) or white colonies arising from an additional copy of *SUP11* (non-disjunction). (B) The indicated haploid strains encode *ade2-101* and carry the non-essential chromosome fragment CFIII (*CEN3.L.YPH278)* encoding *SUP11*. In WT cells the *ade2-101* allele confers a red colony phenotype, while the presence of *SUP11* fully suppresses *ade2-101* producing white colonies. Cells were grown and plated as described in A. Loss of CFIII during the first mitotic division was indicated by the formation of half-red, half-white colonies. For each strain, the frequency of chromosome loss is plotted on the y-axis and the total number of colonies examined indicated (n). (C) Sister chromatid cohesion was evaluated in WT, *nup60Δ*, and *ctf18Δ* haploid cells containing ~256 *lacO* repeats integrated at the *LEU2* locus and P_{HIS3}-*GFP-lacI*. Cells were grown to mid-logarithmic growth phase in YPD medium, washed three times with SC medium lacking histidine (SC-his) and resuspended in SC-his supplemented with 40 mM 3-amino triazole for 40 min at 23˚C to induce P_{HIS3}-*GFP-lacI*. Cells were washed and resuspended in YPD medium containing 15 μg/mL nocodazole for 3 h at 23˚C. Cells arrested in G2/M-phase were imaged using fluorescence microscopy. Representative images are shown on the left. Defects in sister chromatid cohesion are indicated by the presence of two GFP foci in metaphase arrested cells. For each strain the percentage of large-budded cells containing two GFP foci are plotted on the y-axis and the number of large-budded cells examined is indicated (n).

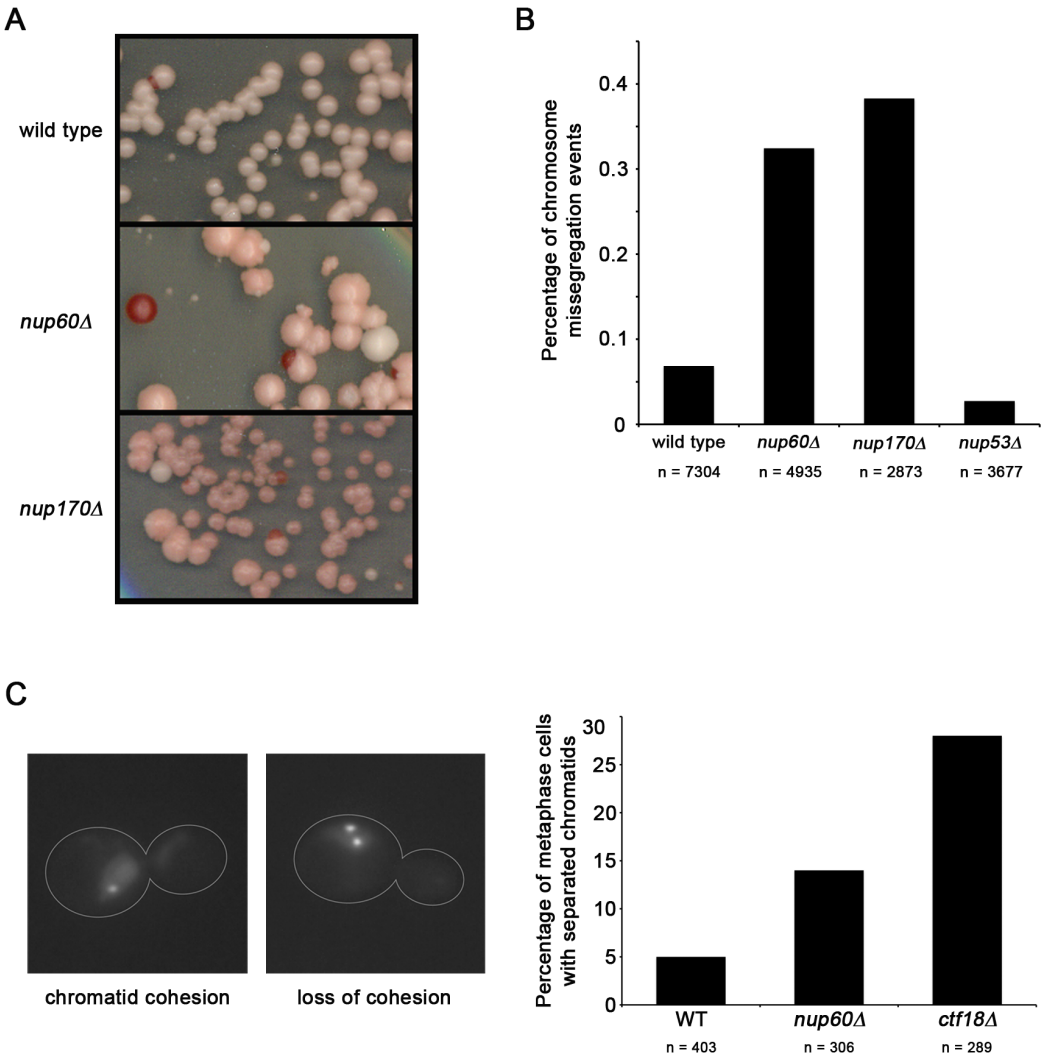

Figure 7-1. Nup60p functions in chromosome segregation.

Figure 7-2. Expression of a *NUP170* C-terminal domain suppresses the growth defect of an *elm1Δ nup170Δ* mutant.

(A) To assess growth rates of the indicated strains, an equal number of cells from each cell culture were serially diluted and spotted onto YPD plates and incubated at 30˚C for 3 d (*top panel*). Cellular morphology was examined in cells grown to mid-logarithmic growth phase and imaged by light microscopy. Representative bright field images are shown (*bottom panels*). (B) The growth rate of the *itc1Δ nup170Δ* mutant was examined in cells expressing various *NUP170* truncations under control of a galactose inducible promoter ($P_{GAL1/10}$). Plasmids pNS-276 (empty vector), pNS288 ($NUP170^{1\text{-}1502}$; expressing full length *NUP170*; amino acids 1-1502), pNS-312 ($NUP170^{1\text{-}750}$), pNS-313 ($NUP170^{750\text{-}1502}$), pNS-333 ($NUP170^{500\text{-}1502}$), and pNS-337 ($NUP170^{1000\text{-}1502}$) were introduced into the *itc1Δ nup170Δ* strain. Cells were grown to mid-logarithmic growth phase and an equal number of cells from each cell culture were serially diluted and spotted onto SC medium containing glucose and incubated at 30˚C for 5 d (*left panel*). Cellular morphology of the indicated strains was determined as described in A for cells grown in the presence of glucose (*right panels*). Note, in the presence of glucose (repressive conditions) leaky expression from $P_{GAL1/10}$ of full-length $NUP170^{1\text{-}1502}$, $NUP170^{750\text{-}1502}$, and $NUP170^{1000\text{-}1502}$ was sufficient to rescue growth of the *itc1Δ nup170Δ* double mutant while the severe morphology defect was partially suppressed by leaky expression of $NUP170^{1\text{-}1502}$ and $NUP170^{1000\text{-}1502}$.

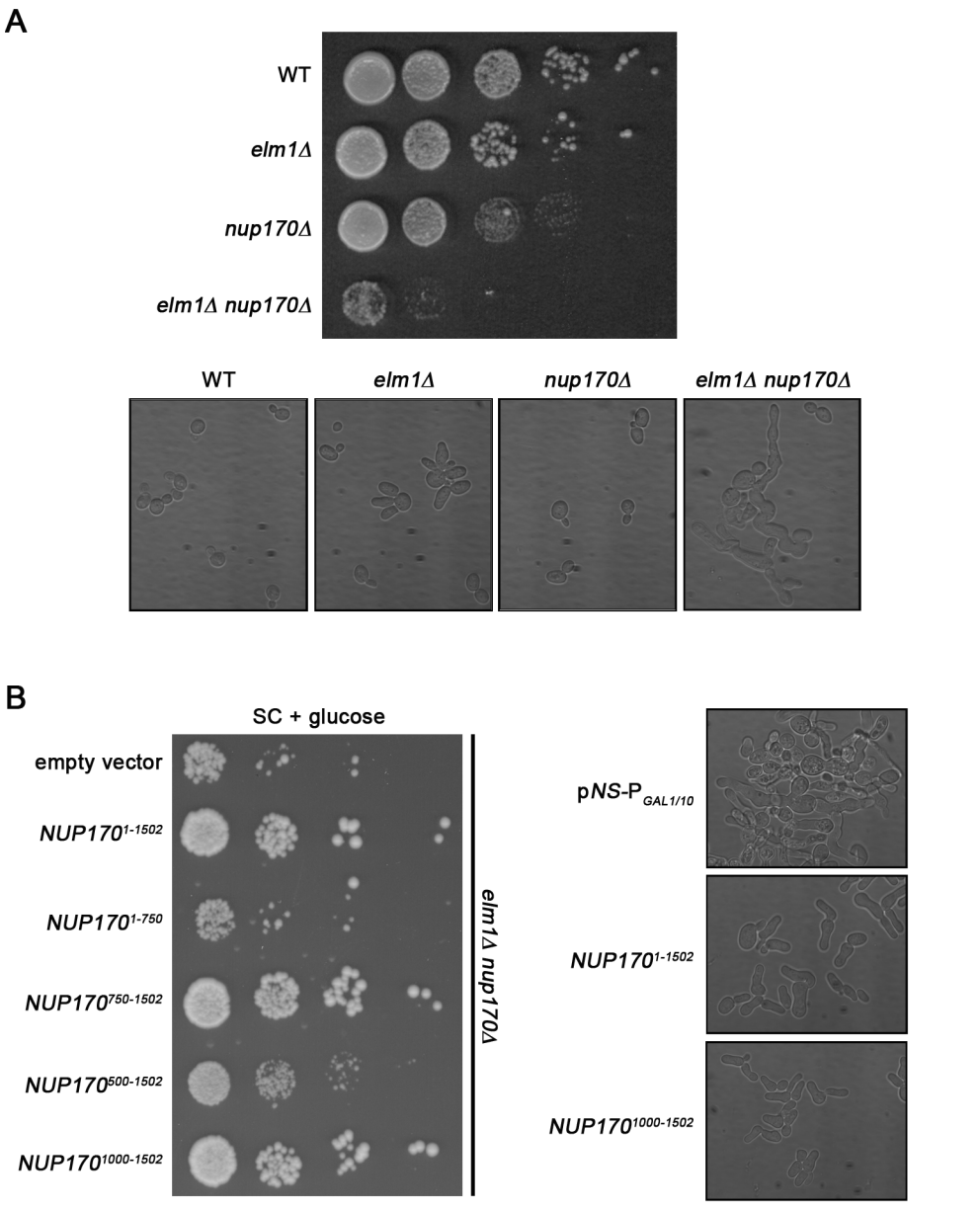

Figure 7-2. Expression of a *NUP170* C-terminal domain suppresses the growth defect of an *elm1Δ nup170Δ* mutant.

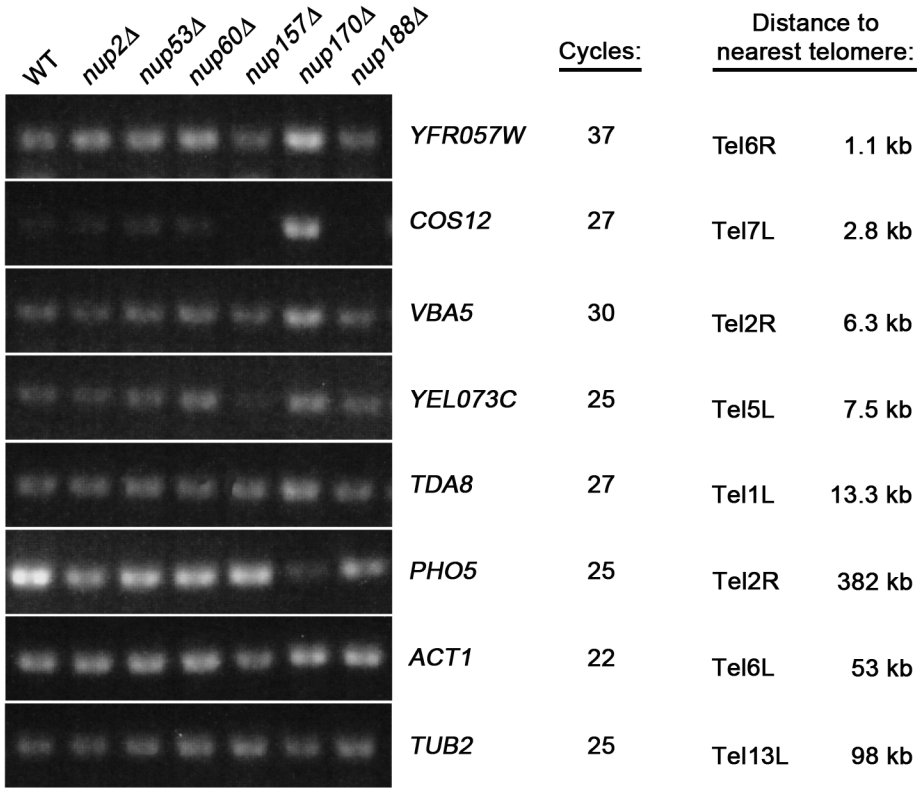

Figure 7-3. Derepression of subtelomeric genes was not detected in other *nup* null mutants.

Repression of subtelomeric genes was assessed in a WT strain and the indicated *nup* null mutants. Total RNA was isolated from cells grown to mid-logarithmic growth phase in YPD medium and expression of the subtelomeric genes *YFR057W*, *COS12*, *VBA5*, *YEL073C*, and *TDA8* and the non-subtelomeric phosphate metabolism gene *PHO5* were determined by semi-quantitative reverse-transcription PCR (RT-PCR) using primer sets specific to each target cDNA. *ACT1* and *TUB2* served as a loading control and the *nup170Δ* mutant served as positive control for derepression. The number of cycles for optimal, logarithmic amplification of each target cDNA and the distance of each gene to the nearest telomere are indicated.

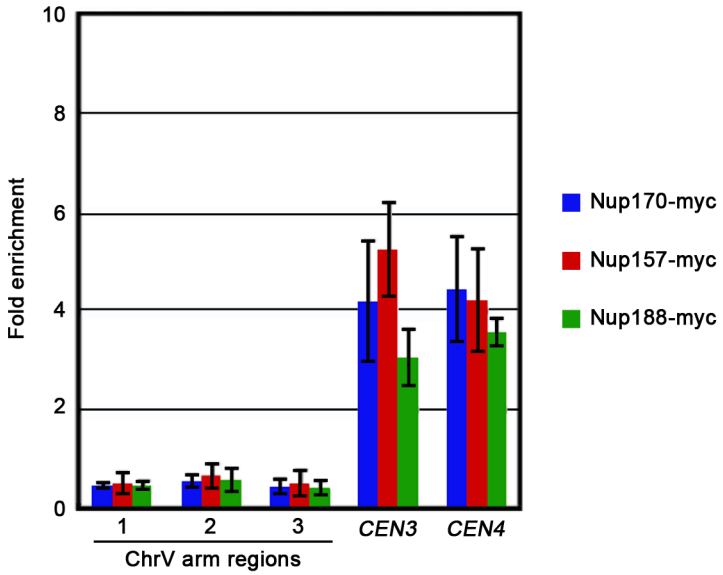

Figure 7-4. Nup170p, Nup157p, and Nup188p associate with centromeric DNA.

Isogenic yeast strains synthesizing the C-terminal Myc-fusion proteins Nup170-9xMyc (blue), Nup157-9xMyc (red), and Nup188-9xMyc (green) were constructed from the BY4742 background. Centromeric association of the Myc-tagged fusion proteins was analyzed by chromatin immunoprecipitation (ChIP) and qPCR using primer sets positioned within the centromeric regions of chromosome III and IV (*CEN3* and *CEN4*) and along the right arm of chromosome V (ChrV arm regions 1, 2, and 3; positioned at 534 kb, 542 kb, and 549.7 kb) as negative controls. Mean relative enrichment of three independent ChIP experiments is plotted on the y-axis with standard error.
* ChIP and qPCR analysis was performed by YW.

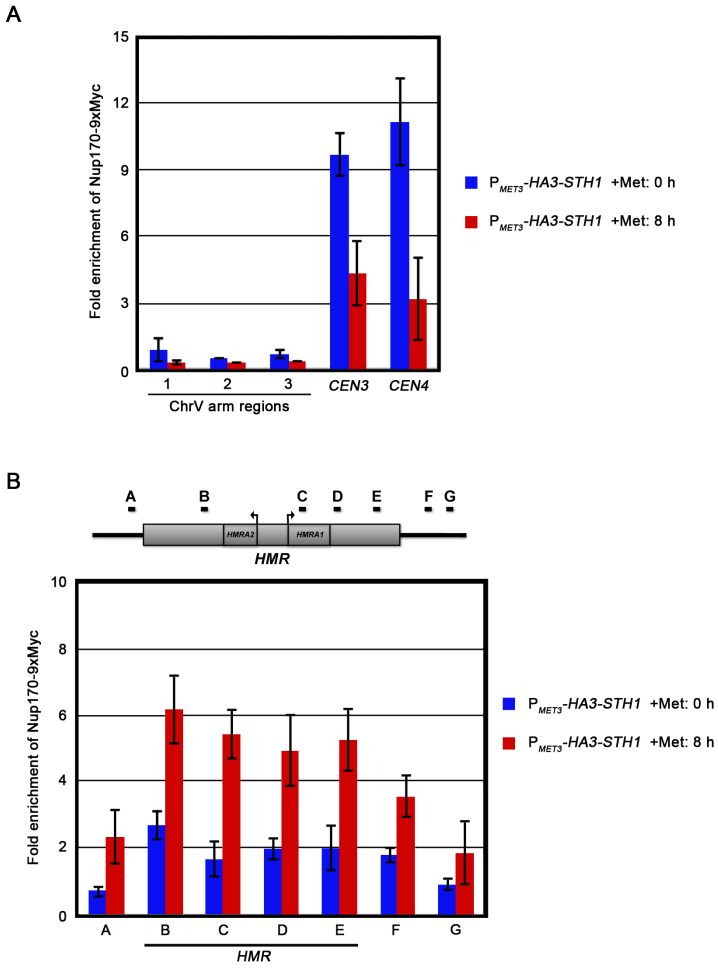

Figure 7-5. Association of Nup170p with centromeric DNA and *HMR* are differentially affected by loss of Sth1p.

(A-B) In a strain expressing *NUP170-9xMYC*, the *STH1* promoter was replaced with the repressible *MET3* promoter (P_{MET3}-*HA3-STH1*) such that *STH1* is repressed in the presence of methionine. P_{MET3}-*HA3-STH1* cells producing Nup170-9xMyc were grown to early-logarithmic growth phase in SC medium lacking methionine (SC-met) and *STH1* was repressed by the addition of 200 μg/mL methionine for 8 h. Chromatin immunoprecipitation of Nup170-9xMyc was performed before (+Met: 0 h; blue) and after depletion of Sth1p for 8 h (+Met: 8 h; red). ChIP samples were analyzed by qPCR to examine Nup170-9xMyc association with centromeric DNA (A) and *HMR* (B) in the presence and absence of Sth1p. For each histogram, the mean relative enrichment and standard error are plotted on the y-axis. Primer sets for panel A are located along the right arm of chromosome V (1, 2, and 3) as negative controls and within the centromeric regions of chromosome III and IV (*CEN3* and *CEN4*). Primer sets for panel B are positioned within *HMR* (primers B to E) and flanking *HMR* (primers A, F, and G).

* ChIP and qPCR analysis was performed by YW.

Figure 7-6. Colocalization amongst nucleoporins.

Strains producing the indicated C-terminally-tagged fusion proteins were grown to mid-logarithmic growth phase in YPD medium, washed twice with SC medium and immobilized on agarose pads immediately prior to imaging by confocal microscopy. During image acquisition, objective movement was driven by a piezoelectric actuator to allow rapid acquisition of z-stacks. Stacks of 37 optical sections spaced 0.16 μm apart were acquired. Data sets were deconvolved with *Huygens Professional* software using an iterative algorithm to reduce background noise and reassign blur. Shown are representative deconvolved single focal plane images of the green (GFP), red (mRFP or mCherry) and merged channels. Deconvolved images were displayed in *Imaris 7*.0 software and the Spot detection feature was used to assign signals to three-dimensional spheres representative of NPCs. Colocalization of spheres from the corresponding red and green channels was determined using *Matlab* software for the indicated number of cells (n). For each strain, the mean percentage of colocalizing spheres within an individual cell is plotted on the y-axis with standard deviation. The number of cells examined is indicated (n).

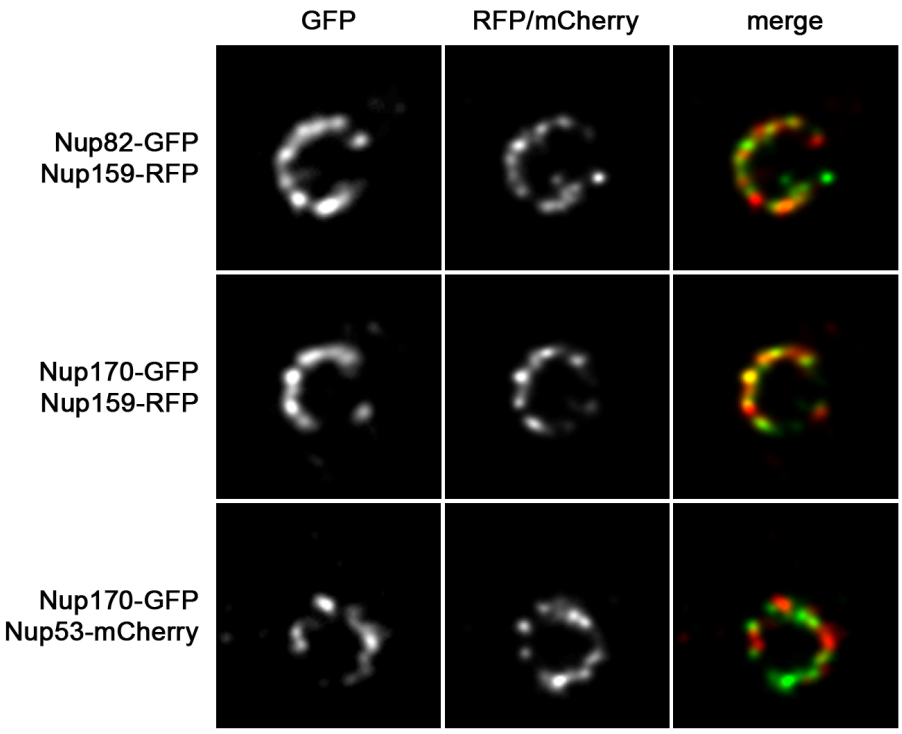

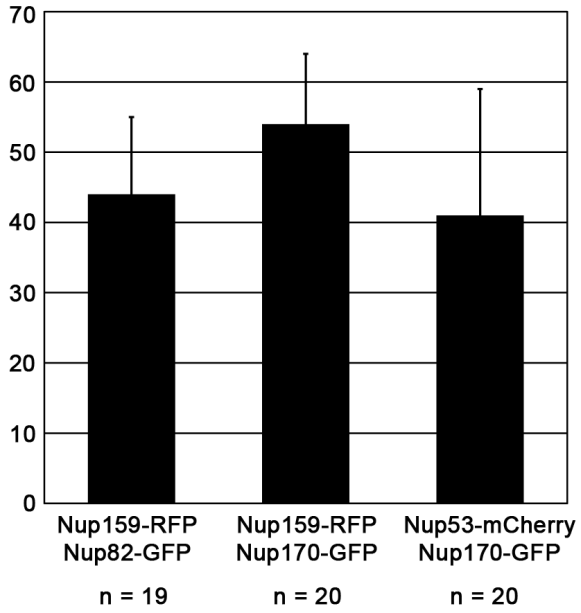

Figure 7-6. Colocalization amongst nucleoporins.

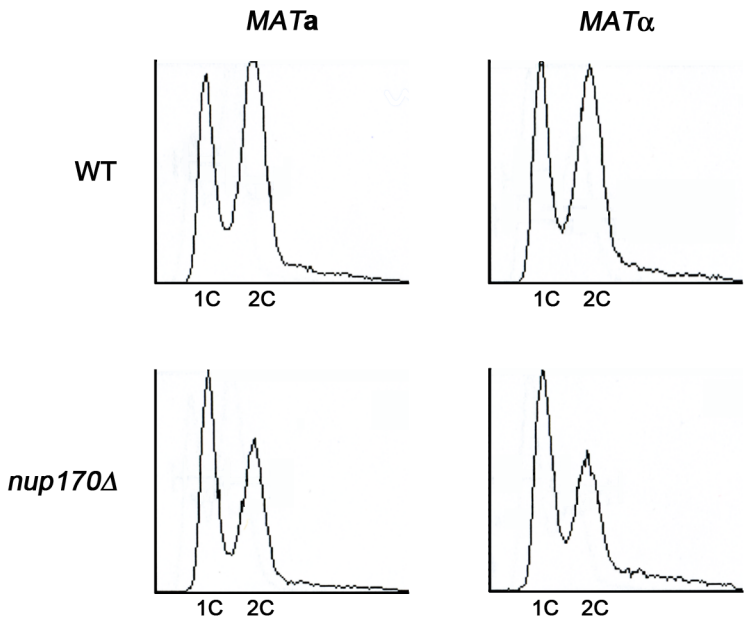

Figure 7-7. A *nup170Δ* cell culture contains an increased number of G1-phase cells compared to WT.

Asynchrounous cultures of WT and *nup170Δ* cells of the indicated mating types (*MAT***a** and *MAT*α) were grown to an OD_{600} of 0.8 and assessed for DNA content. Shown are profiles of DNA content for the indicated strains as determined by FACS analysis. Cells with a 1C DNA content are indicative of cells in G1-phase of the cell cycle.

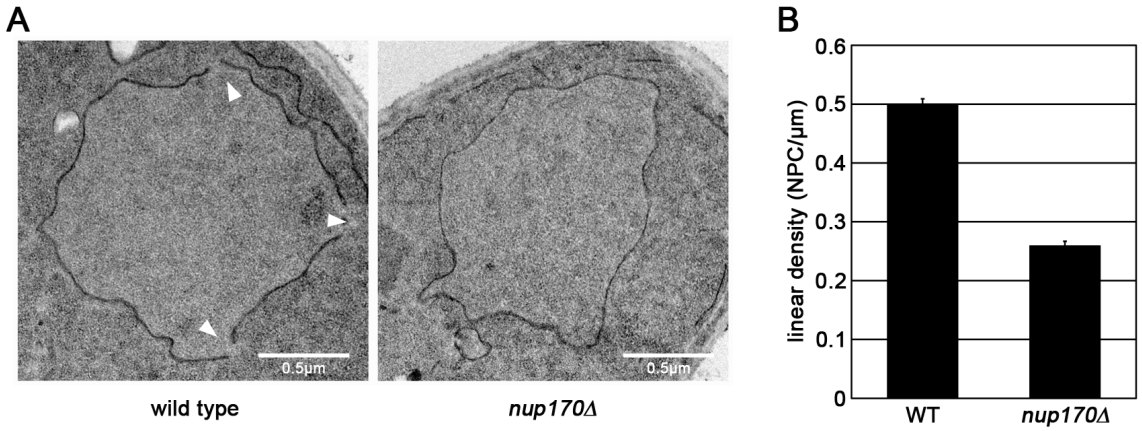

Figure 7-8. Loss of Nup170p leads to a reduced number of NPCs.

Isogenic WT and *nup170Δ* strains were isolated through tetrad dissection of a *nup170Δ* heterozygous diploid strain (DVY1150). Cells were grown in YPD medium to an OD_{600} of ~0.8 and processed for examination by transmission electron microscopy (TEM). To visualize membranous structures, cells were stained with potassium permanganate. (A) Representative TEM micrographs of a WT and *nup170Δ* cell. Arrowheads indicate gaps in the NE consistent in size with NPCs. Scale bars, 0.5 μm. (B) The number of NPCs in each section was counted and divided by the linear length of the NE to calculate the linear density of NPCs (NPCs/μm). A minimum of 50 cells was analyzed in each experiment and the mean linear density of NPCs and standard error from two independent experiments (WT) or three independent experiments (*nup170Δ)* are shown.

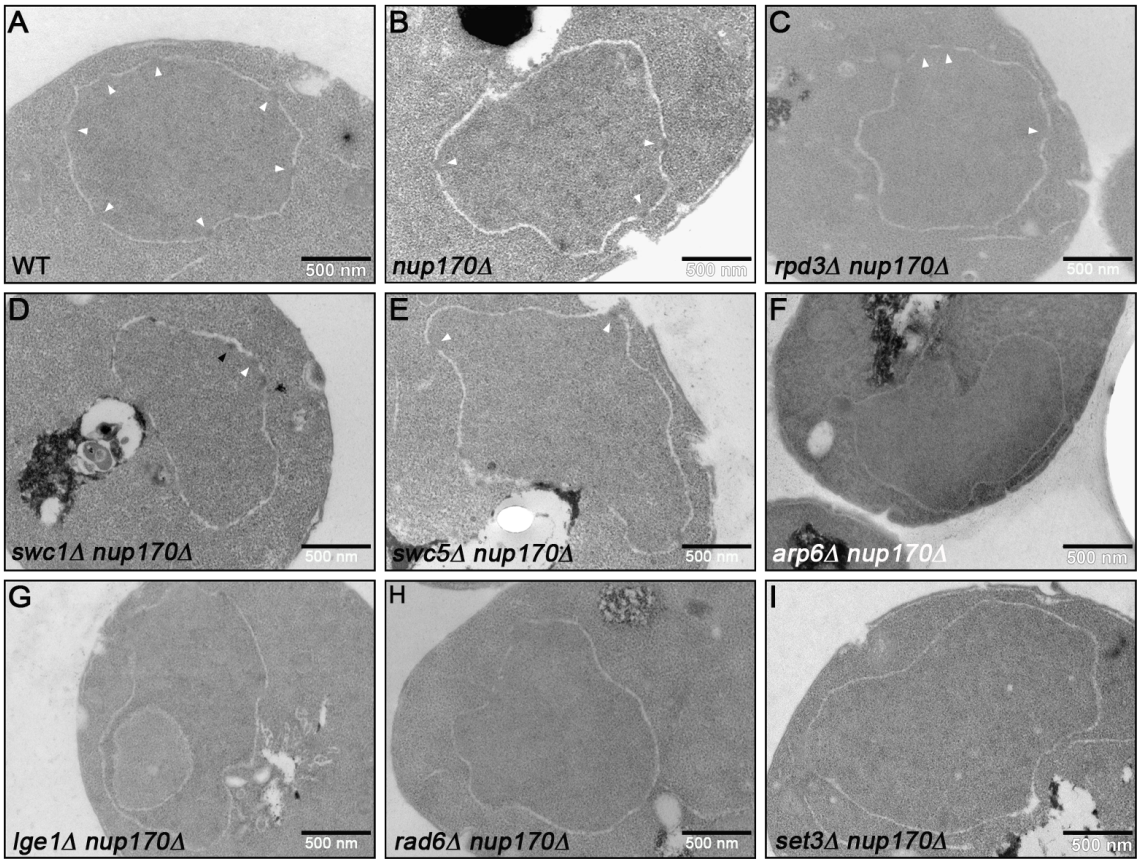

Figure 7-9. Chromatin complexes are required for nuclear morphology and NPC assembly.

Haploid yeast strains of the indicated genotypes were grown in YPD medium to an OD_{600} of ~0.8 and cells were processed for examination by transmission electron microscopy (TEM). To visualize proteinaceous structures, cells were stained with osmium tetroxide. Representative TEM micrographs are shown. White arrowheads indicate mature NPCs. The black arrowhead in panel (D) indicates an electron dense structure attached to the inner nuclear membrane consistent in size with an NPC. Scale bars, 500 nm. Note, NPCs were rarely identified in sections of the double null mutants. Additionally, defects in NE morphology such as herniations, invaginations, and membrane expansion were commonly observed in the double null mutants. Importantly, NPC assembly intermediates were detected attached to the inner nuclear membrane of *swc1Δ nup170Δ* cells.

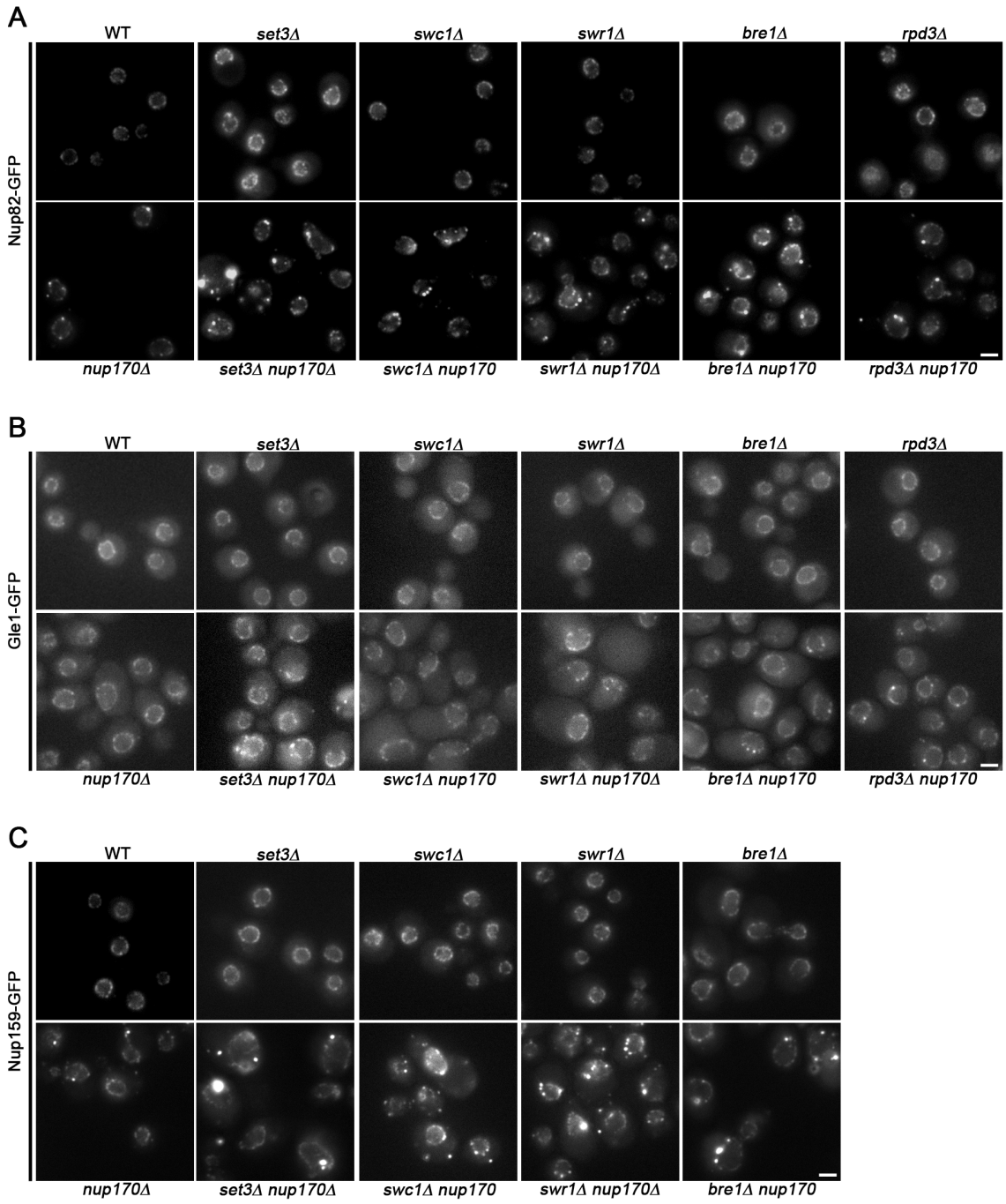

Figure 7-10. Chromatin complexes are required for localization of cytoplasmic Nups at the NE.

The indicated null mutations were introduced into strains expressing *NUP82-GFP* (A), *GLE1-GFP* (B), and *NUP159-GFP* (C) from their endogenous promoters. Cells of mid-logarithmically growing cultures were collected, washed with SC medium and immobilized on agarose pads immediately prior to imaging by epifluorescence microscopy. Scale bars, 2 μm.

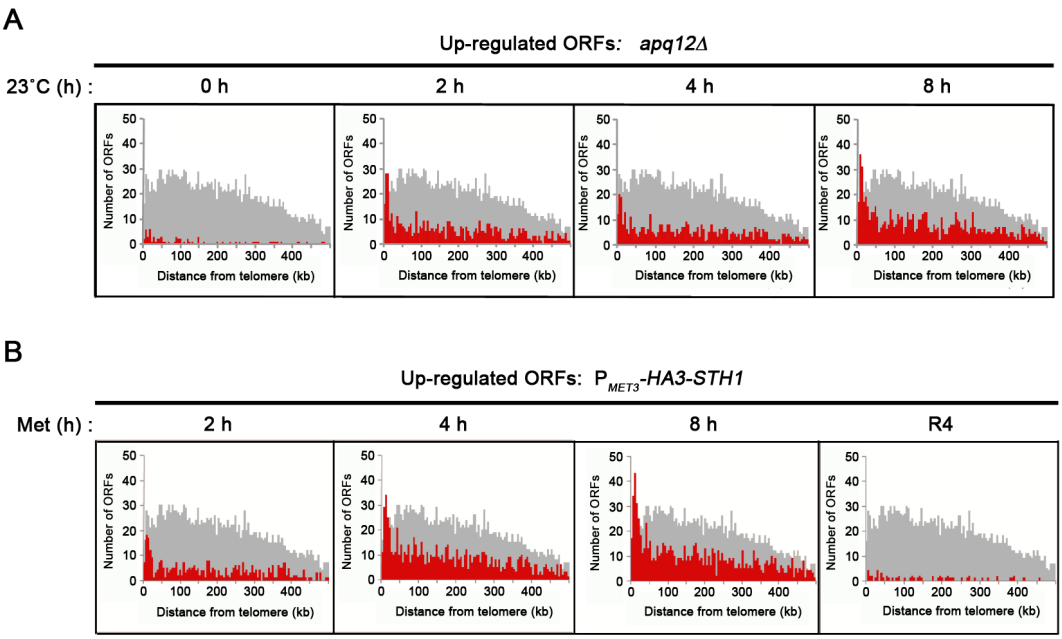

Figure 7-11. NPC assembly mutants exhibit derepression of subtelomeric genes.

(A) Asynchronous cultures of WT and *apq12Δ* cells were grown to early logarithmic growth phase at the permissive temperature (37˚C) and then shifted to the non-permissive temperature (23˚C) in which *apq12Δ* cells exhibit defects in NPC assembly. The gene expression profile of *apq12Δ* cells was determined by DNA microarray analysis comparing RNA isolated from WT and *apq12Δ* cells at the indicated times. Differentially expressed genes were identified by maximum likelihood analysis (lambda ≥ 100) and ORFs with a ≥ 2-fold change in expression were considered significantly affected. To visualize the positions of differentially up-regulated ORFs, the distances of these ORFs to the nearest telomere were determined and the number of ORFs within 5 kb bins were plotted versus their distance from telomeres. Shaded histograms (grey) indicate the total number of ORFs within the 5 kb bins at one-third scale. (B) Gene expression profiles were determined for the NPC assembly mutant P_{MET3}-*HA3-STH1* following repression of the *MET3* promoter (P_{MET3}) by the addition of 200 μg/mL methionine for the times indicated. DNA microarray analysis compared RNA isolated at the indicated times to RNA isolated prior to repression (i.e. 0 h versus 8h) and the positions of ORFs exhibiting significant changes in expression were analyzed as described in panel A, with the exception of lamba ≥ 50. Similar analyses were also performed on P_{MET3} cells repressed for 8 h followed by reinduction of P_{MET3}-*HA3-STH1* for 4 h (R4).

* RNA isolation was performed by DWV. cDNA labeling and hybridization were performed by YW. Data analysis and image processing were performed by WMC, YW, and DWV.

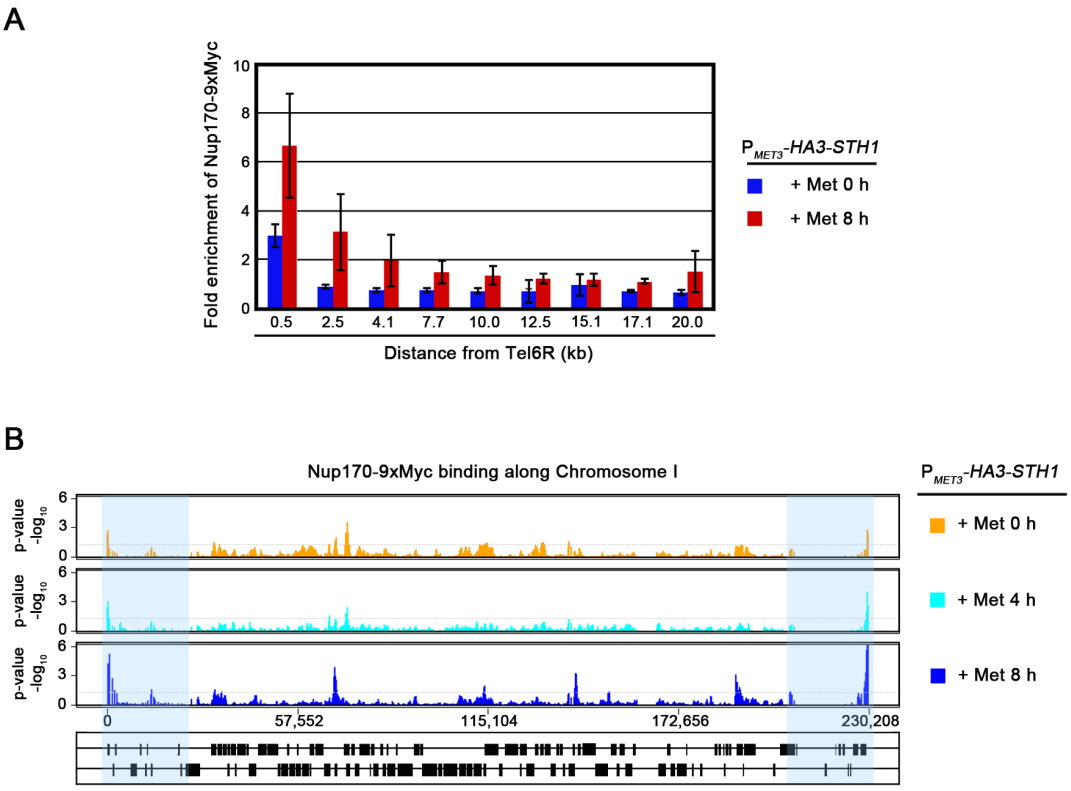

Figure 7-12. Association of Nup170p with subtelomeric DNA is enhanced in the absence of Sth1p.

Association of Nup170p with subtelomeric DNA was assessed in cells depleted of Sth1p. (A) Chromatin immunoprecipitation of Nup170-9xMyc was performed from P$_{MET3}$-*HA3-STH1* cells either producing Sth1p (blue; + Met 0 h) or depleted of Sth1p for 8 h (red; + Met 8 h). ChIP samples were analyzed by qPCR using primer sets positioned along a 20 kb subtelomeric region of the right arm of chromosome VI (x-axis). Mean relative enrichment of three independent ChIP experiments is plotted on the y-axis with standard error. (B) The genome-wide binding profile of Nup170p in the presence and absence of Sth1p was determined by ChIP-chip analysis. Shown are the binding profiles of Nup170-9xMyc obtained from P$_{MET3}$-*HA3-STH1* cells depleted of Sth1p for 0 h (gold), 4 h (light blue), and 8 h (dark blue) along a representative chromosome (Chromosome I). Nup170p DNA binding sites are plotted along the y-axis as a logarithmic function of their p-values (-log$_{10}$). Black rectangles represent ORFs located on the Watson and Crick strands. Subtelomeric regions are indicated by blue shading.
* ChIP experiments were performed by YW, data analysis was performed by YW and WMC and figure processing was performed by YW, WMC, and DWV.

Figure 7-13. a-specific genes are derepressed in NPC assembly mutants.

Repression of the **a**-specific genes *BAR1* and *STE2* was assessed in the NPC assembly mutants, *apq12Δ* and *nup157Δ* P_{MET3}-*HA3-NUP170*. (A) *MAT*α WT and *apq12Δ* cells were grown to an OD_{600} of 0.4 at 37˚C, the permissive temperature in which the NPC-assembly defects of the *apq12Δ* mutant are minimized. Cells were then shifted to the non-permissive temperature (23˚C) to illicit NPC assembly defects (Nup mislocalization) and RNA was isolated at the times indicated. Following 8 h at 23˚C, benzyl alcohol was added to a final concentration of 0.1% for 1 h to mediate Nup re-localization to the NE. Expression of *BAR1* and *STE2* were determined by semi-quantitative, reverse-transcription PCR (RT-PCR) of isolated RNA using primer sets specific to each target cDNA. *TUB2* served as a loading control. The number of cycles for optimal, logarithmic amplification of each target cDNA is indicated. (B) Expression of *BAR1* and *STE2* were determined by RT-PCR as described in A for the indicated strains. Cells were grown in SC medium lacking methionine (SC-met) to an OD_{600} of ~0.4 and P_{MET3}-*HA3-NUP170* was repressed by addition of 200 μg/mL methionine for the indicated times. Following 8 h of repression, cells were washed extensively with SC-met and resuspended in SC-met for an additional 6 h to reinduce P_{MET3}-*HA3-NUP170*. For each time point protein samples were taken and analyzed by SDS-PAGE and Western blotting to monitor HA3-Nup170p levels (IB: HA3-Nup170p) and RNA was isolated for RT-PCR analysis. Note, the mutant strains *nup170Δ* and P_{MET3}-*HA3-NUP170* served as positive and negative controls, respectively.

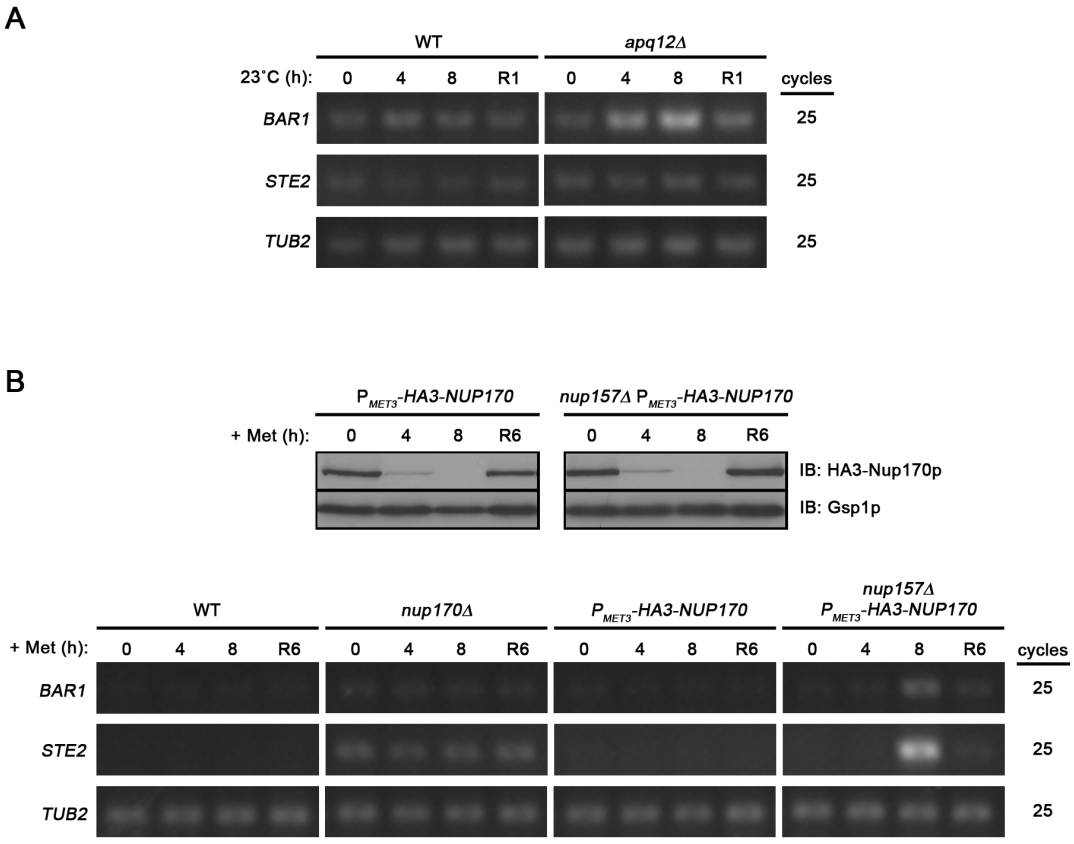

Figure 7-13. a-specific genes are derepressed in NPC assembly mutants.